PREDICTIVE IMAGABLE BIOMARKERS FOR BRAIN DISORDERS

EDITED BY: Pravat K. Mandal and Lars Ersland
PUBLISHED IN: Frontiers in Neurology and Frontiers in Neuroscience

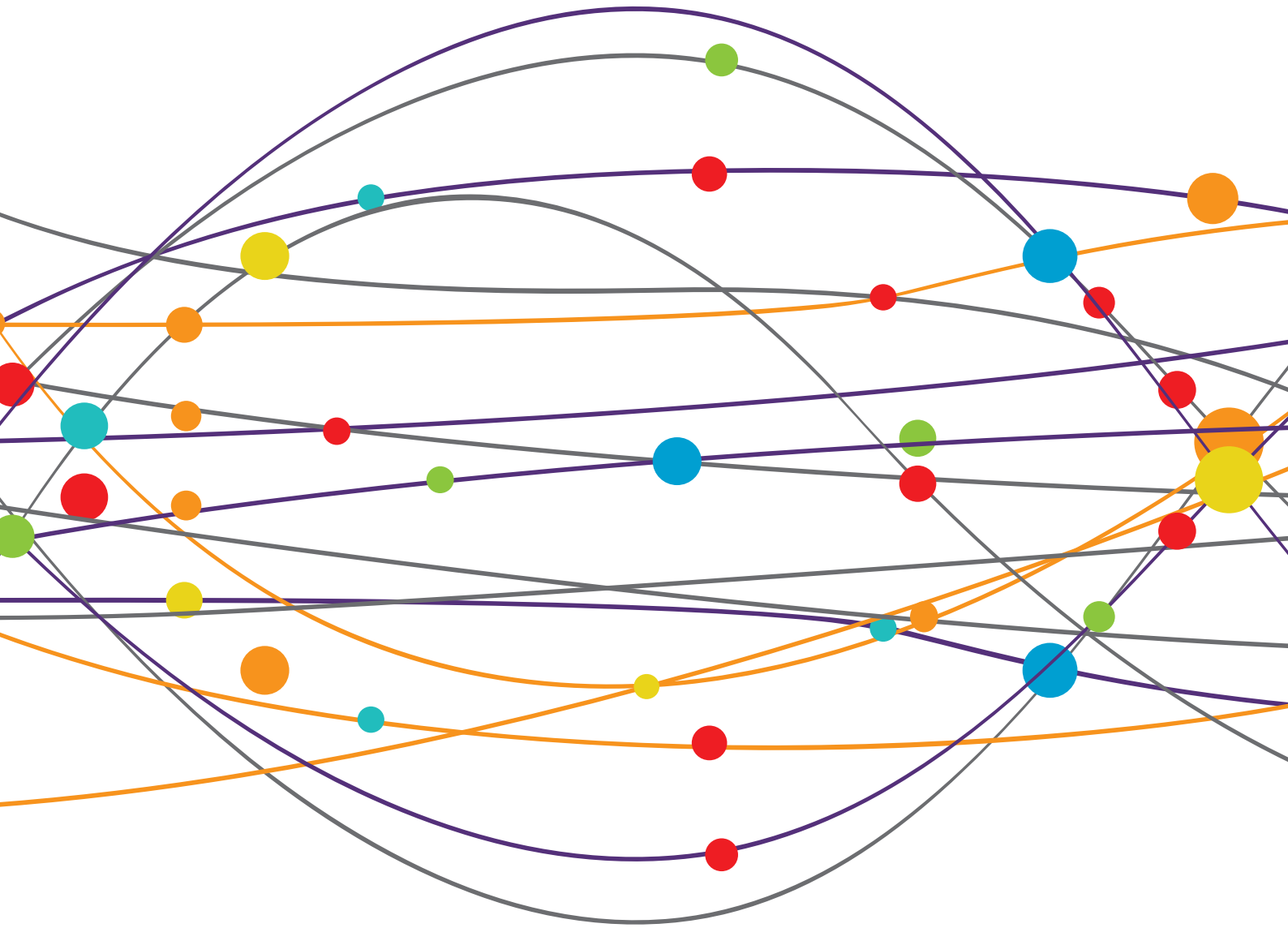

frontiers Research Topics

ISSN 1664-8714
ISBN 978-2-88963-048-6
DOI 10.3389/978-2-88963-048-6

About Frontiers

Frontiers is more than just an open-access publisher of scholarly articles: it is a pioneering approach to the world of academia, radically improving the way scholarly research is managed. The grand vision of Frontiers is a world where all people have an equal opportunity to seek, share and generate knowledge. Frontiers provides immediate and permanent online open access to all its publications, but this alone is not enough to realize our grand goals.

Frontiers Journal Series

The Frontiers Journal Series is a multi-tier and interdisciplinary set of open-access, online journals, promising a paradigm shift from the current review, selection and dissemination processes in academic publishing. All Frontiers journals are driven by researchers for researchers; therefore, they constitute a service to the scholarly community. At the same time, the Frontiers Journal Series operates on a revolutionary invention, the tiered publishing system, initially addressing specific communities of scholars, and gradually climbing up to broader public understanding, thus serving the interests of the lay society, too.

Dedication to Quality

Each Frontiers article is a landmark of the highest quality, thanks to genuinely collaborative interactions between authors and review editors, who include some of the world's best academicians. Research must be certified by peers before entering a stream of knowledge that may eventually reach the public - and shape society; therefore, Frontiers only applies the most rigorous and unbiased reviews.
Frontiers revolutionizes research publishing by freely delivering the most outstanding research, evaluated with no bias from both the academic and social point of view. By applying the most advanced information technologies, Frontiers is catapulting scholarly publishing into a new generation.

What are Frontiers Research Topics?

Frontiers Research Topics are very popular trademarks of the Frontiers Journals Series: they are collections of at least ten articles, all centered on a particular subject. With their unique mix of varied contributions from Original Research to Review Articles, Frontiers Research Topics unify the most influential researchers, the latest key findings and historical advances in a hot research area! Find out more on how to host your own Frontiers Research Topic or contribute to one as an author by contacting the Frontiers Editorial Office: researchtopics@frontiersin.org

PREDICTIVE IMAGABLE BIOMARKERS FOR BRAIN DISORDERS

Topic Editors:
Pravat K. Mandal, National Brain Research Center, India and Florey Institute of Neuroscience and Mental Health, Australia
Lars Ersland, Haukeland University Hospital, Norway

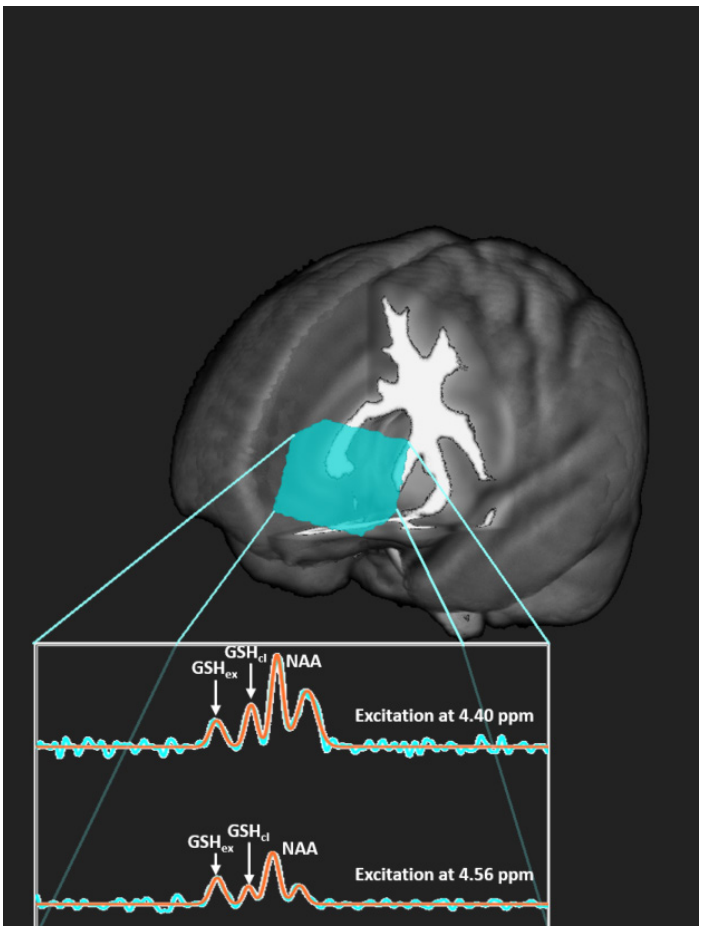

Image caption: Characterization of two glutathione (GSH) conformers (Extended and Closed forms) in the brain using MEGA-PRESS sequence.
Image credit: Dr. Praful P. Pai and Khushboo Punjabi, NBRC, India.

Recent research on Neurodegenerative disorders such as Alzheimer's Disease, Parkinson's Disease, etc. and Neuropsychiatric disorders such as Schizophrenia, has shown strong evidence that altered brain tissue structure, physiology, and connectivity reflect the extent of severity of behavioral and physical abnormalities. With the advancement of high field strength MR technologies like MRS (Magnetic Resonance Spectroscopy), fMRI (functional Magnetic Resonance Imaging) and DTI (Diffusion Tensor Imaging), it has become possible to non-invasively measure these changes brain microenvironment in terms of levels of antioxidants; neurotransmitters;

regional activity, susceptibility and connectivity during transition from healthy to pathological conditions, and during progression of disease stages.

Advanced Machine Learning (ML) and Statistical modeling algorithms are utilizing features extracted from multimodal MR based, neuropsychological and neurophysiological data to build classifiers that identify highly sensitive and specific biomarkers to aid in understanding the causal processes of these brain disorders and can be translated from bench to bedside clinical practices for non-invasive diagnostic testing. It is also important to have global clinical research data sharing platforms that utilize data mining and ML to identify early biomarkers and test the sensitivity of old ones from time to time with advancement in research.

This Research Topic updates the reader about the latest research in imagable biomarkers using MR methodologies and use of AI for testing the sensitivity of these biomarkers.

Citation: Mandal, P. K., Ersland, L., eds. (2019). Predictive Imagable Biomarkers for Brain Disorders. Lausanne: Frontiers Media. doi: 10.3389/978-2-88963-048-6

Table of Contents

SECTION 3

REVIEWS

frontiers in Neurology

EDITORIAL
published: 13 June 2019
doi: 10.3389/fneur.2019.00583

Editorial: Predictive Imagable Biomarkers for Neurodegenerative and Neurodevelopmental Diseases

Pravat K. Mandal[1,2]* *and Lars Ersland*[3,4,5]

[1] Neuroimaging and Neurospectroscopy Laboratory (NINS), National Brain Research Centre, Gurgaon, India, [2] Florey Institute of Neuroscience and Mental Health, Melbourne, VIC, Australia, [3] Department of Clinical Engineering, Haukeland University Hospital, Bergen, Norway, [4] Department of Biological and Medical Psychology, University of Bergen, Bergen, Norway, [5] NORMENT Center of Excellence, Haukeland University Hospital, Bergen, Norway

Keywords: imagable biomarkers, neurodevelopmental, neurodegenerative, glutathione conformations, imaging techniques

Editorial on the Research Topic

Predictive Imagable Biomarkers for Neurodegenerative and Neurodevelopmental Diseases

In the last four decades, tremendous economic and technological development has helped to improve the quality of life and average life span has increased substantially. As a consequence, the number of people with much higher age is increasing and reports of aging associated disorders are multiplying due to various neurodegenerative disorders such as Alzheimer's, Parkinson's frontotemporal, dementia with Lewy body disease etc. The causal process of these neurodegenerative disorders is not known yet; however, oxidative stress is recognized to play an important role (1–3). At the same time, the number of cases with neurodevelopmental disorders [Autism Spectrum Disorders (ASD) (4), Epilepsy (5) and Attention Deficit Hyperactivity Disorder (6)] is increasing rapidly in the early part of the life due to multifactorial reasons. Two major health related issues in two distinct age groups need urgent attention to identify the causal process and subsequently a therapeutic development for cure.

The advancements in different imaging techniques [e.g., Magnetic Resonance Imaging (MRI), MR Spectroscopy (MRS), functional MRI (fMRI), functional MRS, Magnetic Encephalography, Diffusion Tensor Imaging etc.] provide various critical features for reliably predicting the individuals who will progress from asymptomatic pre-clinical phase to clinical phases.

In this context, it is critical to investigate the factors which may impact the brain microenvironment these could trigger the early causal processes. In neurodevelopmental and neurodegenerative disorders, the roles of various neurochemicals receptors or antioxidants and their abnormal modulations are getting huge attention for more in-depth research. Recently it was discovered that brain microenvironment has the role to modulate the two distinct conformations of glutathione (GSH), a major antioxidant involved in neutralizing harmful radicals (**Figure 1**). GSH exists in two conformational states (extended and closed form) in the brain (7, 10, 11). It is therefore paramount to identify novel imagable diagnostic biomarkers involving antioxidants, neurotransmitters and physiological parameters that can aid in discovering the causal processes of these brain disorders and can be translated into clinical practices for simplified diagnostic tests and advocating appropriate lifestyle changes to delay the onset of symptoms.

This special issue has a total of ten articles from various laboratories. Mandal and co-workers have developed a Hadoop-based big data framework (BHARAT) integrating non-invasive MRI, MRS as well as neuropsychological test outcomes to identify early diagnostic biomarkers of AD. The framework for AD incorporates the three "V"s (volume, variety and velocity) with advanced data mining, machine learning, and statistical modeling algorithms Sharma et al.

OPEN ACCESS

Edited by:
Jan Kassubek,
University of Ulm, Germany

Reviewed by:
Hans-Peter Müller,
University of Ulm, Germany

***Correspondence:**
Pravat K. Mandal
pravat.mandal@gmail.com;
pravat@nbrc.ac.in;
pravat.mandal@florey.edu.au

Specialty section:
This article was submitted to Applied Neuroimaging, a section of the journal Frontiers in Neurology

Received: *13 May 2019*
Accepted: *17 May 2019*
Published: *13 June 2019*

Citation:
Mandal PK and Ersland L (2019) Editorial: Predictive Imagable Biomarkers for Neurodegenerative and Neurodevelopmental Diseases. Front. Neurol. 10:583. doi: 10.3389/fneur.2019.00583

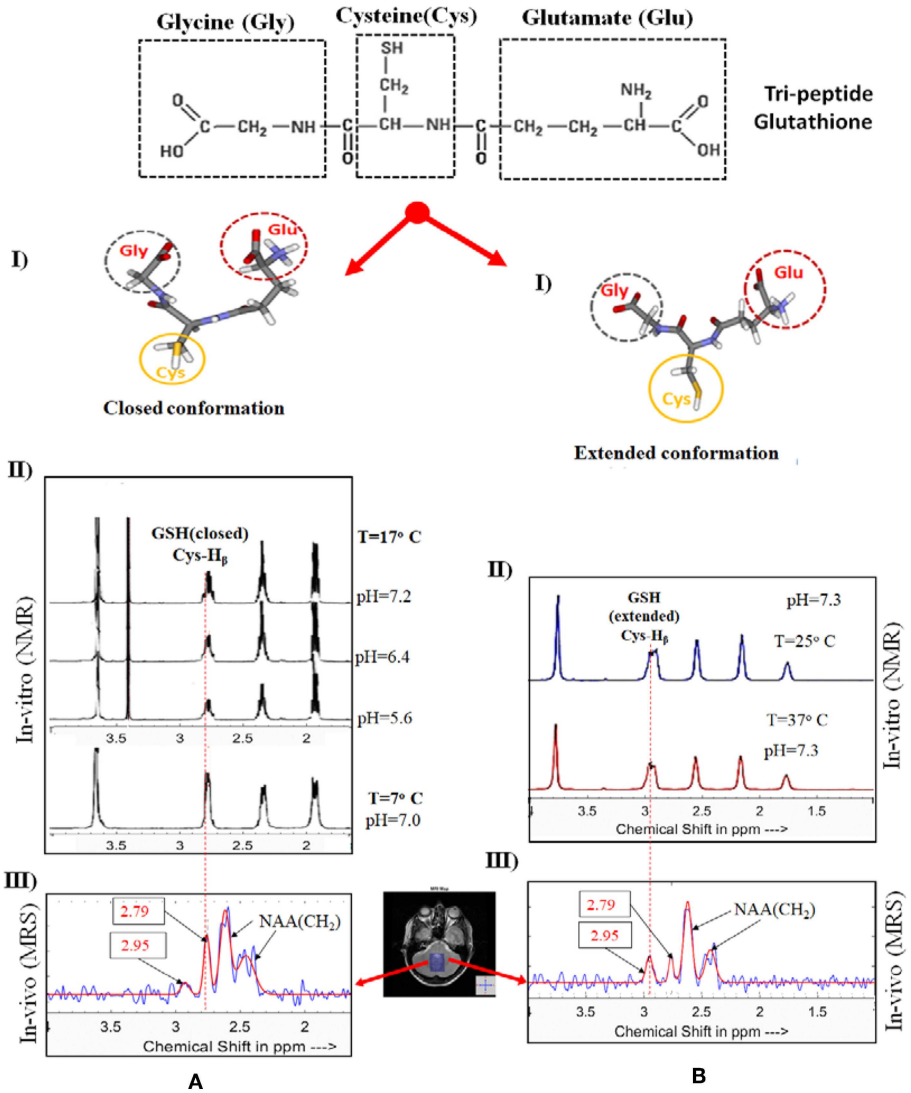

FIGURE 1 | Impact of brain microenvironment on the conformational changes of GSH as evidenced by *in vitro* and *in vivo* MR spectroscopy. Tripeptide GSH is available in two forms. In the panel **(A)**, (I and II), represents the structure of closed form of GSH and the NMR spectra. The second panel **(B)**, (I and II), presents the extended conformation of GSH form and the NMR spectra. Necessary permissions [processed using KALPANA package (1)] were taken to reproduce GSH structure and the NMR spectra from the publishers [IOS PRESS (7), FEBS (8) and Springer (9)]. **(A,B)** (III) display MEGA-PRESS spectra of the cerebellum of the same subject for closed form of GSH (with 180° excitation pulse at 4.40 ppm and TE/TR 130/2500 ms) and extended GSH form (with selective 180° pulse applied at 4.56 ppm and TE/TR 130/2500 ms) using 3T Philips Achieva at NINS Lab, NBRC, India). The NMR spectrum of GSH (closed and extended forms) is aligned with MR spectra of GSH from human brain.

Feng et al. have used corpus callosum (CC) radiomic features related to the diagnosis of AD. They have aimed to identify the CC radiomic features related to the diagnosis of AD and build classification model based on machine learning for the diagnosis of AD.

Teipel et al. have used MRI and cognitive data from 124 patients, derived from ANDI-1 cohort (follow up period 0.4–3.1 years). They conclude that basal forebrain volume, but not hippocampus volume, is a significant predictor of rates for global cognitive decline to predict subsequent cognitive decline during cholinergic treatment.

Yamasakhi et al. have studied the driving ability in the Alzheimer's Disease Spectrum (ADS) and have hypothesized that feasibility of event-related potentials can be a possible predictive biomarker of driving ability in ADS. Interestingly, even in the early stage of the disease, patients with ADS are characterized by the impairment of visuospatial function such as radial optic flow perception related to self-motion perception.

Oishi et al., using functional MRI, found a significant relationship between low Gray Matter (GM) volume in the right inferior parietal lobule (IPL) and severity of mental disorientation. They hypothesize that right IPL is responsible for mental disorientation in amnestic MCI (aMCI) based on voxel-based morphometry. A significant decreased GM volume has been found in the right IPL, which correlates with lower orientation scores on the COGNISTAT cognitive testing tool.

O'Gorman Tuura et al. have investigated the relationship between the axial symptoms of PD and GABA and glutamate levels have quantified using MRS (PD patients $N = 20$ and 17 healthy control). The study showed associations between GABA and Glx and axial symptoms scores are typically more prominent in akinetic-rigid patients than in tremor-dominant patients.

Emamzadeh et al. have presented various risk factors for PD and PD treatment options. Potential risk factors include environmental toxins, drugs, pesticides, brain microtrauma, focal cerebrovascular damage, and genomic defects. Conventional pharmacological treatment of PD is based on the replacement of dopamine using dopamine precursors (levodopa, L-DOPA, L-3,4 dihydroxyphenylalanine), dopamine agonists (amantadine, apomorphine) and MAO-B inhibitors (selegiline, rasagiline), which can be used alone or in combination with each other.

Amyotrophic lateral sclerosis (ALS) is a progressive neurodegenerative process affecting upper and lower motor neurons as well as non-motor systems. Wirth and corworkers report the precentral and postcentral cortical thinning detected by structural MRI combined with clinical (ALS-specific functional rating scale revised, ALSFRS-R) and neurophysiological (motor unit number index, MUNIX) biomarkers in both cross-sectional and longitudinal analyses. Their study concludes that a combinatory use of structural MRI, neurophysiological and clinical biomarkers allows for an appropriate and detailed assessment of clinical state and course of disease of ALS Wirth et al.

Dwyer et al. have reported that no significant changes in GABA, Glx, or NAA levels are observed as a result of anodal stimulation, or between active and sham stimulation, suggesting that a single session of anodal tDCS to the pSTG may be less effective than in other cortical areas.

Winklewski et al. report that DTI can reveal strategic information with respect to white matter tracts, disconnection mechanisms, and related symptoms. Axial and radial diffusivity are likely to provide quite consistent information in healthy subjects, and in pathological conditions with limited edema and inflammatory changes. DTI remains one of the most promising non-invasive diagnostic tools in medicine.

It is our sincere efforts to bring the latest research from leading laboratories to enrich the area, and we believe that multi-centric research collaboration could immensely help to identify various factors responsible for brain microenvironment changes. These critical features can be used in big data analytics, and it should subsequently help in setting a successful clinical trial (9, 12).

AUTHOR CONTRIBUTIONS

PKM conceptualized the idea and wrote the first draft. LE discussed and participated in the draft finalization. The final version was approved by both authors.

FUNDING

This work was supported by TATA INNOVATION AWARD (Award No. BT/HRD/01/05/2015 to PKM) from the ministry of Science and Technology, Government of India and India-Australia Biotechnology funding (Grant no BT/Indo-Aus/10/31/2016 to PKM).

ACKNOWLEDGMENTS

PKM and LE thank Dr. Deepika Shukla (Scientist, NINS lab) as well as Ms. Khushboo Punjabi (Ph.D. student, NINS Lab) for excellent academic support. Thanks to Ms. Avinash Kalyani, (R&D Engineer, NINS lab) for preparing the **Figure 1**. Ms. Kanika Sandal (Research Manager, NINS lab) is appreciated for getting the necessary permission from publishers.

REFERENCES

1. Mandal PK, Saharan S, Tripathi M, Murari G. Brain glutathione levels–a novel biomarker for mild cognitive impairment and Alzheimer's disease. *Biol Psychiatry*. (2015) 78:702–10. doi: 10.1016/j.biopsych.2015.04.005
2. Mandal PK, Tripathi M, Sugunan S. Brain oxidative stress: detection and mapping of anti-oxidant marker 'Glutathione' in different brain regions of healthy male/female, MCI and Alzheimer patients using non-invasive magnetic resonance spectroscopy. *Biochem Biophys Res Commun*. (2012) 417:43–8. doi: 10.1016/j.bbrc.2011.11.047
3. Markesbery WR. Oxidative stress hypothesis in Alzheimer's disease. *Free Radic Biol Med*. (1997) 23:134–47. doi: 10.1016/S0891-5849(96)00629-6
4. Mikhail AG, King BH. Autism spectrum disorders: update of evaluation and treatment. *Curr Psychiatry Rep*. (2001) 3:361–5. doi: 10.1007/s11920-996-0027-x
5. Bozzi Y, Casarosa S, Caleo M. Epilepsy as a neurodevelopmental disorder. *Front Psychiatry*. (2012) 3:19. doi: 10.3389/fpsyt.2012.00019
6. Vaidya CJ. Neurodevelopmental abnormalities in ADHD. *Curr Top Behav Neurosci*. (2012) 9:49–66. doi: 10.1007/7854_2011_138
7. Shukla D, Mandal PK, Ersland L, Gruner ER, Tripathi M, Raghunathan P, et al. A multi-center study on human brain glutathione conformation using magnetic resonance spectroscopy. *J Alzheimers Dis*. (2018) 66:517–32. doi: 10.3233/JAD-180648
8. Delalande O, Desvaux H, Emmanuel Godat E. Cadmium – glutathione solution structures provide new insights into heavy metal detoxification. *FEBS J*. (2010) 277:5086–96. doi: 10.1111/j.1742-4658.2010.07913.x
9. Zhang R, Wu W, Luo S. Different behaviors of glutathione in aqueous and DMSO solutions: molecular dynamics simulation and NMR experimental study. *J Solution Chem*. (2011) 40:1784–95. doi: 10.1007/s10953-011-9752-9
10. Mandal PK, Shukla D, Govind V, Boulard Y, Ersland L. Glutathione Conformations and its implications for *in vivo* magnetic resonance spectroscopy. *J Alzheimers Dis*. (2017) 59:537–41. doi: 10.3233/JAD-170350
11. Mandal PK, Shukla D. Brain metabolic, structural, and behavioral pattern learning for early predictive diagnosis of Alzheimer's disease. *J Alzheimers Dis*. (2018) 63:935–9. doi: 10.3233/JAD-180063
12. Mandal PK, Shukla D, Tripathi M, Ersland L. Cognitive improvement with glutathione supplement in Alzheimer's disease: a way forward. *J Alzheimers Dis*. (2019) 68:531–5. doi: 10.3233/JAD-181054

Conflict of Interest Statement: The authors declare that the research was conducted in the absence of any commercial or financial relationships that could be construed as a potential conflict of interest.

frontiers in Neurology

ORIGINAL RESEARCH
published: 30 July 2018
doi: 10.3389/fneur.2018.00614

Combinatory Biomarker Use of Cortical Thickness, MUNIX, and ALSFRS-R at Baseline and in Longitudinal Courses of Individual Patients With Amyotrophic Lateral Sclerosis

Anna M. Wirth[1,2], Andrei Khomenko[1], Dobri Baldaranov[1], Ines Kobor[1], Ohnmar Hsam[1], Thomas Grimm[1], Siw Johannesen[1], Tim-Henrik Bruun[1], Wilhelm Schulte-Mattler[1], Mark W. Greenlee[2] and Ulrich Bogdahn[1]†*

[1] Department of Neurology, University Hospital of Regensburg, Regensburg, Germany, [2] Department of Experimental Psychology, University of Regensburg, Regensburg, Germany

OPEN ACCESS

Edited by:
Pravat K. Mandal,
National Brain Research Centre (NBRC), India

Reviewed by:
Tino Prell,
Friedrich-Schiller-Universität-Jena, Germany
Senthil S. Kumaran,
All India Institute of Medical Sciences, India

***Correspondence:**
Ulrich Bogdahn
uli.bogdahn@ukr.de

†Senior authorship.

Specialty section:
This article was submitted to Applied Neuroimaging, a section of the journal Frontiers in Neurology

Received: 15 February 2018
Accepted: 09 July 2018
Published: 30 July 2018

Citation:
Wirth AM, Khomenko A, Baldaranov D, Kobor I, Hsam O, Grimm T, Johannesen S, Bruun T-H, Schulte-Mattler W, Greenlee MW and Bogdahn U (2018) Combinatory Biomarker Use of Cortical Thickness, MUNIX, and ALSFRS-R at Baseline and in Longitudinal Courses of Individual Patients With Amyotrophic Lateral Sclerosis. Front. Neurol. 9:614. doi: 10.3389/fneur.2018.00614

Objective: Amyotrophic lateral sclerosis (ALS) is a progressive neurodegenerative process affecting upper and lower motor neurons as well as non-motor systems. In this study, precentral and postcentral cortical thinning detected by structural magnetic resonance imaging (MRI) were combined with clinical (ALS-specific functional rating scale revised, ALSFRS-R) and neurophysiological (motor unit number index, MUNIX) biomarkers in both cross-sectional and longitudinal analyses.

Methods: The unicenter sample included 20 limb-onset classical ALS patients compared to 30 age-related healthy controls. ALS patients were treated with standard Riluzole and additional long-term G-CSF (Filgrastim) on a named patient basis after written informed consent. Combinatory biomarker use included cortical thickness of atlas-based dorsal and ventral subdivisions of the precentral and postcentral cortex, ALSFRS-R, and MUNIX for the musculus abductor digiti minimi (ADM) bilaterally. Individual cross-sectional analysis investigated individual cortical thinning in ALS patients compared to age-related healthy controls in the context of state of disease at initial MRI scan. Beyond correlation analysis of biomarkers at cross-sectional group level ($n = 20$), longitudinal monitoring in a subset of slow progressive ALS patients ($n = 4$) explored within-subject temporal dynamics of repeatedly assessed biomarkers in time courses over at least 18 months.

Results: Cross-sectional analysis demonstrated individually variable states of cortical thinning, which was most pronounced in the ventral section of the precentral cortex. Correlations of ALSFRS-R with cortical thickness and MUNIX were detected. Individual longitudinal biomarker monitoring in four slow progressive ALS patients revealed evident differences in individual disease courses and temporal dynamics of the biomarkers.

Conclusion: A combinatory use of structural MRI, neurophysiological and clinical biomarkers allows for an appropriate and detailed assessment of clinical state and course of disease of ALS.

Keywords: amyotrophic lateral sclerosis, magnetic resonance imaging, cortical thickness, MUNIX, ALSFRS-R

INTRODUCTION

Amyotrophic lateral sclerosis (ALS) is a rapidly progressive neurodegenerative disorder affecting upper and lower motor neurons as well as non-motor systems (1). The degeneration of motor neurons results in muscular fasciculation, progressive weakness, and eventual paralysis (2). Average survival in ALS is 3–5 years, but patients evidently vary in phenotype and disease progression (2, 3). The great clinical heterogeneity in ALS is reflected by different phenotypes with variability regarding the involvement of upper motor neuron (UMN) and lower motor neuron (LMN) signs, site of onset (bulbar, limb), rate of progression, and involvement of neurobehavioral deficits (2, 4). Therefore, clinical and biological biomarkers are helpful in describing disease severity and progression (3).

Magnetic resonance imaging (MRI) has produced potential biomarkers that clarify the role of brain structure and function in the progress of the disease (5, 6). In structural morphometric studies, cortical thickness compared to surface and volume was most sensitive to disease-related changes (7). A variety of studies investigating structural surface-based morphometry showed reduced cortical thickness primarily in the precentral cortex (8–16). Cortical thinning was not restricted to the primary motor cortex. Several studies reported cortical thinning to spread to non-motor cortex areas like the temporal, frontal, parietal, and postcentral cortex (8, 10, 15). However, not all published MRI studies detected alterations in the cortical thickness (17) or cortical volume (18, 19) of the precentral cortex of ALS patients. Essentially, precentral cortical thinning was reported to be focal, and dependent on the clinical phenotype, rate of progression, and age (8, 11, 13). Additionally, several longitudinal MRI studies revealed no further cortical thinning of the precentral cortex in the course of disease (9, 14–17).

In addition to MRI, clinical and electrophysiological biomarkers are among the most currently used and prominent biomarkers (20). The widely used ALS-specific functional rating scale revised (ALSFRS-R) and its subscales are correlated with survival (3). However, correlations between precentral cortical thickness and ALSFRS-R scores were rather weak (10, 21) or not detected in several neuroimaging studies so far (9, 12, 13, 16, 22). While MRI is considered a suitable biomarker for UMN function, neurophysiological motor unit number estimation (MUNE) and motor unit number index (MUNIX) are treated as biomarkers for the estimation of functional lower motor units (23, 24). MUNE is calculated from the division of maximal compound muscle action potential (CMAP) by the mean surface single motor unit action potential (SMUP) (25). In contrast, MUNIX is derived from a mathematical model based on CMAP and electromyographic surface interference patterns (SIP) (26). MUNE and MUNIX scores are inter-correlated in ALS patients (23). As the acquisition of MUNIX is easier and less time consuming than that of MUNE, MUNIX has become a promising biomarker of motor unit loss (27, 28). MUNIX scores were correlated with ALSFRS-R scores (26), but they declined faster than ALSFRS-R scores over time in ALS patients (29). Only few studies investigated the relationship between neurophysiological biomarkers and cortical thickness and failed to find a significant correlation with MUNE or other motor evoked potential indices (21, 30). To our knowledge, no published study investigated correlations between cortical thickness and MUNIX as a biomarker potentially affected by both lower and UMN function (23).

Aim of the study was to investigate individual states of cortical thinning of the precentral and postcentral cortex in a limb-onset ALS sample with respect to young-onset, and slow disease progression. It is the first study to analyze combinatory biomarker use of MRI cortical thickness, neurophysiological MUNIX, and routine ALSFRS-R in both cross-sectional group analysis of the whole sample, and in longitudinal monitoring exploring differences in temporal dynamics between biomarkers in a subgroup of slow progressive ALS patients.

MATERIALS AND METHODS

Participants

Cross-sectional group analysis included 20 limb-onset classical ALS patients (5 females, $M = 48$ years, $SD = 11$) compared to 30 age-related healthy controls (14 females, $M = 45$ years, $SD = 13$). Mean age of ALS patients was lower than that reported in other ALS studies, as the sample included several young-onset patients. Mean ALSFRS-R score across all 20 patients at the time point of first MRI scan was 36 score points ($SD = 8$; range: 23–48). The sample included both slow and fast progressive ALS patients indicated by disease progression rates ($M = 0.51$, $SD = 0.27$; range: 0.00–1.00). The presence of both UMN and LMN signs in all patients allowed no clear differentiation in UMN or LMN predominance of disease. Patients' characteristics are

Abbreviations: ADM, abductor digiti minimi; ALS, amyotrophic lateral sclerosis; ALSFRS-R, ALS-specific functional rating scale revised; CMAP, compound muscle action potential; G-CSF, granulocyte-colony stimulating factor; LMN, lower motor neuron; MNI, Montreal Neurological Institute; MPRAGE, magnetization prepared rapid gradient echo sequence; MRI, magnetic resonance imaging; MUNE, motor unit number estimation; MUNIX, motor unit number index; PoD, postcentral dorsal; PoV, postcentral ventral; PreD, precentral dorsal; PreV, precentral ventral; ROI, region of interest; SIP, surface interference pattern; SMN, sensorimotor network; SMUP, single motor unit potential; UMN, upper motor neuron.

TABLE 1 | Patients' characteristics at baseline.

#	Range of age	ALSFRS-R [0 48]	MUNIX left	MUNIX right	Time span since onset	Onset	Progression rate
1	21–25	30	6.63	10.43	49	Arm	0.37
2	26–30	35	8.20	29.21	28	Arm	0.46
3	31–35	24	6.94	2.83	28	Leg	0.86
4	41–45	24	*	*	28	Leg	0.86
5	41–45	41	54.12	38.00	19	Leg	0.37
6	41–45	28	4.85	0.70	38	Arm	0.53
7	41–45	46	*	*	16	Arm	0.13
8	46–50	39	138.40	41.88	56	Leg	0.16
9	46–50	48	170.10	187.30	19	Leg	0.00
10	46–50	24	48.37	18.51	24	Arm	1.00
11	46–50	46	213.60	193.00	3	Leg	0.67
12	46–50	40	114.50	97.18	21	Leg	0.38
13	46–50	38	*	*	25	Leg	0.40
14	51–55	42	27.25	21.62	7	Arm	0.86
15	51–55	35	*	*	33	Leg	0.39
16	56–60	38	123.90	101.60	29	Leg	0.34
17	56–60	44	126.90	0.00	13	Leg	0.31
18	61–65	42	83.10	119.00	10	Leg	0.60
19	61–65	24	12.34	9.66	33	Leg	0.73
20	66–70	21	6.94	2.83	36	Leg	0.75

*Summary of baseline characteristics of all 20 limb-onset ALS patients including age (in ranges of years), ALSFRS-R sum score upon initial MRI scan (48 in clinical non affected), neurophysiological MUNIX scores for left and right ADM upon initial MRI scan, the length of time span between symptom onset and initial MRI scan in months, onset of disease (arm, leg), and progression rate. In four out of 20 ALS patients (marked with *), neurophysiological assessment was still conducted using MUNE technique (patient 4: left MUNE = 2, right MUNE = 1; patient 7: left MUNE =3, MUNE right = 77; patient 13: left MUNE = 275, right MUNE = 85; patient 15: left MUNE = 240, right MUNE = 120). No MUNIX scores were obtained in these four patients. Progression rates were calculated by [48-ALSFRS-R sum score/months since symptom onset; see (8)]. Neuropsychological assessment using the Edinburgh Cognitive and Behavioral ALS Screen (ECAS) was conducted only in patient 3 (129/136 score points) and patient 9 (100/136 score points).*

summarized in **Table 1**. These included age (in ranges of years), ALSFRS-R sum scores and neurophysiological MUNIX scores for left and right ADM upon initial MRI scan, time interval between symptom onset and initial T1 MRI scan (in months), onset of disease (arm, leg), and progression rates [(48-ALSFRS-R)/months since symptom onset] (8). Genetic background of ALS was exhibited in one patient only (patient 8). All other patients were diagnosed as sporadic ALS.

All patients received standard Riluzole treatment and additional G-CSF (granulocyte-colony stimulating factor, Filgrastim) treatment on a named patient basis. Application modes and doses of G-CSF were individually adapted, treatment duration was up to 7 years. For safety and monitoring of progression, structural MRI and MUNIX were assessed every 3 months. ALSFRS-R scores were acquired monthly, but were integrated in the analysis only at the time points of MRI scanning. MRI cortical thickness was combined with ALSFRS-R sum scores, and MUNIX scores for left and right ADM in both cross-sectional analysis and longitudinal biomarker monitoring.

The unicenter project was carried out in accordance with the Declaration of Helsinki (31) and approved by the ethics committee at the University of Regensburg (ethics approval: 15-101-0106). Written informed consent was obtained prior to participation in all participants.

Data Acquisition

Structural MRI was conducted at a 1.5 Tesla clinical scanner (Aera, Siemens Medical, Erlangen, Germany). For each patient, a high-resolution T1-weighted structural scan was obtained by a magnetization prepared rapid gradient echo sequence (MPRAGE; time-to-repeat TR: 2220 ms, time-to-echo TE: 5.97 ms, flip angle FA: 15°, voxel size: $1 \times 1 \times 1$ mm^3, field of view FOV: 256×256 mm^2, 176 sagittal slices covering the whole brain).

MUNIX estimates the number of motor units in a muscle by a mathematical algorithm involving both the compound muscle action potentials (CMAP) and the continuous electromyographic surface interference pattern (SIP) of the muscles (23, 27). In contrast to original MUNIX, MUNIX recordings of this project implicated continuous SIP recordings during increasing muscle contraction. SIP data were modified by baseline correction, filter settings, rectifications, and SIP intervals. Artifacts were corrected by exclusion of SIP intervals below a specified baseline threshold. As MUNIX was introduced more recently as a neurophysiological biomarker, four out of 20 ALS patients received the assessment of MUNE only (see **Table 1**).

MRI Data Preprocessing

T1-weighted structural images were reconstructed by Freesurfer software version 5.3 (Martinos Center for Biomedical Imaging,

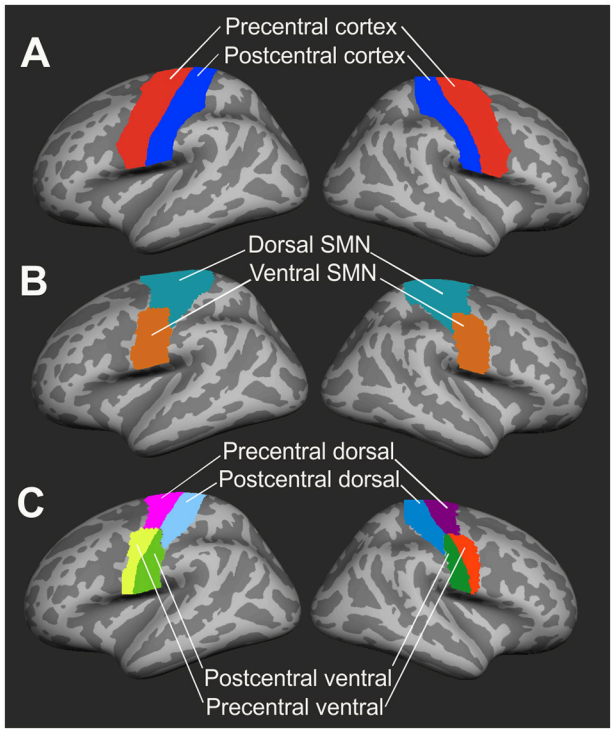

FIGURE 1 | Definition of regions of interest. **(A)** Precentral (red) and postcentral (blue) cortex were identified by the Desikan-Killiany parcellation atlas (34). **(B)** The resting-state-fMRI based atlas of Yeo et al. (35) was used to define dorsal (marine blue) and ventral (brown) segments of the sensorimotor network (SMN). **(C)** Final subdivision of the precentral and postcentral cortex into dorsal and ventral segments resulted in four ROIs (precentral dorsal, precentral ventral, postcentral dorsal, postcentral ventral) in both left and right hemisphere. ROIs were mapped upon the Freesurfer average brain surface.

Charlestown, MA). The reconstruction procedure included automatic segmentation of gray matter and subcortical white matter (32) and tessellation and registration of the cortical surface to a spherical atlas (33). For group analysis, T1-weighted images of the 20 individual patients' brains were registered to the Freesurfer average structural brain by using the Freesurfer linear and non-linear image registration tools (FLIRT, FNIRT).

ROI Definition

Cortical thickness analysis focused on precentral and postcentral regions of interest (ROI) as defined by the Desikan-Killiany parcellation atlas [(34); see **Figure 1A**]. Dorsal and ventral subdivisions of the sensorimotor network were defined by a resting-state-functional MRI (fMRI) data-based atlas (35) in volumetric MNI (Montreal Neurological Institute) space. These ROIs were subsequently registered to the Freesurfer volumetric space and then to the Freesurfer average brain surface (see **Figure 1B**). As all ROIs were mapped upon the Freesurfer average brain space, ROIs were identically sized in each patient and healthy control.

Computation of Cortical Thickness

Cortical thickness was computed according to a workflow recommended by Freesurfer software. Individual surface-based cortical thickness data were mapped upon the Freesurfer average brain surface. By the use of a segmentation statistical tool of Freesurfer software, cortical thickness in each of the four ROIs (PreD: precentral dorsal, PreV: precentral ventral, PoD: postcentral dorsal, PoV: postcentral ventral, see **Figure 1C**) was calculated and extracted as a mean value across vertices.

Cross-Sectional Group Analysis

Group-analysis of mean cortical thickness was conducted using a repeated measures ANOVA with the within-subject factors region (PreD, PreV, PoD, PoV) and hemisphere (left vs. right), and the between-subject factors group (ALS vs. controls), gender (male vs. female), and the covariate age. Differences in cortical thickness between regions were investigated by paired *t*-tests and differences between patients and controls were analyzed using independent-samples *t*-tests. *T*-tests were corrected by Bonferroni correction. Correlation analyses were conducted to investigate relations between cortical thickness, ALSFRS-R sum scores and subscores, and MUNIX by the Bravais-Pearson correlation coefficient. Significance level was set to $p < 0.05$. Multiple comparison errors were controlled by Bonferroni correction procedure in *post-hoc* analyses.

Individual Cortical Thickness Analysis

In addition to cross-sectional group analysis, this project focused on the interindividual variability of cortical thinning. For this purpose, we compared the cortical thickness of all 20 patients to age-related controls, resulting in individual *z*-transformed deviations of cortical thickness from healthy control level. As age effects on cortical thickness are well described (36), ALS patients were compared to one out of two possible age groups. Based on the mean age of ALS patients, the 30 healthy controls were differentiated into two comparably sized subgroups (1: age <48 years, $n = 17$; 2: age ≥48 years, $n = 13$). Furthermore, *z*-transformed deviations of cortical thickness from healthy controls as well as biomarkers MUNIX and ALSFRS-R were monitored in four individual slow progressive ALS patients over a time course of at least 18 months (patient 1, 2, 8, 9, see **Table 1**). All other patients exhibited MRI time courses of a maximum of 9 months only (3 scans: $n = 2$; 2 scans $n = 6$; 1 scan: $n = 8$) due to high disability and lack of T1 MRI data.

RESULTS

Cross-Sectional Group Analysis

As Mauchly's test indicated that the assumption of sphericity was violated [$\chi^2_{(5)} = 22.42$, $p < 0.001$], degrees of freedom were corrected using Greenhouse-Geisser estimates of sphericity ($\varepsilon = 0.79$). Cortical thickness was not significantly different between patients and healthy controls [$F_{(1, 45)} = 1.314$; $p = 0.258$] at cross-sectional group level. Cortical thickness significantly varied across cerebral regions [$F_{(3, 135)} = 23.351$, $p < 0.001$] and with respect to age [$F_{(1, 45)} = 21.776$, $p < 0.001$]. Cortical thickness was significantly higher in precentral than in

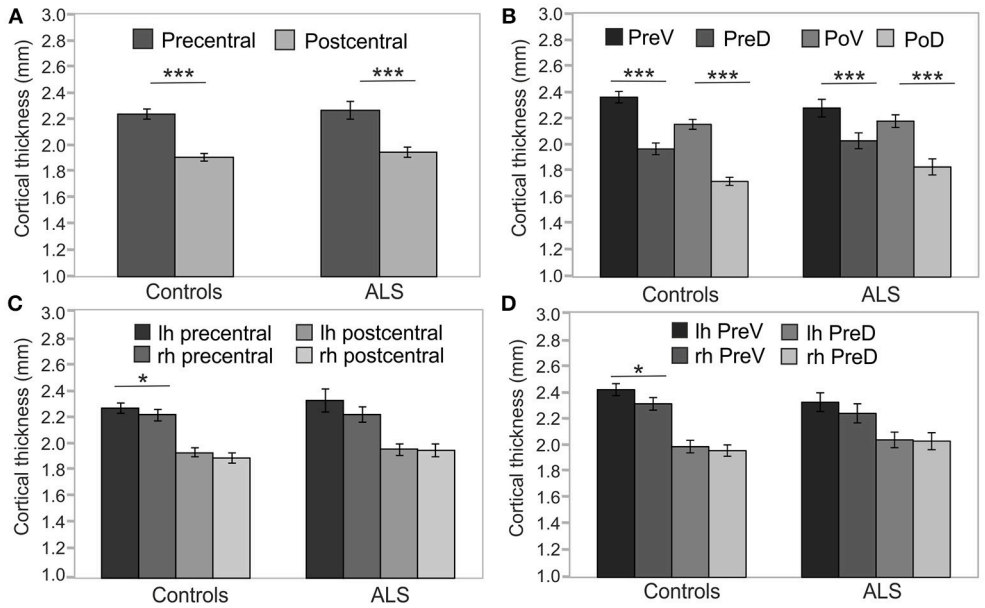

FIGURE 2 | Precentral and postcentral cortical thickness. Cross-sectional analyses of cortical thickness of ALS patients ($n = 20$) and healthy controls ($n = 30$). **(A)** Precentral cortical thickness averaged across left (lh) and right (rh) hemisphere was significantly higher than postcentral cortical thickness in both ALS patients and healthy controls. **(B)** Cortical thickness of ventral segments of both precentral (PreV) and postcentral (PoV) cortex were similarly higher than in dorsal segments (PreD, PoD) in both ALS patients and healthy controls. Hemispheric differences were detected only in the precentral **(C)** and precentral ventral cortex **(D)** of healthy controls. Significance level was set to $p < 0.05$. Bonferroni correction was used for multiple comparisons. Lh, left hemisphere; Rh, right hemisphere; PreV, precentral ventral; PreD, precentral dorsal; PoV, postcentral ventral; PoD, postcentral dorsal. Asterisks refer to the height of p-value: $^{*}p < 0.05$, $^{***}p < 0.001$.

postcentral regions in both ALS patients [$T_{(19)} = 8.584$, $p < 0.05$, corrected], and healthy controls [$T_{(29)} = 16.521$, $p < 0.05$, corrected] (**Figure 2A**). Ventral subdivisions of precentral and postcentral cortex showed greater cortical thickness than dorsal subdivisions in both ALS patients [$T_{(19)} = 9.906$, $p < 0.05$, corrected] and healthy controls [$T_{(29)} = 12.389$; $p < 0.05$, corrected] (**Figure 2B**). The ANOVA revealed no significant main effect of hemisphere, as significant hemispheric differences in cortical thickness were restricted to the precentral [$T_{(29)} = 3.445$, $p < 0.05$, corrected] (**Figure 2C**) and precentral ventral cortex [$T_{(29)} = 3.596$, $p < 0.05$, corrected] of healthy controls (**Figure 2D**). ALSFRS-R sum scores correlated with cortical thickness of the precentral ventral cortex ($r = 0.570$, $p = 0.009$) and the postcentral ventral region ($r = 0.481$, $p = 0.032$). Cortical thickness did not significantly correlate with MUNIX scores for left and right ADM in any ROI. MUNIX scores for the left ($r = 0.767$, $p < 0.05$, corrected) and right ($r = 0.791$, $p < 0.05$, corrected) ADM correlated with ALSFRS-R sum scores. Highest correlations of cortical thickness with ALSFRS-R subscores were found for turning (PreV: $r = 0.501$, $p = 0.024$; PoV: $r = 0.652$, $p = 0.002$), walking (PoV: $r = 0.603$, $p = 0.005$), and cutting (PreV: $r = 0.453$, $p = 0.045$). MUNIX scores predominantly correlated with ALSFRS-R subscores on handwriting (left ADM: $r = 0.637$, $p = 0.008$; right ADM: $r = 0.678$, $p = 0.005$), cutting (left ADM: $r = 0.840$, $p < 0.001$; right ADM: $r = 0.834$, $p < 0.001$), dressing (left ADM: $r = 0.793$, $p < 0.001$, right ADM: $r = 0.806$, $p < 0.001$), turning (left ADM: $r = 0.609$, $p = 0.012$; right ADM: $r = 0.663$, $p = 0.007$), and climbing stairs (left ADM: $r = 0.563$, $p = 0.023$; right ADM: $r = 0.611$, $p = 0.016$). ALS patients were separated *post-hoc* in arm-onset ($n = 7$) and leg-onset ($n = 13$) groups. Arm-onset patients showed significantly lower MUNIX scores for ADM (left: $M = 19$, $SD = 19$; right: $M = 16$, $SD = 11$) than leg-onset patients (left: $M = 95$, $SD = 69$; right: $M = 72$, $SD = 72$) [left ADM: $T_{(14)} = -3.399$, $p < 0.05$, corrected; right ADM: $T_{(14)} = -2.506$; $p = 0.029$]. Arm-onset and leg-onset patients did not significantly differ in disease progression, ALSFRS-R sum scores and subscores.

Variability of Cortical Thinning

Thirty healthy controls were differentiated into two groups of age (1. age <48 years, 2. age ≥48 years, see section Individual Cortical Thickness Analysis). In each of the two subgroups, means of cortical thickness of all precentral and postcentral ROIs (see **Table 2**) were calculated. These mean values were used as reference values for the calculation of z-transformed deviations of ROI-specific cortical thickness of individual ALS patients (for patient numbers see **Table 1**) from healthy control level.

Cortical thickness alterations below at least one deviation from healthy control level were detected in eleven out of twenty patients (patients 1, 2, 3, 4, 6, 10, 14, 16, 18, 19, 20) and marginally indicated in two patients (patients 5, 9). Cortical thinning was primarily observed in the precentral cortex, especially in the ventral segment (**Figure 3A**). Most pronounced cortical thinning in all precentral ROIs was detected in patient 10 and patient 19. Leg-onset patient 19 was characterized by older age (range: 61–65 years), low ALSFRS-R score (24 score points), low MUNIX

TABLE 2 | References values of cortical thickness.

		Lh PreV (mm)	Rh PreV (mm)	Lh PreD (mm)	Rh PreD (mm)	Lh PoV (mm)	Rh PoV (mm)	Lh PoD (mm)	Rh PoD (mm)
1	*M*	2.542	2.442	2.106	2.068	2.276	2.205	1.804	1.798
	SD	0.205	0.139	0.194	0.158	0.165	0.188	0.158	0.163
2	*M*	2.249	2.132	1.827	1.807	2.072	2.016	1.663	1.584
	SD	0.184	0.275	0.242	0.232	0.198	0.244	0.141	0.145

Cortical thickness (mm) of healthy control participants subdivided into two age groups (1: age <48 years, 2: age ≥48 years). Mean age of the two subgroups: Group 1: M = 36, SD = 7, n = 17; Group 2: M = 52, SD = 15, n = 13. Lh, left hemisphere; Rh, right hemisphere; PreV, precentral ventral; PreD, precentral dorsal; PoV, postcentral ventral; PoD, postcentral dorsal.

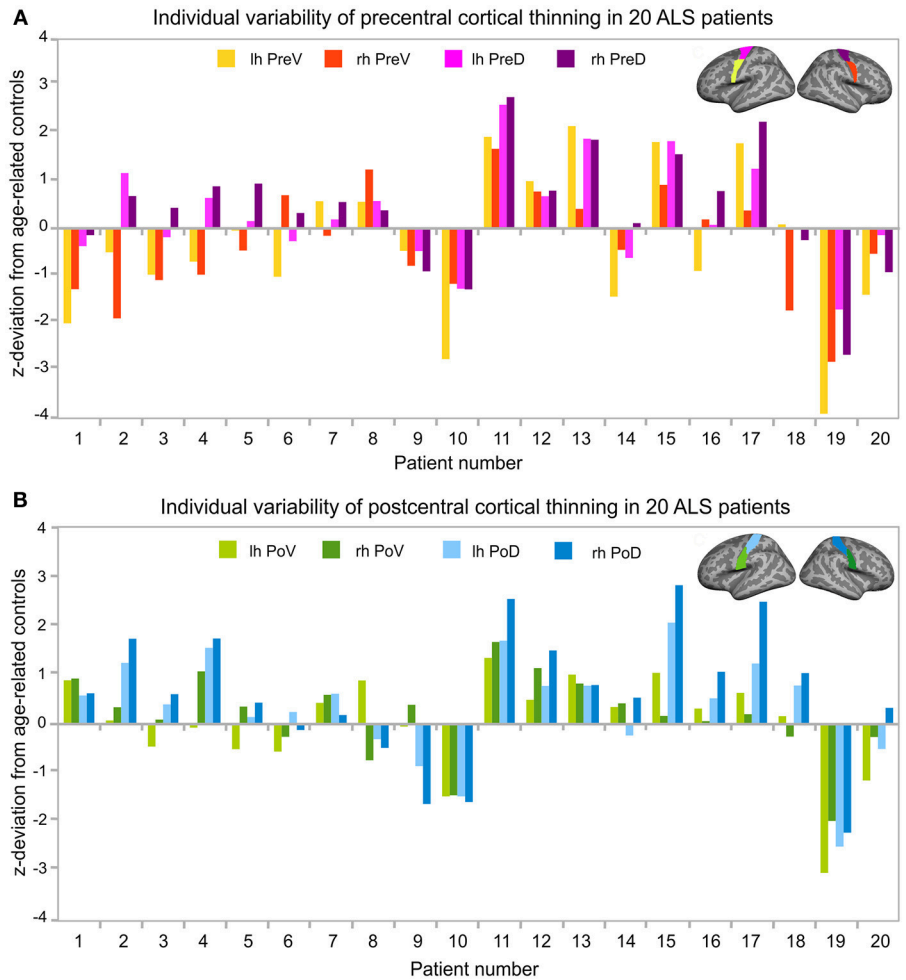

FIGURE 3 | Individual variability of cortical thinning in ALS patients. Z-transformed deviation of cortical thickness from age-related healthy controls (see **Table 2**) in all 20 individual ALS patients. Patient numbers refer to **Table 1**. Patients were sorted by age. *Z*-transformed deviations of cortical thickness were considered relevant at least one deviation from healthy controls. **(A)** Individual variability of cortical thickness of the left (lh, yellow) and right (rh, red) precentral ventral (PreV) and left (lh, pink) and right (rh, purple) precentral dorsal (PreD) ROIs. **(B)** Deviations of individual cortical thickness of the left (lh, light green) and right (rh, dark green) postcentral ventral (PoV) and the left (lh, bright blue) and right (rh, dark blue) postcentral dorsal (PoD) region in the same 20 individual patients. Precentral **(A)** and postcentral **(B)** ROIs were visualized upon the Freesurfer average brain surface. Lh, left hemisphere; Rh, right hemisphere; PreV, precentral ventral; PreD, precentral dorsal; PoV, postcentral ventral; PoD, postcentral dorsal.

scores of ADM, and high disease progression rate (0.73). Patient 10 was much younger (range: 46–50 years), but showed low ALSFRS-R score (24 score points), and the highest progression rate (1.00) of the entire patient sample (see **Table 1**). The two youngest ALS patients (patients 1–2, age ranges: 21–25 and 26–30 years) shared similar patterns of cortical thinning, similar mode

of disease (arm-onset), low ALSFRS-R scores, low MUNIX scores for ADM, and similar disease progression rates (see **Table 1**, see **Figure 3A**). Cortical thinning in the postcentral cortex was detected in four patients (patients 9, 10, 19, 20; **Figure 3B**). Three out of these four patients also exhibited evident precentral cortical thinning. Leg-onset patient 9 stood out of the sample with the highest ALSFRS-R score, high MUNIX scores for ADM, lowest progression rate (0.00), and more pronounced cortical thinning of the postcentral cortex than of the precentral cortex. Increased levels of cortical thickness above healthy control level were more prominent in the postcentral cortex than in the precentral cortex. Seven patients exhibited unremarkable levels of cortical thickness (patients 7, 8, 11, 12, 13, 15, 17). Six (patients 7, 8, 12, 13, 15, 17) out of these seven patients exhibited disease progression rates less or equal to 0.40 (see **Table 1**).

Longitudinal Monitoring of Cortical Thickness, ALSFRS-R, and MUNIX

Repeated long-term follow-up T1 MRI data exceeding 18 months were available in two leg-onset patients (patients 8, 9) and two arm-onset patients (patients 1, 2). The four patients presented different initial levels and longitudinal courses of ALSFRS-R sum scores (**Figure 4A**), MUNIX scores (**Figure 4B**), and cortical thickness alterations (**Figures 4C–F**). Both patients 1 and 2 have in common young-onset (21–30 years), arm-onset diagnosis, low levels of ALSFRS-R scores (patient 1: 30 score points, patient 2: 35 score points) upon first MRI scan, low MUNIX scores for left and right ADM (see **Table 1**), and similar progression rates (patient 1: 0.37, patient 2: 0.46). In both patients, ALSFRS-R sum scores decreased over time (patient 1: blue; patient 2: green; **Figure 4A**). In contrast, MUNIX for left and right ADM stagnated at low level (patient 1: blue; patient 2: green;

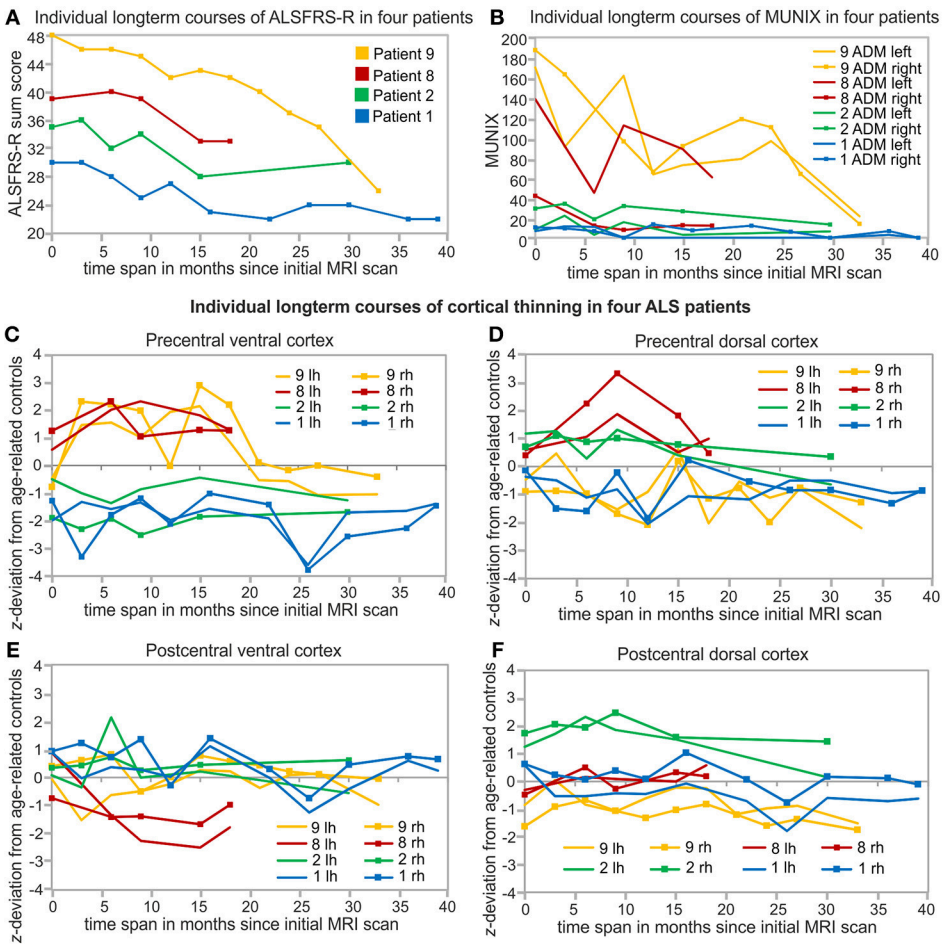

FIGURE 4 | Individual and long-term biomarker monitoring over at least 18 months. Arm-onset and young-onset patients (patient 1, 2) showed higher progression rates (see **Table 1**) than leg-onset similarly aged patients 8 and 9. Patient 9 (yellow), Patient 8 (red), Patient 2 (green), patient 1 (blue) are sorted based on the initial levels of ALSFRS-R sum scores. **(A)** Courses of ALSFRS-R sum scores of the four individual patients starting at different baseline values and developed differently over the measured time span. **(B)** Long-term courses of MUNIX scores for the left and right ADM of the same four patients. Individual long-term monitoring of cortical thickness of these four patients in the precentral ventral (PreV, **C)** and dorsal cortex (PreD, **D)** and postcentral ventral (PoV, **E)** and dorsal (PoD, **F)** cortex of both hemispheres. Individual cortical thickness is *z*-transformed to age-related healthy control level (see **Table 2**). Lh, left hemisphere; Rh, right hemisphere.

Figure 4B). Cortical thickness of the precentral ventral cortex persisted below healthy control level over time in both patients (patient 1: blue, patient 2: green; **Figure 4C**). Cortical thickness of the precentral dorsal cortex decreased below healthy control level in patient 1 in the longitudinal course (**Figure 4D**). No cortical thinning consistently below healthy control level was found for the postcentral ROIs in both patients 1 and 2 (**Figures 4E,F**). Patient 8 and 9 (both aged 46–50 years) were diagnosed with leg-onset disease and obtained high ALSFRS-R sum scores at time point of initial MRI scan (**Table 1**). Progression rates of patient 8 (0.16) and 9 (0.00) were much lower than for patients 1 and 2. In both patients, ALSFRS-R sum scores declined over time (patient 8: red, patient 9: yellow, **Figure 4A**). MUNIX scores of patient 9 similarly decreased for the left and right ADM (yellow, **Figure 4B**). In patient 8, MUNIX scores for the left ADM started at much higher level than for the right ADM and showed a more pronounced decline of scores over time (red, **Figure 4B**). Patient 8 exhibited progressive cortical thinning only in the postcentral ventral cortex (**Figure 4E**). In patient 9, cortical thinning of the right precentral dorsal cortex spread to the left hemisphere over the time course (yellow, **Figure 4D**). Cortical thickness of the postcentral dorsal cortex further decreased over time (yellow, **Figure 4F**). Despite fluctuations, ventral sections of precentral and postcentral cortex of patient 9 persisted at healthy control level (yellow, **Figures 4C,E**).

DISCUSSION

Cortical thinning was heterogenous and most pronounced in the precentral ventral cortex. ALSFRS-R sum score was associated with both cortical thickness and MUNIX scores. Individual longitudinal monitoring of clinical ALSFRS-R, neurophysiological MUNIX, and MRI cortical thickness indicated both interindividual differences among ALS patients as well as differences in temporal dynamics between biomarkers over the course of disease.

Cortical Thickness of the Precentral and Postcentral Cortex

Cortical thickness was highly age-dependent and significantly different between precentral and postcentral cortex as well as between ventral and dorsal subdivisions of precentral and postcentral cortex. Postmortem (37) and MRI (38, 39) studies showed approximately 1.5 times greater cortical thickness of the precentral compared to the postcentral cortex. The only study addressing gradients of postcentral cortical thickness in humans (40) reported greatest cortical thickness in the area defined as ventral segment in our study. Age effects on precentral and postcentral cortical thickness have been well described (36).

Variability of Cortical Thinning

Individual cross-sectional analysis revealed heterogenous individual states of cortical thinning, which was more pronounced in the precentral than in the postcentral cortex. Postcentral cortical thinning was only present in four patients. Three out of these four patients also showed pronounced cortical thinning of the precentral cortex. These observations are consistent with studies reporting postcentral atrophy was rather less prominent or not detectable (12, 41). Instead, postcentral atrophy was discussed to result from the spread of cortical degeneration in the course of disease (41, 42). With respect to the spread of disease, interestingly, individual longitudinal analysis revealed that patient 8 developed postcentral cortical thinning despite lack of precentral cortical thinning. Cortical thinning was most pronounced in the ventral segment of the precentral cortex. The precentral ventral cortex as defined here was also reported to exhibit alterations in ALS patients in other studies (14, 43, 44). Seven out of twenty patients exhibited no indications of cortical thinning. This finding is supported by a meta-analysis reporting cortical atrophy only in a percentage of ALS cases (45) and other MRI studies failing to find alterations in the precentral cortex of ALS patients (17–19). The lack of cortical thinning in ALS patients may be explained by low progression rates and young-onset. Cortical thinning was primarily observed in ALS patients with faster progression or advanced stage of disease (46). Six out of seven patients exhibiting no indications of cortical thinning were characterized with disease progression rates less or equal to 0.40. Moreover, the ALS sample of the current study was much younger than ALS patients involved in most MRI studies (8, 13, 17, 43, 47, 48). Individual cross-sectional analysis also revealed enhanced levels of cortical thickness predominantly in the postcentral cortex. Future studies may investigate if enhanced levels of cortical thickness may be associated with processes of neuroplasticity or treatment effects. Finally, heterogeneous alterations in cortical thickness (including increases and decreases) argue for the need of individual perspective on ALS patients beyond group averages (6).

Longitudinal Monitoring of Cortical Thickness, ALSFRS-R, and MUNIX

Longitudinal monitoring of cortical thickness in four patients revealed differences in temporal dynamics of clinical ALSFRS-R, neurophysiological MUNIX, and MRI cortical thickness in the same individual patients. The long-term biomarker monitoring was limited to the patients who survived for longer periods of time and who underwent more than three MRI scans. All other patients of the sample received three MRI scans or less due to short survival or lack of scan capability. Similar to Abhinav et al. (49), patients showed very different baseline levels and various progression types of ALSFRS-R sum scores over time. While the decline of high-level ALSFRS-R sum scores of patient 9 (ALSFRS-R baseline: 48) was evidently observable, changes in ALSFRS-R sum scores of progressed stage patient 1 (ALSFRS-R baseline: 30) were less evident. These observations are consistent with ALSFRS-R being considered to be less sensitive for short-term time windows and slow disease progression (3, 24, 50). ALSFRS-R is also regarded as a rather general severity summary scale without sensitivity for mode of disease (17, 29). The unspecific character of ALSFRS-R may also explain why correlations between ALSFRS-R and cortical thickness were weak or not detectable (9, 15, 21). In contrast to ALSFRS-R, MUNIX significantly differentiated

between arm and leg-onset of disease. Corresponding to Grimaldi et al. (26), MUNIX scores significantly correlated with ALSFRS-R scores, but showed much faster longitudinal dynamics than ALSFRS-R scores as reported by Neuwirth et al. (29). Once at very low level MUNIX scores stagnated across time in arm-onset patients 1 and 2. The phenomenon of a floor effect of MUNIX measurements at low level in completely wasted muscles was described by Neuwirth et al. (51). In contrast, higher level MUNIX scores for ADM in leg-onset patients 8 and 9 showed a fast decrease over time. Consistent with these observations, clinical markers are considered to be more sensitive to changes than MRI markers (17). Although MUNIX is considered a candidate biomarker like MUNE for LMN function (24), MUNIX scores may be influenced by both lower and UMN function (23). Existing studies investigating correlations of cortical thickness to MUNE or other neurophysiological techniques failed to find significant correlations (21, 30). As the first study combining MRI cortical thickness with MUNIX, we also found no significant correlations. Differences in both individual state of disease and within-subject temporal dynamics of various biomarkers may explain the difficulty to find significant correlations in multimodal biomarker use.

Methodological Limitations

Some methodological limitations need to be considered. First, the sample size was limited to 20 patients. As ALS MRI studies suffer from high costs and high drop-out rates due to increasing disability of patients (50), many published unicenter ALS MRI studies included samples smaller than 20 ALS patients (12, 41, 52, 53). Second, the MRI magnetic field strength was 1.5T. Although MRI magnetic field strength of 3T may have been beneficial, 1.5T still was sufficient for the detection of gray matter alterations in ALS MRI studies (11, 12, 22, 41, 54). Third, by the use of a more conservative ROI based approach than a vertex-based approach, the study may have failed to detect very focal cortical thinning inside of the ROIs. However, this approach did not only reduce the influence of false positive results but still successfully detected cortical thinning. Fourth, MUNIX scores were not assessed in leg muscles. However, this study is the first cross-sectional and longitudinal study combining cortical thickness analysis with both ALSFRS-R and MUNIX with respect to the individual patient. Fifth, longitudinal monitoring of biomarkers was limited to four patients of the sample due to high disability ($n = 6$), death ($n = 4$), lack of T1 data ($n = 6$). Still, our long-term biomarker monitoring analysis is unique, as to our knowledge, none of the published longitudinal MRI studies showed longitudinal courses of both MRI cortical thickness and MUNIX biomarkers using as many repeated measures in a time course longer than 18 months as presented in the current study. Moreover, most MRI studies focused on group analysis irrespective of the individual patient (9, 10, 14–17), although the individual perspective has been increasingly demanded in ALS neuroimaging research (6, 24, 55, 56).

CONCLUSIONS

The present study demonstrated that MRI is a potential biomarker for the differentiation of individual states of cortical thinning in an ALS sample including young-onset and slow progressive patients. Longitudinal monitoring of MRI, clinical, and neurophysiological biomarkers in the same patient reveal substantial differences in temporal dynamics. Combinatory biomarker use contributes a substantial gain of information about individual state of disease beyond group averages. Future studies may expand the idea of combining neuroimaging techniques with other clinical or molecular biomarkers to deepen our understanding of multisystem/multifactorial ALS disease progression.

AUTHOR CONTRIBUTIONS

AW: substantial contribution to the conception and the design of the study, acquisition, analysis, interpretation of the MRI data, and composition of the manuscript. AK and DB: substantial contribution to the conception of the study, data acquisition, interpretation of the data, and revision of the manuscript. IK, TG, SJ, WS-M, T-HB, and UB: substantial contribution to the conception of the study, acquisition, analysis, and interpretation of clinical and neurophysiological data, and revision of the manuscript. SJ, OH, AK, DB, WS-M, and UB: care for ALS patients in outpatient clinic, treatment concept. MG: substantial contribution to the conception of the study, supervision of MRI data analysis and data interpretation, and revision of the manuscript.

FUNDING

This work was supported by the German Federal Ministry of Education and Research (BMBF, Project GO-Bio, 031A386).

REFERENCES

1. Riva N, Agosta F, Lunetta C, Filippi M, Quattrini A. Recent advances in amyotrophic lateral sclerosis. *J Neurol*. (2016) 263:1241–54. doi: 10.1007/s00415-016-8091-6
2. Calvo AC, Manzano R, Mendonca DMF, Munoz MJ, Zaragoza P, Osta R. Amyotrophic lateral sclerosis: a focus on disease progresssion. *Biomed Res Int*. (2014) 2014:925101. doi: 10.1155/2014/925101
3. Rosenfeld J, Strong MJ. Challenges in the understanding and treatment of Amyotrophic Lateral Sclerosis/Motor Neuron disease. *Neurotherapeutics* (2015) 12:317–25. doi: 10.1007/s13311-014-0332-8
4. Chio A, Calvo A, Moglia C, Mazzini L, Mora G, PARALS study group, et al. Phenotypic heterogeneity of amyotrophic lateral sclerosis: a population based study. *J Neurol Neurosurg Psychiatry* (2011) 82:740–6. doi: 10.1136/jnnp.2010.235952
5. Agosta F, Chio A, Cosottini M, De Stefano N, Falini A, Mascalchi M, et al. The present and the future of neuroimaging in amyotrophic lateral sclerosis. *Am J Neuroradiol*. (2010) 31:1769–77. doi: 10.3174/ajnr.A2043

6. Simon NG, Turner MR, Vucic S, Al-Chalabi A, Shefner J, Lomen-Hoerth C, et al. Quantifying disease progression in amyotrophic lateral sclerosis. *Ann Neurol*. (2014) 76:643–57. doi: 10.1002/ana.24273
7. Turner MR, Verstraete E. What does imaging reveal about the pathology of amyotrophic lateral sclerosis. *Curr Neurol Neurosci Rep*. (2015) 15:45. doi: 10.1007/s11910-015-0569-6
8. Agosta F, Valsasina P, Riva N, Copetti M, Messina MJ, Prelle A, et al. The cortical signature of amyotrophic lateral sclerosis. *PLoS ONE* (2012) 7:e42816. doi: 10.1371/journal.pone.0042816
9. De Albuquerque M, Branco LMT, Rezende TJR, de Andrade HMT, Nucci A, Franca, M. C. F. Jr. Longitudinal evaluation of cerebral and spinal cord damage in Amyotrophic Lateral Sclerosis. *Neuroimage Clin*. (2017) 14:269–76. doi: 10.1016/j.nicl.2017.01.024
10. Kwan JY, Meoded A, Danielian LE, Wu T, Floeter MK. Structural imaging differences in longitudinal changes in primary lateral sclerosis and amyotrophic lateral sclerosis. *NeuroImage Clin*. (2013) 2:151–60. doi: 10.1016/j.nicl.2012.12.003
11. Mezzapesa DM, D'Errico E, Tortelli R, Distaso E, Cortese R, Tursi M, et al. (2013). Cortical Thinning and clinical heterogeneity in Amyotrophic Lateral Sclerosis. *PLoS ONE* 8:e80748. doi: 10.1371/journal.pone.0080748
12. Roccatagliata L, Bonzano L, Mancardi G, Canepa C, Caponnetto C. Detection of motor cortex thinning and corticospinal tract involvement by quantitative MRI in amyotrophic lateral sclerosis. *Amyotroph Lateral Scler*. (2009) 10:47–52. doi: 10.1080/17482960802267530
13. Schuster C, Kasper E, Matchts J, Bittner D, Kaufmann J, Benecke R, et al. Focal thinning of the motor cortex mirrors clinical features of amyotrophic lateral sclerosis and their phenotypes: a neuroimaging study. *J Neurol*. (2013) 260:2856–64. doi: 10.1007/s00415-013-7083-z
14. Schuster C, Kasper E, Machts J, Bittner D, Kaufmann J, Benecke R, et al. Longitudinal course of cortical thickness decline in amyotrophic lateral sclerosis. *J Neurol*. (2014) 261:1871–80. doi: 10.1007/s00415-014-7426-4
15. Verstraete E, Veldink JH, Hendrikse J, Schelhaas HJ, van den Heuvel MP, van den Berg LH. Structural MRI reveals cortical thinning in amyotrophic lateral sclerosis. *J Neurol Neurosurg Psychiatry* (2012) 83:383–8. doi: 10.1136/jnnp-2011-300909
16. Walhout R, Westeneng HJ, Verstraete E, Hendrikse J, Veldink JH, van den Heuvel MP, et al. Cortical thickness in ALS: towards a marker for upper motor neuron involvement. *J Neurol Neurosurg Psychiatry* (2015) 86:288–94. doi: 10.1136/jnnp-2013-306839
17. Cardenas-Blanco A, Machts J, Acosta-Cabronero J, Kaufman J, Abdulla S, Kollewe K, et al. Structural and diffusion imaging versus clinical assessment to monitor amyotrophic lateral sclerosis. *Neuroimage Clin*. (2016) 11:408–14. doi: 10.1016/j.nicl.2016.03.011
18. Ellis CM, Suckling J, Amaro, E. Jr., Bullmore ET, Simmons A, Williams SC, et al. Volumetric analysis reveals corticospinal tract degeneration and extramotor involvement in ALS. *Neurology* (2001) 57:1571–8. doi: 10.1212/WNL.57.9.1571
19. Mezzapesa DM, Ceccarelli A, Dicuonzo F, Carella A, De Caro MF, Lopez M, et al. Whole-brain and regional brain atrophy in amyotrophic laterals sclerosis. *Am. J. Neuroradiol*. (2007) 28:255–259.
20. Benatar M, Boylan K, Jeromin A, Rutkove SB, Berry J, Atassi N, et al. ALS Biomarkers for therapy development: State of the field and future directions. *Muscle Nerve* (2016) 53:169–82. doi: 10.1002/mus.24979
21. Cosottini M, Donatelli G, Costagli M, Caldarazzo Ienco E, Frosini D, Pesaresi I, et al. High-resolution 7T MR imaging of the motor cortex in amyotrophic lateral sclerosis. *Am J Neuroradiol*. (2016) 37:455–61. doi: 10.3174/ajnr.A4562
22. Thorns J, Jansma H, Peschel T, Grosskreutz J, Mohammadi B, Dengler R, et al. Extent of cortical involvement in amyotrophic lateral sclerosis – an analysis based on cortical thickness. *BMC Neurol*. (2013) 13:148. doi: 10.1186/1471-2377-13-148
23. Stein F, Kobor I, Bogdahn U, Schulte-Mattler W. Toward the validation of a new method (MUNIX) for motor unit number assessment. *J Electromyogr Kinesiol*. (2016) 27:73–7. doi: 10.1016/j.jelekin.2016.02.001
24. Van Es MS, Hardiman O, Chio A, Al-Calabi A, Pasterkamp RJ, Veldink JH, et al. Amyotrophic lateral sclerosis. *Lancet* (2017) 390:2084–98. doi: 10.1016/S0140-6736(17)31287-4
25. Gooch CL, Doherty TJ, Chan KM, Bromberg MB, Lewis RA, Stashuk DW, et al. Motor unit number estimation: a technology and literature review. *Muscle Nerve* (2014) 50:884–93. doi: 10.1002/mus.24442
26. Grimaldi S, Duprat L, Grapperon AM, Verschueren A, Delmont E, Attarian S. Global motor unit number index sum score for assessing the loss of lower motor neurons in amyotrophic lateral sclerosis. *Muscle Nerve* (2017) 56:202–6. doi: 10.1002/mus.25595
27. Grimm T, Schulte-Mattler W. Update – Neurophysiologische Methoden zur Bestimmung motorischer Einheiten in menschlichen Muskeln. *Klinische Neurophysiol*. (2017) 48:14–150. doi: 10.1055/s-0043-115149
28. Escorcio-Bezerra ML, Abrahao A, de Castro I, Chieia MAT, de Avezado LA, Pinheiro DS, et al. MUNIX: Reproducibility and clinical correlations in Amyotrophic Lateral Sclerosis. *Clin Neurophysiol*. (2016) 127:2979–84. doi: 10.1016/j.clinph.2016.06.011
29. Neuwirth C, Barkhaus PE, Burkhardt C, Castro J, Czell D, de Carvalho M, et al. Motor Unit Number Index (MUNIX) detects motor neuron loss in pre-symptomatic muscles in Amyotrophic Lateral Sclerosis. *Clin Neurophysiol*. (2017) 128:495–500. doi: 10.1016/j.clinph.2016.11.026
30. Mitsumoto H, Ulug AM, Pullman SL, Gooch CL, Chan S, Tang MX, et al. Quantitative objective markers for upper and lower motor neuron dysfunction in ALS. *Neurology* (2007) 68:1402–10. doi: 10.1212/01.wnl.0000260065.57832.87
31. World Medical Association. World medical association declaration of Helsinki: Ethical principles for medical research involving human subjects. *JAMA* (2013) 310:2191–4. doi: 10.1001/jama.2013.281053
32. Fischl B, Salat DH, Busa E, Albert M, Dieterich M, Haselgrove C, et al. Whole brain segmentation: automated labeling of neuroanatomical structures in the human brain. *Neuron* (2002) 33:341–355. doi: 10.1016/S0896-6273(02)00569-X
33. Fischl B, Sereno MI, Dale AM. Cortical surface-based analysis. II: inflation, flattening, and a surface-based coordinate system. *Neuroimage* (1999) 9:195–207. doi: 10.1006/nimg.1998.0396
34. Desikan RS, Ségonne F, Fischl B, Quinn BT, Dickerson BC, Blacker D, et al. An automated labeling system for subdividing the human cerebral cortex on MRI scans into gyral based regions of interest. *Neuroimage* (2006) 31:968–80. doi: 10.1016/j.neuroimage.2006.01.021
35. Yeo BTY, Krienen FM, Sepulcre J, Sabuncu MR, Lashkari D, Hollinshead M, et al. The organization of the human cerebral cortex estimated by intrinsic functional connectivity. *J Neurophysiol*. (2011) 106:1125–65. doi: 10.1152/jn.00338.2011
36. Salat DH, Buckner RL, Snyder AZ,Greve DN, Desikan RSR, Busa E, et al. Thinning of the cerebral cortex in aging. *Cereb Cortex* (2004) 14:721–30. doi: 10.1093/cercor/bhh032
37. Meyer JR, Roychowdhury S, Russell EJ, Callahan C, Gitelman D, Mesulam MM. Location of the central sulcus via cortical thickness of the precentral and postcentral gyri on MRI. *Am J Neuroradiol*. (1996) 17:1699–706.
38. Fischl B, Dale AM. Measuring the thickness of the human cerebral cortex from magnetic resonance images. *Proc Natl Acad Sci USA*. (2000) 97:11050–5. doi: 10.1073/pnas.200033797
39. Sahin N, Mohan S, Maralani PJ, Duddukuri S, O'Rourke DM, Melhem ER, et al. Assignment confidence in localization of the hand motor cortex: comparison of structural imaging with functional MRI. *Am J Roentgenl*. (2016) 207:1263–1270. doi: 10.2214/AJR.15.15119
40. Wagstyl K, Ronan L, Goodyer IM, Fletcher PC. Cortical thickness gradients in structural hierarchies. *Neuroimage* (2015) 111:241–50. doi: 10.1016/j.neuroimage.2015.02.036
41. Grosskreutz J, Kaufmann J, Fradrich J, Dengler R, Heinze HJ, Peschel T. Widespread sensorimotor and frontal cortical atrophy in Amyotrophic Lateral Sclerosis. *BMC Neurol*. (2006) 6:17. doi: 10.1186/1471-2377-6-17
42. Brettschneider J, Del Tredici K, Toledo JB, Robinson JL, Irwin DJ, Grossman M, et al. Stages of pTDP-3 pathology in amyotrophic lateral sclerosis. *Ann Neurol*. (2013) 74:20–38. doi: 10.1002/ana.23937
43. Lillo P, Mioshi E, Burrell JR, Kiernan MC, Hodges JR, Hornberger M. (2012). Grey and white matter changes across the amyotrophic lateral sclerosis-frontotemporal dementia continuum. *PLoS ONE* 7:e43993. doi: 10.1371/journal.pone.0043993.

44. Schuster C, Hardiman O, Bede P. Survival prediction in Amyotrophic lateral sclerosis based on MRI measures and clinical characteristics. *BMC Neurol.* (2017) 17:73. doi: 10.1186/s12883-017-0854-x
45. Chen Z, Ma L. Grey matter volume changes over the whole brain in amyotrophic lateral sclerosis: a voxel-wise meta-analysis of voxel based morphometry studies. *Amyotroph Lateral Scler*. (2010) 11:549–54. doi: 10.3109/17482968.2010.516265
46. Meadowcroft MD, Mutic NJ, Bigler DC, Wang JL, Simmons Z, Connor JR, et al. Histological-MRI correlation in the primary motor cortex of patients with amyotrophic lateral sclerosis. *J Magn Reson Imaging* (2015) 41:665–75. doi: 10.1002/jmri.24582
47. Agosta F, Ferraro PM, Riva N, Spinelli EG, Cio A, Canu E, et al. Structural brain correlates of cognitive and behavioral impairment in MND. *Hum Brain Mapping* (2016) 37:1614–26. doi: 10.1002/hbm.23124
48. Spinelli EG, Agosta F, Ferraro PM, Riva N, Lunetta C, Falzone YM, et al. Brain MR imaging in patients with lower motor neuron-predominant disease. *Radiology* (2016) 280:545–56. doi: 10.1148/radiol.2016151846
49. Abhinav K, Yeh FC, El-Doklar A, Ferrando LM, Chang YF, Lacomis D, et al. Use of diffusion spectrum imaging in preliminary longitudinal evaluation of amyotrophic lateral sclerosis: development of an imaging biomarker. *Front Neurosci.* (2014) 8:270. doi: 10.3389/fnhum.2014.00270
50. Rutkove SB. Clinical measures of disease progression in amyotrophic lateral sclerosis. *Neurotherapeutics* (2015) 12:338–93. doi: 10.1007/s13311-014-0331-9
51. Neuwirth C, Barkhaus PE, Burkhardt C, Castro J, Czell D, de Carvalo M, et al. Tracking motor neuron loss in a set of six muscles in amyotrophic lateral sclerosis using the Motor Unit Number Index (MUNIX): a 15-month longitudinal multicentre trial. *J Neurol Neurosurg Psychiatry* (2015) 86:1172–9. doi: 10.1136/jnnp-2015-310509
52. Cosottini M, Cecchi P, Piazza S, Pesaresi I, Fabbri S, Diciotti S, et al. Mapping cortical degeneration in ALS with magnetization transfer ratio and voxel-based morphometry. *PLoS ONE* (2013) 8:e68279. doi: 10.1371/journal.pone.0068279
53. Verstraete E, van den Heuvel MP, Veldink JH, Blanken N, Mandl RC, Hulshoff Pol HE, et al. (2010). Motor network degeneration in amyotrophic lateral sclerosis: a structural and functional connectivity study. *PLoS ONE* 5:e13664. doi: 10.1371/journal.pone.0013664
54. Tavazzi E, Lagana MM, Bergsland N, Tortorella P, Pinardi G, Luneta C, et al. Grey matter damage in progressive multiple sclerosis versus amyotrophic lateral sclerosis: a voxel-based morphometry MRI study. *Neurol Sci.* (2015) 36:371–7. doi: 10.1007/s10072-014-1954-7
55. Turner MR, Bowser R, Brujn L, Dupuis L, Ludolph A, McGrath M, et al. Mechanisms, models and biomarkers in amyotrophic lateral sclerosis.Amyotroph. *Lateral Scler Frontotemporal Degener*. (2013) 14:19–32. doi: 10.3109/21678421.2013.778554
56. Verstraete E, Foerster BR. Neuroimaging as a new diagnostic modality in amyotrophic lateral sclerosis. *Neurotherapeutics* (2015) 12:403–16. doi: 10.1007/s13311-015-0347-9

Conflict of Interest Statement: The authors declare that the research was conducted in the absence of any commercial or financial relationships that could be construed as a potential conflict of interest.

frontiers in Neurology

ORIGINAL RESEARCH
published: 14 August 2018
doi: 10.3389/fneur.2018.00642

Basal Forebrain Volume, but Not Hippocampal Volume, Is a Predictor of Global Cognitive Decline in Patients With Alzheimer's Disease Treated With Cholinesterase Inhibitors

Stefan J. Teipel[1,2], Enrica Cavedo[3,4,5,6,7], Harald Hampel[3,4,5,6] and Michel J. Grothe[1] for the Alzheimer's Disease Neuroimaging Initiative† and Alzheimer Precision Medicine Initiative (APMI)*

[1] German Center for Neurodegenerative Diseases-Rostock/Greifswald, Rostock, Germany, [2] Department of Psychosomatic Medicine, University of Rostock, Rostock, Germany, [3] AXA Research Fund and Sorbonne University Chair, Paris, France, [4] Sorbonne University, GRC n° 21, Alzheimer Precision Medicine, AP-HP, Pitié-Salpêtrière Hospital, Boulevard de l'Hôpital, Paris, France, [5] Brain and Spine Institute (ICM), INSERM U 1127, CNRS UMR 7225, Boulevard de l'Hôpital, Paris, France, [6] Department of Neurology, Institute of Memory and Alzheimer's Disease (IM2A), Pitié-Salpêtrière Hospital, AP-HP, Boulevard de l'Hôpital, Paris, France, [7] IRCCS Istituto Centro San Giovanni di Dio-Fatebenefratelli, Brescia, Italy

Background: Predicting the progression of cognitive decline in Alzheimer's disease (AD) is important for treatment selection and patient counseling. Structural MRI markers such as hippocampus or basal forebrain volumes might represent useful instruments for the prediction of cognitive decline. The primary objective was to determine the predictive value of hippocampus and basal forebrain volumes for global and domain specific cognitive decline in AD dementia during cholinergic treatment.

Methods: We used MRI and cognitive data from 124 patients with the clinical diagnosis of AD dementia, derived from the ADNI-1 cohort, who were on standard of care cholinesterase inhibitor treatment during a follow-up period between 0.4 and 3.1 years. We used linear mixed effects models with cognitive function as outcome to assess the main effects as well as two-way interactions between baseline volumes and time controlling for age, sex, and total intracranial volume. This model accounts for individual variation in follow-up times.

Results: Basal forebrain volume, but not hippocampus volume, was a significant predictor of rates of global cognitive decline. Larger volumes were associated with smaller rates of cognitive decline. Left hippocampus volume had a modest association with rates of episodic memory decline. Baseline performance in global cognition and memory was significantly associated with hippocampus and basal forebrain volumes; in addition, basal forebrain volume was associated with baseline performance in executive function.

Conclusions: Our findings indicate that in AD dementia patients, basal forebrain volume may be a useful marker to predict subsequent cognitive decline during cholinergic treatment.

Keywords: cholinergic treatment, MRI, prediction, memory, executive function, basal forebrain, hippocampus

OPEN ACCESS

Edited by:
Lars Ersland, Haukeland University Hospital, Norway

Reviewed by:
Elizabeth J. Coulson, The University of Queensland, Australia
Karsten Specht, University of Bergen, Norway

****Correspondence:***
Stefan J. Teipel
stefan.teipel@med.uni-rostock.de

† Data used in preparation of this article were obtained from the Alzheimer's Disease Neuroimaging Initiative (ADNI) database (adni.loni.usc.edu/). As such, the investigators within the ADNI contributed to the design and implementation of ADNI and/or provided data but did not participate in analysis or writing of this report. A complete listing of ADNI investigators can be found at: http://adni.loni.usc.edu/wp-content/uploads/how_to_apply/ADNI_Acknowledgement_List.pdf

Specialty section:
This article was submitted to Applied Neuroimaging, a section of the journal Frontiers in Neurology

Received: *10 November 2017*
Accepted: *17 July 2018*
Published: *14 August 2018*

Citation:
Teipel SJ, Cavedo E, Hampel H and Grothe MJ (2018) Basal Forebrain Volume, but Not Hippocampal Volume, Is a Predictor of Global Cognitive Decline in Patients With Alzheimer's Disease Treated With Cholinesterase Inhibitors. Front. Neurol. 9:642. doi: 10.3389/fneur.2018.00642

INTRODUCTION

A prediction of the individual course of cognitive change in Alzheimer's disease (AD) would help adequate resource allocation, patient care, and counseling. Evidence suggests that the hippocampus supports the consolidation of long-term declarative memory (1, 2), showing neurodegeneration in autopsy data and atrophy in *in vivo* MRI scans as early as in predementia stages of AD (3, 4). Its measurement is standardized, robust, accessible and feasible for *in vivo* studies using established volumetric protocols, with the most recent advance being an internationally harmonized protocol for a consistent delineation of the hippocampus' anatomical borders on MRI scans (5). The cholinergic basal forebrain is the main source of neocortical acetylcholine (6), and is involved in attentional processes, such as immediate recall and executive function (7). Autopsy studies found degeneration of cholinergic basal forebrain neurons in early clinical stages of AD (8, 9), and the resulting reduction of cholinergic cortical activity represents the rationale for the use of cholinergic treatment in AD dementia. The hippocampus represents a key input area of cholinergic projections from the basal forebrain (10). In recent years, MRI based protocols for an automated measurement of cholinergic basal forebrain volumes have been established that make use of stereotactic information derived from combined post mortem MRI and histology (11–13). Based on these protocols, several MRI volumetric studies have shown consistent pattern of hippocampus and cholinergic basal forebrain atrophy in AD dementia (11, 14) and prodromal at-risk stages of AD dementia, such as amnestic mild cognitive impairment (MCI) (15, 16) or individuals with amyloid positive MCI (17).

Based on these findings, hippocampus and cholinergic basal forebrain volumes may help to predict cognitive change and response to cholinergic treatment in patients with AD dementia or prodromal AD. A previous study found that the thickness of the substantia innominata, a potential proxy of cholinergic basal forebrain integrity (18), was associated with rates of cognitive change in 82 AD dementia patients during 9 months of treatment with a cholinesterase inhibitor, with smaller rates of cognitive decline in people with a lower thickness of the substantia innominata (19). In people with MCI, hippocampus volume was associated with rates of cognitive decline with a moderate effect size (20–24). In 37 AD dementia cases, smaller hippocampus volume was associated with faster global cognitive decline during cholinergic treatment (25). In a recent randomized controlled trial of donepezil, we found that hippocampus volume, but not basal forebrain volume, was a predictor of subsequent cognitive decline in 216 MCI cases (26); this effect, however, was independent of treatment. In summary, in MCI cases hippocampus volume, but not basal forebrain volume, was found to be a significant predictor of cognitive decline, irrespective of treatment. In studies on AD dementia cases, hippocampus volume and a proxy for basal forebrain volume were found significant predictors of cognitive decline during cholinergic treatment.

Here, we used longitudinal cognitive data of 124 AD dementia cases retrieved from the Alzheimer's Disease Neuroimaging Initiative (ADNI-1) database, all receiving cholinergic treatment. Based on the previous evidence on the potential predictive value of these brain regions in AD, we determined the association of hippocampus and basal forebrain volume with rates of global and domain-specific cognitive decline during cholinergic treatment. We expected that lower basal forebrain (hippocampus) volume would predict a faster rate of global and executive (global and episodic memory) function. Secondly, we determined the predictive use of basal forebrain and hippocampus volumes for the identification of cognitively stable vs. cognitively declining patients, where we expected that cognitively stable patients would have larger basal forebrain and hippocampus volumes at baseline. These data help to assess the potential usefulness of volumetric MRI to identify people with a more rapid disease progression; such data would support clinical decision making on allocation of treatment resources and care.

METHODS

Study Population

Data used in the preparation of this article were obtained from the Alzheimer's Disease Neuroimaging Initiative (ADNI) database (adni.loni.usc.edu). The ADNI was launched in 2003 as a public-private partnership, led by Principal Investigator Michael W. Weiner, MD. The primary goal of ADNI has been to test whether serial magnetic resonance imaging (MRI), positron emission tomography (PET), other biological markers, and clinical and neuropsychological assessment can be combined to measure the progression of mild cognitive impairment (MCI) and early Alzheimer's disease (AD). A fuller description of ADNI and up-to-date information is available at www.adni-info.org. We retrieved data of participants of the ADNI-1 study who had a clinical diagnosis of AD dementia at baseline, a baseline MRI scan, neuropsychological testing at baseline and follow-up and documented treatment with any cholinesterase inhibitor during follow-up time. We retrieved 124 cases, 56 women, fulfilling these conditions. We included only people with a clinical diagnosis of AD dementia, because cholinesterase inhibitor treatment is only approved for this diagnosis, but not for MCI or other diagnoses.

Neuropsychological Tests

We used ADAScog11 as measure of global cognitive decline (27–29). ADAScog 11 has frequently been used in clinical efficacy trials of cholinesterase inhibitors in AD as primary endpoint (30, 31). In addition, we used composite measures for memory and executive function, respectively, to account for the different versions of the word lists of neuropsychological tests employed in the ADNI psychometric assessment. The ADNI composite scores have been previously defined and they appear to: (i) have good validity, (ii) include additional information, incorporating all of the domain-specific information available from the neuropsychological battery administered in ADNI, and (iii) be strongly associated with a priori specified neuroimaging parameters selected on the basis of their known association with the respective cognitive domain (32, 33).

MRI Acquisition

ADNI MRI data were acquired on multiple 1.5 Tesla MRI scanners using phantom-calibrated scanner-specific T1-weighted sagittal 3D MPRAGE sequences. In order to increase signal uniformity across the multicenter scanner platforms, original MPRAGE acquisitions in ADNI undergo standardized image pre-processing correction steps. Standardization of MRI sequences across ADNI sites and centralized image pre-processing steps have been described in detail previously (34) and are documented on the ADNI website (http://adni.loni.usc.edu/methods/).

MRI Data Processing

The processing of structural MRI scans was implemented through statistical parametric mapping, SPM8 (Wellcome Dept. of Imaging Neuroscience, London), and the VBM8-toolbox (http://dbm.neuro.uni-jena.de/vbm/) implemented in MATLAB 7.1 (Mathworks, Natwick), and has been described in detail previously (35, 36). Briefly, MRI scans were automatically segmented into gray matter (GM), white matter (WM), and cerebrospinal fluid (CSF) partitions of 1.5 mm isotropic voxel-size, using the segmentation routine of the VBM8-toolbox. The resulting GM and white matter partitions of each subject in native space were then high-dimensionally registered to an aging/AD-specific reference template based on a completely independent cohort (37) using the Diffeomorphic Anatomic Registration using Exponentiated Lie algebra (DARTEL) algorithm (38). Individual flow-fields obtained from the DARTEL registration to the reference template were used to warp the GM segments and voxel-values were modulated for volumetric changes introduced by the high-dimensional normalization, such that the total amount of GM volume present before warping was preserved. All preprocessed GM maps passed a visual inspection for overall segmentation and registration accuracy.

The total intracranial volume (TIV) was calculated as the sum of the total segmented GM, WM, and CSF volumes (38). GM volumes of the hippocampus and basal forebrain cholinergic nuclei were automatically extracted by summing up the modulated GM voxel values within respective regions of interest (ROI) in the reference space. The basal forebrain ROI was based on a recently published cytoarchitectonic map of basal forebrain cholinergic nuclei in MNI space, derived from combined histology, and in cranio MRI of a post-mortem brain (13). This cytoarchitectonic map matches standard MNI space and was projected into the aging-AD specific template space using non-linear warping parameters obtained from a DARTEL registration. Although the cytoarchitectonic basal forebrain map comprises detailed outlines of different cholinergic subdivisions within the basal forebrain, including cell clusters corresponding to the medial septum, diagonal band, nucleus subputaminalis, and nucleus basalis Meynert, in the current study we only considered the entire volume of the map, including all cholinergic subdivisions, as a proxy for overall basal forebrain cholinergic system integrity. The ROI mask for the hippocampus was obtained by manual delineation of the hippocampus in the reference template of aging-AD specific anatomy (37) using the interactive software package Display (McConnell Brain Imaging Centre at the Montreal Neurological Institute) and a previously described protocol for segmentation of the medial temporal lobe (39). An illustration of both ROIs in the gray matter fraction of the reference space template employed in our current study can be found in the previous publications (15, 40, 41).

Statistical Analysis

We conducted two types of analysis. The first analysis determined associations of volumetric markers with rates of change in cognitive scores as continuous outcomes. The second analysis determined the accuracy of response prediction in cognitive scores as binary outcome.

Association With Rates of Change

We determined the main effects and the two-way interactions of baseline volumes by time on neuropsychological performance as dependent variable using linear mixed effects models with subject-related random effects for intercept and time, controlling for age, sex, and TIV. The model fit was compared between nested models (random intercept vs. uncorrelated random intercept and slope vs. correlated random intercept and slope) using Akaike's information criterion (AIC) (42). Significance of parameters was determined using t-statistics with degrees of freedom determined according to the Satterthwaite approximation. Mixed effect model analyses were calculated in R, including the libraries "lme4" and "lmerTest," available at http://cran.r-project.org/web/packages.

Response Prediction

We originally had planned to determine response prediction. Similarly to previous studies (43), we defined response as more than 4 points improvement (i.e., at least 4 points decline) in ADAScog11 over one year. This criterion, however, yielded only three responders so that an analysis was not feasible. Consequently, we relaxed the response criterion and discriminated between non-decliners (zero change or better) vs. decliners in the cognitive endpoints. Rates of change in cognitive scores were derived from the coefficients of the subject-related random effect for time on the cognitive scores, controlling for age and sex. We determined logistic regression models regressing the binary endpoint of decline vs. non-decline on those volumetric markers that had shown a significant association with the continuous rates of cognitive decline in the previous models.

We used block-wise cross validation with repeated random sampling, based on Gaussian-distributed random numbers generated in R. We repeatedly split the data set into 63.2% of training data and 36.8% of test data. For each of the repeatedly drawn training samples, the logistic regression parameters were estimated and subsequently applied to the remaining test data set. Bootstrapping aimed to assess levels of predictive accuracy in the test data so to avoid overestimation of accuracy levels that occurs when assessment is based on the training data. We recorded areas under the receiver operating characteristic curves (AUC) for each test data set; different to the rate of correctly identified cases, the AUC is insensitive to an uneven distribution of outcomes. The entire cross-validation process was iterated 100 times to determine the variability of the estimates of accuracy

TABLE 1 | Baseline demographic characteristics.

N (women)	124 (56)
Age, mean (*SD*) in years	75.3 (7.4)
MMSE, mean (*SD*)	23.5 (1.9)
ADAScog11, mean (*SD*)	19.0 (6.4)
ADNI-MEM, mean (*SD*)	−0.9 (0.5)
ADNI-EXE, mean (*SD*)	−0.9 (0.8)
L. hippocampus volume (*SD*) in mm^3	2,038 (337)
R. hippocampus volume (*SD*) in mm^3	2,212 (374)
Basal forebrain volume (*SD*) in mm^3	481 (85)

ADAScog11 - 11-items version of the Alzheimer's Disease Assessment Scale–Cognitive subscale, higher values indicate worse performance.
ADNI-MEM - ADNI memory score (32); this scale provides z-standardized performance scores, lower values indicate worse performance.
ANDI-EXE - ADNI executive function score (33); this scale provides z-standardized performance scores, lower values indicate worse performance.

across runs. We determined nonparametric bootstrap confidence intervals with the 2.5 and 97.5 percentiles defining the lower and upper limits of the confidence interval [(44), Chapter 13]. Logistic regression analysis was calculated in R, using function glm with the parameter family = binary.

All analyses were performed with RStudio, version 0.98.1102, a user interface of R Project for Statistical Computing Analyses.

RESULTS

Sample

We retrieved 124 (56 women) cases with AD dementia fulfilling the inclusion criteria. Follow-up times ranged between 0.4 and 3.1 years, number of follow-up time points ranged between 1 and 5. Baseline demographic characteristics and hippocampus and basal forebrain volumes are given in **Table 1.**

Association With Global and Domain-Specific Cognitive Rates of Change

For **ADAScog11**, the best fit was achieved with a model allowing for a correlated random intercept and slope. Detailed results are shown in **Table 2.** ADAScog11 showed a significant worsening over time with 4.3 points increase per year. Left and right hippocampus and basal forebrain volumes were significantly correlated with ADAScog11 baseline performance, with better performance with higher volume. In addition, basal forebrain volume was associated with less worsening in ADAScog11 performance over time ($t = -2.9$, 115 df, $p < 0.005$) with the effect amounting to 1.6 points less increase in ADAScog11 per year when the volume of basal forebrain was one standard deviation higher (**Figure 1**). The partial correlation coefficient (controlling for TIV) between slopes of ADAScog11 change from the mixed effects model and basal forebrain baseline volume was $r = -0.23$, $p < 0.01$. Left and right hippocampus volumes had no significant effects on the ADAScog11 rates of change over time ($p > 0.22$ for all comparisons).

For **ADNI memory score,** the best fit was achieved with a model allowing for an uncorrelated random intercept and slope. Detailed results are shown in **Table 2.** On average, patients lost 0.21 z-score points per year. Left and right hippocampus and basal forebrain volumes were significantly associated with baseline memory performance, with higher performance associated with higher volume. In addition, left hippocampus volume was associated with less worsening in the ADNI memory score over time ($t = -2.0$, 109 df, $p < 0.05$) with the effect amounting to 0.04 less z-score points lost per year when the volume was one standard deviation higher (**Figure 2**). The partial correlation coefficient (controlling for TIV) between slopes of ADNI memory rates of change from the mixed effects model and left hippocampus baseline volume was −0.15, $p < 0.1$. Right hippocampus and basal forebrain volumes had no significant effects on the ADNI memory rates of change over time ($p > 0.16$ for all comparisons).

For **ADNI executive function score** the best fit was achieved with a model allowing for an uncorrelated random intercept and slope. Detailed results are shown in **Table 2**. On average, patients lost 0.29 z-score points per year ($t = -10.1$, 98 df, $p < 0.001$). Basal forebrain was significantly associated with baseline executive function performance ($t = 3.2$, 123 df, $p < 0.002$), with better performance associated with higher volume; there was no effect for left or right hippocampus volume. Neither bilateral hippocampus nor basal forebrain volumes had a significant effect on the executive function rates of change over time ($p > 0.20$ for all comparisons).

The covariates that were used in the model showed no effect of age, sex or total intracranial volume on ADAScog; age had a significant effect on ADNI memory and executive function scores ($p < 0.05$), but sex and TIV had no significant effects on these scores.

Response Prediction

Basal forebrain volume was significantly associated with the outcome of non-decline in ADAScog11 with an odds ratio of 2.5 ($p < 0.05$), i.e., a one standard deviation higher basal forebrain volume increased the odds of non-decline by a factor of 2.5. The corresponding bootstrapped AUC in the test data was 0.78, the 2.5/97.5 percentile confidence interval was 0.50 to 0.98. For the ADNI memory score there were no non-decliners, rendering further analysis infeasible.

DISCUSSION

We found significant decline of global cognitive function as well as memory and executive function in AD dementia cases during follow-up. Higher basal forebrain volume was associated with slower global cognitive decline, and higher left hippocampus volume was associated with slower memory decline. The prognostic use of basal forebrain volume to discriminate between cognitive decliners and cognitive stable persons based on the global ADAScog11 score reached a cross-validated area under the ROC curve of 0.78, indicating a fair accuracy, however with a broad bootstrapped confidence interval including the random guessing level of AUC = 0.5.

The clear decline of global cognitive function as assessed by ADAScog11 is consistent with previous studies on the course of

TABLE 2 | Summary of predictor effects.

		Left Hp t(df); *p*	Right Hp t(df); *p*	BF t(df); *p*
ADAScog11	Volume	−2.1(120); <0.04	−3.6 (120); <0.001	−3.0(119); <0.004
	Time	8.0(109); 10^{-11}	8.0(109); 10^{-11}	8.0(109); 10^{-11}
	Time*Volume	n.s.	n.s.	−2.9(115); <0.005
ADNI-MEM	Volume	2.3(129); <0.03	3.3(128); <0.002	3.9(128); <0.001
	Time	−10.7(112); 10^{-14}	−10.7(112); 10^{-14}	−10.7(112); 10^{-14}
	Time*Volume	−2.0(109); <0.05	n.s.	n.s.
ADNI-EXE	Volume	n.s.	n.s.	3.2(123); <0.002
	Time	−10.1(98); 10^{-14}	−10.1(98); 10^{-14}	−10.1(98); 10^{-14}
	Time*Volume	n.s.	n.s.	n.s.

Reported are the main effect of time and volume and the interaction effects of volume by time. All models were controlled for age, sex, and total intracranial volume.
Data are given as: t-values (t); number of degrees of freedom (df); p-value (p).
Please note: the sign of the t-value gives the direction of the effect, i.e., a positive t-value indicates that test scores were higher with higher volume and vice versa.
Hp, hippocampus.
BF, basal forebrain.
ADAScog11, 11-items version of the Alzheimer's Disease Assessment Scale–Cognitive subscale.
ADNI-MEM, ADNI memory score (32).
ANDI-EXE, ADNI executive function score (33).

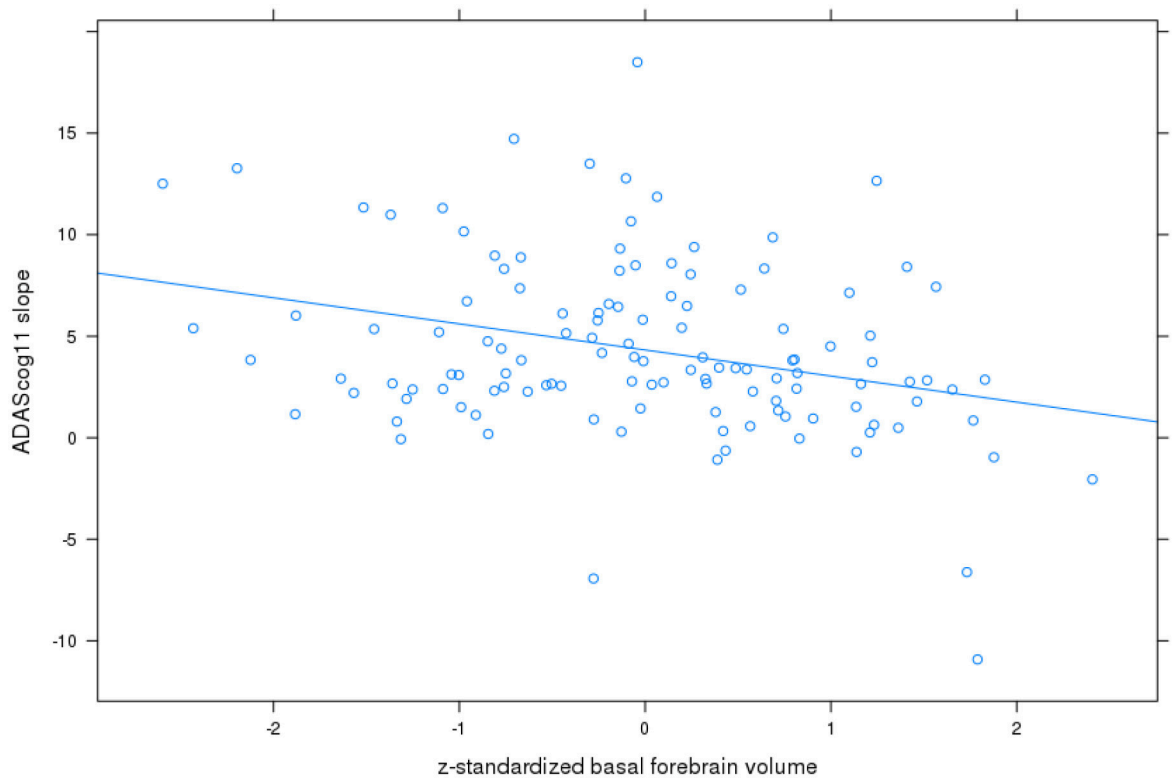

FIGURE 1 | Basal forebrain volume and rates of change in ADAScog11. Plot of z-standardized basal forebrain volume on mixed effects linear model estimates of rates of change in ADAScog score controlling for age and sex, with linear regression line.

cognitive decline in dementia stages of AD (45). A large cohort study of 622 cases with cholinesterase inhibitor treatment and paired assessments of MMSE at baseline and after 3 to 4 months showed a response rate of 37%, when defining response by at least 2 points MMSE increase (46). The findings in this large cohort study agree with findings in randomized controlled trials with cholinesterase inhibitors showing an increase of MMSE or decrease in ADAScog scores in the first 3 to 6 months of treatment with subsequent decline (47, 48). Here, we assessed longer term follow-up, between 0.4 and 3.1 years, accounting for

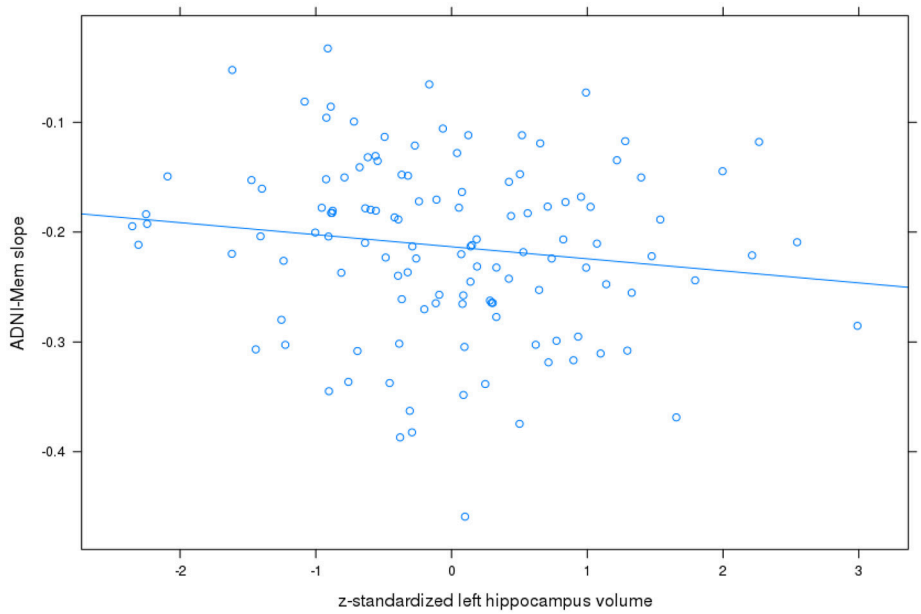

FIGURE 2 | Left hippocampus volume and rates of change in ADNI memory score. Plot of z-standardized left hippocampus volume on mixed effects linear model estimates of rates of change in ADNI memory (ADNI-Mem) score controlling for age and sex, with linear regression line.

the low number of cases fulfilling response criteria (only 10 of 124 cases, even when defining response as non-decline).

In the cross-sectional analyses, baseline volumes of basal forebrain, and left and right hippocampus were associated with global cognitive function as well as memory performance, as assessed by the ADNI memory composite score. These findings agree with previous studies showing that hippocampus volume was associated with episodic memory (49) and global cognitive (50) performance in AD patients. Similarly, previous studies have described associations of basal forebrain volume with global cognitive and episodic memory performance in AD dementia and MCI cases in cross-sectional analysis (15, 40, 41). In addition, in the current study, basal forebrain volume was associated with the executive function composite score. This agrees with the observation that cholinergic activity subserves executive function and attention that is supported by the adverse effects of anticholinergic treatment on executive function and attention (51–53), and by findings of similar associations in independent cohorts (15, 40, 41).

Cholinergic basal forebrain volume was significantly associated with subsequent global cognitive decline as assessed by ADAScog11. AD dementia cases with a one standard deviation higher basal forebrain volume had 1.6 points less worsening in ADAScog11 per year, accounting for 37% of the annual overall rate of ADAScog11 worsening. Basal forebrain volume allowed correct discrimination between cognitive non-decliners and cognitive decliners with an AUC of 0.78. We used the AUC as measure of accuracy, because this measure is less sensitive to the proportion of non-decliners; in contrast, the level of correct case identification would have been uninformative, because with only 10 non-decliners simply predicting non-conversion in all cases would already yield correct classification in 114 out of 124 cases. Our findings indicate that in the presence of cholinergic treatment, a high cholinergic basal forebrain volume is associated with more benign global cognitive decline. Our findings agree with a previous exploratory study, where response to cholinergic treatment over 9 months as measured by the MMSE score was significantly associated with gray matter volume in basal forebrain regions from a voxel based regression analysis in 23 AD cases (54). Our findings disagree with a study in 82 AD dementia patients using the substantia innominata thickness as a proxy of cholinergic basal forebrain integrity (18); here smaller rate of cognitive decline was found associated with a smaller thickness of the substantia innominata during 9 months cholinergic treatment (19). The number of subjects was higher and the average follow-up time was longer in our study compared to the previous study. In addition, manual measurement of the thickness of the substantia innominata is prone to intra- and inter-rater variability, and assesses only a small subsection of the cholinergic basal forebrain compared to the automated measurement of basal forebrain volume based on a post mortem reference map (11).

Hippocampus volume was not associated with the subsequent rate of global cognitive decline. In a small sample of 37 AD patients, a previous study found a higher hippocampus volume associated with less worsening of ADAScog score over 0.5 to 2 years of follow-up (25). A part of these 37 individuals had been classified as very mild AD, resembling rather the prodromal MCI than the dementia stage of AD. This outcome therefore

agrees with the results of our previous study on 216 MCI cases, where we found that higher hippocampus volume, rather than basal forebrain volume, was associated with more benign rates of global cognitive and memory decline (26). Taken together these findings suggest that hippocampus volume may be a proxy of reserve capacity in MCI individuals, but no more in AD dementia patients. This interpretation would agree with the notion that hippocampus atrophy begins to degenerate earlier than basal forebrain and reaches a plateau in the dementia stage of AD so that the functional relevance of hippocampus volume variation would be limited in the dementia stage of the disease. In contrast, changes in basal forebrain volume may still dynamically progress during AD dementia and may thus serve as a better predictor of disease progression in more advanced disease stages (37).

In contrast to global cognitive decline, left hippocampus volume was significantly associated with the rate of episodic memory score decline, consistent with previous evidence in subjects with MCI (26, 55). Different to global cognitive decline we could not determine the predictive accuracy of hippocampus volume for non-decline, as non-decline did not occur in our sample. The partial r of −0.15, however, points to a small effect size for left hippocampus volume on subsequent rate of memory decline, consistent with a limited role of hippocampus volume for predicting subsequent cognitive decline in the AD dementia stage, even when considering the hippocampus-specific functional measure of episodic memory performance.

Beyond structural markers, such as hippocampus or basal forebrain volumes, a previous study found cortical network functional integrity in functional MRI as a significant predictor of cholinergic treatment response, but the study included only 18 cases (56).

Several limitations have to be considered with our study. First, similar to previous studies in AD dementia (19, 25) we determined the predictive value of hippocampus and basal forebrain volumes for cognitive decline in patients who all received treatment. Therefore, we can only derive conclusions on prediction of cognitive decline during treatment, but not on prediction of treatment effects; in our view this distinction is sometimes not made explicit enough in the literature (19, 25). We had decided to exclude AD dementia cases without documentation of cholinergic treatment since the lack of documentation of treatment may not be a reliable indicator for the lack of treatment in the ADNI cohort. In addition, the lack of treatment in a cohort like ADNI will likely be related to selection bias; the ADNI cohort by design features no random allocation to treatment. Furthermore, information on the duration of treatment before inclusion in the ADNI cohort was not available so that stratification according to duration of treatment was not possible. Our findings encourage the analysis of prospective controlled clinical trials in AD dementia for a potential association of basal forebrain and hippocampus volumes with rates of subsequent cognitive change in dependency of treatment. Secondly, observation periods were very heterogeneous in the ADNI cohort. We used a mixed effects model to explicitly model variability in observation periods. Indeed, the models including a random effects term for time provided a better fit than models excluding such term. Thirdly, it would have been interesting following previous evidence on the corticotopic organization of the cholinergic basal forebrain to analyze a differential involvement of antero-medial vs. postero-lateral basal forebrain subregions. Anterior-medial basal forebrain nuclei project mainly to the hippocampus and ventromedial cortical regions, whereas posterior-lateral nuclei project more densely to lateral neocortical areas (6, 57, 58), which may also be related to different functional representation of these subnuclei. However, the overall small size of the basal forebrain volume restricts the accuracy of subregional assessments so that we did not include such an analysis. Fourthly, we had selected the ADNI memory and executive function composite scores to reduce the dimensionality of our analyses. Previous studies had shown that both composite measures exhibited more consistent rates of change in MCI and AD dementia individuals than the respective single tests (32, 33). Finally, we aimed to determine odds ratios of volumes for predicting clinically significant response to treatment. Such response has previously been defined to equal at least 4 points decrease in ADAScog11 (43). Since only 3 cases fulfilled this response criterion, we could not conduct the intended analysis. When we used a more liberal criterion of no cognitive decline, i.e., ≤ 0 points change in ADAScog11, we found a significant odds ratio of 2.5. This indicates that a person with a one standard deviation higher basal forebrain volume has a 2.5 higher chance of no decline, all other variables kept constant. However, this analysis detects a clinically potentially less relevant endpoint than the originally planned analysis of 4 points change.

In summary, we found significant decline of global cognitive function as well as memory and executive function in AD dementia patients treated with cholinesterase inhibitors. Basal forebrain volume, but not hippocampus volume, was a predictor of global cognitive decline with a cross-validated accuracy of approximately 78% to discriminate between non-decliners and decliners, albeit based on a small sample of non-decliners. In contrast, left hippocampus volume showed only a modest association with subsequent rates of memory decline during cholinergic treatment. Our data suggest that with the transition from prodromal MCI to AD dementia the brain areas with biologically meaningful dynamic variation and ensuing predictive value may shift from the hippocampus to the basal forebrain region. The use of hippocampus and basal forebrain volumes to predict response to cholinergic treatment in AD dementia needs to be studied in cohorts with controlled treatment.

ETHICS APPROVAL AND CONSENT TO PARTICIPATE

All procedures performed in the ADNI studies involving human participants were in accordance with the ethical standards of the institutional research committees and with the 1964 Helsinki declaration and its later amendments. Written informed consent was obtained from all participants or their authorized representatives.

The study procedures were approved by the institutional review boards of all participating centers (https://adni.loni.usc.edu/wp-content/uploads/how_to_apply/ADNI_Acknowledgement_List.pdf:) Oregon Health and Science University; University of Southern California; University of California—San Diego; University of Michigan; Mayo Clinic, Rochester; Baylor College of Medicine; Columbia University Medical Center; Washington University, St. Louis; University of Alabama at Birmingham; Mount Sinai School of Medicine; Rush University Medical Center; Wien Center; Johns Hopkins University; New York University; Duke University Medical Center; University of Pennsylvania; University of Kentucky; University of Pittsburgh; University of Rochester Medical Center; University of California, Irvine; University of Texas Southwestern Medical School; Emory University; University of Kansas, Medical Center; University of California, Los Angeles; Mayo Clinic, Jacksonville; Indiana University; Yale University School of Medicine; McGill University, Montreal-Jewish General Hospital; Sunnybrook Health Sciences, Ontario; U.B.C. Clinic for AD & Related Disorders; Cognitive Neurology—St. Joseph's, Ontario; Cleveland Clinic Lou Ruvo Center for Brain Health; Northwestern University; Premiere Research Inst (Palm Beach Neurology); Georgetown University Medical Center; Brigham and Women's Hospital; Stanford University; Banner Sun Health Research Institute; Boston University; Howard University; Case Western Reserve University; University of California, Davis—Sacramento; Neurological Care of CNY; Parkwood Hospital; University of Wisconsin; University of California, Irvine—BIC; Banner Alzheimer's Institute; Dent Neurologic Institute; Ohio State University; Albany Medical College; Hartford Hospital, Olin Neuropsychiatry Research Center; Dartmouth-Hitchcock Medical Center; Wake Forest University Health Sciences; Rhode Island Hospital; Butler Hospital; UC San Francisco; Medical University South Carolina; St. Joseph's Health Care Nathan Kline Institute; University of Iowa College of Medicine; Cornell University and University of South Florida: USF Health Byrd Alzheimer's Institute.

AVAILABILITY OF DATA AND MATERIALS

The datasets analyzed during the current study are available in the ADNI repository, www.adni-info.org.

AUTHOR CONTRIBUTIONS

ST and MG have made substantial contributions to conception and design of the study, and the analysis and interpretation of data, drafted the manuscript, given final approval of the version to be published, agreed to be accountable for all aspects of the work in ensuring that questions related to the accuracy or integrity of any part of the work are appropriately investigated and resolved. EC and HH have made substantial contributions to analysis and interpretation of data, been involved in revising the manuscript critically for important intellectual content, given final approval of the version to be published, agreed to be accountable for all aspects of the work in ensuring that questions related to the accuracy or integrity of any part of the work are appropriately investigated and resolved.

FUNDING

Data collection and sharing for this project was funded by the Alzheimer's Disease Neuroimaging Initiative (ADNI) (National Institutes of Health Grant U01 AG024904) and DOD ADNI (Department of Defense award number W81XWH-12-2-0012). ADNI is funded by the National Institute on Aging, the National Institute of Biomedical Imaging and Bioengineering, and through generous contributions from the following: AbbVie,Alzheimer's Association; Alzheimer's Drug Discovery Foundation; Araclon Biotech; BioClinica, Inc.; Biogen;Bristol-Myers Squibb Company; CereSpir, Inc.; Cogstate; Eisai Inc.; Elan Pharmaceuticals, Inc.; Eli Lilly and Company; EuroImmun; F. Hoffmann-La Roche Ltd and its affiliated company Genentech, Inc.; Fujirebio; GE Healthcare; IXICO Ltd.; Janssen Alzheimer Immunotherapy Research & Development, LLC.; Johnson & Johnson Pharmaceutical Research & Development LLC.; Lumosity; Lundbeck; Merck & Co., Inc.; Meso Scale Diagnostics, LLC.; NeuroRx Research; Neurotrack Technologies; Novartis Pharmaceuticals Corporation; Pfizer Inc.; Piramal Imaging; Servier; Takeda Pharmaceutical Company; and Transition Therapeutics. The Canadian Institutes of Health Research is providing funds to support ADNI clinical sites in Canada. Private sector contributions are facilitated by the Foundation for the National Institutes of Health (www.fnih.org). The grantee organization is the Northern California Institute for Research and Education, and the study is coordinated by the Alzheimer's Therapeutic Research Institute at the University of Southern California. ADNI data are disseminated by the Laboratory for Neuro Imaging at the University of Southern California. HH is supported by the AXA Research Fund, the Fondation Partenariale Sorbonne Université' and the Fondation pour la Recherche sur Alzheimer, Paris, France. The research leading to these results has received funding from the program Investissements d'Avenir ANR-10-IAIHU-06 (Agence Nationale de la Recherche-10-IA Agence Institut Hospitalo-Universitaire-6). This publication benefited from the support of the Program PHOENIX® led by the Sorbonne University Foundation and sponsored by la Fondation pour la Recherche sur Alzheimer.

ACKNOWLEDGMENTS

Data used in the preparation of this article were obtained from the Alzheimer's Disease Neuroimaging Initiative (ADNI) database (adni.loni.usc.edu). The ADNI was launched in 2003 by the National Institute on Aging (NIA), the National Institute of Biomedical Imaging and Bioengineering (NIBIB), the Food and Drug Administration (FDA), private pharmaceutical companies and non-profit organizations, as a $60 million, 5-year public-private partnership. The primary goal of ADNI has been to test whether serial magnetic resonance imaging (MRI), positron emission tomography (PET), other biological markers, and clinical and neuropsychological assessment can be combined to

measure the progression of mild cognitive impairment (MCI) and early Alzheimer's disease (AD). Determination of sensitive and specific markers of very early AD progression is intended to aid researchers and clinicians to develop new treatments and monitor their effectiveness, as well as lessen the time and cost of clinical trials.

The Principal Investigator of this initiative is Michael W. Weiner, MD, VA Medical Center and University of California—San Francisco. ADNI is the result of efforts of many co-investigators from a broad range of academic institutions and private corporations, and subjects have been recruited from over 50 sites across the U.S. and Canada. The initial goal of ADNI was to recruit 800 subjects but ADNI has been followed by ADNI-GO and ADNI-2. To date these three protocols have recruited over 1500 adults, ages 55 to 90, to participate in the research, consisting of cognitively normal older individuals, people with early or late MCI, and people with early AD. The follow up duration of each group is specified in the protocols for ADNI-1, ADNI-2, and ADNI-GO. Subjects originally recruited for ADNI-1 and ADNI-GO had the option to be followed in ADNI-2. For up-to-date information, see www.adni-info.org.

Contributors to the Alzheimer precision medicine initiative - working group (APMI-WG): Lisi Flores Aguilar (Montréal), Claudio Babiloni (Rome), Filippo Baldacci (Pisa), Norbert Benda (Bonn), Keith L. Black (Los Angeles), Arun L. W. Bokde (Dublin), Ubaldo Bonuccelli (Pisa), Karl Broich (Bonn), René S. Bun (Paris), Francesco Cacciola (Siena), Juan Castrillo† (Derio), Enrica Cavedo (Paris), Roberto Ceravolo (Pisa), Patrizia A. chiesa (Paris), Olivier Colliot (Paris), Cristina-Maria Coman (Paris), Jean-Christophe Corvol (Paris), Augusto Claudio Cuello (Montréal), Jeffrey L. Cummings (Las Vegas), Herman Depypere (Gent), Bruno Dubois (Paris), Andrea Duggento (Rome), Stanley Durrleman (Paris), Valentina Escott-price (Cardiff), Howard Federoff (Irvine), Maria Teresa Ferretti (Zürich), Massimo Fiandaca (Irvine), Richard A. Frank (Malvern), Francesco Garaci (Rome), Remy Genthon (Paris), Nathalie George (Paris), Filippo S. Giorgi (Pisa), Manuela Graziani (Roma), Marion Haberkamp (Bonn), Marie-Odile Habert (Paris), Harald Hampel (Paris), Karl Herholz (Manchester), Eric Karran (Cambridge), Seung H. KIM (Seoul), Yosef Koronyo (Los Angeles), Maya Koronyo-Hamaoui (Los Angeles), Foudil Lamari (Paris), Todd Langevin (Minneapolis-Saint Paul), Stéphane Lehéricy (Paris), Simone Lista (Paris), Jean Lorenceau (Paris), Mark Mapstone (Irvine), Christian Neri (Paris), Robert Nisticò (Rome), Francis Nyasse-Messene (Paris), Sid E. O'Bryant (Fort Worth), George Perry (San Antonio), Craig Ritchie (Edinburgh), Katrine Rojkova (Paris), Simone Rossi (Siena), Amira Saidi (Rome), Emiliano Santarnecchi (Siena), Lon S. Schneider (Los Angeles), Olaf Sporns (Bloomington), Nicola Toschi (Rome), Steven R. Verdooner (Sacramento), Andrea Vergallo (Paris), Nicolas Villain (Paris), Lindsay A. Welikovitch (Montréal), Janet Woodcock (Silver Spring), Erfan Younesi (Esch-sur-Alzette).

REFERENCES

1. Carr VA, Viskontas IV, Engel SA, Knowlton BJ. Neural activity in the hippocampus and perirhinal cortex during encoding is associated with the durability of episodic memory. *J Cogn Neurosci.* (2010) 22:2652–62. doi: 10.1162/jocn.2009.21381
2. Deweer B, Pillon B, Pochon JB, Dubois B. Is the HM story only a "remote memory"? Some facts about hippocampus and memory in humans. *Behav Brain Res.* (2001) 127:209–24. doi: 10.1016/S0166-4328(01)00366-7
3. Price JL, Morris JC. Tangles and plaques in nondemented aging and "preclinical" Alzheimer's disease. *Ann Neurol.* (1999) 45:358–68. doi: 10.1002/1531-8249(199903)45:3<358::AID-ANA12>3.0.CO;2-X
4. Kaye JA, Swihart T, Howieson D, Dame A, Moore MM, Karnos T, et al. Volume loss of the hippocampus and temporal lobe in healthy elderly persons destined to develop dementia. *Neurology* (1997) 48:1297–304.
5. Frisoni GB, Jack CR Jr, Bocchetta M, Bauer C, Frederiksen KS, Liu Y, et al. The EADC-ADNI Harmonized Protocol for manual hippocampal segmentation on magnetic resonance: evidence of validity. *Alzheimers Dement* (2015) 11:111–25. doi: 10.1016/j.jalz.2014.05.1756
6. Mesulam MM, Mufson EJ, Levey AI, Wainer BH. Cholinergic innervation of cortex by the basal forebrain: cytochemistry and cortical connections of the septal area, diagonal band nuclei, nucleus basalis (substantia innominata), and hypothalamus in the rhesus monkey. *J Comp Neurol.* (1983) 214:170–97. doi: 10.1002/cne.902140206
7. Bracco L, Bessi V, Padiglioni S, Marini S, Pepeu G. Do cholinesterase inhibitors act primarily on attention deficit? A naturalistic study in Alzheimer's disease patients. *J Alzheimers Dis.* (2014) 40:737–42. doi: 10.3233/JAD-131154
8. Mesulam M, Shaw P, Mash D, Weintraub S. Cholinergic nucleus basalis tauopathy emerges early in the aging-MCI-AD continuum. *Ann Neurol.* (2004) 55:815–28. doi: 10.1002/ana.20100
9. Sassin I, Schultz C, Thal DR, Rub U, Arai K, Braak E, et al. Evolution of Alzheimer's disease-related cytoskeletal changes in the basal nucleus of Meynert. *Acta Neuropathol.* (2000) 100:259–69. doi: 10.1007/s004019900178
10. Mesulam MM. Cholinergic circuitry of the human nucleus basalis and its fate in Alzheimer's disease. *J Comp Neurol.* (2013) 521:4124–44. doi: 10.1002/cne.23415
11. Teipel SJ, Flatz WH, Heinsen H, Bokde AL, Schoenberg SO, Stockel S, et al. Measurement of basal forebrain atrophy in Alzheimer's disease using MRI. *Brain* (2005) 128(Pt 11):2626–44. doi: 10.1093/brain/awh589
12. Zaborszky L, Hoemke L, Mohlberg H, Schleicher A, Amunts K, Zilles K. Stereotaxic probabilistic maps of the magnocellular cell groups in human basal forebrain. *NeuroImage* (2008) 42:1127–41. doi: 10.1016/j.neuroimage.2008.05.055
13. Kilimann I, Grothe M, Heinsen H, Alho EJ, Grinberg L, Amaro Jr E, et al. Subregional basal forebrain atrophy in Alzheimer's Disease: a multicenter study. *J Alzheimers Dis.* (2014) 40:687–700. doi: 10.3233/JAD-132345
14. Teipel SJ, Meindl T, Grinberg L, Grothe M, Cantero JL, Reiser MF, et al. The cholinergic system in mild cognitive impairment and Alzheimer's disease: an *in vivo* MRI and DTI study. *Human Brain Mapp.* (2011) 32:1349–62. doi: 10.1002/hbm.21111
15. Grothe M, Zaborszky L, Atienza M, Gil-Neciga E, Rodriguez-Romero R, Teipel SJ, et al. Reduction of basal forebrain cholinergic system parallels cognitive impairment in patients at high risk of developing Alzheimer's disease. *Cereb Cortex* (2010) 20:1685–95. doi: 10.1093/cercor/bhp232
16. Muth K, Schonmeyer R, Matura S, Haenschel C, Schroder J, Pantel J. Mild cognitive impairment in the elderly is associated with volume loss of the cholinergic basal forebrain region. *Biol Psychiatry* (2010) 67:588–91. doi: 10.1016/j.biopsych.2009.02.026
17. Teipel S, Heinsen H, Amaro E, Jr., Grinberg LT, Krause B, Grothe M, et al. Cholinergic basal forebrain atrophy predicts amyloid burden in Alzheimer's disease. *Neurobiol Aging* (2013) 35:482–91. doi: 10.1016/j.neurobiolaging.2013.09.029
18. Hanyu H, Asano T, Sakurai H, Tanaka Y, Takasaki M, Abe K. MR analysis of the substantia innominata in normal aging, Alzheimer disease, and other types of dementia. *Am J Neuroradiol.* (2002) 23:27–32.
19. Tanaka Y, Hanyu H, Sakurai H, Takasaki M, Abe K. Atrophy of the substantia innominata on magnetic resonance imaging predicts response to donepezil

treatment in Alzheimer's disease patients. *Dement Geriatr Cogn Disord.* (2003) 16:119–25. doi: 10.1159/000070998
20. Jack CR, Jr., Petersen RC, Xu YC, O'Brien PC, Smith GE, Ivnik RJ, et al. Prediction of AD with MRI-based hippocampal volume in mild cognitive impairment. *Neurology* (1999) 52:1397–403.
21. Erten-Lyons D, Howieson D, Moore MM, Quinn J, Sexton G, Silbert L, et al. Brain volume loss in MCI predicts dementia. *Neurology* (2006) 66:233–5. doi: 10.1212/01.wnl.0000194213.50222.1a
22. Apostolova LG, Dutton RA, Dinov ID, Hayashi KM, Toga AW, Cummings JL, et al. Conversion of mild cognitive impairment to Alzheimer disease predicted by hippocampal atrophy maps. *Arch Neurol* (2006) 63:693–9. doi: 10.1001/archneur.63.5.693
23. Macdonald KE, Bartlett JW, Leung KK, Ourselin S, Barnes J, investigators A. The value of hippocampal and temporal horn volumes and rates of change in predicting future conversion to AD. *Alzheimer Disease Assoc Disord.* (2013) 27:168–73. doi: 10.1097/WAD.0b013e318260a79a
24. Ewers M, Walsh C, Trojanowski JQ, Shaw LM, Petersen RC, Jack CR Jr, et al. Prediction of conversion from mild cognitive impairment to Alzheimer's disease dementia based upon biomarkers and neuropsychological test performance. *Neurobiol Aging* (2012) 33:1203–14. doi: 10.1016/j.neurobiolaging.2010.10.019
25. Csernansky JG, Wang L, Miller JP, Galvin JE, Morris JC. Neuroanatomical predictors of response to donepezil therapy in patients with dementia. *Arch Neurol.* (2005) 62:1718–22. doi: 10.1001/archneur.62.11.1718
26. Teipel SJ, Cavedo E, Grothe MJ, Lista S, Galluzzi S, Colliot O, et al. Predictors of cognitive decline and treatment response in a clinical trial on suspected prodromal Alzheimer's disease. *Neuropharmacology* (2016) 108:128–35. doi: 10.1016/j.neuropharm.2016.02.005
27. Wessels AM, Dowsett SA, Sims JR. Detecting Treatment Group Differences in Alzheimer's disease clinical trials: a comparison of alzheimer's disease assessment scale - Cognitive Subscale (ADAS-Cog) and the Clinical Dementia Rating - Sum of Boxes (CDR-SB). *J Prev Alzheimers Dis.* (2018) 5:15–20. doi: 10.14283/jpad.2018.2
28. Sevigny JJ, Peng Y, Liu L, Lines CR. Item analysis of ADAS-Cog: effect of baseline cognitive impairment in a clinical AD trial. *Am J Alzheimers Dis Other Demen.* (2010) 25:119–24. doi: 10.1177/1533317509350298
29. Wouters H, van Gool WA, Schmand B, Zwinderman AH, Lindeboom R. Three sides of the same coin: measuring global cognitive impairment with the MMSE, ADAS-cog and CAMCOG. *Int J Geriatr Psychiatry* (2010) 25:770–9. doi: 10.1002/gps.2402
30. Birks JS, Grimley Evans J. Rivastigmine for Alzheimer's disease. *Cochrane Database Syst Rev.* (2015) 4:CD001191. doi: 10.1002/14651858.CD001191.pub3
31. Loy C, Schneider L. Galantamine for Alzheimer's disease. *Cochrane Database Syst Rev.* (2004) 4:CD001747. doi: 10.1002/14651858.CD001747.pub2
32. Crane PK, Carle A, Gibbons LE, Insel P, Mackin RS, Gross A, et al. Development and assessment of a composite score for memory in the Alzheimer's Disease Neuroimaging Initiative (ADNI). *Brain Imaging Behav.* (2012) 6:502–16. doi: 10.1007/s11682-012-9186-z
33. Gibbons LE, Carle AC, Mackin RS, Harvey D, Mukherjee S, Insel P, et al. A composite score for executive functioning, validated in Alzheimer's Disease Neuroimaging Initiative (ADNI) participants with baseline mild cognitive impairment. *Brain Imaging Behav.* (2012) 6:517–27. doi: 10.1007/s11682-012-9176-1
34. Jack CR Jr., Bernstein MA, Fox NC, Thompson P, Alexander G, Harvey D, et al. The Alzheimer's Disease Neuroimaging Initiative (ADNI): MRI methods. *J Magn Reson Imaging* (2008) 27:685–91. doi: 10.1002/jmri.21049
35. Teipel SJ, Flatz W, Ackl N, Grothe M, Kilimann I, Bokde AL, et al. Brain atrophy in primary progressive aphasia involves the cholinergic basal forebrain and Ayala's nucleus. *Psychiatry Res.* (2014) 221:187–94. doi: 10.1016/j.pscychresns.2013.10.003
36. Grothe MJ, Schuster C, Bauer F, Heinsen H, Prudlo J, Teipel SJ. Atrophy of the cholinergic basal forebrain in dementia with Lewy bodies and Alzheimer's disease dementia. *J Neurol.* (2014) 261:1939–48. doi: 10.1007/s00415-014-7439-z
37. Grothe M, Heinsen H, Teipel S. Longitudinal measures of cholinergic forebrain atrophy in the transition from healthy aging to Alzheimer's disease. *Neurobiol Aging* (2013) 34:1210–20. doi: 10.1016/j.neurobiolaging.2012.10.018
38. Ashburner J. A fast diffeomorphic image registration algorithm. *NeuroImage* (2007) 38:95–113. doi: 10.1016/j.neuroimage.2007.07.007
39. Pruessner JC, Li LM, Serles W, Pruessner M, Collins DL, Kabani N, et al. Volumetry of hippocampus and amygdala with high-resolution MRI and three-dimensional analysis software: minimizing the discrepancies between laboratories. *Cerebral Cortex* (2000) 10:433–42. doi: 10.1093/cercor/10.4.433
40. Grothe MJ, Ewers M, Krause B, Heinsen H, Teipel SJ. Basal forebrain atrophy and cortical amyloid deposition in nondemented elderly subjects. *Alzheimers Dement* (2014) 10(5 Suppl.):S344–53. doi: 10.1016/j.jalz.2013.09.011
41. Grothe MJ, Heinsen H, Amaro E, Jr., Grinberg LT, Teipel SJ, Alzheimer's disease neuroimaging i. cognitive correlates of basal forebrain atrophy and associated cortical hypometabolism in mild cognitive impairment. *Cereb Cortex* (2016) 26:2411–26. doi: 10.1093/cercor/bhv062
42. Sakamoto Y, Ishiguro M, Kitagawa G. *Akaike Information Criterion Statistics*. Boston: D. Reidel Publishing Company (1986).
43. Ohnishi T, Sakiyama Y, Okuri Y, Kimura Y, Sugiyama N, Saito T, et al. The prediction of response to galantamine treatment in patients with mild to moderate Alzheimer's disease. *Curr Alzheimer Res.* (2014) 11:110–8. doi: 10.2174/1567205011310660167
44. Efron B, Tibshirani RJ. *An Introduction to the Bootstrap*. New York, NY: Chapman & Hall/CRC (1994). Available online at: https://www.crcpress.com/An-Introduction-to-the-Bootstrap/Efron-Tibshirani/p/book/9780412042317
45. Raghavan N, Samtani MN, Farnum M, Yang E, Novak G, Grundman M, et al. The ADAS-Cog revisited: novel composite scales based on ADAS-Cog to improve efficiency in MCI and early AD trials. *Alzheimers Dement* (2013) 9(1 Suppl):S21–31. doi: 10.1016/j.jalz.2012.05.2187
46. Van Der Putt R, Dineen C, Janes D, Series H, McShane R. Effectiveness of acetylcholinesterase inhibitors: diagnosis and severity as predictors of response in routine practice. *Int J Geriatr Psychiatry* (2006) 21:755–60. doi: 10.1002/gps.1557
47. Birks J, Grimley Evans J, Iakovidou V, Tsolaki M, Holt FE. Rivastigmine for Alzheimer's disease. *Cochrane Database Syst Rev.* (2009) 2:CD001191. doi: 10.1002/14651858.CD001191.pub2
48. Birks J, Harvey RJ. Donepezil for dementia due to Alzheimer's disease. *Cochrane Database Syst Rev.* (2006) 1:CD001190. doi: 10.1002/14651858.CD001190.pub2
49. Kasper E, Brueggen K, Grothe MJ, Bruno D, Pomara N, Unterauer E, et al. Neuronal correlates of serial position performance in amnestic mild cognitive impairment. *Neuropsychology* (2016) 30:906–14. doi: 10.1037/neu0000287
50. Colliot O, Chetelat G, Chupin M, Desgranges B, Magnin B, Benali H, et al. Discrimination between Alzheimer disease, mild cognitive impairment, and normal aging by using automated segmentation of the hippocampus. *Radiology* (2008) 248:194–201. doi: 10.1148/radiol.2481070876
51. Pomara N, Nolan K, Halpern G. Scopolamine-induced impairment as a potential predictor of Alzheimer's disease in individuals with Apolipoprotein E type 4 alleles. *Neurochem Res.* (1995) 20:1519–20. doi: 10.1007/BF00970602
52. Snyder PJ, Lim YY, Schindler R, Ott BR, Salloway S, Daiello L, et al. Microdosing of scopolamine as a "cognitive stress test": rationale and test of a very low dose in an at-risk cohort of older adults. *Alzheimers Dement* (2014) 10:262–7. doi: 10.1016/j.jalz.2014.01.009
53. Dumas JA, Newhouse PA. The cholinergic hypothesis of cognitive aging revisited again: cholinergic functional compensation. *Pharmacol Biochem Behav.* (2011) 99:254–61. doi: 10.1016/j.pbb.2011.02.022
54. Bottini G, Berlingeri M, Basilico S, Passoni S, Danelli L, Colombo N, et al. GOOD or BAD responder? Behavioural and neuroanatomical markers of clinical response to donepezil in dementia. *Behav Neurol.* (2012) 25:61–72. doi: 10.1155/2012/538542
55. Mielke MM, Okonkwo OC, Oishi K, Mori S, Tighe S, Miller MI, et al. Fornix integrity and hippocampal volume predict memory decline and progression to Alzheimer's disease. *Alzheimers Dement* (2012) 8:105–13. doi: 10.1016/j.jalz.2011.05.2416

56. Miettinen PS, Jauhiainen AM, Tarkka IM, Pihlajamaki M, Grohn H, Niskanen E, et al. Long-Term Response to Cholinesterase Inhibitor Treatment Is Related to Functional MRI Response in Alzheimer's Disease. *Dement Geriat Cogn Disord.* (2015) 40:243–55. doi: 10.1159/000435948
57. Zaborszky L, Csordas A, Mosca K, Kim J, Gielow MR, Vadasz C, et al. Neurons in the basal forebrain project to the cortex in a complex topographic organization that reflects corticocortical connectivity patterns: an experimental study based on retrograde tracing and 3D reconstruction. *Cereb Cortex* (2015) 25:118–37. doi: 10.1093/cercor/bht210
58. Ghashghaei HT, Barbas H. Neural interaction between the basal forebrain and functionally distinct prefrontal cortices in the rhesus monkey. *Neuroscience* (2001) 103:593–614. doi: 10.1016/S0306-4522(00)00585-6

Conflict of Interest Statement: The authors declare that the research was conducted in the absence of any commercial or financial relationships that could be construed as a potential conflict of interest.

The reviewer KS and handling Editor declared their shared affiliation.

frontiers in Neurology

ORIGINAL RESEARCH
published: 26 September 2018
doi: 10.3389/fneur.2018.00806

Beyond Dopamine: GABA, Glutamate, and the Axial Symptoms of Parkinson Disease

Ruth L. O'Gorman Tuura[1]*, *Christian R. Baumann*[2] *and Heide Baumann-Vogel*[2]

[1] *Center for MR Research, University Children's Hospital Zurich, Zurich, Switzerland,* [2] *Department of Neurology, University Hospital Zurich, Zurich, Switzerland*

Introduction: The axial symptoms of Parkinson disease (PD) include difficulties with balance, posture, speech, swallowing, and locomotion with freezing of gait, as well as axial rigidity. These axial symptoms impact negatively on quality of life for many patients, yet remain poorly understood. Dopaminergic treatments typically have little effect on the axial symptoms of PD, suggesting that disruptions in other neurotransmitter systems beyond the dopamine system may underlie these symptoms. The purpose of the present study was to examine the relationship between the axial symptoms of PD and GABA and glutamate levels quantified with magnetic resonance spectroscopy.

Methods: The participant group included 20 patients with PD and 17 healthy control participants. Water-scaled GABA and Glx (glutamate + glutamine) concentrations were derived from GABA-edited MEGA-PRESS spectra acquired from the left basal ganglia and prefrontal cortex, and additional water-scaled Glx concentrations were acquired from standard PRESS spectra acquired from the pons. Spectra were analyzed with LCModel. The axial symptoms of PD were evaluated from subscales of the Unified Parkinson's Disease rating scale (MDS-UPDRS).

Results: PD patients demonstrated significantly higher GABA levels in the basal ganglia, which correlated with the degree of gait disturbance. Basal ganglia Glx levels and prefrontal GABA and Glx levels did not differ significantly between patient and control groups, but within the PD group prefrontal Glx levels correlated negatively with difficulties turning in bed. Results from an exploratory subgroup analysis indicate that the associations between GABA, Glx, and axial symptoms scores are typically more prominent in akinetic-rigid patients than in tremor-dominant patients.

Conclusion: Alterations in GABAergic and glutamatergic neurotransmission may contribute to some of the axial symptoms of PD.

Keywords: Parkinson disease, magnetic resonance spectroscopy, GABA, glutamate, basal ganglia, prefrontal cortex, gait, axial symptoms

OPEN ACCESS

Edited by:
Lars Ersland, Haukeland University Hospital, Norway

Reviewed by:
Mark Mikkelsen, Johns Hopkins University, United States
Fabiana Novellino, Consiglio Nazionale Delle Ricerche (CNR), Italy

***Correspondence:**
Ruth L. O'Gorman Tuura
Ruth.tuura@kispi.uzh.ch

Specialty section:
This article was submitted to Neurodegeneration, a section of the journal Frontiers in Neurology

Received: *18 May 2018*
Accepted: *07 September 2018*
Published: *26 September 2018*

Citation:
O'Gorman Tuura RL, Baumann CR and Baumann-Vogel H (2018) Beyond Dopamine: GABA, Glutamate, and the Axial Symptoms of Parkinson Disease. Front. Neurol. 9:806. doi: 10.3389/fneur.2018.00806

INTRODUCTION

Parkinson disease (PD) is a progressive neurodegenerative disorder thought to affect over 4 million patients worldwide (1). The core motor symptoms of PD include akinesia, rigidity, resting tremor, and postural and balance difficulties, but patients can also suffer from a broad spectrum of non-motor symptoms (2). While some of the motor symptoms can be improved by dopaminergic (e.g., levodopa) therapy, the non-motor symptoms and the "axial" motor symptoms, including difficulties with gait, posture, speech, swallowing, and postural stability, typically do not respond well to dopaminergic therapy (3). These axial symptoms have a severe, long-lasting negative impact on quality of life and have been identified as a top research priority by patients, family members, and carers affected by PD, second only to the overarching aim to find an effective cure (2).

The neural origin of the axial symptoms of PD is not well-understood, and treatment options are limited. However, converging evidence indicates that disruptions in other neurotransmitter systems beyond the dopamine system are present in PD and may underlie some of the non-motor and axial symptoms (4–6).

Two of the other major neurotransmitter systems implicated in basal ganglia regulation and in PD, namely the glutamate and γ-amino butyric acid (GABA) systems, can be probed non-invasively using magnetic resonance spectroscopy (MRS) (7). Previous MRS studies in PD have reported increased GABA in the pons, basal ganglia, and thalamus (8–10), decreased cortical glutamate (11), and an increased GABA/glutamate ratio in the substantia nigra (12). In other neurodegenerative disorders, altered GABA and glutamate levels have been linked to symptoms which are also present in PD, including cognitive impairment (13, 14) and depression (15). In mice, altered GABA and Glycine neurotransmission was observed to trigger the cardinal features of rapid eye movement sleep behavior disorder (RBD) (16), a premotor symptom of PD which may represent a biomarker for overall disease severity (17). However, few studies have examined altered GABA and glutamate levels in relation to PD symptomatology, and currently the link between alterations in the GABAergic and glutamatergic systems and the axial symptoms of PD remains unclear. The purpose of the present study was to examine the relationship between the axial symptoms of PD, GABA, and glutamate levels in the basal ganglia and prefrontal cortex, and glutamate levels in the pons. Based on previous reports, we hypothesized that patients with PD would show increased GABA levels in the basal ganglia and decreased glutamate in the prefrontal cortex and pons, and that more pronounced abnormalities in the GABA and glutamate levels would correlate positively with the severity of the axial symptoms of PD.

MATERIALS AND METHODS

Participants

The patient group consisted of 20 patients with PD (4 female, mean age 63 years, range 50–75) recruited from the Neurology Department of the University Hospital of Zürich, Switzerland (see **Table 1** for demographics). All 20 patients had bilateral impairment, and 9/20 patients were treated with levodopa without dopamine agonists, while 11/20 patients were treated with a combination of levodopa and dopamine agonists. Patients were enrolled consecutively. Seventeen healthy control participants (4 female, mean age 62 years, range 28–77) with no history of neurological or psychiatric illness were also recruited. All participants gave written and verbal informed consent to participate in the study, which was approved by the cantonal ethics committee of the Canton of Zürich, Switzerland.

MRI/MRS Acquisition and Analysis

Magnetic resonance imaging and spectroscopy data were acquired with a 3T GE MR750 scanner (GE Healthcare, Milwaukee, WI, USA), using an 8-channel receive-only head coil. On the day of the scan, patients were scanned at a time when their dopaminergic medication was wearing off, before their next dose could be taken. The MRI protocol included a 3D T1-weighted fast spoiled gradient echo (SPGR) scan (echo time (TE) = 3 ms, repetition time (TR) = 8 ms, inversion time (TI)=600 ms; voxel resolution = $1 \times 1 \times 1$ mm^3, flip angle=8°), used for localisation of the MRS voxels and correction of the GABA and glutamate levels for partial volume CSF contamination (18).

Single voxel PRESS spectra were acquired from a 3.4 mL ($15 \times 15 \times 15$ mm3) voxel in the pons, with TE = 35 ms, TR = 3000 ms, 128 spectral averages, and 16 unsuppressed water reference lines, resulting in a total scan time of 7 min, (see **Figure 1** for an illustration of the voxel positions and representative spectra).

Single-voxel GABA-edited spectra were acquired from a 30 mL voxel centered on the left basal ganglia using the MEGAPRESS method (19), with TE = 69 ms, TR = 1800 ms, 320 spectral averages (160 edit ON/OFF pairs), and an eight-step phase cycle. MEGA-editing was achieved with 16-ms Gaussian editing pulses applied at 1.9 and 7.5 ppm in alternate spectral lines. For each metabolite spectrum, 16 unsuppressed water reference lines were also acquired, resulting in a total acquisition time of 10 min. To achieve a consistent voxel position between participants, voxels were prescribed on an axial plane where the putamen was widest in the lateral (right-left) direction, such that the anterior and medial borders of the voxel were aligned with the anterior and medial margins of the head of the caudate nucleus.

Additional GABA-edited MEGAPRESS spectra were collected from a subset of $n = 31$ participants ($n = 16$ PD patients, $n = 15$ controls), using a 30 mL voxel in in the left prefrontal cortex, with TE = 69 ms, TR = 1800 ms, 320 spectral averages (160 edit ON/OFF pairs), and an eight-step phase cycle. MEGA-editing was achieved as described above for the basal ganglia. In order to achieve a consistent voxel position between participants, the voxel was localized according to a standard set of anatomical measurements. (20).

Spectra were analyzed with LCModel version 6.31-H (21). Edited MEGA-PRESS spectra were analyzed with a simulated basis set including basis spectra for GABA, N-acetyl aspartate (NAA), glutamate (Glu), Glutamine (Gln), glutathione, and N-acetyl aspartyl glutamate (NAAG), using the control parameter sptype=mega-press-3 to avoid mis-assignment of the spectral baseline to the GABA peak (22). Since no attempt was

TABLE 1 | Patient characteristics and MDS-UPDRS scores.

Patient	Disease duration (years)	PD Type	Most affected side	LED	MDS-UPDRS			
					I	II	III	IV
1	18	Akinetic rigid	Right	1500	22	14	31	8
2	14	Tremor-dominant	Right	1300	18	10	41	6
3	5	Tremor-dominant	Right	600	8	15	13	6
4	6	Tremor-dominant	Left	900	17	16	31	4
5	11	Akinetic rigid	Left	1550	15	14	46	9
6	11	Akinetic rigid	Right	1200	10	12	18	1
7	8	Tremor-dominant	Left	800	8	7	25	6
8	8	Akinetic rigid	Left	1500	11	10	27	10
9	16	Akinetic rigid	Right	950	12	14	26	10
10	9	Tremor-dominant	Left	800	13	17	21	8
11	5	Akinetic rigid	Left	750	11	17	26	8
12	11	Akinetic rigid	Left	1500	20	14	31	10
13	12	Akinetic rigid	Right	1550	7	17	33	6
14	8	Tremor-dominant	Left	450	12	14	20	10
15	3	Akinetic rigid	Left	650	23	11	32	0
16	10	Akinetic rigid	Right	850	14	10	21	9
17	12	Akinetic rigid	Right	900	3	5	17	5
18	12	Tremor-dominant	Left	1050	8	12	40	7
19	4	Tremor-dominant	Left	1600	13	15	31	7
20	2	Tremor-dominant	Left	775	15	5	29	6

made to quantify the co-edited macromolecule underlying the GABA peak in the edited MEGAPRESS spectra, the GABA concentrations should be considered to represent GABA+ rather than pure GABA.

PRESS spectra from the pons were analyzed using a standard GE basis set including basis spectra for Alanine, Aspartate, Creatine, GABA, Glucose, Gln, Glu, glycerophosphorylcholine, phosphorylcholine, lactate, myo-inositol, NAA, NAAG, Scyllo-inositol, and Taurine. For all pontine PRESS spectra the default LCModel baseline fit settings were used.

Metabolite concentrations were calculated in institutional units (I.U.) after referencing each metabolite signal to the unsuppressed water signal and correcting both the metabolite and water signals for partial volume CSF contamination within the voxel (18). Additional water and metabolite relaxation time corrections were not performed. Since our hypotheses focused on alterations in the GABA and glutamate systems, only the GABA and Glx (Glu+Gln) levels from the basal ganglia and prefrontal cortex, and the Glx levels from the pons were entered into the statistical analysis (see below for statistical methods).

Symptom Evaluation

Axial symptoms were evaluated from subscales of the Unified Parkinson's Disease rating scale (MDS-UPDRS) (23) including speech/dysarthria (2.1), swallowing (2.3), turning in bed (2.9), arising from a chair (3.9), freezing of gait (2.13, 3.11), gait (3.10), postural stability (3.12), and posture (3.13). Since several symptom scores pertain to gait disturbance, a summary score for the gait symptoms was derived by summing together the individual scores for items 2.13, 3.10, and 3.11, and an overall summary score of the axial symptoms was also derived by adding together the symptom scores from each of the axial subscales. The UPDRS scores were derived while the patients were in the ON medication state.

Statistical Analysis

GABA and Glx concentrations and symptom scores were tested for normality with a Shapiro-Wilk test. Group comparisons (PD vs. control) were assessed with a two-sided *t*-test for normally-distributed variables and a Mann-Whitney test for non-normally distributed variables. A non-parametric bivariate correlation (Spearman's rho) was used to investigate the association between GABA and Glx levels and axial symptom scores from the MDS-UPDRS. In the event of a significant group difference or correlation emerging for Glx, *post-hoc* tests were performed to ascertain if this difference or association was driven by Glu or Gln. Since the patient group included both tremor-dominant and akinetic-rigid PD patients who are known to demonstrate differences in the progression of axial motor symptoms, (24–26) the relationship between GABA and Glx levels and the overall axial summary score was evaluated in the tremor-dominant and akinetic-rigid subgroups separately, after dichotomising patients according to their motor signs at disease onset (27). In the event of a significant association between the axial summary score and neurotransmitter levels emerging in one or both of the

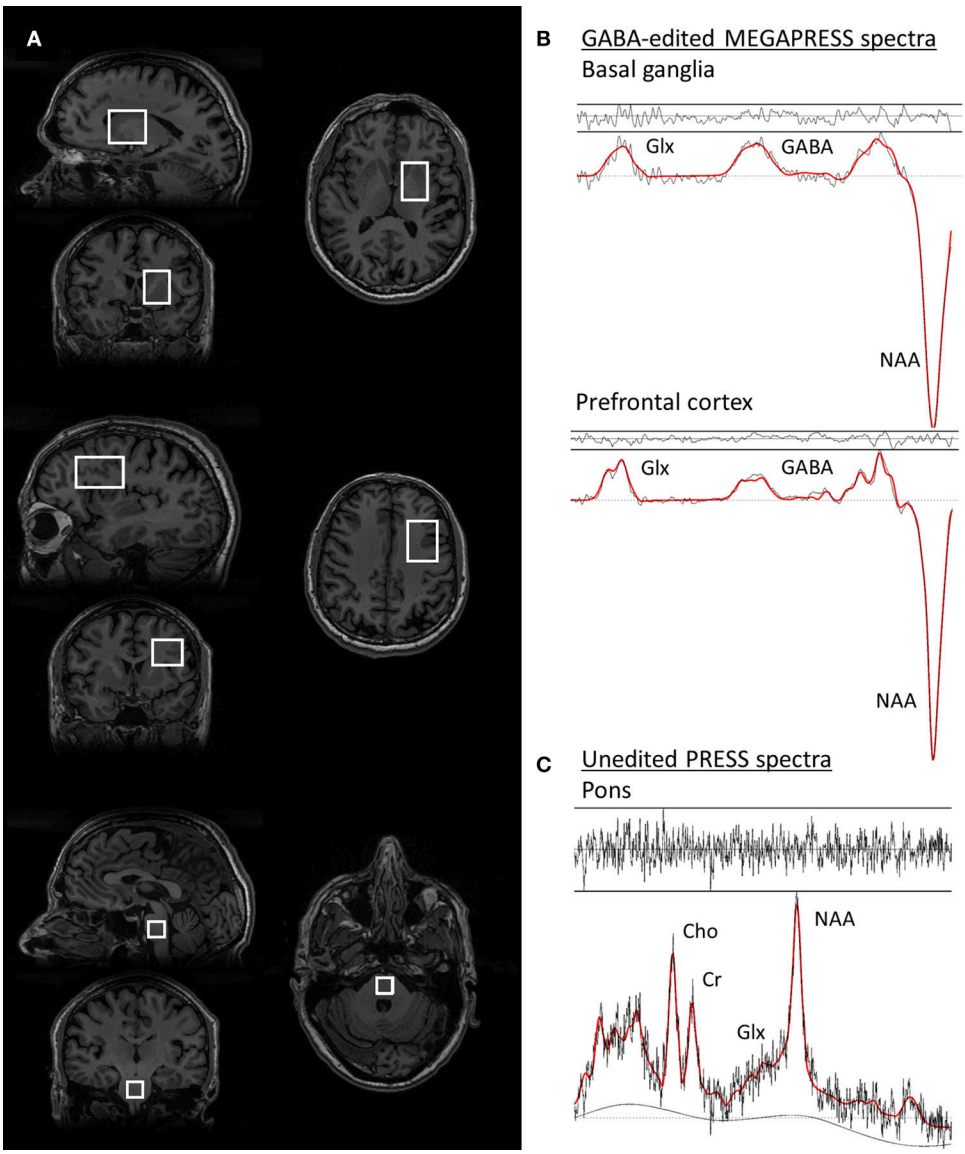

FIGURE 1 | Voxel positions and representative spectra from one PD patient. **(A)** voxel positions from the basal ganglia, prefrontal cortex, and pons voxels, respectively. **(B)** GABA-edited MEGAPRESS spectra from the basal ganglia (top) and prefrontal cortex (middle). The spectral data are plotted in black and the LCModel fit for each spectrum is overlaid in red. **(C)** PRESS spectrum from the pons, with the LCModel fit overlaid in red. For all spectra, the residuals of the fit are plotted above each spectrum.

subgroups, additional *post-hoc* correlations with the individual symptom scores were performed in the relevant subgroup(s) in order to ascertain which symptoms were likely to underly the observed association with neurotransmitter levels. In order to investigate the influence of medication on the association between neurotransmitter levels and symptom scores, additional *post-hoc* correlations were also performed for all significant associations between GABA, Glx, and symptom scores after controlling for the levodopa equivalent dose. All statistical analyses were performed with SPSS version 22, with a two-tailed significance threshold of $p < 0.05$. No correction was made for multiple comparisons.

RESULTS

Representative spectra from the pons, basal ganglia, and prefrontal cortex in one PD participant are shown in **Figure 1**, together with images depicting the voxel positions.

GABA-edited MEGAPRESS data was not collected from one patient with a lesion in the basal ganglia, and the basal ganglia Glx levels were excluded for one patient in whom an artifact was visible over the Glx doublet in the MEGA-PRESS subtraction spectrum.

Glx levels in the pons and GABA levels in the basal ganglia followed a normal distribution, but GABA and Glx levels in the

TABLE 2 | Demographic data and neurotransmitter levels for the PD and control groups.

	PD	Controls	PD vs. Control
Age (Median ± IQR)	62.9 ± 11.5	66.2 ± 12.4	$p = 0.563$
(Mean ± SD)	63.6 ± 6.8	62.5 ± 12.8	
Gender	16 M, 4 F	13 M, 4 F	$p = 0.798$
Left Basal Ganglia GABA§	4.61 ± 0.57	3.93 ± 0.75	$p = 0.005$*
Left Basal Ganglia Glx	8.27 ± 3.5	6.66 ± 2.0	$p = 0.069$
Left Prefrontal GABA	3.48 ± 0.90	2.96 ± 0.96	$p = 0.114$
Left Prefrontal Glx	8.19 ± 0.98	7.98 ± 0.84	$p = 0.114$
Pons Glx§	13.6 ± 4.02	14.2 ± 3.16	$p = 0.58$

§*Indicates a normally distributed variable, described by Mean ± SD.*
Data are summarized as median ± inter-quartile range and tested with a Mann-Whitney U test unless indicated otherwise. [MRS levels are given in institutional units (I.U.)].

prefrontal cortex and Glx levels in the basal ganglia were not normally distributed ($p < 0.05$, Shapiro–Wilk test). The axial symptom scores and the corresponding summary score were also not normally distributed ($p < 0.05$, Shapiro–Wilk test).

PD and control groups did not differ in terms of age or gender ($p > 0.5$, Mann–Whitney test, see **Table 2**). PD patients demonstrated increased GABA in the basal ganglia ($t = 2.874$, $p = 0.007$, 2-tailed t-test). After removal of one outlier in the PD group with a GABA level 6 standard deviations away from the mean, GABA levels in the basal ganglia remained significantly higher in the PD group ($t = 3.009$, $p = 0.005$, 2-tailed t-test). The corresponding Glx data for this outlier was also removed from further statistical analyses. No significant differences were observed between GABA and Glx levels in the prefrontal cortex or Glx levels in the basal ganglia and pons between the PD and control groups.

Significant associations between GABA and Glx concentrations and axial symptom scores are plotted in **Figure 2**. GABA levels in the left basal ganglia correlated positively with the gait summary score (Spearman's rho = 0.491, $p = 0.038$), as well as the individual gait (MDS 3.10) subscore (Spearman's rho = 0.495, $p = 0.037$) of the motor part of the MDS-UPDRS. Both correlations were present at trend level in the subgroup of akinetic-rigid patients (Gait summary score: Spearman's rho = 0.580, $p = 0.079$, MDS 3.10: Spearman's rho = 0.604, $p = 0.064$), but not in the tremor-dominant subgroup. For the summary score incorporating all the axial symptoms from the UPDRS, basal ganglia GABA levels showed a trend-level association in the full patient group (Spearman's rho = 0.441, $p = 0.067$), which was significant in the subgroup of akinetic rigid patients (Spearman's rho = 0.671, $p = 0.034$), but not in the subgroup of tremor-dominant patients (Spearman's rho = 0.345, $p = 0.403$). In the subgroup of akinetic-rigid patients, basal ganglia GABA levels were significantly correlated with difficulties arising from a chair (MDS 3.9, Spearman's rho = 0.838, p = 0.002 and with posture (MDS 3.13, Spearman's rho = 0.838, $p = 0.002$).

No significant correlations were observed between basal ganglia or pontine Glx levels and the axial symptom scores, but prefrontal Glx levels were negatively correlated with the turning in bed (MDS 2.9) subscore, both in the full patient group (Spearman's rho= −0.546, $p = 0.029$), and in the subgroup of akinetic-rigid patients (Spearman's rho = −0.686, $p = 0.041$). Prefrontal GABA levels were negatively correlated with the postural stability score (MDS 3.12, Spearman's rho = - 0.842, $p = 0.004$), in the akinetic-rigid subgroup only.

The correlations between basal ganglia GABA and the gait subscore and summary score became non-significant after controlling for the levodopa equivalent dose (Spearman's rho=0.324/0.341, $p = 0.224/0.196$ for the gait summary score and subscore, respectively), as did the correlation between basal ganglia GABA levels and the axial symptom summary score in the akinetic-rigid subgroup (Spearman's rho =0.403, $p = 0.322$) However, correlations between basal ganglia GABA levels and difficulties arising from a chair (MDS 3.9) remained significant in the akinetic-rigid subgroup after controlling for levodopa equivalent dose (Spearman's rho = 0.845, $p = 0.008$), as did the correlation between basal ganglia GABA and problems with posture (MDS 3.13, Spearman's rho = 0.845, $p = 0.008$). The correlation between prefrontal Glx and turning in bed diminished to trend level after controlling for levodopa equivalent dose (Spearman's rho = −0.491, $p = 0.074$), but the correlation between prefrontal GABA and difficulties with postural stability (MDS 3.12) in the akinetic-rigid subgroup remained significant after controlling for the levodopa equivalent dose (Spearman's rho = −0.76, $p = 0.047$).

DISCUSSION

Gait and locomotion, turning in bed, arising from a chair, and postural stability all depend on efficient sensorimotor integration (28, 29), which is affected in PD (30–32). The basal ganglia act as an important hub for sensorimotor integration (33, 34) and descending basal ganglia projections to the midbrain have been reported to play an important role in gait and postural control (35, 36). One of the ways in which the basal ganglia are thought to influence sensorimotor integration is by gating or controlling the access of sensory information to motor neurons, via a balance of neurotransmitter activity (30, 37, 38). In PD, the motor systems can become hypo-excitable following an increased inhibition of sensory inputs to the basal ganglia, leading to a diminished motor response to certain sensory stimuli (30). This diminished responsiveness to sensory stimuli is thought to underly the observed difficulties experienced by PD patients in regulating the amplitude of movements in the absence of external visual or auditory cues, when they are dependent on sensory feedback for accurate motor control, (31, 32, 38) and may also contribute to the axial symptoms.

In the present study, the observed link between increased GABA levels in the left basal ganglia in PD patients and the degree of gait disturbance (**Figure 2**) may be associated with an over-inhibition of the processing of sensory inputs necessary for maintaining posture and initiating locomotion. This observation is consistent with the reported role of GABAergic outputs from the basal ganglia in the control of posture and locomotion (35, 39, 40). However, since locomotion can be initiated by stimulation

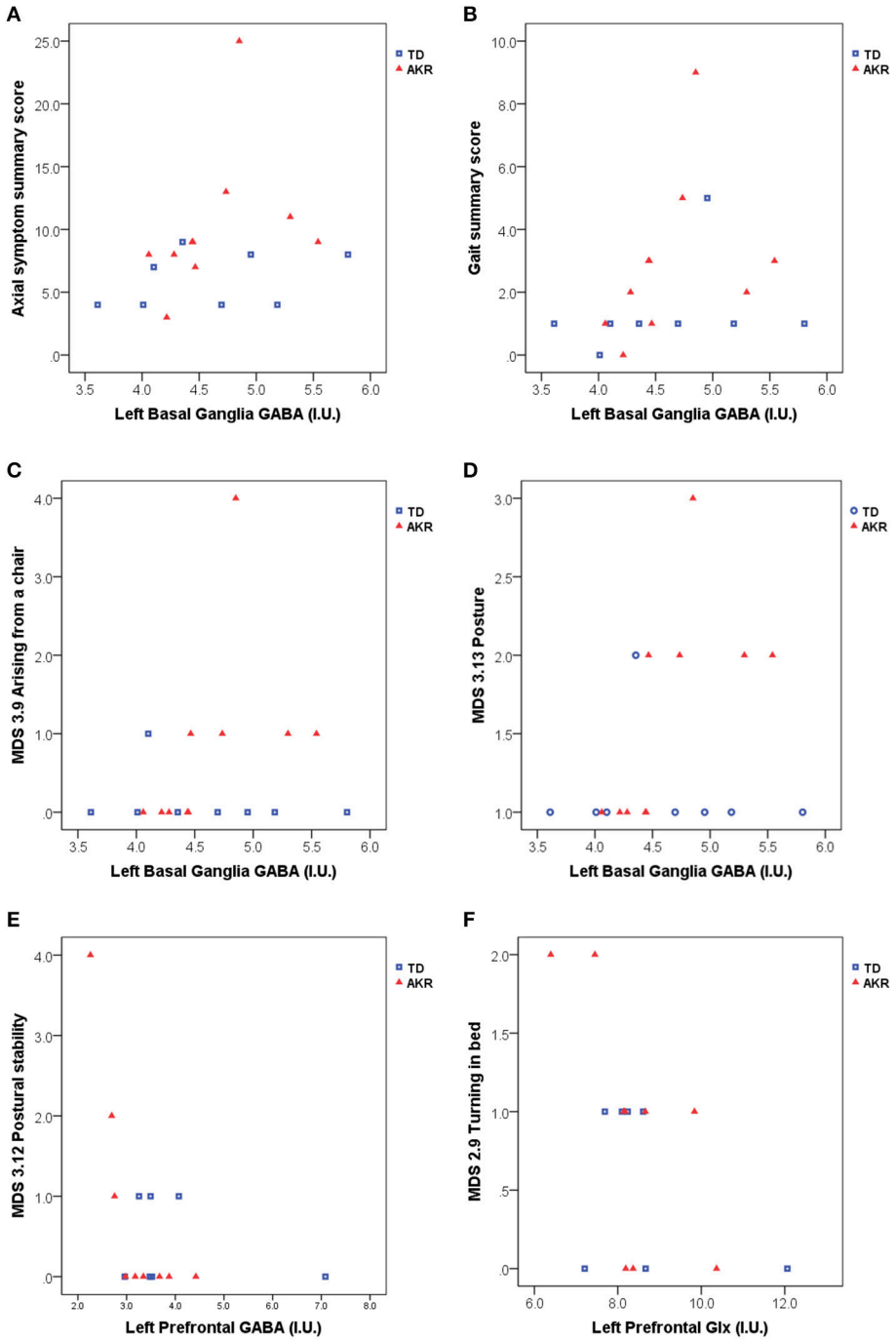

FIGURE 2 | Basal ganglia GABA, prefrontal GABA and prefrontal Glx appear to be associated with axial symptom scores including gait and postural difficulties assessed with the MDS-UPDRS. **(A)** left basal ganglia GABA levels were significantly associated with higher axial symptom summary scores in akinetic-rigid (AKR) patients ($p = 0.034$), but not in tremor-dominant (TD) patients ($p = 0.403$), while the full patient group showed a trend-level association between basal ganglia GABA and axial summary scores ($p = 0.067$). **(B)** Elevated GABA levels were also associated higher gait summary scores ($p = 0.038$, full group). In the AKR subgroup, increased GABA levels were significantly positively associated with difficulties arising from a chair (**C**, $p = 0.002$) and difficulties with posture (**D**, $p = 0.002$). Left prefrontal GABA levels were negatively associated with postural stability in the AKR subgroup ($p = 0.004$, **E**), while left prefrontal Glx levels were negatively associated difficulties turning in bed, both in the full group ($p = 0.029$, **F**), and in the AKR subgroup ($p = 0.041$, **F**).

of the midbrain locomotor region, (36) one would expect corresponding neurotransmitter abnormalities to be observed in the pons, related to problems with gait. In the present study, we were not able to measure GABA in the pons due to the large voxel size required for GABA measurement with MEGA-PRESS, but we did not observe any apparent relationship between

the pontine Glx concentrations (from standard PRESS) and problems with gait. However, since the PRESS voxel volume (3.4 mL) is large in comparison to the size of the midbrain locomotor region or the peduculopontine nucleus of the pons, two of the pontine regions implicated in gait control and muscle tone regulation, the lack of an apparent relationship between pontine Glx and posture or gait symptoms may be due to a lack of regional specificity of the pontine MRS measurement. Future studies at higher field strengths (e.g., 7T), where smaller voxel volumes can be used and where GABA can be quantified without the need for spectral editing, may be able to extend the present findings to clarify the link between gait difficulties and pontine neurotransmitter levels.

In the subgroup analysis, the observed link between basal ganglia GABA levels and the gait and axial summary scores seemed to be mostly driven by GABA and symptom changes in the akinetic-rigid subgroup of patients rather than the tremor-dominant patients. Longitudinal studies have shown that the akinetic-rigid subtype of PD presents a risk factor for greater progression of the motor symptoms, including freezing of gait and other axial symptoms. (24–26) Akinetic-rigid PD patients have also been shown to demonstrate differences in structural and functional connectivity in comparison to tremor-dominant patients, (41–43) and differences in iron deposition between the subtypes indicates that different pathological mechanisms may underly the observed differences in symptom progression (44). In light of the small group sizes, the subgroup analysis in the present study should be considered exploratory, and we hope these results can be replicated in a larger sample. Given the evidence for differences in brain structure and function as well as symptom progression in different subtypes of PD, it would be interesting to examine differences in the metabolite profile, including neurotransmitter changes, between akinetic-rigid and tremor-dominant PD patients in more detail in a larger cohort.

While basal ganglia GABA levels appeared to be related to gait difficulties, prefrontal Glx levels correlated negatively with difficulties turning in bed (**Figure 2**), and prefrontal GABA levels correlated negatively with postural stability, in the akinetic-rigid subgroup. The negative correlation between prefrontal Glx and symptom scores would be consistent with previous reports of decreased cortical Glx in PD, (11) under the assumption that patients more severely affected by axial symptoms like turning in bed would have lower prefrontal Glx levels. However, since in the present study no significant differences in prefrontal Glx were observed at the group level, the apparent correlation between frontal Glx and symptom scores seen in the present study cannot be interpreted in the context of abnormal Glx levels in the patient group. The link between prefrontal GABA and posture is also consistent with the putative role of prefrontal and parietal cortical regions in maintaining postural equilibrium, (45) but should also be interpreted with caution in light of the lack of a significant difference in prefrontal GABA between the patient and control groups. It is possible that these associations with individual symptom scores may be affected by outliers, given the small group sizes and the limited distribution of symptoms in some domains. These results should therefore be considered with caution until they can be replicated in a larger sample.

Since the symptom scores were assessed while patients were in the ON medication state, while the MRS was performed just before the next dose was due and thus rather in an OFF state, medication effects could potentially confound the comparison between GABA and Glx levels and the axial symptom scores. While most of the axial symptoms do not typically respond well to levodopa, dopamine replacement therapy has been reported to reduce freezing of gait in patients with PD, (46) and in the present sample the levodopa equivalent dose showed a trend-level association with basal ganglia GABA ($p = 0.09$, Spearman's rho). The effect of levodopa on freezing of gait may explain why the correlations between basal ganglia GABA levels and the gait and axial symptom summary scores diminished in significance after controlling for the levodopa equivalent dose, particularly in akinetic-rigid patients. In contrast, the association between neurotransmitter levels and other symptom scores such as rising from a chair, turning in bed, posture, and postural stability, seemed relatively independent of levodopa effects, but in addition to levodopa 11 patients were additionally medicated with dopamine agonists. Previous studies in children with attention deficit hyperactivity disorder (ADHD) have reported that treatment with dopamine agonists like methylphenidate can reduce striatal Glx levels (47), although methylphenidate did not appear to influence frontal Glx levels, (47) and another study of medication-naïve and medicated adults with ADHD failed to find differences in Glx related to medication status (48). However, since treatment with dopamine agonists or other medications may introduce additional variability into the Glx and GABA signals measured MRS, it would be instructive to clarify the effects of dopaminergic and other medications on the GABA and Glx levels in a future study, where the cohort of PD patients is sufficiently large to enable separation into subgroups according to medication status.

CONCLUSION

MRS offers a unique opportunity to study the complex interplay between excitatory and inhibitory neurotransmitter activity both within and outside the motor network. The present pilot study provides evidence of a link between alterations in GABA and glutamate levels and the axial symptoms of Parkinson's disease, lending important insight into the neural origin of these symptoms, and opening up potential avenues for treatment.

AUTHOR CONTRIBUTIONS

RO: conception, organization, and execution of research project, design and execution of data analysis, and writing of the first draft of the manuscript. CB: conception of Research Project, design and review and critique of data analysis, and review and critique of the manuscript. HB-V: conception, organization, and execution of research project, design and review and critique of data analysis, and review and critique of the manuscript.

REFERENCES

1. Dorsey ER, Constantinescu R, Thompson JP, Biglan KM, Holloway RG, Kieburtz F. Projected number of people with Parkinson disease in the most populous nations, 2005 through 2030. *Neurology* (2007) 68:384–6. doi: 10.1212/01.wnl.0000247740.47667.03
2. Deane KH, Flaherty H, Daley DJ, Pascoe R, Penhale B, Clarke CE. et al. Priority setting partnership to identify the top 10 research priorities for the management of Parkinson's disease. *BMJ Open* (2014) 4:e006434. doi: 10.1136/bmjopen-2014-006434
3. Jankovic J, and Aguilar LG. Current approaches to the treatment of Parkinson's disease. *Neuropsychiatr Dis Treat* (2008) 4:743–57. doi: 10.2147/NDT.S2006
4. Bonnet AM. Involvement of non-dopaminergic pathways in Parkinson's disease. *CNS Drugs* (2000) 13:351–64. doi: 10.2165/00023210-200013050-00005
5. Barone P. Neurotransmission in Parkinson's disease: beyond dopamine. *Eur J Neurol*. (2010) 17:364–376. doi: 10.1111/j.1468-1331.2009.02900.x
6. Karachi C, Grabli D, Bernard FA, Tande D, Wattiez N, Belaid H. et al. Cholinergic mesencephalic neurons are involved in gait and postural disorders in Parkinson disease. *J Clin Invest*. (2010) 120:2745–54. doi: 10.1172/JCI42642
7. Rae CD. A guide to the metabolic pathways and function of metabolites observed in human brain 1H magnetic resonance spectra. *Neurochem Res*. (2014) 39:1–36. doi: 10.1007/s11064-013-1199-5
8. Emir UE, Tuite PJ, Oz G. Elevated pontine and putamenal GABA levels in mild-moderate Parkinson disease detected by 7 tesla proton MRS. *PLoS ONE* (2012) 7:e30918. doi: 10.1371/journal.pone.0030918
9. Dharmadhikari S, Ma R, Yeh CL, Stock AK, Snyder S, Zauber SE, et al. Striatal and thalamic GABA level concentrations play differential roles for the modulation of response selection processes by proprioceptive information. *Neuroimage* (2015) 120:36–42. doi: 10.1016/j.neuroimage.2015.06.066
10. O'Gorman Tuura RL, Baumann CR, Baumann-Vogel H. Neurotransmitter activity is linked to outcome following subthalamic deep brain stimulation in Parkinson's disease. *Parkins Relat Disord*. (2018) 50:54–60. doi: 10.1016/j.parkreldis.2018.02.014
11. Griffith, HR, Okonkwo OC, O'Brien T, Hollander JA. Reduced brain glutamate in patients with Parkinson's disease. *NMR Biomed*. (2008) 21:381–7. doi: 10.1002/nbm.1203
12. Oz G, Terpstra M, Tkac I, Aia P, Lowary J, Gruetter PJ. Proton MRS of the unilateral substantia nigra in the human brain at 4 tesla: detection of high GABA concentrations. *Magn Reson Med*. (2006) 55:296–301. doi: 10.1002/mrm.20761
13. Foy CM, Daly EM, Glover A, O'Gorman R, Simmons A, Murphy DG. et al. Hippocampal proton MR spectroscopy in early Alzheimer's disease and mild cognitive impairment. *Brain Topogr*. (2011) 24:316–22. doi: 10.1007/s10548-011-0170-5
14. Riese F, Gietl A, Zolch N, Henning A, O'Gorman R, Kalin AM, et al. Posterior cingulate gamma-aminobutyric acid and glutamate/glutamine are reduced in amnestic mild cognitive impairment and are unrelated to amyloid deposition and apolipoprotein E genotype. *Neurobiol Aging* (2015) 36:53–9. doi: 10.1016/j.neurobiolaging.2014.07.030
15. Kalueff AV, Nutt DJ. Role of GABA in anxiety and depression. *Depress Anxiety* (2007) 24:495–517. doi: 10.1002/da.20262
16. Brooks PL, Peever JH. Impaired GABA and glycine transmission triggers cardinal features of rapid eye movement sleep behavior disorder in mice. *J Neurosci*. (2011)31:7111–21. doi: 10.1523/JNEUROSCI.0347-11.2011
17. Chahine LM, Kauta SR Daley JT, Cantor CR, Dahodwala N. Surface EMG activity during REM sleep in Parkinson's disease correlates with disease severity. *Parkins Relat Disord*. (2014) 20:766–71. doi: 10.1016/j.parkreldis.2014.04.011
18. Chowdhury FA, O'Gorman RL, Nashef L, Elwes RD, Edden RA, Murdoch JB. et al. Investigation of glutamine and GABA levels in patients with idiopathic generalized epilepsy using megapress. *J Magn Reson Imaging* (2015) 41:694–99. doi: 10.1002/jmri.24611
19. Mescher M, Merkle H, Kirsch J, Garwood M, Gruetter R. Simultaneous *in vivo* spectral editing and water suppression. *NMR Biomed*. (1998) 11:266–72. doi: 10.1002/(SICI)1099-1492(199810)11:6<266::AID-NBM530>3.0.CO;2-J
20. Michels L, Martin E, Klaver P, Edden R, Zelaya F, LythgoeDJ. et al. Frontal GABA levels change during working memory. *PLoS ONE* (2012) 7:e31933. doi: 10.1371/journal.pone.0031933
21. Provencher SW. Estimation of metabolite concentrations from localized *in vivo* proton NMR spectra. *Magn Reson Med*. (1993) 30:672–9. doi: 10.1002/mrm.1910300604
22. Mullins PG, McGonigle DJ, O'Gorman RL, Puts NA, Vidyasagar R, Evans CJ, et al. Current practice in the use of MEGA-PRESS spectroscopy for the detection of GABA. *Neuroimage* (2014) 86:43–52. doi: 10.1016/j.neuroimage.2012.12.004
23. Goetz CG, Tilley BC, Shaftman SR, Stebbins GT, Fahn S, Martinez-Martin P. et al. Movement disorder society-sponsored revision of the unified parkinson's disease rating scale (MDS-UPDRS): scale presentation and clinimetric testing results. *Mov Disord*. (2008) 23:2129–70. doi: 10.1002/mds.22340
24. Post B, Merkus MP, de Haan RJ, Speelman JD. Prognostic factors for the progression of Parkinson's disease: a systematic review. *Mov Disord*. (2007) 22:1839–51; quiz 1988. doi: 10.1002/mds.21537
25. Reinoso G, Allen JC, Au WL, Seah SH, Tay KY, Tan LC. Clinical evolution of Parkinson's disease and prognostic factors affecting motor progression: 9-year follow-up study. *Eur J Neurol*. (2015) 22:457–63. doi: 10.1111/ene.12476
26. Zhang H, Yin X, Ouyang Z, Chen J, Zhou S, Zhang C. et al. A prospective study of freezing of gait with early Parkinson disease in Chinese patients. *Medicine (Baltimore)* (2016) 95:e4056. doi: 10.1097/MD.0000000000004056
27. Baumann CR, Held U, Valko PO, Wienecke M, Waldvogel D. Body side and predominant motor features at the onset of Parkinson's disease are linked to motor and nonmotor progression. *Mov Disord*. (2014) 29:207–13. doi: 10.1002/mds.25650
28. Peterka RJ. Sensorimotor integration in human postural control. *J Neurophysiol*. (2002) 88:1097–118. doi: 10.1152/jn.2002.88.3.1097
29. Hickok G, Houde J, Rong F. Sensorimotor integration in speech processing: computational basis and neural organization. *Neuron* (2011) 69:407–22. doi: 10.1016/j.neuron.2011.01.019
30. Schneider JS, Diamond SG, Markham CH. Deficits in orofacial sensorimotor function in Parkinson's disease. *Ann Neurol*. (1986) 19:275–82. doi: 10.1002/ana.410190309
31. Lewis GN, Byblow WD. Altered sensorimotor integration in Parkinson's disease. *Brain* (2002) 125(Pt. 9):2089–99. doi: 10.1093/brain/awf200
32. Abbruzzese G, Berardelli A. Sensorimotor integration in movement disorders. *Mov Disord*. (2003) 18:231–40. doi: 10.1002/mds.10327
33. De Long MR, Alexander GE. *The Basal Ganglia and Sensorimotor Integration*. Berlin: Springer Berlin Heidelberg (1987).
34. Albin RL, Young AB, Penney JB. The functional anatomy of basal ganglia disorders. *Trends Neurosci*. (1989) 12:366–75. doi: 10.1016/0166-2236(89)90074-X
35. Takakusaki K, Habaguchi T, Ohtinata-Sugimoto J, Saitoh K, Sakamoto T. Basal ganglia efferents to the brainstem centers controlling postural muscle tone and locomotion: a new concept for understanding motor disorders in basal ganglia dysfunction. *Neuroscience* (2003) 119:293–308. doi: 10.1016/S0306-4522(03)00095-2
36. Hikosaka O. GABAergic output of the basal ganglia. *Prog Brain Res*. (2007) 160:209–26. doi: 10.1016/S0079-6123(06)60012-5
37. Schneider JS, Denaro FJ, Lidsky TI. Basal ganglia: motor influences mediated by sensory interactions. *Exp Neurol*. (1982) 77:534–43. doi: 10.1016/0014-4886(82)90226-6
38. Adamovich SV, Berkinblit MB, Hening W, Sage J, Poizner H. The interaction of visual and proprioceptive inputs in pointing to actual and remembered targets in Parkinson's disease. *Neuroscience* (2001) 104:1027–1041. doi: 10.1016/S0306-4522(01)00099-9
39. Garcia-Rill E. The basal ganglia and the locomotor regions. *Brain Res*. (1986) 396:47–63. doi: 10.1016/0165-0173(86)90009-3
40. Takakusaki K, Saitoh K, Harada H, Kashiwayanagi M. Role of basal ganglia-brainstem pathways in the control of motor behaviors. *Neurosci Res*. (2004) 50:137–51. doi: 10.1016/j.neures.2004.06.015
41. Lewis MM, Du G, Sen S, Kawaguchi A, Truong Y, Lee S, et al. Differential involvement of striato- and cerebello-thalamo-cortical pathways in tremor- and akinetic/rigid-predominant Parkinson's disease. *Neuroscience* (2011) 177:230–9. doi: 10.1016/j.neuroscience.2010.12.060

42. Guan X, Xuan M, Gu Q, Xu X, Huang P, Wang N, et al. Influence of regional iron on the motor impairments of Parkinson's disease: a quantitative susceptibility mapping study. *J Magn Reson Imaging* (2017) 45:1335–42. doi: 10.1002/jmri.25434
43. Luo C, Song W, Chen Q, Yang J, Gong Q, Shang HF. White matter microstructure damage in tremor-dominant Parkinson's disease patients. *Neuroradiology* (2017) 59:691–8. doi: 10.1007/s00234-017-1846-7
44. Jin L, Wang J, Jin H, Fei G, Zhang Y, Chen W, et al. Nigral iron deposition occurs across motor phenotypes of Parkinson's disease. *Eur J Neurol*. (2012) 19:969–76. doi: 10.1111/j.1468-1331.2011.03658.x
45. Jacobs, J. V and Horak, F. B. Cortical control of postural responses. *J Neural Transm (Vienna)* (2007) 114:1339–48. doi: 10.1007/s00702-007-0657-0
46. Schaafsma JD, Balash Y, Gurevich T, Bartels AL, Hausdorff JM, Giladi N. Characterization of freezing of gait subtypes and the response of each to levodopa in Parkinson's disease. *Eur J Neurol*. (2003) 10:391–98. doi: 10.1046/j.1468-1331.2003.00611.x
47. Carrey N, MacMaster FP, Sparkes SJ, Khan SC, Kusumakar V. Glutamatergic changes with treatment in attention deficit hyperactivity disorder: a preliminary case series. *J Child Adolesc Psychopharmacol*. (2002) 12:331–36. doi: 10.1089/104454602762599871
48. Maltezos S, Horder J, Coghlan S, Skirrow C, O'Gorman R, Lavender, T. J. et al. Glutamate/glutamine and neuronal integrity in adults with ADHD: a proton MRS study. *Transl Psychiatry* (2014) 4:e373. doi: 10.1038/tp.2014.11

Conflict of Interest Statement: The authors declare that the research was conducted in the absence of any commercial or financial relationships that could be construed as a potential conflict of interest.

frontiers in Neurology

BRIEF RESEARCH REPORT
published: 14 December 2018
doi: 10.3389/fneur.2018.01086

Decreased Gray Matter Volume of Right Inferior Parietal Lobule Is Associated With Severity of Mental Disorientation in Patients With Mild Cognitive Impairment

Ayame Oishi[1,2]*, *Takao Yamasaki*[1,2], *Ayako Tsuru*[1], *Motozumi Minohara*[1] and *Shozo Tobimatsu*[2]

[1] Department of Neurology, Minkodo Minohara Hospital, Fukuoka, Japan, [2] Department of Clinical Neurophysiology, Neurological Institute, Graduate School of Medical Sciences, Kyushu University, Fukuoka, Japan

OPEN ACCESS

Edited by:
Pravat K. Mandal, National Brain Research Centre (NBRC), India

Reviewed by:
Ying Han, Capital Medical University, China
Kiyotaka Nemoto, University of Tsukuba, Japan

***Correspondence:**
Ayame Oishi
aooishi@med.kyushu-u.ac.jp

Specialty section:
This article was submitted to Applied Neuroimaging, a section of the journal Frontiers in Neurology

Received: *17 June 2018*
Accepted: *27 November 2018*
Published: *14 December 2018*

Citation:
Oishi A, Yamasaki T, Tsuru A, Minohara M and Tobimatsu S (2018) Decreased Gray Matter Volume of Right Inferior Parietal Lobule Is Associated With Severity of Mental Disorientation in Patients With Mild Cognitive Impairment. Front. Neurol. 9:1086. doi: 10.3389/fneur.2018.01086

Background: Mental disorientation in time, space, and with respect to people is common in patients with Alzheimer's disease (AD) and mild cognitive impairment (MCI). Recently, a high-resolution functional MRI (fMRI) study revealed that the inferior parietal lobule (IPL) and precuneus are important regions related to mental orientation in healthy individuals. We hypothesized that the IPL and/or precuneus are crucial regions for mental disorientation in patients with amnestic MCI (aMCI). Therefore, our aim was to assess our hypothesis in these patients using voxel-based morphometry (VBM).

Methods: Fifteen patients with aMCI participated. The Neurobehavioral Cognitive Status Examination (COGNISTAT) as well as the Mini-Mental State Examination (MMSE) were used to evaluate mental disorientation. Subsequently, we used VBM analysis to identify brain regions that exhibited gray matter (GM) volume loss associated with mental disorientation. Based on our hypothesis, four brain regions (bilateral IPLs and precuneus) were selected as regions of interest (ROIs).

Results: We found a significant decreased GM volume in the right IPL, which was correlated with lower orientation scores on the COGNISTAT. In contrast, GM volume in other ROIs did not show a significant positive correlation with mental disorientation. Regarding the MMSE, no significant reduction in GM associated with decline in orientation were observed in any ROI.

Conclusion: We found the significant relationship between low GM volume in the right IPL and severity of mental disorientation. Therefore, the right IPL is responsible for mental disorientation in aMCI.

Keywords: mild cognitive impairment, mental disorientation, Neurobehavioral Cognitive Status Examination (COGNISTAT), Mini-Mental State Examination, inferior parietal lobule, voxel-based morphometry, magnetic resonance imaging

INTRODUCTION

Alzheimer's disease (AD) is a progressive neurodegenerative disorder and the most common form of dementia in older people. It is characterized by numerous cognitive deficits including memory disturbance, disorientation, and visuospatial deficits (1, 2). In contrast, mild cognitive impairment (MCI) is an intermediate state between normal aging and dementia (3) and is classified into two subtypes: amnestic and non-amnestic MCI. Amnestic MCI (aMCI) is widely viewed as a preclinical stage of AD (4).

Orientation in time, space, and to people is fundamental for one's own behavior. Recently, a high-resolution functional magnetic resonance imaging (fMRI) study has revealed that common cortical activity related to orientation for time, space and people is mainly localized in the IPL and precuneus in healthy people (5). AD is a pathology known to preferentially involve temporo-parietal association areas, and this is true even in MCI (6). Nevertheless, which brain regions are associated with disorientation is still unclear in aMCI, even though disorientation is a major symptom.

Mini-Mental State Examination (MMSE) is the most commonly used tool for assessing cognitive functions including orientation to time (5 points) and space (5 points) for clinical and research purposes. However, it does not assess, orientation to people. Recently, the Neurobehavioral Cognitive Status Examination (COGNISTAT) has been introduced as a way to evaluate cognitive functions. COGNISTAT is a short cognitive battery that contains subtests for orientation to people (2 points), time (6 points), and space (4 points). Furthermore, AD patients exhibited significantly lower scores on many subtests of COGNISTAT compared with healthy older individuals (7). The total number of impaired scores on COGNISTAT is also useful for discriminating AD from non-AD dementia (7). Thus, COGNISTAT is likely a better tool than MMSE for studying the core brain regions associated with overall mental disorientation (including time, space, and people) in aMCI and AD.

Voxel-based morphometry (VBM) is a brain imaging method that can measure gray matter (GM) volume (GMV). The results can be used to assess the relationship between GMV and scores on neuropsychological tests related to various neurodegenerative disorders (8, 9). Therefore, VBM can reveal which brain regions are related to disorientation in aMCI and AD. The aim of this study was to use VBM to identify the brain regions associated with overall mental disorientation in aMCI using neuropsychological tests (COGNISTAT and MMSE). Based on the recent fMRI finding showing the important role of the IPL and precuneus on orientation in healthy humans (5), we tested the hypothesis that the IPL and/or precuneus are brain regions crucial for overall mental disorientation in aMCI.

MATERIALS AND METHODS

We analyzed data from the orientation subtests of COGNISTAST and MMSE (Japanese versions) and from high-resolution three-dimensional (3D) T1-weighted MRI images obtained from 15 aMCI patients who visited the Memory Clinic (outpatient dementia service) at the Minohara Hospital. The protocol for the present study was approved by the internal ethics review boards of Minohara Hospital.

Patients

We retrospectively reviewed the medical records of 15 aMCI patients (9 females; age: 63–84 [mean: 75.3 ± 6.8] years; education: 9–16 [mean: 12.7 ± 2.0] years) from their first visit until September 2017. At the first visit, all patients underwent clinical neurological examinations by an experienced neurologist (T.Y.). Neuropsychological assessments were also performed by a clinical psychologist (A.T.), including the administration of COGNISTAT and MMSE, the delayed recall of logical memory on the Wechsler Memory Scale-Revised (delayed LM WMS-R), the Clinical Dementia Rating (CDR) scale, and the Geriatric Depression Scale (GDS). Furthermore, all patients completed electroencephalography, MRI, single photon emission computed tomography (SPECT), and standard laboratory tests. Inclusion criteria for aMCI followed the criteria of the Japanese Alzheimer's Disease Neuroimaging Initiative (10).

MRI Acquisition and Analysis

T1-weighted 3D sagittal images were acquired using a 1.5-Tesla MRI scanner (MRT200PP3, Toshiba Medical Systems Corporation, Japan). The acquisition parameters were as follows; repetition time = 13.5 ms; echo time = 5.5 ms; flip angle = 20°; field of view = 220 mm; acquisition matrix = 256 × 256, and slice thickness = 1.5 mm.

T1 images were processed using the VBM in SPM12 (Functional Imaging Laboratory, University College London, UK) running on MATLAB R2015b (The Mathworks, Inc., USA). In the segmentation, registration, normalization and modulation process, we used default settings for all parameters but "Preserve" was changed from "Preserve Concentrations" to "Preserve Amount" for converting to volume. The images were segmented according to tissue type into GM, white matter (WM), and cerebrospinal fluid images (CSF), and non-tissue types (bones, soft tissue, and air). Then, the Diffeomorphic Anatomical Registration using Exponentiated Lie Algebra (DARTEL) tool box in SPM12 for registration, normalization, and modulation. DARTEL templates were created from all the present data (11). The registered images were transformed to Montreal Neurological Institute (MNI) space. Finally, the normalized and modulated images were smoothed with 8-mm full width half maximum Gaussian kernel and analyzed with SPM12 software. The volumes of the different tissue classes and the total intracranial volume (TIV, sum of GM, WM, and CSF) were calculated using a MATLAB script (http://www0.cs.ucl.ac.uk/staff/g.ridgway/vbm/get_totals.m).

Statistical analysis of GMV data was performed using SPM12. To test our hypothesis that the IPL and/or precuneus are important regions for disorientation in aMCI, four brain regions (bilateral IPLs and precuneus) were selected as regions of interest (ROIs). These ROIs were based on the anatomically defined ROIs in the WFU PickAtlas toolbox (12). For each ROI, small volume correction was performed (voxel-level FWE corrected, $p < 0.05$) with TIV as a covariate. Furthermore, for the peak MNI

coordinate within each ROI, Pearson's correlation coefficient was calculated to evaluate the relationship between the GMV resulting from SPM12 analysis to extract raw voxel values within each ROI (13) and orientation scores on COGNISTAT and MMSE. We also adjusted the *p*-values to determine the effects of age, sex, and length of education for COGNISTAT and MMSE analyses, and additionally total MMSE score for COGNISTAT analysis. The difference of GMV loss associated with orientation scores between converters and non-converters were compared by the two-sample *t*-test. Further, a *post-hoc* statistical power analysis was conducted using G*power 3.1.9.2 [power (1-β)> 0.8 was generally acceptable] (14).

RESULTS

Progression From MCI to AD

During the follow-up period (mean 19 ± 17 months), 10 of 15 patients who were diagnosed with aMCI converted to probable AD on the basis of medical records, neurological evaluation, or interviews.

Neuropsychological Tests

The mean score on the orientation subtest of COGNISTAT was 10.6 ± 1.5 (full = 12, higher scores indicate better orientation). For the MMSE, the mean scores of total and orientation subtest were 25.8 ± 2.3 (full = 30) and 8.9 ± 1.1 (full = 10), respectively. The mean score on the Delayed LM WMS-R was 2.8 ± 2.3 (full = 25), and that for the GDS was 4.4 ± 3.1 (normal < 6). The mean CDR score was 0.5 (range = 0–3).

VBM Analysis

Regarding COGNISTAT, we found a regional cluster (15, 16) that exhibited a significant positive correlation between GMV and orientation scores in the right IPL. In this ROI, the peak location (MNI coordinate) was $x = 45$, $y = -48$, $z = 21$ (cluster size = 15 voxels; voxel-level FWE corrected, $p < 0.05$, (1-β) = 0.949; **Figure 1A**). The correlation coefficient (r) between GMV in the right IPL and the orientation scores was 0.63 (**Figure 1B**), which suggested the positive correlation. Although there was no statistically significant difference after adjusting for sex, age, length of education and total MMSE score (FWE corrected, $p = 0.193$, (1-β) = 0.934), there was a statistical significance or a trend toward significance for the adjustment for sex, age, length of education, and total MMSE score, respectively (FWE corrected, $p < 0.05$, (1-β) = 0.947; $p = 0.054$, (1-β) = 0.947; $p = 0.063$, (1-β) = 0.947; $p < 0.05$, (1-β) = 0.947). In contrast, other ROIs (left IPL and bilateral precuneus) did not exhibit a significant positive correlation between GMV and orientation scores. Regarding MMSE, we did not find any significant correlations between GMV and orientation score in any ROI. Finally, we could not find statistically significant differences in any brain regions between converters and non-converters.

DISCUSSION

MMSE is a frequently used assessment tool for cognitive function (7) that can identify disorientation in early AD and in those at high-risk of cognitive decline (17). COGNISTAT has recently been introduced to evaluate cognitive function because its diagnostic accuracy and clinical utility were better than those for MMSE in a primary care population (18). COGNISTAT includes an orientation subtest for people, besides those for time and space. Thus, we used COGNISTAT as the primarily means to evaluate orientation. To our knowledge, this is the first VBM study to identify core brain regions associated with overall mental disorientation in aMCI.

We found that brain atrophy (lower GMV) was related to greater severity of overall mental disorientation in the right IPL of aMCI patients. This finding partially supports our hypothesis that IPL and/or the precuneus is important for

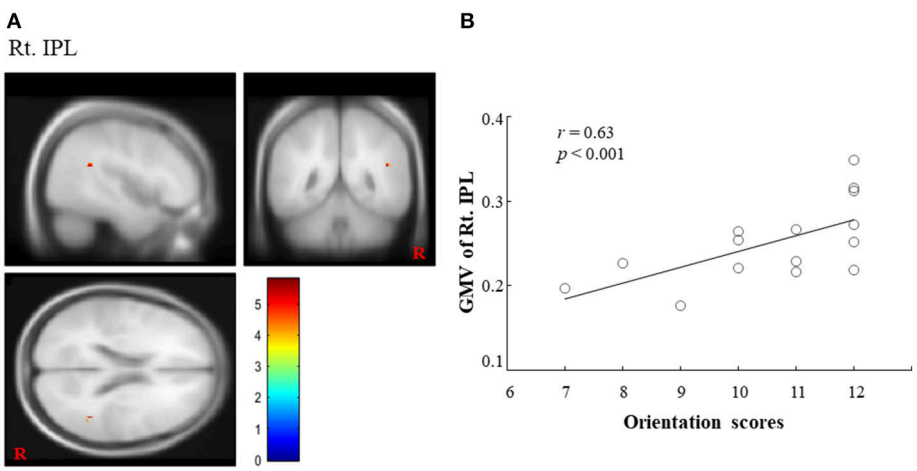

FIGURE 1 | Importance of right IPL on COGNISTAT scores. **(A)** A regional cluster is shown in the right IPL (voxel-level FWE corrected, $p < 0.05$). **(B)** We found a significant positive correlation between the GMV in the right IPL and overall orientation scores on the COGNISTAT. IPL, inferior parietal lobule; GMV, gray matter volume; COGNISTAT, Neurobehavioral Cognitive Status Examination.

disorientation in aMCI. However, we did not find any significant correlation between disorientation as assessed by MMSE and any of our hypothesized brain regions. These results suggest that COGNISTAT may be superior to MMSE in its ability to identify overall mental disorientation related to brain atrophy.

Only the right IPL showed a significant correlation between GMV and disorientation. Brain regions related to disorientation are mostly localized in the right hemisphere, which partially overlaps with the default mode network (DMN) (19–21). Furthermore, a previous neuropathological study on AD demonstrated that the relationship between disorientation (time and place) and parietal lobe was stronger in the right hemisphere (22). Taken together, the right IPL of aMCI may be more involved in overall mental disorientation than the left IPL.

Recent fMRI study demonstrated that common cortical activity related to orientation in time, space, and to people are precisely localized to the IPL and precuneus (5). This finding partially supports our findings that the IPL plays an important role in disorientation in aMCI. Among aMCI and AD, the distribution of amyloid deposition is remarkably similar to the spatial pattern of the DMN (23). Therefore, the orientation network is probably impaired in aMCI because pathological changes in it were observed in AD (22).

Although a previous SPECT study of AD showed hypoperfusion of the precuneus (24), we could not observe a relationship between GMV in the precuneus and disorientation. Interestingly, a recent diffusion MRI study revealed that the IPL was anatomically connected with the precuneus by short-range bilateral white matter tracts (25). This functional communication between areas is important for processing cognitive functions, including orientation. Accordingly, low GMV in the IPL might induce dysfunction of the precuneus, which results in disorientation in aMCI.

It is interesting to note that glutathione (GSH) serves as a marker of oxidative stress that is an important factor in MCI and AD (26–29). Mandal et al. (27) reported that GSH levels in hippocampus measured by magnetic resonance spectroscopy (MRS) accurately discriminated MCI from healthy individuals and that GSH levels correlated with cognitive function. The parietal cortex has more GSH content than other brain regions in healthy people in MRS (26). Decreased GSH level in the parietal cortex may underlie low orientation scores of aMCI in this study. Thus, the combined use of GSH-MRS and VBM analysis is useful to clarify the neural correlates of disorientation in aMCI.

This study was limited by the relatively small sample size. Particularly, we could not find a positive correlation between the right IPL and orientation scores after adjusting for demographical variables. There was also no significant difference in GMV loss between converters and non-converters. We could not assess the correlation with orientation subtests. Since orientation scores of COGNISTAT does not show normal distribution, it may be smeared by celling effect. Further longitudinal and larger scale VBM studies should be considered to verify the brain regions associated with disorientation in time, space, and to people in aMCI.

In conclusion, the right IPL is responsible for overall mental disorientation in aMCI. Therefore, brain atrophy in the right IPL can be useful for early detection of aMCI.

AUTHOR CONTRIBUTIONS

AO, TY, AT, and MM collected data. AO analyzed the data. AO, TY, and ST wrote the manuscript. AO, TY, ST, AT, and MM have read and approved the final version of the manuscript.

FUNDING

This study was supported in part by a Grant-in-Aid for Scientific Research on Innovative Areas, MEXT KAKENHI 15H05875 (ST), and by JSPS KAKENHI Grant Number JP17K09801 to TY.

ACKNOWLEDGMENTS

We thank Adam Phillips, PhD, from Edanz Group (www.edanzediting.com/ac) for editing a draft of this manuscript.

REFERENCES

1. Lesourd M, Le Gall D, Baumard J, Croisile B, Jarry C, Osiurak F. Aplaxia and Alzheimer's disease: review and perspctives. *Neuropsychol Rev.* (2013) 23:234–56. doi: 10.1007/s11065-013-9235-4
2. Alzheimer's Association. 2018 Alzheimer's disease fact and figures. *Alzheimers Dement.* (2018) 14:367–429. doi: 10.1016/j.jalz.2018.02.001
3. Petersen RC. Clinical practice. mild cognitive impairment. *N Engl J Med.* (2011) 364:2227–34. doi: 10.1056/NEJMcp0910237
4. Petersen RC. Mild cognitive impairment as a diagnostic entity. *J Intern Med.* (2004) 256:183–94. doi: 10.1111/j.1365-2796.2004.01388.x
5. Peer M, Salomon R, Goldberg I, Blanke O, Arzy S. Brain system for mental orientation in space, time, and person. *Proc Natl Acad Sci USA.* (2015) 112:11072–7. doi: 10.1073/pnas.1504242112
6. McKee AC, Au R, Cabral HJ, Kowall NW, Seshadri S, Kubilus CA, et al. Visual association pathology in preclinical Alzheimer disease. *J Neuropathol Exp Neurol.* (2006) 65:621–30. doi: 10.1097/00005072-200606000-00010
7. Tsuruoka Y, Takahashi M, Suzuki M, Sato K, Shirayama Y. Utility of the Neurobehavioral Cognitive Status Examination (COGNISTAT) in differentiating between depressive status in late-life depression and late-onset Alzheimer's disease: a preliminary study. *Ann Gen Psychiatry* (2016) 15:3. doi: 10.1186/s12991-016-0091-5
8. Baxter LC, Sparks DL, Johnson SC, Lenoski B, Lopez JE, Connor DJ, et al. Relationship of cognitive measures and gray and white matter in Alzheimer's disease. *J Alzheimers Dis.* (2006) 9:253–60. doi: 10.3233/JAD-2006-9304
9. Gao Y, Nie K, Huang B, Mei M, Guo M, Xiea S, et al. Changes of brain structure in Parkinson's disease patients with mild cognitive impairment analyzed via VBM technology. *Neurosci Lett.* (2016) 658:121–32. doi: 10.1016/j.neulet.2017.08.028
10. Yamasaki T, Horie S, Ohyagi Y, Tanaka E, Nakamura N, Goto Y, et al. A potential VEP biomarker for mild cognitive impairment: evidence from selective visual deficit of higher-level dorsal pathway. *J Alzheimers Dis.* (2016) 53:661–76. doi: 10.3233/JAD-150939
11. Goto M, Abe O, Aoki S, Kamagata K, Hori M, Miyati T, et al. Combining segmented grey and white matter images improves voxel-based morphometry for the case of dilated lateral ventricle. *Magn Reson Med Sci.* (2018) 17:293–300. doi: 10.2463/mrms.mp.2017-0127

12. Maldjian JA, Laurienti PJ, Kraft RA, Burdette JH. An automated method for neuroanatomic and cytoarchitectonic atlas-based interrogation of fMRI data sets. *Neuroimage* (2003) 19:1233–9. doi: 10.1016/S1053-8119(03)00169-1
13. Beheshti I, Demirel H, for the Alzheimer's Disease Neuroimaging Initiative. Probability distribution function- based classification of structural MRI for the detection of Alzheimer's disease. *Comput Biol Med.* (2015) 64:208–16. doi: 10.1016/j.compbiomed.2015.07.006
14. Faul F, Erdfelder E, Buchner A, Lang AG. Statistical power analyses using G*Power 3.1: tests for correlation and regression analysis. *Behav Res Methods* (2009) 41:1149–60. doi: 10.3758/BRM.41.4.1149
15. Scarpazza C, Tognin A, Frisciata S, Sartori G, Mechelli A. False positive rates in voxel-based morphometry studies of the human brain: should we be worried? *Neurosci Biobehav Rev.* (2015) 52:49–55. doi: 10.1016/j.neubiorev.2015.02.008
16. Shi Y, Chen L, Chen T, Li L, Dai J, Lui S, et al. A meta-analysis of voxel-based brain morphometry studies in obstructive sleep apnea. *Sci Rep.* (2017) 7:10095. doi: 10.1038/s41598-017-09319-6
17. Guerrero-Berroa E, Luo X, Schmeidler J, Rapp MA, Dahlman K, Grossman HT, et al. The MMSE orientation for time domain is a strong predictor of subsequent cognitive decline in the elderly. *Int J Geriatr Psychiatry* (2009) 24:1429–37. doi: 10.1002/gps.2282
18. Johansson MM, Kvitting AS, Wressle E, Marcusson J. Clinical utility of cognistat in multiprofessional team evaluations of patients with cognitive impairment in Swedish primary care. *Int J Family Med.* (2014) 2014:649253. doi: 10.1155/2014/649253
19. Peer M, Lyon R, Arzy S. Orientation and disorientation: lessons from patients with epilepsy. *Epilepsy Behav*. (2014) 41:149–57. doi: 10.1016/j.yebeh.2014.09.055
20. Buckner RL, Carroll DC. Self-projection and the brain. *Trends Cogn Sci.* (2006) 11:49–57. doi: 10.1016/j.tics.2006.11.004
21. Buckner RL, Andrews-Hanna JR, Schacter DL. The brain's default network. anatomy, function, and relevance to disease. *Ann N Y Acad Sci.* (2008) 1124:1–38. doi: 10.1196/annals.1440.011
22. Giannakopoulos P, Gold G, Duc M, Michel JP, Hof PR, Bouras C. Neural substarates of spatial and temporal disorientation in Alzheimer's disease. *Acta Neuropathol.* (2000) 100:189–95. doi: 10.1007/s004019900166
23. Buckner RL, Snyder AZ, Shannon BJ, LaRossa G, Sachs R, Fotenos AF, et al. Molecular, structural, and functional characterization of Alzheimer's disease: evidence for a relationship between default activity, amyloid, and memory. *J Neurosci.* (2005) 25:7709–17. doi: 10.1523/JNEUROSCI.2177-05.2005
24. Yamashita KI, Taniwaki Y, Utsunomiya H, Taniwaki T. Cerebral blood flow reduction associated with orientation for time in amnestic mild cognitive impairment and Alzheimer disease patients. *J Neuroimaging* (2014) 24:590–4. doi: 10.1111/jon.12096
25. Uesaki M, Takemura H, Ashida H. Computational neuroanatomy of human stratum proprium of interparietal sulcus. *Brain Struct Funct.* (2018) 223:489–507. doi: 10.1007/s00429-017-1492-1
26. Mandal PK, Tripathi M, Sugunan S. Brain oxidative stress: detection and mapping of anti-oxidant marker 'glutathione' in different brain regions of healthy male/female, MCI and Alzheimer patients using non-invasive magnetic resonance spectroscopy. *Biochem Biophys Res Commun.* (2012) 417:43–8. doi: 10.1016/j.bbrc.2011.11.047
27. Mandal PK, Saharan S, Tripathi M, Murari G. Brain glutathione levels - a novel biomarker for mild cognitive impairment and Alzheimer's disease. *Biol Psychiatry* (2015) 78:702–10. doi: 10.1016/j.biopsych.2015.04.005
28. Shukla D, Mandal PK, Ersland L, Grüner ER, Tripathi M, Raghunathan P, et al. A multi-center study on human brain glutathione conformation using magnetic resonance spectroscopy. *J Alzheimers Dis.* (2018) 66:517–32. doi: 10.3233/JAD-180648
29. Bermejo P, Martín-Aragón S, Benedí J, Susín C, Felici E, Gil P, et al. Peripheral levels of glutathione and protein oxidation as markers in the development of Alzheimer's disease from mild cognitive impairment. *Free Radic Res.* (2008) 42:162–70. doi: 10.1080/10715760701861373

Conflict of Interest Statement: The authors declare that the research was conducted in the absence of any commercial or financial relationships that could be construed as a potential conflict of interest.

frontiers in Neurology

ORIGINAL RESEARCH
published: 08 January 2019
doi: 10.3389/fneur.2018.01145

No Effects of Anodal tDCS on Local GABA and Glx Levels in the Left Posterior Superior Temporal Gyrus

Gerard E. Dwyer[1,2]*, *Alexander R. Craven*[1,2], *Marco Hirnstein*[1,2], *Kristiina Kompus*[1,2], *Jörg Assmus*[3], *Lars Ersland*[1,2,4], *Kenneth Hugdahl*[1,2,5,6] and *Renate Grüner*[6,7]

[1] Department of Biological and Medical Psychology, University of Bergen, Bergen, Norway, [2] NORMENT Centre of Excellence, Haukeland University Hospital, Bergen, Norway, [3] Centre for Clinical Research, Haukeland University Hospital, Bergen, Norway, [4] Department of Clinical Engineering, Haukeland University Hospital, Bergen, Norway, [5] Division of Psychiatry, Department of Clinical Medicine, Haukeland University Hospital, Bergen, Norway, [6] Department of Radiology, Haukeland University Hospital, Bergen, Norway, [7] Department of Physics and Technology, University of Bergen, Bergen, Norway

A number of studies investigating the biological effects of transcranial direct current stimulation (tDCS) using magnetic resonance spectroscopy (MRS) have found that it may affect local levels of γ-aminobutyric acid (GABA), glutamate and glutamine (commonly measured together as "Glx" in spectroscopy), and N-acetyl aspartate (NAA), however, these effects depend largely on the stimulation parameters used and the cortical area targeted. Given that different cortical areas may respond to stimulation in different ways, the purpose of this experiment was to assess the as yet unexplored biological effects of tDCS in the posterior superior temporal gyrus (pSTG), an area that has attracted some attention as a potential target for the treatment of auditory verbal hallucinations in schizophrenia patients. Biochemical changes were monitored using continuous, online MRS at a field strength of 3 Tesla. Performing intrascanner stimulation, with continuous spectroscopy before, during and after stimulation, permitted the assessment of acute effects of tDCS that would otherwise be lost when simply comparing pre- and post-stimulation differences. Twenty healthy participants underwent a repeated-measures experiment in which they received both active anodal and sham intrascanner stimulation in a stratified, randomized, double-blind experiment. No significant changes in GABA, Glx, or NAA levels were observed as a result of anodal stimulation, or between active and sham stimulation, suggesting that a single session of anodal tDCS to the pSTG may be less effective than in other cortical areas that have been similarly investigated.

Keywords: tDCS, GABA, Glultamate, magnetic resonance spectroscopy, MRS

OPEN ACCESS

Edited by:
Peter Sörös,
University of Oldenburg, Germany

Reviewed by:
Samuel James Westwood,
Aston University, United Kingdom
Dieter J. Meyerhoff,
University of California, San Francisco, United States

***Correspondence:**
Gerard E. Dwyer
gerard.dwyer@uib.no

Specialty section:
This article was submitted to Applied Neuroimaging, a section of the journal Frontiers in Neurology

Received: *07 April 2018*
Accepted: *11 December 2018*
Published: *08 January 2019*

Citation:
Dwyer GE, Craven AR, Hirnstein M, Kompus K, Assmus J, Ersland L, Hugdahl K and Grüner R (2019) No Effects of Anodal tDCS on Local GABA and Glx Levels in the Left Posterior Superior Temporal Gyrus. Front. Neurol. 9:1145. doi: 10.3389/fneur.2018.01145

INTRODUCTION

Transcranial direct current stimulation (tDCS) is a non-invasive neurostimulation technique that uses constant, low level (0.5–2.0 mA) direct current to modulate cortical excitability in a polarity dependent manner (1). Nitsche and Paulus (2) used the magnitude of motor-evoked potentials (MEP) as generated by transcranial magnetic stimulation (TMS) as an indication of changes in excitability and found that tDCS was able to induce changes in excitability of up to 40%, with anodal stimulation having an excitatory effect, and cathodal stimulation having an inhibitory

effect. Subsequent studies showed that effects may outlast the duration of stimulation, with short applications inducing excitability shifts during stimulation, and ∼10 min or more of stimulation producing persistant effects lasting up to 90 min after current flow has ceased (3) suggesting that tDCS has the ability to induce long term potentiation (LTP)-like effects on synaptic plasticity (4).

Due to its purported effects on excitability and synaptic plasticity, tDCS has been investigated as a potential treatment for a range of neurological and psychiatric disorders such as Parkinson's disease (5), depression (6), and for the treatment of auditory verbal hallucinations in schziophrenia. A case reported by Homan et al. (7) found that cathodal tDCS halfway between T3 and P3 in the 10–20 electroencephelography (EEG) system was successful in alleviating both hallucinations (−60% Hallucination Change Scale (HCS) score) and global symptoms (−20% Postive and Negative Syndrome Scale (PANSS) score). A randomized control trial conducted by Brunelin et al. (8) using a similar stimulation paradigm at 2.0 mA also showed improvement in hallucinations (−31% Auditory Hallucination Rating Scale (AHRS) score) and global symptoms (−13% PANSS score). Subsequent studies, using similar stimulation parameters have found both reductions (9) and no significant differences (10, 11) in symptoms. While tDCS shows great promise as a potential treatment for schizophrenia, the lack of consistent findings between these studies highlight the need for a deeper understanding of the effects of tDCS.

Although generally accepted that anodal stimulation typically facilitates excitability and cathodal stimulation inhibits excitability (12), studies have shown that the effects of tDCS on excitability are not so simplistic, and depend on a number of factors such as electrode size and placement, stimulation intensity and duration, as well as the orientation of neurons relative to the stimulating electrodes (12–14). Furthermore, Batsikadze et al. (15) found that while 20 min of cathodal stimulation at 1.0 mA had an inhibitory effect, 20 min of cathodal stimulation at 2.0 mA had an excitatory effect, increasing the magnitude of measured MEPs. Esmaeilpour et al. (16) showed that the dose-response relationship in tDCS is not necessarily linear, and that although increasing current produces a corresponding increase in brain electric field, it may not necessarily enhance a neurophysiological, behavioral or clinical outcome. As Woods et al. (14) caution, it cannot be taken for granted that what is effective in a particular cortical area is transferable and applicable to others, rather recommending a "titration" of parameters.

Abbreviations: BOLD, Blood Oxygen Level Dependent; EEG, Electroencephalography; ERETIC, Electronic reference to access *in vivo* concentrations; FWHM, Full width at half maximum; GABA, Gamma-aminobutyric acid; Glx, Glutamate and glutamine; GSH, Glutathione; LTP, Long-term potentiation; MEGA-PRESS, Mescher-Garwood point resolved spectroscopy; MEP, Motor evoked potential; MRS, Magnetic Resonance Spectroscopy; NAA, N-acetylaspartate; NAAG, N-acetylaspartylglutamate; pSTG, Posterior superior temporal gyrus; tDCS, Transcranial direct current stimulation; TE, Echo time; TMS, Transcranial Magnetic Stimulation; TR, Repetition time

Despite the observed effectiveness of tDCS, the exact mechanisms by which it works are not yet fully understood. Horvath et al. (17) show that changes in cognitive effects alone may be an unreliable measure of effectiveness. Computational forward models and simulations have been useful in imaging current flow, aiding in the design of stimulation paradigms (18) but do not provide information about neuronal responses to delivered current or whether the effect is excitatory or inhibitory in nature.

Krause et al. (19) suggest that tDCS may modulate the excitation/inhibition balance, that is, the relative contributions of excitatory and inhibitory inputs to a neural circuit corresponding to a neuronal event. Using *in vivo* magnetic resonance spectroscopy (MRS), the excitation-inhibition balance may be characterized in terms of the local concentrations of the excitatory neurotransmitter glutamate and inhibitory neurotransmitter gamma-aminobutyric acid (GABA). Studies that have used MRS to investigate the effect of tDCS have found anodal tDCS to reduce local cortical GABA concentration in the motor cortex (20, 21) and to increase local concentrations of glutamate and glutamine, measured together as "Glx," and N-acetyl aspartate (NAA) in the intraparietal and prefrontal cortices (22, 23), the observed reduction in inhibitory neurotransmitter levels and concurrent increases in excitatory neurotransmitter levels being consistent with the facilitatory nature of anodal stimulation. Thus, *in vivo* MRS provides a window into the biochemical events underlying tDCS that may also be used as a biomarker indicating the effectiveness and nature of a stimulation paradigm.

In this study, MRS was used to investigate the acute biochemical effects of tDCS in validating its potential for use as a treatment for auditory-verbal hallucinations in schizophrenia. However, rather than simply comparing pre- and post-stimulation spectral acquisitions, biochemical changes were measured continuously using online MRS in a manner similar to those used by Bachtiar et al. (24) and Hone-Blanchet et al. (23). By acquiring spectra continuously over the course of stimulation, spectral frames could be combined in such a way that metabolite levels could be measured and tracked before, during and post stimulation, allowing better insight into the acute effects of stimulation as opposed to the lasting effects. Findings in other cortical areas suggest that if anodal tDCS were to have a similar effect on the local excitation-inhibition balance, it may be measured as a statistically significant increase in Glx and NAA levels (22, 25) and decrease in GABA levels (20, 21, 24) and that these changes would be significantly different under active stimulation when compared to sham.

MATERIALS AND METHODS

This study was carried out in accordance with the recommendations and ethical approval of the regional committee for medical and health research ethics (REK-Vest) REK case number 2013/2342. All subjects gave written informed consent in accordance with the Declaration of Helsinki and the

guidelines drawn up by The Norwegian National Research Ethics Committee for medical and health research (NEM).

Participants

Twenty healthy participants (mean age: 25 years, range: 19–32; 10 male) participated in the study. All participants were required to complete a Norwegian language version of the Edinburgh handedness inventory (26) to determine right-handedness in an attempt to control for issues related to lateralization of cortical areas, such that stimulation in the left hemisphere affects approximately the same functional area in each participant. The test assessed dominance of right and left hand in performing 10 everyday activities to produce a score ranging between −100 (exclusively left handed) and +100 (exclusively right handed), participants with a score greater than +40 were considered to be right handed and were permitted into the study (mean score: +80, SD: 24). Based on self-report, participants were free from psychiatric and neurologic conditions and had not used any psychoactive/psychotropic substances, including no smoking or other tobacco based or nicotine containing products, for 6 months prior to participating in the experiment. Participants were also instructed not to consume alcohol for at least 24 h prior to participation.

Data from one female participant was omitted from final analyses due to abnormally high measurements of Glx more than three standard deviations above the group mean (Glx levels almost 5 times higher than average values), suggesting an error in spectral acquisition.

tDCS Stimulation

Stimulation was performed using an MR-compatible DC-Stimulator MR (neuroConn GmbH, Ilmenau, Germany) fitted with two 5 × 7 cm (35 cm^2) MR compatible rubber electrodes. Given that the motivation for this study was the potential for tDCS to be used as a treatment for schizophrenia, stimulation parameters were chosen to emulate those used in previous studies. Intensity was set at 2.0 mA (27) and although the majority of studies using tDCS as a treatment for auditory-verbal hallucinations have stimulated for 20 min, the prohibitively long scan time this would necessitate in order to have three equally long spectroscopy windows meant that stimulation had to be limited to 10 min. The anodal electrode was placed with the center of the pad on an area over the pSTG, such that the lower corners of the 7 cm edge of the electrode touch points T3 and T5 in the EEG 10-20 system. The cathodal electrode was placed over the contralateral orbitofrontal cortex, a site commonly used in tDCS montages for placement of the reference electrode (2, 12) such that the center of the electrode covered point AF8 in the EEG 10–20 system. Each electrode was coated with a layer of Ten20 conductive paste (Weaver and Company, Aurora, United States of America) at the interface between electrode and skin to improve both adhesion and conductivity. Once the electrodes were in place, participants were placed in the scanner with electrodes attached but not connected to the stimulation box. Electrodes were only connected prior to spectroscopy sequences.

This study followed a stratified, randomized, double-blind design, with both participants and experimenters blind to the stimulation condition. Each subject participated in two MR-scanning sessions with tDCS: one with active and one with sham stimulation, separated by a wash-out period of 1 h outside of the scanner (12, 28) counterbalanced for order. Double-blinding was performed by having the stimulation condition determined by a code, independently predetermined by a researcher not present at the stimulation, such that each participant underwent both active and sham stimulation conditions and that equal numbers experienced active and sham stimulation as the first condition.

MR-Imaging and Spectroscopy

All imaging and spectroscopy was performed on a 3 T GE 750 Discovery Scanner from GE Healthcare (General Electric, Milwaukee, United States of America) using a standard 8-channel head coil from Invivo (Invivo corp., Gainsville, Florida, United States of America).

Following a 3-plane localizer sequence (2D Spin Echo, TE = 80 ms, FOV = 240 mm, slice thickness = 8 mm, slice spacing = 15 mm) structural anatomical imaging was performed using a 3D T1 weighted fast spoiled gradient sequence (FSPGR) (number of slices = 192, slice thickness = 1.0 mm, repetition time (TR) = 7.8 ms, echo time (TE) = 2.95 ms, field of view = 260 × 260 mm^2, flip angle = 14 degrees, matrix = 256 × 256). These structural images were used to position a 24 × 24 × 24 mm^3 voxel for the spectroscopy component of this experiment in the left pSTG, centered around the primary auditory cortex, aligned orthogonally in the axial scan plane with no angulation (**Figure 1**).

Since the aim of this study was to characterize acute biochemical changes in terms of the excitation-inhibition balance, a GABA specific MEGA-PRESS sequence (29) was used as it provides accurate and stable measurements of GABA, as well as a measurement of glutamate and glutamine combined as "Glx" (30). Spectroscopy was performed using a MEGA-PRESS sequence (TE = 68 ms, TR = 1,500 ms, 8-way phase cycling, editing at 1.9 and 7.5 ppm in alternating frames) of 628 paired repetitions, followed by 16 unsuppressed reference acquisitions for a total scan time of 31 min and 48 s. Once 10 min of spectroscopy had elapsed, stimulation was initiated at the control box located outside the scanner at the control room. Active stimulation was delivered for 10 min with 24 s of ramping time both before and after the stimulation/sham period at a constant intensity of 2.0 mA. For the sham stimulation condition, intensity was ramped up to 2.0 mA over 24 s, then delivered for another 40 s, before being ramped down to zero, giving participants a similar sensation to that they would experience during active stimulation. Spectroscopy acquisition continued for 10 min in order to assess post-stimulation effects (**Figure 2**).

Spectral Analysis

While no spectral artifacts were observed during steady-state tDCS stimulation, mild artifacts were seen in spectral frames acquired during the ramping periods for both active and sham stimulation. Frames from these periods were omitted from all subsequent analyses.

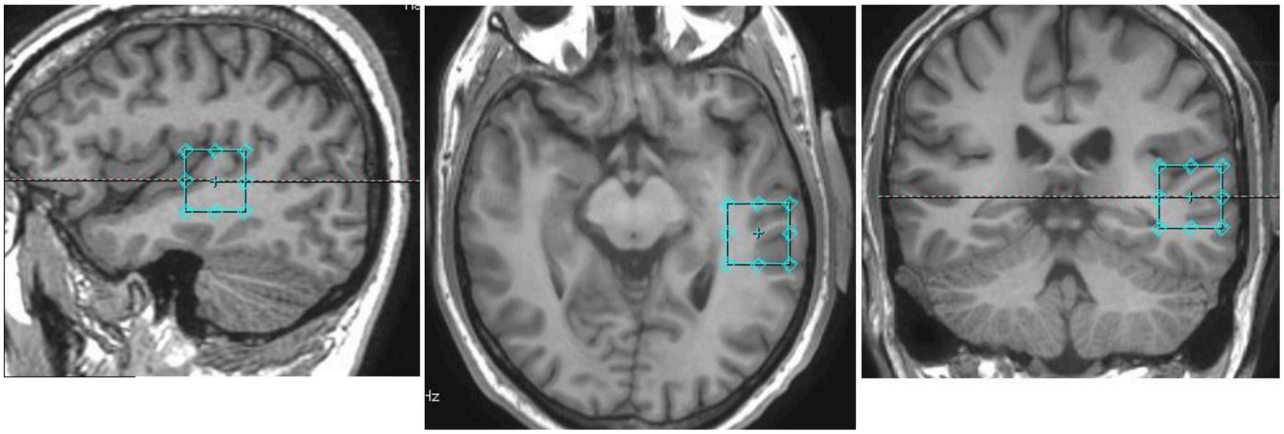

FIGURE 1 | Voxel placement in the pSTG in one participant: Sagittal (left), axial (middle), and coronal (right) views overlayed on an anatomical scan.

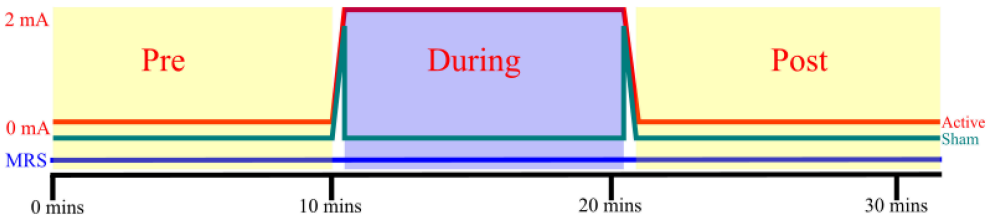

FIGURE 2 | tDCS and MRS: Each participant received both active and sham stimulation, separated by a washout period of 1 h, counterbalanced for order. 24 s of ramping up and down were incorporated into both active and sham stimulation. MRS was acquired constantly throughout each session. The pre-, during, and post-stimulation spectroscopy windows did not include frames acquired during ramping.

Following phase adjustment, coil combination, and realignment, each continuous acquisition was first subdivided into three smaller blocks of ∼10 min, with exact length depending on how many frames were excluded due to ramping artifacts, comprising a pre-, during-, and post stimulation block for each session, hereafter referred to as a three point analysis. Frames within each block were then averaged together and within each block, ON, and OFF spectrum pairs were subtracted to produce a difference spectrum then subjected to quantitative analysis with LCModel (version 6.3-1J) (31, 32) using a simulated basis set (33) with Kaiser coupling constants (34) to provide an estimate of average levels of GABA, glutamate and glutamine measured together as Glx, glutathione (GSH), NAA, and N-acetyl aspartate glutamate (NAAG). Metabolite levels were scaled relative to the unsuppressed water signal acquired at the end of each spectroscopy sequence.

One issue that affects MEGA-edited GABA spectroscopy is co-editing of macromolecule (MM) resonances at 1.7 ppm contaminating the GABA signal in the difference spectrum. GABA, in this report, refers to both GABA and the co-edited macromolecule, typically denoted GABA+ (35).

To further investigate acute effects of tDCS, and eliminate the possibility short-lived metabolic fluctuations being obscured through averaging, a second analysis was performed in which the during- and post-stimulation blocks were further subdivided into two smaller windows in an attempt to uncover any changes in metabolite concentration during this period, thus providing five time points over the acquisition, hereafter referred to as the five point analysis: one 10 min pre-stimulation window, two 5 min during-, and two 5 min post-stimulation windows.

MRS signals have been demonstrated to be susceptible to line-broadening artifacts associated with local blood-oxygen-level dependent (BOLD) effects (36). As an indication of potential BOLD interference, the full width at half maximum (FWHM) values as determined by LCModel were used as a measure of quality control, to ensure the MRS signal had not been significantly affected between time points.

Statistical Analysis

Statistical analyses were performed using R (37) and the nlme package (38) to perform a linear mixed effects model analysis of the effect of tDCS on the concentrations of three metabolites of interest, namely NAA, Glx, and GABA, over time. This model specified two groups of participants (active-first and sham-first) and time period as fixed effects as well as an interaction effect between the two, with the subject as a random effect. This model was also used to investigate crossover effects between the active and sham stimulation conditions due to the within-subject design of the study, to determine whether order of stimulation, active first or sham first, may have had

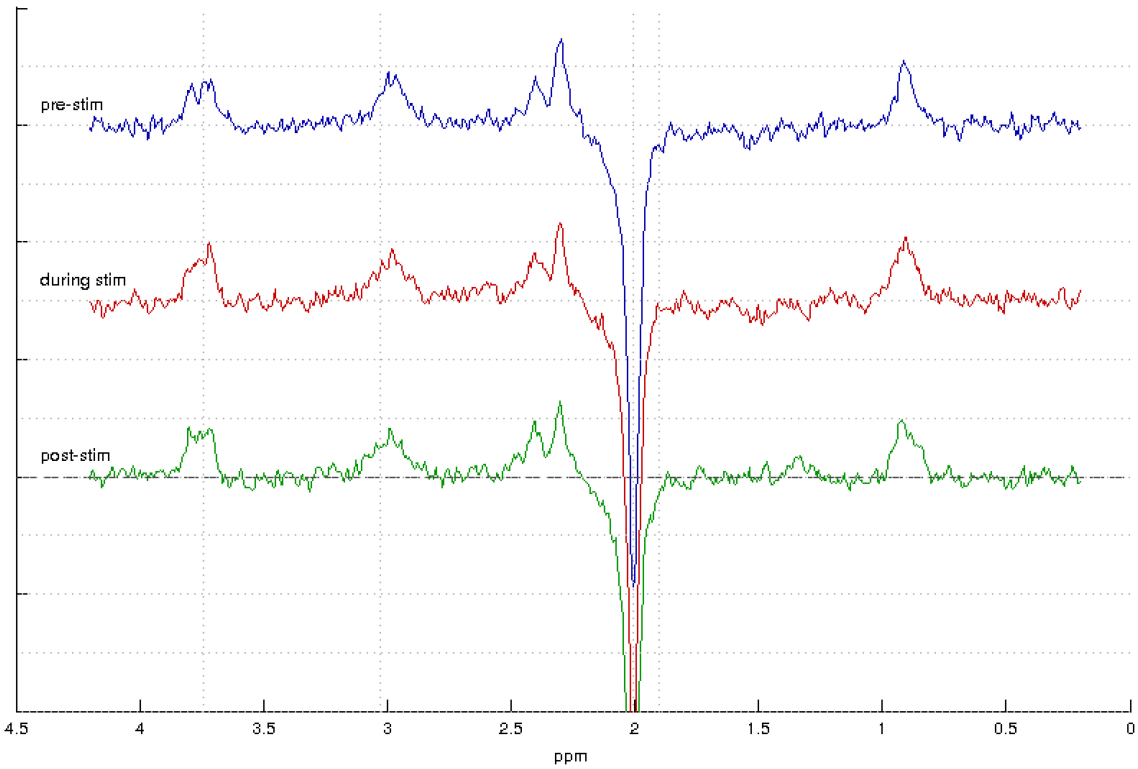

FIGURE 3 | MEGA-PRESS spectra from one participant showing spectra acquired during the pre-stimulation window (top, blue) during stimulation (middle, red) and post-stimulation (bottom, green).

any significant effect on results and whether the stimulation condition in the first session had any lasting effect on the second. The same model was used for both the 3-point and 5-point analyses.

RESULTS

Sample spectra from the three-point analysis of an individual participant are shown in **Figure 3** along with spectral quality metrics for all participants in **Table 1**. A linear mixed effects model of the average metabolite concentration across three time windows (pre-, during-, and post-stimulation) revealed no significant fluctuations in any of the metabolites of interest between any time points (**Figure 4** and **Appendix A**). Similarly, no significant fluctuations in any of the metabolites of interest were found between any time points in the five-time point analysis (**Figure 4** and **Appendix B**).

No significant crossover effects were found (**Figure 4**, **Appendices A, B**) indicating both that the order in which participants received the two different stimulation conditions had no significant effect on results and that there were no crossover effects from the first session significantly affecting the second. There was no significant difference in the change between groups over time, indicating no difference in fluctuations for any of the metabolite levels between active and sham conditions.

The FWHM as reported by LCModel was used as an indication of potential BOLD interference (**Tables 2**, **3**), but saw very little fluctuation between time points, making BOLD interference an unlikely source of error.

DISCUSSION

The montage and stimulation parameters used in this experiment did not induce a statistically significant effect on Glx, GABA, or NAA levels as measured with the MRS sequence used, and there was no significant difference in response observed between the active and sham stimulation conditions.

The active hypothesis for this experiment was informed by previous studies in which active anodal stimulation was found to be associated with increases in Glx and NAA levels (22, 23) and decreases in GABA levels (20, 21, 24) as measured by MRS. In comparing these studies with the findings presented here, there are three key elements to be considered, namely the stimulation parameters, the MRS acquisition parameters and the site of stimulation and spectroscopy.

As stated in section tDCS Stimulation, due to limitations of the experimental design, stimulation could only be delivered for 10 min as opposed to the 20 min previously used in the treatment of schizophrenia symptoms. Although as little as 7 min of stimulation has been

shown to induce lasting effects after stimulation has ceased (39), it cannot be taken for granted that the 10 min delivered in this session was sufficient to induce a change. While the stimulation window was shorter than the 30 min used by both Clark et al. (22) and Hone-Blanchet et al. (23) and the 20 min and 15 min used by Bachtiar et al. (24) and Kim et al. (20), respectively, Stagg et al. (21) were able to detect significant changes in GABA and Glx levels in the left sensorimotor cortex using a similar

TABLE 1 | Spectral Quality: FWHM, SNR, and mean %CRLB for GABA and Glx for each stimulation window.

Window	FWHM (Hz)	SNR	Mean GABA %CRLB	Mean Glx %CRLB
Pre Stim	8.22 ± 2.34	20.47 ± 4.71	5.12	4.54
During Stim	8.39 ± 2.41	20.83 ± 4.20	5.16	4.41
Post Stim	8.03 ± 2.18	21.67 ± 4.04	4.91	4.24

TABLE 2 | Average FWHM and standard deviation (sd) as estimated by LCModel for the 3-point analysis.

	Mean FWHM−3-point analysis (Hz)					
	Pre	sd	During	sd	Post	sd
Active	7.95	1.86	7.98	1.79	7.59	1.38
Sham	8.46	2.24	8.64	2.24	8.32	2.30

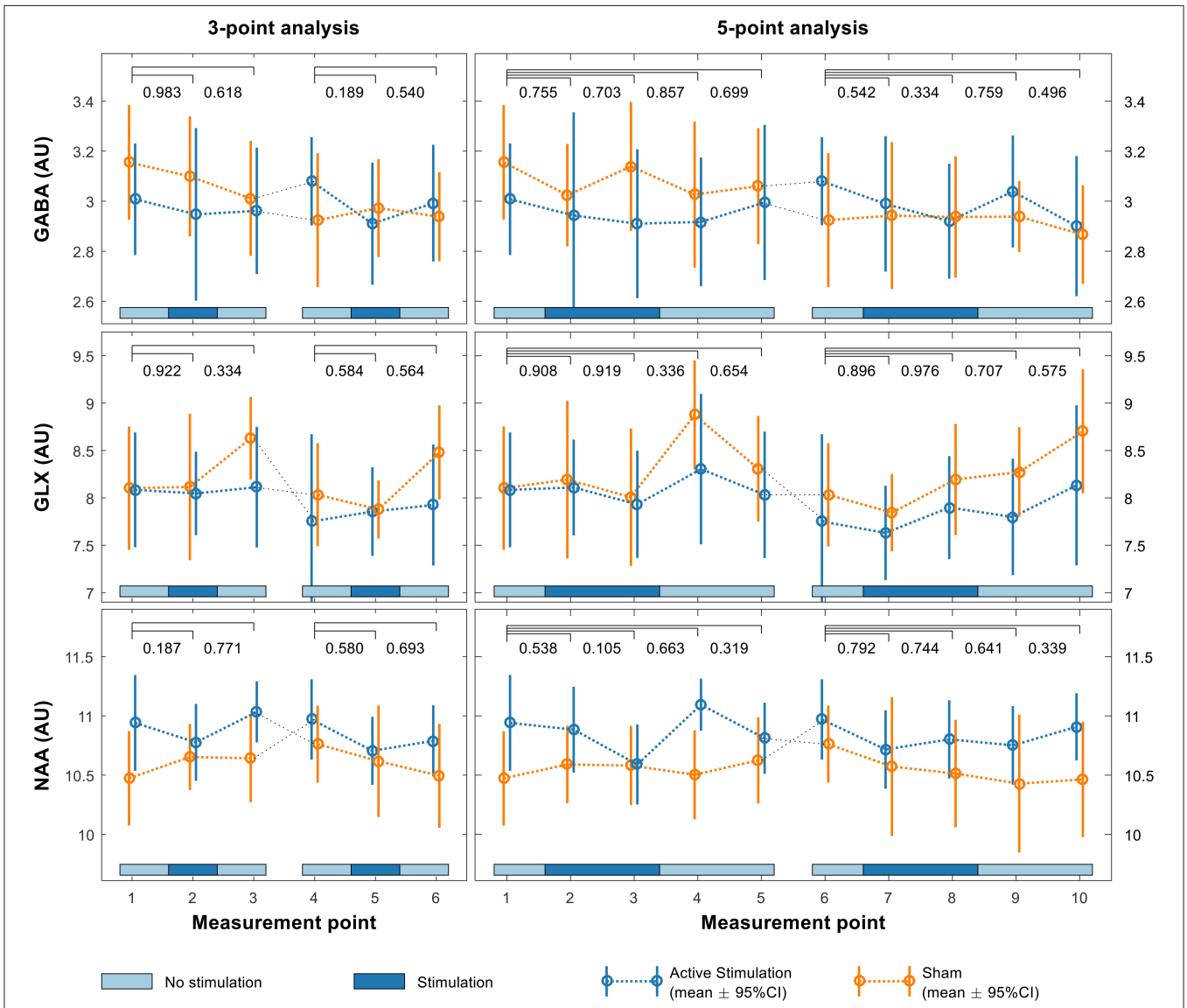

FIGURE 4 | Linear mixed effects model of GABA (upper row), Glx (middle row) and NAA (lower row) levels in the pSTG for both the first and second sessions using both 3-point (left) and 5-point (right) analyses. *p*-values shown above each plot indicate significance of interaction effects at each time point relative to baseline.

TABLE 3 | Average FWHM and standard deviation (sd) as estimated by LCModel for the 5-point analysis.

	Mean FWHM−5-point analysis (Hz)									
	Pre	**sd**	**During1**	**sd**	**During2**	**sd**	**Post1**	**Sd**	**Post2**	**sd**
Active	7.95	1.86	8.00	1.77	7.94	1.69	7.74	1.73	7.77	1.55
Sham	8.46	2.24	8.50	0.02	8.46	2.06	8.28	2.42	8.46	1.96

MEGA-PRESS sequence at 3 T given only 10 min of anodal stimulation at 1.0 mA. The findings of Batsikadze et al. (15) and Esmaeilpour et al. (16) suggest it is possible that stimulating at 2.0 mA had a different effect to the one predicted. However, studies conducted by Brunelin et al. (8) and Mondino et al. (9) both found significant reductions in symptoms of auditory-verbal hallucinations using stimulation in this area following cathodal stimulation at 2.0 mA, suggesting an issue more likely related to electrode polarity than stimulation intensity. While no significant changes, nor non-significant tendencies toward changes in any of the metabolites under investigation were seen during stimulation, even in the five-point analysis, it is unlikely that allowing a full 20 min of stimulation would induce a measureable effect, though it cannot be ruled out conclusively.

One of the unique features of this study was the use of continuous, online MRS as opposed to separate acquisitions. While Hone-Blanchet et al. (23) also acquired spectra during stimulation, also using a MEGA-PRESS sequence with an echo time of 68 ms and 11 min acquisition blocks, their study does not include a pre-stimulation window. Similarly, Clark et al. (22) acquired multiple spectra during the pre- and post-stimulation windows, also using a MEGA-PRESS sequence with an echo time of 68 ms, but with spectra acquired sequentially rather than continuously in blocks of 4 min and 48 s. While there is little difference in terms of the resultant spectra whether acquired continuously or sequentially, acquiring separate scans may introduce more variability as each pre-scan affects parameters such as shim, gain adjustment and center-frequency tuning between each segment. It may be considered more robust to acquire all spectra with the same parameters, as was done in this study with single continuous acquisitions. Compared with previous studies using similar sequences, comparable or shorter acquisition times, and smaller voxel sizes, i.e., $20 \times 20 \times 20$ mm^3 (21, 22, 24), there is little evidence to suggest an error in the MRS acquisition. Intuitively, a larger voxel size provides a higher signal-to-noise ratio, but may come at the expense of some focality in terms of covering the site of stimulation. It is possible that the larger voxel size used in this study may have incorporated spectra from cells not affected by stimulation. However, the voxel dimensions are still small compared to the surface area of the stimulating electrode, and tDCS is not a particularly focused stimulation technique.

The most significant difference between this study and other studies that have measured biochemical changes associated with tDCS with MRS is the cortical region being investigated, both as a stimulation site and volume of interest in spectroscopy. As Woods et al. (14) illustrated, it cannot be taken for granted that all cortical areas will respond to stimulation in the same manner, and compared to areas such as the sensorimotor cortex and frontal areas such as the dorsolateral prefrontal cortex, the temporoparietal and temporal regions have not been quite as thoroughly investigated. One study investigating the use of anodal tDCS in an adjacent cortical area, namely the left mid-posterior temporal gyrus, on improving performance in a range or reading and naming tasks (40) did not find any significant improvement in performance. Although different stimulation parameters were used, the agreement between the null-findings of this and the present study suggest it is possible that the pSTG and adjacent areas in the region, are not as responsive to anodal stimulation as other areas that have been investigated, but that the effectiveness of tDCS as a treatment for hallucinations is based on its ability to modulate over-active areas in the brain with cathodal stimulation. That is to say, anodal stimulation may not affect excitability in the pSTG, but cathodal stimulation may be effective in modulating activity in over-active or pathologically active networks such as those that might be associated with hallucinations. Computer modeling may be able to determine whether the responsiveness of this cortical area may be due to anatomical features such as skull thickness or cerebrospinal fluid density. It may be of interest to repeat a similar experiment looking at the effects of cathodal stimulation in this area in conjunction with computer models that may be able to determine whether the absence of an observed affect may be attributed to issues of anatomy and current flow.

In an investigation into the effect of active, intrascanner tDCS on the BOLD response as measured with functional MRI, Antal et al. (41) found that the presence of an electric current in the magnetic field inside an MRI scanner produces artifacts that may result in confounding false-positive activity patterns. While mild artifacts were observed during the ramping periods before and after stimulation, and these spectral frames were removed from subsequent analyses, there were no artifacts observed during active or sham stimulation periods. Furthermore, there were no statistically significant differences observed between the pre- and post-stimulation windows, where no ongoing active or sham stimulation was present. This, coupled with the findings of previous studies using online MRS acquired during stimulation (23, 24) suggest that interfence caused by ongoing intrascanner tDCS during spectral acquisition is not a likely source of error.

Another potential explanation for the null findings of this experiment is insufficient power as a result of too few participants. An analysis conducted in G*Power (42) determined

there were enough participants to detect at least a medium sized effect (i.e., effect size > 0.6, 1-$\beta = 0.8$, $\alpha = 0.05$). Many of the studies that have previously investigated biochemical effects of tDCS have noted significant findings with smaller sample sizes than the 19 used in this study, including $N = 12$ (22), $N = 17$ (23), and $N = 11$ (21). To this end it is believed that the study was sufficiently powered, in terms of the participant sample size, to detect a comparable effect. One of the problems with statistical power as outlined by Button et al. (43) is that while problems of low statistical power are typically associated with reduced chances of detecting a true effect, they may also reduce the likelihood of a statistically significant result being indicative of a true effect. That is, finding false positive effects due to inflated effect sizes. As Westwood et al. (40) illustrate, while it may be of value to include more participants in future studies, it calls the effectiveness of a single session of tDCS into question if the effects are so small. Referring to a meta-analysis in preparation, Westwood et al. (40) discuss an analysis of pooled studies looking at anodal stimulation in the frontal and temporal lobes which produced a sample size of almost 200 participants in which there was still no evidence of an effect of a single session of tDCS. In light of this, it is not believed that an increased sample size would have improved the outcome of this experiment.

One problem affecting the spectroscopy aspect of this study is that of how to quantify metabolite levels. Typical methods make use of water as an endogenous reference, or report the concentration as a ratio relative to an internal reference such as creatine or NAA. While creatine is typically favored as an internal reference (44) its use is complicated when using the MEGA-PRESS sequence as creatine signals are eliminated during subtraction and are not present in the difference edited spectrum, though they may be recovered from the spectra acquired without an editing pulse (commonly referred to as the "OFF" spectrum in the spectral pairs used to create the difference spectrum). NAA was not used as an internal reference as it has been demonstrated to be affected by anodal tDCS (22, 23), although no changes in NAA levels were measured over the course of the acquisition. The use of water as an endogenous reference can be problematic for studies such as this that attempt to measure metabolic changes in a dynamic manner, i.e., in relation to activity over time, as MRS signals have been shown to be susceptible to line-broadening artifacts associated with local BOLD effects (36). Using a fixed water reference taken at the end of the acquisition, as was done in this study, the reference signal was not subject to fluctuations as the result of a BOLD effect throughout the scan as the metabolites of interest were, i.e., comparing an unchanging reference to a signal subject to interference may increase the likelihood of a false change being detected. As a single, fixed water reference was used, it is difficult to decisively rule out any incidental BOLD-related fluctuations. However, such fluctuations would likely be manifest across all metabolites in the FWHM estimate given by LCModel, which is not seen in our data (**Tables 2**, **3**), making it unlikely to be a significant source of error. Ideally, an experiment such as this would benefit from the use of external referencing, such as the Electronic Reference To access *in vivo* Concentrations (ERETIC) method (45, 46).

In interpreting these findings, it is important to consider that tDCS is regarded as a neuromodulatory technique, it does not induce activity or action potentials, but rather facilitates increases or decreases in neuronal excitability. Bikson and Rahman (47) discuss the idea of activity-selectivity and task-specific modulation, that is, that tDCS will preferentially modulate a neuronal network that is already active, while not modulating a separate network that is inactive. One of the problems with the region of interest in this study is that it contains the primary auditory cortex and adjacent areas responsible for the sensation of sound and processing of speech (48). While other paradigms have investigated cortical areas that may be associated with a task, e.g., the primary motor cortex and force adaptation task (20), that may distinguish between blocks of activity and rest, the auditory cortex will experience ongoing sensory input during scanning. It is possible that no biochemical changes were observed between blocks as the local cortical circuit was already in an active state during the pre-stimulation window and that tDCS was not able to drive a higher level of activity.

In conclusion, using continuous online MRS, no significant change in the levels of Glx, GABA, or NAA in the left pSTG was observed that could be attributed to an effect of active, anodal tDCS. Despite this, the method provides a useful insight into the acute effects of stimulation paradigms and their effect on local neuronal circuitry. Further research investigating an effect of tDCS in this area suggests performing a similar experiment using cathodal tDCS, redesigning the experiment to allow 20 min of stimulation, perhaps combining this experiment with computer models and also using an external referencing method to avoid possible confounding variables associated with how metabolite levels are measured.

AUTHOR CONTRIBUTIONS

GD, AC, MH, KK, KH, and RG were involved in the conception and design of the study. GD, AC, MH, and KK contributed to planning and performing of the experiments. AC performed the spectral analysis component of this study. JA performed statistical analyses. LE contributed to acquisition of MR-Spectra. GD wrote the manuscript with the assistance and critical feedback of all contributing authors.

FUNDING

The current research was partly funded by grants from the Research Council of Norway (#221550), European Research Council, ERC (#693124), and the Health Authority of Western Norway (#911783) to KH; the Bergen Research Foundation (grant BFS2016REK03) to MH; and Norway Grants (EMP180) to KK.

SUPPLEMENTARY MATERIAL

The Supplementary Material for this article can be found online at: https://www.frontiersin.org/articles/10.3389/fneur.2018.01145/full#supplementary-material

REFERENCES

1. Zaghi S, Acar M, Hultgren B, Boggio PS, Fregni F. Noninvasive brain stimulation with low-intensity electrical currents: putative mechanisms of action for direct and alternating current stimulation. *Neuroscientist* (2010) 16:285–307. doi: 10.1177/1073858409336227
2. Nitsche MA, Paulus W. Excitability changes induced in the human motor cortex by weak transcranial direct current stimulation. *J Physiol.* (2000) 527:633–9. doi: 10.1111/j.1469-7793.2000.t01-1-00633.x
3. Nitsche MA, Paulus W. Sustained excitability elevations induced by transcranial DC motor cortex stimulation in humans. *Neurology* (2001) 57:1899. doi: 10.1212/WNL.57.10.1899
4. Stagg CJ, Nitsche MA. Physiological basis of transcranial direct current stimulation. *Neuroscientist* (2011) 17:37–53. doi: 10.1177/1073858410386614
5. Benninger DH, Hallett M. Non-invasive brain stimulation for Parkinson's disease: current concepts and outlook 2015. *NeuroRehabilitation* (2015) 37:11–24. doi: 10.3233/NRE-151237
6. Brunoni AR, Moffa AH, Fregni F, Palm U, Padberg F, Blumberger DM, et al. Transcranial direct current stimulation for acute major depressive episodes: meta-analysis of individual patient data. *Br J Psychiatry* (2016) 208:522–31. doi: 10.1192/bjp.bp.115.164715
7. Homan P, Kindler J, Federspiel A, Flury R, Hubl D, Hauf M, et al. Muting the voice: a case of arterial spin labeling-monitored transcranial direct current stimulation treatment of auditory verbal hallucinations. *Am J Psychiatry* (2011) 168:853–4. doi: 10.1176/appi.ajp.2011.11030496
8. Brunelin J, Mondino M, Gassab L, Haesebaert F, Gaha L, Suaud-Chagny M-F, et al. Examining transcranial Direct-Current Stimulation (tDCS) as a treatment for hallucinations in schizophrenia. *Am J Psychiatry* (2012) 169:719–24. doi: 10.1176/appi.ajp.2012.11071091
9. Mondino M, Jardri R, Suaud-Chagny M-F, Saoud M, Poulet E, Brunelin J. Effects of fronto-temporal transcranial direct current stimulation on auditory verbal hallucinations and resting-state functional connectivity of the left temporo-parietal junction in patients with schizophrenia. *Schizophr Bull.* (2016) 42:318–26. doi: 10.1093/schbul/sbv114
10. Fitzgerald PB, McQueen S, Daskalakis ZJ, Hoy KE. A negative pilot study of daily bimodal transcranial direct current stimulation in schizophrenia. *Brain Stimul.* (2014) 7:813–6. doi: 10.1016/j.brs.2014.08.002
11. Fröhlich F, Burrello TN, Mellin JM, Cordle AL, Lustenberger CM, Gilmore JH, et al. Exploratory study of once-daily transcranial direct current stimulation (tDCS) as a treatment for auditory hallucinations in schizophrenia. *Eur Psychiatry* (2016) 33:54–60. doi: 10.1016/j.eurpsy.2015.11.005
12. Nitsche MA, Cohen LG, Wassermann EM, Priori A, Lang N, Antal A, et al. Transcranial direct current stimulation: state of the art 2008. *Brain Stimul.* (2008) 1:206–23. doi: 10.1016/j.brs.2008.06.004
13. Radman T, Ramos RL, Brumberg JC, Bikson M. Role of cortical cell type and morphology in subthreshold and suprathreshold uniform electric field stimulation *in vitro*. *Brain Stimul.* (2009) 2:215–28.e3. doi: 10.1016/j.brs.2009.03.007
14. Woods AJ, Antal A, Bikson M, Boggio PS, Brunoni AR, Celnik P, et al. A technical guide to tDCS, and related non-invasive brain stimulation tools. *Clin Neurophysiol.* (2016) 127:1031–48. doi: 10.1016/j.clinph.2015.11.012
15. Batsikadze G, Moliadze V, Paulus W, Kuo MF, Nitsche MA. Partially non-linear stimulation intensity-dependent effects of direct current stimulation on motor cortex excitability in humans. *J Physiol.* (2013) 591:1987–2000. doi: 10.1113/jphysiol.2012.249730
16. Esmaeilpour Z, Marangolo P, Hampstead BM, Bestmann S, Galletta E, Knotkova H, et al. Incomplete evidence that increasing current intensity of tDCS boosts outcomes. *Brain Stimul.* (2018) 11:310–21. doi: 10.1016/j.brs.2017.12.002
17. Horvath JC, Forte JD, Carter O. Quantitative review finds no evidence of cognitive effects in healthy populations from single-session transcranial Direct Current Stimulation (tDCS). *Brain Stimul.* (2015) 8:535–50. doi: 10.1016/j.brs.2015.01.400
18. Bikson M, Rahman A, Datta A. Computational models of transcranial direct current stimulation. *Clin EEG Neurosci.* (2012) 43:176–83. doi: 10.1177/1550059412445138
19. Krause B, Márquez-Ruiz J, Cohen Kadosh R. The effect of transcranial direct current stimulation: a role for cortical excitation/inhibition balance? *Front Hum Neurosci.* (2013) 7:602. doi: 10.3389/fnhum.2013.00602
20. Kim S, Stephenson MC, Morris PG, Jackson SR. tDCS-induced alterations in GABA concentration within primary motor cortex predict motor learning and motor memory: a 7T magnetic resonance spectroscopy study. *Neuroimage* (2014) 99:237–43. doi: 10.1016/j.neuroimage.2014.05.070
21. Stagg CJ, Best JG, Stephenson MC, Shea J, Wylezinska M, Kincses ZT, et al. Polarity-sensitive modulation of cortical neurotransmitters by transcranial stimulation. *J Neurosci.* (2009) 29:5202–6. doi: 10.1523/JNEUROSCI.4432-08.2009
22. Clark VP, Coffman BA, Trumbo MC, Gasparovic C. Transcranial direct current stimulation (tDCS) produces localized and specific alterations in neurochemistry: a 1H magnetic resonance spectroscopy study. *Neurosci Lett.* (2011) 500:67–71. doi: 10.1016/j.neulet.2011.05.244
23. Hone-Blanchet A, Edden RA, Fecteau S. Online effects of transcranial direct current stimulation in real time on human prefrontal and striatal metabolites. *Biol Psychiatry* (2016) 80:432–8. doi: 10.1016/j.biopsych.2015.11.008
24. Bachtiar V, Near J, Johansen-Berg H, Stagg CJ. Modulation of GABA and resting state functional connectivity by transcranial direct current stimulation. *Elife* (2015) 4:e08789. doi: 10.7554/eLife.08789
25. Hone-Blanchet A, Fecteau, S. Chapter 15 - The use of non-invasive brain stimulation in drug addictions. In: Kadosh RC, editor. *The Stimulated Brain*. San Diego, CA: Academic Press. (2014). p. 425–452. doi: 10.1016/B978-0-12-404704-4.00015-6
26. Oldfield RC. The assessment and analysis of handedness: the Edinburgh inventory. *Neuropsychologia* (1971) 9:97–113. doi: 10.1016/0028-3932(71)90067-4
27. Mondino M, Bennabi D, Poulet E, Galvao F, Brunelin J, Haffen E. Can transcranial direct current stimulation (tDCS) alleviate symptoms and improve cognition in psychiatric disorders? *World J Biol Psychiatry* (2014) 15:261–75. doi: 10.3109/15622975.2013.876514
28. Nitsche MA, Seeber A, Frommann K, Klein CC, Rochford C, Nitsche MS, et al. Modulating parameters of excitability during and after transcranial direct current stimulation of the human motor cortex. *J Physiol.* (2005) 568:291–303. doi: 10.1113/jphysiol.2005.092429
29. Mescher M, Merkle H, Kirsch J, Garwood M, Gruetter R. Simultaneous *in vivo* spectral editing and water suppression. *NMR Biomed.* (1998) 11:266–72. doi: 10.1002/(SICI)1099-1492(199810)11:6<266::AID-NBM530>3.0.CO;2-J
30. Henry ME, Lauriat TL, Shanahan M, Renshaw PF, Jensen JE. Accuracy and stability of measuring GABA, glutamate, and glutamine by proton magnetic resonance spectroscopy: a phantom study at 4Tesla. *J Magn Reson.* (2011) 208:210–8. doi: 10.1016/j.jmr.2010.11.003
31. Provencher SW. Estimation of metabolite concentrations from localized *in vivo* proton NMR spectra. *Magn Reson Med.* (1993) 30:672–9. doi: 10.1002/mrm.1910300604
32. Provencher SW. Automatic quantitation of localized *in vivo* 1H spectra with LCModel. *NMR Biomed.* (2001) 14:260–4. doi: 10.1002/nbm.698
33. Dydak U, Jiang Y-M, Long L-L, Zhu H, Chen J, Li W-M, et al. *In vivo* measurement of brain GABA concentrations by magnetic resonance spectroscopy in smelters occupationally exposed to manganese. *Environ Health Perspect.* (2011) 119:219–24. doi: 10.1289/ehp.1002192
34. Kaiser LG, Young K, Meyerhoff DJ, Mueller SG, Matson GB. A detailed analysis of localized J-difference GABA editing: theoretical and experimental study at 4 T. *NMR Biomed.* (2008) 21:22–32. doi: 10.1002/nbm.1150
35. Edden RAE, Puts NAJ, Barker PB. Macromolecule-suppressed GABA-edited magnetic resonance spectroscopy at 3T. *Magn Reson Med.* (2012) 68:657–61. doi: 10.1002/mrm.24391
36. Zhu X-H, Chen W. Observed BOLD effects on cerebral metabolite resonances in human visual cortex during visual stimulation: a functional 1H MRS study at 4 T. *Magn Reson Med.* (2001) 46:841–7. doi: 10.1002/mrm.1267
37. R Development Core Team. *R: A Language and Environment for Statistical Computing*. Vienna: R Foundation for Statistical Computing. (2016). Available online at: https://www.R-project.org/
38. Pinheiro J, Bates D, DebRoy S, Sarkar D, Team RC. *nlme: Linear and Nonlinear Mixed Effects Models: R Package Version 3.1-128*. (2016). Available online at: http://CRAN.R-project.org/package=nlme

39. Horvath JC, Forte JD, Carter O. Evidence that transcranial direct current stimulation (tDCS) generates little-to-no reliable neurophysiologic effect beyond MEP amplitude modulation in healthy human subjects: a systematic review. *Neuropsychologia* (2015) 66:213–36. doi: 10.1016/j.neuropsychologia.2014.11.021
40. Westwood SJ, Olson A, Miall RC, Nappo R, Romani C. Limits to tDCS effects in language: failures to modulate word production in healthy participants with frontal or temporal tDCS. *Cortex* (2017) 86:64–82. doi: 10.1016/j.cortex.2016.10.016
41. Antal A, Bikson M, Datta A, Lafon B, Dechent P, Parra LC, et al. Imaging artifacts induced by electrical stimulation during conventional fMRI of the brain. *Neuroimage* (2014) 85:1040–7. doi: 10.1016/j.neuroimage.2012.10.026
42. Faul F, Erdfelder E, Lang A-G, Buchner A. G*Power 3: a flexible statistical power analysis program for the social, behavioral, and biomedical sciences. *Behav Res Methods* (2007) 39:175–91. doi: 10.3758/BF03193146
43. Button KS, Ioannidis JPA, Mokrysz C, Nosek BA, Flint J, Robinson ESJ, et al. Power failure: why small sample size undermines the reliability of neuroscience. *Nat Rev Neurosci*. (2013) 14:365–76. doi: 10.1038/nrn3475
44. Bottomley PA, Griffiths JR. *Handbook of Magnetic Resonance Spectroscopy in vivo: MRS Theory, Practice and Applications*. Chichester: John Wiley & Sons Ltd. (2016).
45. Barantin L, Pape AL, Akoka S. A new method for absolute quantitation MRS metabolites. *Magn Reson Med.* (1997) 38:179–82. doi: 10.1002/mrm.1910380203
46. Heinzer-Schweizer S, De Zanche N, Pavan M, Mens G, Sturzenegger U, Henning A, et al. *In-vivo* assessment of tissue metabolite levels using 1H MRS and the Electric REference to access *in vivo* concentrations (ERETIC) method. *NMR Biomed.* (2010) 23:406–13. doi: 10.1002/nbm.1476
47. Bikson M, Rahman A. Origins of specificity during tDCS: anatomical, activity-selective, and input-bias mechanisms. *Front Hum Neurosci.* (2013) 7:688. doi: 10.3389/fnhum.2013.00688
48. Winer JA, Schreiner CE. *The Auditory Cortex*. New York, NY: Springer US. (2010).

Conflict of Interest Statement: We wish to draw to the attention of the Editor that co-authors AC, LE, KH, and RG have shares in the company NordicNeuroLab A/S which produces add-on equipment for MRI examinations that were used in this study.

The remaining authors declare that the research was conducted in the absence of any commercial or financial relationships that could be construed as a potential conflict of interest.

frontiers in Neurology

ORIGINAL RESEARCH
published: 26 July 2018
doi: 10.3389/fneur.2018.00618

Corpus Callosum Radiomics-Based Classification Model in Alzheimer's Disease: A Case-Control Study

*Qi Feng[1,2], Yuanjun Chen[3], Zhengluan Liao[4], Hongyang Jiang[2], Dewang Mao[2], Mei Wang[2], Enyan Yu[4] and Zhongxiang Ding[5]**

[1] Bengbu Medical College, Bengbu, China, [2] Department of Radiology, Zhejiang Provincial People's Hospital, People's Hospital of Hangzhou Medical College, Hangzhou, China, [3] GE Healthcare Life Sciences, Guangzhou, China, [4] Department of Psychiatry, Zhejiang Provincial People's Hospital, People's Hospital of Hangzhou Medical College, Hangzhou, China, [5] Department of Radiology, Affiliated Hangzhou First People's Hospital, Zhejiang University School of Medicine, Hangzhou, China

Background: Alzheimer's disease (AD) is a progressive neurodegenerative disease that causes the decline of some cognitive impairments. The present study aimed to identify the corpus callosum (CC) radiomic features related to the diagnosis of AD and build and evaluate a classification model.

Methods: Radiomics analysis was applied to the three-dimensional T1-weighted magnetization-prepared rapid gradient echo (MPRAGE) images of 78 patients with AD and 44 healthy controls (HC). The CC, in each subject, was segmented manually and 385 features were obtained after calculation. Then, the feature selection were carried out. The logistic regression model was constructed and evaluated according to identified features. Thus, the model can be used for distinguishing the AD from HC subjects.

Results: Eleven features were selected from the three-dimensional T1-weighted MPRAGE images using the LASSO model, following which, the logistic regression model was constructed. The area under the receiver operating characteristic curve values (AUC), sensitivity, specificity, accuracy, precision, and positive and negative predictive values were 0.720, 0.792, 0.500, 0.684, 0.731, 0.731, and 0.583, respectively.

Conclusion: The results demonstrated the potential of CC texture features as a biomarker for the diagnosis of AD. This is the first study showing that the radiomics model based on machine learning was a valuable method for the diagnosis of AD.

Keywords: magnetic resonance imaging, Alzheimer's disease, corpus callosum, radiomics, neuroimaging

OPEN ACCESS

Edited by:
Lars Ersland, Haukeland University Hospital, Norway

Reviewed by:
Cristian E. Leyton, University of Sydney, Australia
Jordi A. Matias-Guiu, Hospital Clínico San Carlos, Spain

***Correspondence:**
Zhongxiang Ding
hangzhoudzx73@126.com

Specialty section:
This article was submitted to Applied Neuroimaging, a section of the journal Frontiers in Neurology

Received: *10 May 2018*
Accepted: *10 July 2018*
Published: *26 July 2018*

Citation:
Feng Q, Chen Y, Liao Z, Jiang H, Mao D, Wang M, Yu E and Ding Z (2018) Corpus Callosum Radiomics-Based Classification Model in Alzheimer's Disease: A Case-Control Study. Front. Neurol. 9:618. doi: 10.3389/fneur.2018.00618

INTRODUCTION

Alzheimer's disease (AD) is a progressive neurodegenerative disease, resulting in the decline of some cognitive impairments that in turn can influence the immediate and delayed memory, language, calculation, attention, and visuospatial abilities. A definitive diagnosis of AD depends on the pathological findings from an invasive autopsy or biopsy that might not be available. Therefore, noninvasive and accurate AD diagnosis is critical. Although current pharmacotherapy cannot cure this disease, early intervention can delay the disease progression and also prolongs the lives of patients with AD.

The corpus callosum (CC) is the largest white matter tract in the human brain, which connects the two hemispheres that is essential for several neurological functions, including integration

of lateralized sensory input, regulation of higher-order cognitive, social function, and emotional processing (1). The CC atrophy has been found in patients with AD (2), and some of these studies have indicated that the CC atrophy might be related to the degree of cognitive impairment. Therefore, the CC atrophy might be ascribed as the neuroanatomy basis for memory decline in AD. Additionally, a recent study showed the relationship between the CC and AD by texture analysis (3).

Radiomics is a newly developed tumor diagnosis and auxiliary detection technique in recent years. It transforms the visual image information into deep features for quantitative research. Radiomics may provide almost unlimited feature information. The information includes the density, shape, size, and texture of the tumor as determined by phenotype and microenvironment, which aids in the evaluation of the efficacy and prognosis in tumor therapy. The radiomics analysis has been applied to various tumor diseases, such as glioma (4), nasopharyngeal cancer (5), breast cancer (6), hepatocellular carcinoma (7), lung cancer (8), and rectal cancer (9). Nowadays, radiomics is also applied in non-tumor areas, for example, attention-deficit hyperactivity disorder (10), Meniere's disease (11), and autism spectrum disorder (12).

In recent years, the most commonly used imaging method in radiomics studies is computed tomography (CT) that quantifies the tissue density. However, as compared to CT, magnetic resonance (MR) images can provide numerous sequences. It reflects not only the structure of the organization but also the functional metabolism and dynamic changes. MR imaging provides an enhanced tissue contrast, has a multidimensional volume, and does not require a radiation dose (13). Several MR methods have been used to study AD, including resting-state functional MRI (14), voxel-based morphometry (15), diffusion tensor imaging (16), and arterial spin labeling (17) among others. Although these methods are greatly valuable in the diagnosis of AD, they are rarely used in the related radiomics features.

In the present study, we used the T1-weighted MR images of the brain for radiomics analysis. A series of characteristics are obtained by analyzing the heterogeneity of the target area. Finally, clinical prediction and feature analysis were realized. Subsequently, we focused on studying the CC as it occupies a crucial position in AD and can be considered suitable for radiomics analysis. Therefore, the CC heterogeneity is investigated to construct a classification model for distinguishing between the patients with AD and HC.

MATERIALS AND METHODS

Patient Population and Data Acquisition

AD subjects were recruited from the Zhejiang Provincial People's Hospital from September 2016 to February 2018. The healthy control (HC) subjects were right-handed volunteers and recruited from the health promotion center of the hospital. All the subjects provided written informed consent. This prospective study was approved by the local Ethics Committee of the hospital (No. 2012KY002). The work has been carried out in accordance with the Declaration of Helsinki.

The patients underwent a set of standard dementia screening including medical history, neuropsychological testing, physical examinations, laboratory tests, and conventional brain MRI scans. Patients with AD were first diagnosed and were required to fulfill the criteria of the revised NINCDS-ADRDA (National Institute of Neurological and Communicative Disorders and Stroke and the Alzheimer's Disease and Related Disorders Association) (18). The subjects were evaluated using the Mini-Mental State Examination (MMSE) (19). Patients with AD received an MMSE score of ≤ 24.

The criteria for HC subjects were as follows: (1) no neurological or psychiatric disorders such as stroke, epilepsy, or depression; (2) no neurological deficiencies such as hearing or visual loss; (3) no infarction, hemorrhage, or tumor lesion on conventional brain MRI; (4) achieved an MMSE score ≥ 28.

The exclusion criteria for all the subjects were as follows: (1) vascular dementia or mixed dementia; (2) stroke; (3) cerebral trauma; (4) disorders that cause memory loss such as brain tumor, epilepsy, Parkinson's disease; (5) systemic diseases such as severe anemia, diabetes, and hypertension; (6) history of administering psychoactive substances or alcohol dependence. Therefore, 85 patients with AD and 50 HC subjects were recruited initially, followed by an MRI-based examination, and those with unusable data due to the head movement were excluded (7 patients in the AD group and 6 controls). Thus, 78 patients with AD and 44 HC subjects were ultimately included in the study.

All examinations were performed using an MR scanner (Discovery MR750 3.0T; GE Healthcare, Waukesha, WI, USA). The three-dimensional T1-weighted magnetization-prepared rapid gradient echo (MPRAGE) sagittal images were collected. The scan parameters were as follows: TR = 6.7 ms, TE = 2.9 ms, TI = 450 ms, FOV = 256 × 256 mm^2, flip angle = 12°, slice thickness/gap = 1/0 mm, in-plane resolution = 256 × 256, and 192 sagittal slices in total. All collected data is from only one MR scanner.

Segmentation

The CC is considered the region of interest (ROI). The manual segmentation of the CC was carried out using the software "ITK-SNAP" (http://www.itksnap.org/). We selected 9 sections from each image sequence in the sagittal view: the central section, 4 to the right and 4 to the left, as the boundary of CC can be recognizable easily in the sagittal images. Consequently, the segmentation was based on anatomy, which was supported by a previous study (20). All segmentations were conducted by a radiologist and checked by an expert neuroradiologist. The differences in the opinions were resolved by integrating another expert neuroradiologist's opinion. Artificial Intelligence Kit (A.K) is a software developed by GE Healthcare Life Sciences for feature extraction and analysis. It can be combined with software "ITK-SNAP" to obtain 3D images.

Feature Calculation

First, we loaded the original three-dimensional T1-weighted MPRAGE data and ROI images in bulk into the A.K software. Then, the features including Histogram, Formfactor, Haralick, gray level co-occurrence matrix (GLCM), and gray level

run-length matrix (RLM), desired for computation were selected in the data selection window. The displacement vectors were selected as 1, 4, and 7 in the relevant window. The histogram parameters were concerned with the properties of individual pixels that described the distribution of the voxel intensities in the image via basic metrics. The Formfactor parameters include descriptors of the three-dimensional shape and size of the tumor ROI. The texture is one of the major characteristics in identifying the ROI in an image. Texture represents the appearance of the surface and the distribution pattern of the voxels. The GLCM $P(i, j \mid \theta, d)$ calculates the number of times a pixel with gray -level $\boldsymbol{i}$ occurs with another pixel with a gray value $\boldsymbol{j}$ jointly. It is defined as the joint probability of specific pixels having certain gray -level values. The rotation angles of an offset are 0°, 45°, 90°, 135°, and the distance to the neighboring pixel is 1, 2, 3...; the same images have different co-occurrence distributions (21). The RLM $P\ r(i,j \mid \theta)$ represents the number of runs for pixels with gray level $\boldsymbol{i}$ and run length $\boldsymbol{j}$ for a given direction $\boldsymbol{\theta}$. The following ten features of RLM were derived: short run emphasis, long run emphasis, gray level non-uniformity, run length non-uniformity, low gray level run emphasis, high gray level run emphasis, short run low gray level emphasis, short run high gray level emphasis, long run low gray level emphasis, and long run high gray level emphasis (22, 23). The formulas for some parameters are displayed in **Table 1**. The total number of features extracted from this data is 385. Then, the AD or HC label was added for each subject.

Feature Selection

The preprocessing before feature selection was divided into three steps. The first step was dealing with the abnormal value. Here, we replaced the abnormal values by mean. The second step was to set the data to the training data proportion of 0.7 and the testing data proportion of 0.3. The third step was to preprocess the training data after division and perform the same operation on the testing data. This method is known as standardization. The feature selection steps are as follows.

Step 1: The software first sought to identify the features that contribute to the result using the T-test ($P < 0.05$). The rank sum test was used to select the features with significant differences ($P < 0.05$), and the features of T-test and rank sum test were selected together.

Step 2: The correlation analysis reduced the dimension. The filter threshold was set to 0.9 for the Spearman rank correlation coefficient analysis that was conducted on any two feature columns. The two features were highly correlated if the correlation coefficient was > 0.9, thereby excluding of one of them.

TABLE 2 | Demographics performances of the AD and healthy controls.

	AD group	HC group	Statistic	*p* value
Sample size	78	44	NA	NA
Age (years, mean ± SD)	69.18 ± 12.23	65.43 ± 9.70	−1.75	0.08
Gender (Male: Female)	25:53	20:24	2.17*	0.14*
Education (years, mean ± SD)	7.54 ± 4.16	7.09 ± 3.38	−0.61	0.54
MMSE	16.94 ± 5.94	29.14 ± 0.77	17.87	<0.01

*SD standard deviation; Statistics were calculated with t tests unless otherwise indicated; *x^2 test was used; MMSE mini-mental state examination.*

TABLE 1 | Definition of the features measures computed in this study after feature selection.

Type of measure	Name	Formula
Texture Parameter	ClusterShade_AllDirection_offset1	$\sum_{i,j}((i-\mu)+(j-\mu))^3 g(i,j)$
GLCM Parameter	InverseDifferenceMoment_AllDirection_offset1	$f_5 = \sum_{i=1}^{N_8}\sum_{j=1}^{N_8}\frac{1}{1+(i-j)^2}p(i,j)$
GLCM parameter	InverseDifferenceMoment_AllDirection_offset4_SD	$f_5 = \sum_{i=1}^{N_8}\sum_{j=1}^{N_8}\frac{1}{1+(i-j)^2}p(i,j)$
RLM parameter	ShortRunEmphasis_angle45_offset1	$SRE(\theta) = \frac{1}{n_r}\sum_{i=1}^{M}\sum_{j=1}^{N}\frac{p(i,j,\theta)}{j^2}$
RLM parameter	RunLengthNonuniformity_AllDirection_offset4_SD	$RLN(\theta) = \frac{1}{n_r}\sum_{j=1}^{N}(\sum_{i=1}^{M}p(i,j,\theta))^2$
RLM parameter	ShortRunHighGreyLevelEmphasis_AllDire ction_offset4_SD	$SRHGE(\theta) = \frac{1}{n_r}\sum_{j=i}^{N}\sum_{i=1}^{M}\frac{p(i,j,\theta)i^2}{j^2}$
RLM parameter	ShortRunEmphasis_angle90_offset7	$SRE(\theta) = \frac{1}{n_r}\sum_{i=1}^{M}\sum_{j=1}^{N}\frac{p(i,j,\theta)}{j^2}$
RLM parameter	LongRunEmphasis_AllDirection_offset4_SD	$LRE(\theta) = \frac{1}{n_r}\sum_{i=1}^{M}\sum_{j=1}^{N}p(i,j,\theta)j^2$
RLM parameter	ShortRunEmphasis_angle0_offset4	$SRE(\theta) = \frac{1}{n_r}\sum_{i=1}^{M}\sum_{j=1}^{N}\frac{p(i,j,\theta)}{j^2}$
RLM parameter	ShortRunEmphasis_angle90_offset4	$SRE(\theta) = \frac{1}{n_r}\sum_{i=1}^{M}\sum_{j=1}^{N}\frac{p(i,j,\theta)}{j^2}$
RLM parameter	GreyLevelNonuniformity_AllDirection_offset7_SD	$GLN(\theta) = \frac{1}{n_r}\sum_{i=1}^{M}(\sum_{j=1}^{N}p(i,j,\theta))^2$

For texture parameter, g is a GLCM, where i,j are the spatial coordinates of g (i,j). For GLCM parameters, i is a gray-level, j is a gray value, N is the number of classes of gray levels. For RLM parameters, n_r is the number of runs, N is the number of classes of gray levels, and M is the size in voxels of the largest region found.

Step 3: In the training data, the most useful features were selected by the least absolute shrinkage and selection operator (LASSO) Cox regression model. We need to minimize the sum of squares of residues, with the sum of the absolute values of the selected features coefficients being not more than a tuning parameter (λ). We chose the λ which got the minimum criteria according to 10-fold cross-validation in the LASSO model. This method was suitable for the regression analysis of high-dimensional data, and patient features could be selected based on the associations with the survival endpoints and time (24).

Machine Learning

Firstly, training data and testing data were loaded for the following up model building and testing. We subsequently selected the logical regression method to establish a classification model for AD diagnosis. This method was based on the linear function; it served as an independent variable into the sigmoid function. According to the probability *P* of the output (probability that the classification result is 1), the classification was determined. It's one of the machine learning methods.

RESULTS

Comparison of Demographic and Neuropsychological Performance

The demographic variables did not differ significantly between patients and control subjects, as assessed by SPSS (version 22.0). However, the neuropsychological performance was significantly different between the two groups (**Table 2**).

Feature Selection Results

Step 1: A total of 385 features were extracted. The selective method was *T* test + MW. The remaining feature number was 196.

Step 2: The selective method was correlation analysis. The threshold value was 0.9, correlation method Spearman, and the remaining feature number was 89 (**Figure 1**).

Step 3: The selective method was Lasso. We found an optimal lambda by using cross-validation. The error-lambda graph is illustrated in **Figure 2**. The coefficients-lambda graph is shown in **Figure 3**. The remaining feature number was 11. The feature name order was as follows: "InverseDifferenceMoment_AllDirection_offset1"; "ClusterShade_AllDirection_offset1"; "ShortRunEmphasis_angle45_offset1"; "InverseDifferenceMoment_AllDirection_offset4_SD"; "RunLengthNonuniformity_AllDirection_offset4_SD"; "ShortRunHighGreyLevelEmphasis_AllDirection_offset4_SD"; "ShortRunEmphasis_angle90_offset7"; "LongRunEmphasis_AllDirection_offset4_SD"; "ShortRunEmphasis_angle0_offset4"; "ShortRunEmphasis_angle90_offset4"; "GreyLevelNonuniformity_AllDirection_offset7_SD" (**Table 1**).

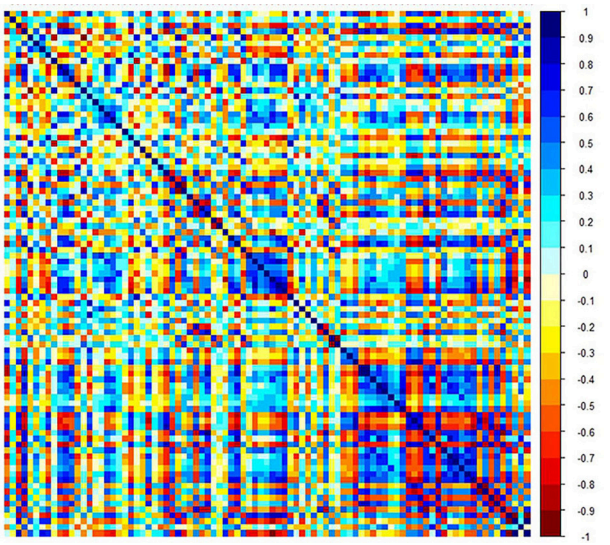

FIGURE 1 | Graph shows correlation analysis between the parameters of training data.

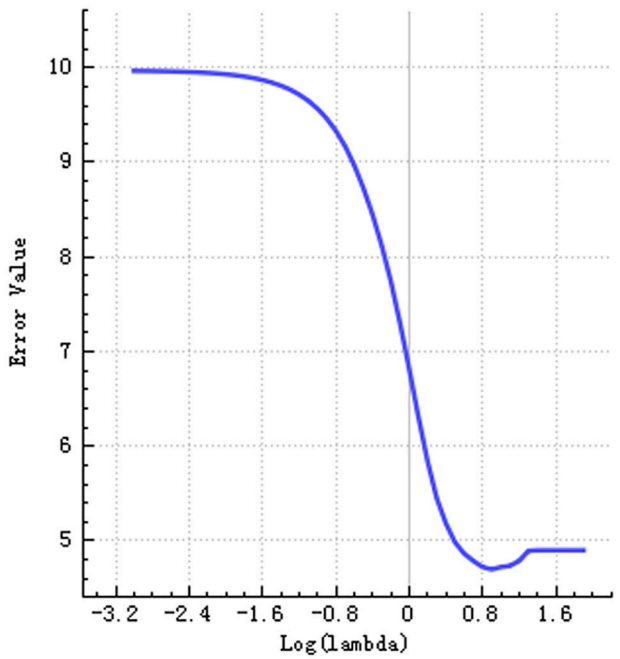

FIGURE 2 | Graph shows error-lambda.

Machine Learning Results

The training and testing data were loaded, the proportion of the training data was 0.7, while that of the testing data was 0.3. While establishing the classifier discriminating the patients with AD from HC subjects, the selected method was logistic regression based on the selected features. The area under the receiver operating characteristic curve values (AUC), sensitivity, specificity, accuracy, precision, positive predictive value, and

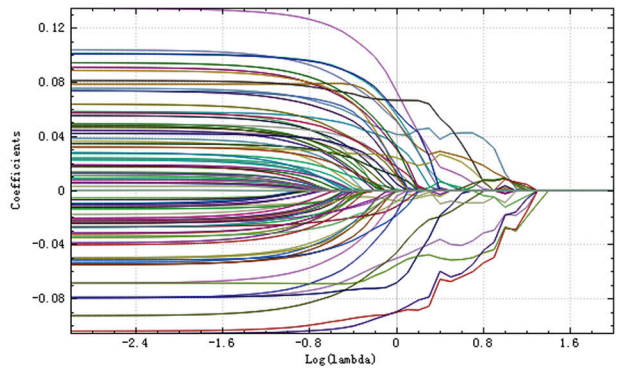

FIGURE 3 | Plot of coefficients-lambda.

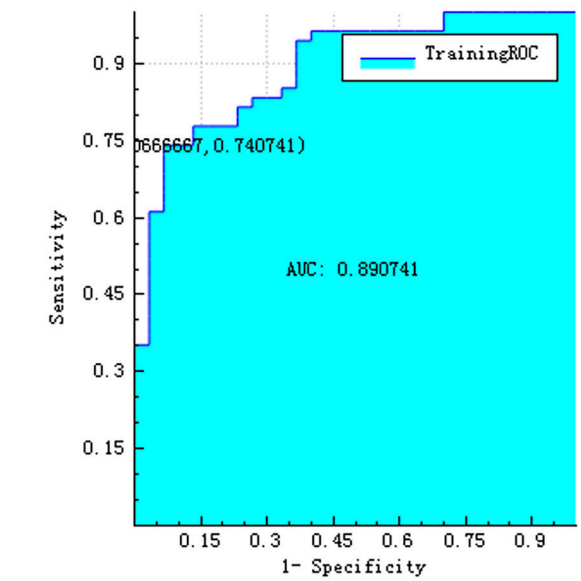

FIGURE 4 | ROC curve of training data.

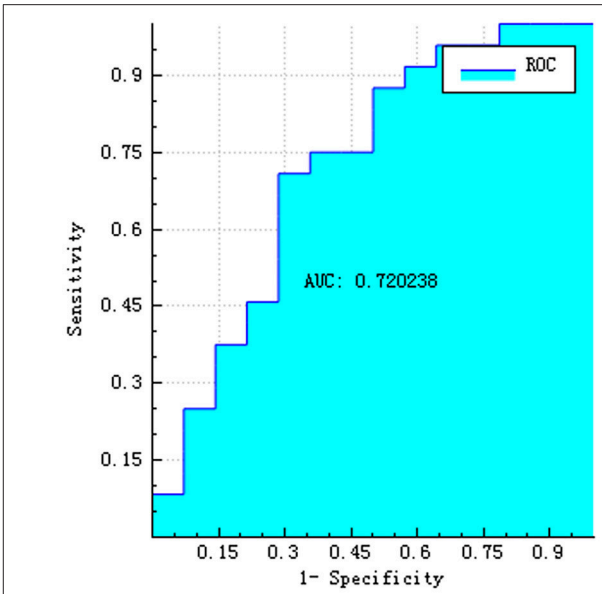

FIGURE 5 | ROC curve of testing data.

negative predictive value were 0.720, 0.792, 0.500, 0.684, 0.731, 0.731, and 0.583, respectively (**Figures 4–6**).

DISCUSSION

The major finding of the present study was that the CC radiomics-based classification model discriminated the patients with AD from HC subjects. After a three-step feature selection, an 11-feature radiomics signature was constructed using logistic regression model for the diagnosis of patients with AD. Although the specificity of this model was not extremely high, its diagnostic value was better than the other indicators.

The radiomics analysis has already been applied to neuropsychiatric disorders. For example, a radiomics study found texture differences between autism spectrum disorder and control groups in the right hippocampus, left choroid-plexus, CC, and cerebellar white matter (25). Another recent radiomics study indicated that cerebral morphometric alterations can allow discrimination between the patients with attention deficit hyperactivity disorder and control subjects and also among the subtypes (10). This study has built random forest classifiers for diagnosis and subtyping. In addition, textures differences in the CC and thalamus were observed in AD and amnestic mild cognitive impairment (3). One study investigated the three-dimensional texture as a putative diagnostic marker of AD (26). However, currently, there is no study describing the establishment of the model in the analysis of AD radiomics studies. Thus, for the first time, the present study attempted to construct a classification model for the diagnosis of AD. In addition, the machine learning method was added to the modeling.

The CC presented abnormality in the surface-based morphometry and microstructural integrity in the patients with AD (27). Another study found significant volume reductions in anterior and posterior of the CC in severe AD patients (28). A voxel-based morphometry study in AD detected significant atrophy of CC in the anterosuperior splenium, the anterior and posterior portions of the body, and the rostral portion of the genu (29). The volume changes in the different portions of the CC might exist in different pathological processes. Reportedly, the anterior portion of CC consists of myelinated axons with a small diameter; however, the posterior portion consists of thick fibers (1). Thus, this abnormal development might result in the differences observed in the texture. In the current study, the texture features derived from the CC were used for differentiating between AD and HC subjects. Herein, we established an analysis framework on the basis of CC radiomics and machine learning methods for AD diagnosis, which suggested that the CC radiomics features could be used as biomarkers for AD diagnosis. Nevertheless, longitudinal developmental studies are essential to substantiate these interpretations. Structural data were involved in the process of classifier building, thereby providing a neuroanatomical evaluation of the disorder.

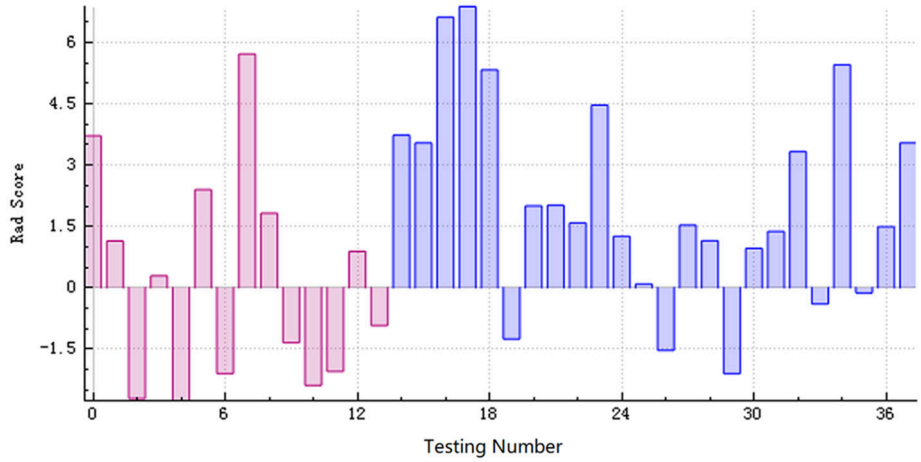

FIGURE 6 | The radiomics score based on the testing data. The red area below the horizontal line and the blue area above the horizontal line represented the accurate prediction. On the contrary, the red area above the horizontal line and the blue area below the horizontal line represented the false prediction.

The radiomics signature consisted of 11 imaging features that were deep features, extracted from the three-dimensional T1-weighted MPRAGE images. The deep features extracted from A.K. performed better than the conventional handcrafted features in the diagnosis of patients with AD. As expected, the deep features reflected higher order imaging patterns and captured more imaging heterogeneity as compared to the low-level shape, intensity, and texture features. Cluster Shade is one of the texture parameters. Cluster analysis is the task of grouping objects such that the objects in the same cluster are rather similar to each other than those in the other clusters. The inverse difference moment is one of the GLCM parameters. Short run emphasis, long run emphasis, run length non-uniformity, short-run high gray level emphasis, and gray level non-uniformity constitute the RLM parameters. They reflect the measurement of nonuniformity of the length and that of the grayscale. Thus, the observed abnormalities in the CC may be clinically relevant with respect to cognitive and behavioral issues in patients with AD. However, the relationship between the radiomics features and the genetic characteristics is yet challenging.

Nevertheless, the present study has several limitations. First, owing to the insufficient sample size, the classification performance may be limited. Thus, a large-scale multicenter study is required to fully assess the generalization ability of the radiomics model in future. Second, although no statistically significant difference was detected between the two groups in the sex ratio analysis, we did not achieve a complete 1:1 match, and hence, it was not possible to completely exclude the effect on the study results. Finally, there is no evaluation of white matter integrity using white matter imaging method, such as DTI and DKI, which need to be further studied.

Future radiomics work can use additional imaging modalities, such as diffusion tensor imaging and functional MRI. These radiomics models might contain additional anatomical structures related to AD, such as the hippocampus, medial temporal lobe, thalamus, as well as, the whole brain. Furthermore, we can improve the classification performance by combining the radiomics analysis with established clinical risk factors such as age and MMSE score.

In conclusion, our findings indicated that a moderately successful diagnostic classification efficiency could be achieved between patients with AD and HC subjects using the CC radiomic features. The workflow was automatic, and therefore, potentially useful in the clinical setting. As a non-invasive MR-based imaging biomarker, the radiomics analysis might provide a valuable and practical method to identify the patients with AD and guide the individualized treatment.

ETHICS STATEMENT

We confirm that we have read the Journal's position on issues involved in ethical publication and affirm that this report is consistent with those guidelines.

AUTHOR CONTRIBUTIONS

QF, HJ, DM, EY, and ZD designed the study. ZL and QF collected patient data and provided clinical expertise. QF and MW segmented the MR images. QF drafted the manuscript. YC interpreted the data for the work. All the authors discussed the results and read and approved the final version of the manuscript.

FUNDING

This research was supported by the Zhejiang Provincial Natural Science Foundation (LY16H180007), the Science Foundation from Health Commission of Zhejiang Province (2016147373), and the Project supported by research innovation program of graduate students of Bengbu Medical College (Byycx1738).

ACKNOWLEDGMENTS

The authors would like to thank the GE Healthcare Life Sciences for supporting this work.

REFERENCES

1. Aboitiz F, Montiel J. One hundred million years of interhemispheric communication: the history of the corpus callosum. *Braz J Med Biol Res.* (2003) 36:409–20. doi: 10.1590/S0100-879X2003000400002
2. Zhu M, Wang X, Gao W, Chen S, Ge H, Hong S, et al. Corpus callosum atrophy and cognitive decline in early Alzheimer's disease: longitudinal MRI study. *Dement Geriatric Cogn Disord.* (2014) 37:214. doi: 10.1159/000350410
3. de Oliveira MS, Balthazar ML, D'Abreu A, Yasuda CL, Damasceno BP, Cendes F, et al. MR imaging texture analysis of the corpus callosum and thalamus in amnestic mild cognitive impairment and mild Alzheimer disease. *AJNR Am J Neuroradiol.* (2011) 32:60. doi: 10.3174/ajnr.A2232
4. Lao J, Chen Y, Li ZC, Li Q, Zhang J, Liu J, et al. A deep learning-based radiomics model for prediction of survival in glioblastoma multiforme. *Sci Rep.* (2017) 7:10353. doi: 10.1038/s41598-017-10649-8
5. Zhang S, Zhang B, Tian J, Dong D, Gu DS, Dong YH, et al. Radiomics features of Multiparametric MRI as novel prognostic factors in advanced nasopharyngeal carcinoma. *Clin Cancer Res Official J Am Assoc Cancer Res.* (2017) 23:4259. doi: 10.1158/1078-0432.CCR-16-2910
6. Cameron A, Khalvati F, Haider M, Wong A. MAPS: a quantitative radiomics approach for prostate cancer detection. *IEEE Trans Bio-Med Eng.* (2015) 63:1145. doi: 10.1109/TBME.2015.2485779
7. Cozzi L, Dinapoli N, Fogliata A, Hsu WC, Reggiori G, Lobefalo F, et al. Radiomics based analysis to predict local control and survival in hepatocellular carcinoma patients treated with volumetric modulated arc therapy. *BMC Cancer* (2017) 17:829. doi: 10.1186/s12885-017-3847-7
8. Yu W, Tang C, Hobbs BP, Li X, Koay EJ, Wistuba II, et al. Development and validation of a predictive radiomics model for clinical outcomes in stage I non-small cell lung cancer. *Int J Radiat Oncol Biol Phys.* (2017). doi: 10.1016/j.ijrobp.2017.10.046. [Epub ahead of print].
9. Nie K, Shi L, Chen Q, Hu X, Jabbour SK, Yue N, et al. Rectal cancer: assessment of neoadjuvant chemoradiation outcome based on radiomics of multiparametric MRI. *Clin Cancer Res.* (2016) 22:5256. doi: 10.1158/1078-0432.CCR-15-2997
10. Sun H, Chen Y, Huang Q, Lui S, Huang X, Shi Y, et al. Psychoradiologic utility of MR imaging for diagnosis of attention deficit hyperactivity disorder: a radiomics analysis. *Radiology* (2017) (Suppl. 11):170226. doi: 10.1148/radiol.2017170226
11. Burg ELVD, Hoof MV, Postma AA, Janssen AML, Stokroos RJ, Kingma H, et al. An exploratory study to detect ménière's disease in conventional MRI scans using radiomics. *Front Neurol.* (2016) 7:170. doi: 10.3389/fneur.2016.00190
12. Chaddad A, Desrosiers C, Hassan L, Tanougast C. Hippocampus and amygdala radiomic biomarkers for the study of autism spectrum disorder. *BMC Neurosci.* (2017) 18:52. doi: 10.1186/s12868-017-0373-0
13. Tang LL, Li WF, Chen L, Sun Y, Chen Y, Liu LZ, et al. Prognostic value and staging categories of anatomic masticator space involvement in nasopharyngeal carcinoma: a study of 924 cases with MR imaging. *Radiology* (2010) 257:151–7. doi: 10.1148/radiol.10100033
14. Yu E, Liao Z, Mao D, Zhang Q, Ji G, Li Y, et al. Directed functional connectivity of posterior cingulate cortex and whole brain in Alzheimer's disease and mild cognitive impairment. *Curr Alzheimer Res.* (2016) 14:628–35. doi: 10.2174/1567205013666161201201000
15. Li X, Cao M, Zhang J, Chen K, Chen Y, Ma C, et al. Structural and functional brain changes in the default mode network in subtypes of amnestic mild cognitive impairment. *J Geriatric Psychiatry Neurol.* (2014) 27:188–98. doi: 10.1177/0891988714524629
16. Lee SH, Coutu JP, Wilkens P, Yendiki A, Rosas HD, Salat DH. Tract-based analysis of white matter degeneration in Alzheimer's disease. *Neuroscience* (2015) 301:79. doi: 10.1016/j.neuroscience.2015.05.049
17. Mattsson N, Tosun D, Insel PS, Simonson A, Jack CR, Beckett LA, et al. Association of brain amyloid-β with cerebral perfusion and structure in Alzheimer's disease and mild cognitive impairment. *Brain A J Neurol.* (2014) 137(Pt 5):1550. doi: 10.1093/brain/awu043
18. Jr JC, Albert MS, Knopman DS, Mckhann GM, Sperling RA, Carrillo MC, et al. Introduction to the recommendations from the National Institute on Aging-Alzheimer's Association workgroups on diagnostic guidelines for Alzheimer's disease. *Alzheimers Dement J Alzheimers Assoc.* (2011) 7:257. doi: 10.1016/j.jalz.2011.03.004
19. Folstein MF, Folstein SE, Mchugh PR. "Mini-mental state". a practical method for grading the cognitive state of patients for the clinician. *J Psychiatr Res.* (1975) 12:189–98. doi: 10.1016/0022-3956(75)90026-6
20. Vidal CN, Nicolson R, Devito TJ, Hayashi KM, Geaga JA, Drost DJ, et al. Mapping corpus callosum deficits in autism: an index of aberrant cortical connectivity. *Biol Psychiatry* (2006) 60:218–25. doi: 10.1016/j.biopsych.2005.11.011
21. Mohanaiah P, Sathyanarayana P, Gurukumar L. Image texture feature extraction using GLCM approach. *Int J Sci Res Pub.* (2013) 3:1.
22. Chu A, Sehgal CM, Greenleaf JF. Use of gray value distribution of run lengths for texture analysis. *Pattern Recogn Lett.* (1990) 11:415–9. doi: 10.1016/0167-8655(90)90112-F
23. Dasarathy BV, Holder EB. Image characterizations based on joint gray level—run length distributions. *Pattern Recogn Lett.* (1991) 12:497–502. doi: 10.1016/0167-8655(91)80014-2
24. Gui J, Li H. Penalized Cox regression analysis in the high-dimensional and low-sample size settings, with applications to microarray gene expression data. *Bioinformatics* (2005) 21:3001–8. doi: 10.1093/bioinformatics/bti422
25. Chaddad A, Desrosiers C, Toews M. Multi-scale radiomic analysis of sub-cortical regions in MRI related to autism, gender and age. *Sci Rep.* (2017) 7:45639. doi: 10.1038/srep45639
26. Zhang J, Yu C, Jiang G, Liu W, Tong L. 3D texture analysis on MRI images of Alzheimer's disease. *Brain Imag Behav.* (2012) 6:61. doi: 10.1007/s11682-011-9142-3
27. Tang X, Qin Y, Zhu W, Miller MI. Surface-based vertexwise analysis of morphometry and microstructural integrity for white matter tracts in diffusion tensor imaging: with application to the corpus callosum in Alzheimer's disease. *Hum Brain Mapp.* (2017) 38:1875–93. doi: 10.1002/hbm.23491
28. Paola MD, Luders E, Iulio FD, Cherubini A, Passafiume D, Thompson PM, et al. Callosal atrophy in mild cognitive impairment and Alzheimer's disease: different effects in different stages. *Neuroimage* (2010) 49:141–9. doi: 10.1016/j.neuroimage.2009.07.050
29. Chaim TM, Duran FL, Uchida RR, Périco CA, de Castro CC, Busatto GF. Volumetric reduction of the corpus callosum in Alzheimer's disease *in vivo* as assessed with voxel-based morphometry. *Psychiatry Res Neuroimaging* (2007) 154:59–68. doi: 10.1016/j.pscychresns.2006.04.003

Conflict of Interest Statement: The authors declare that the research was conducted in the absence of any commercial or financial relationships that could be construed as a potential conflict of interest.

frontiers in Neurology

PERSPECTIVE
published: 08 February 2019
doi: 10.3389/fneur.2019.00009

BHARAT: An Integrated Big Data Analytic Model for Early Diagnostic Biomarker of Alzheimer's Disease

Ankita Sharma[1], *Deepika Shukla*[1], *Tripti Goel*[1] *and Pravat Kumar Mandal*[1,2]*

[1] *Neuroimaging and Neurospectroscopy Laboratory (NINS), National Brain Research Centre, Gurgaon, India,* [2] *Florey Institute of Neuroscience and Mental Health, University of Melbourne Medical School Campus, Melbourne, VIC, Australia*

Alzheimer's disease (AD) is a devastating neurodegenerative disorder affecting millions of people worldwide. Progressive and relentless efforts are being made for therapeutic development by way of advancing understanding of non-invasive imaging modalities for the causal molecular process of AD. We present a Hadoop-based big data framework integrating non-invasive magnetic resonance imaging (MRI), MR spectroscopy (MRS) as well as neuropsychological test outcomes to identify early diagnostic biomarkers of AD. This big data framework for AD incorporates the three "V"s (volume, variety, velocity) with advanced data mining, machine learning, and statistical modeling algorithms. A large *volume* of longitudinal information from non-invasive imaging modalities with colligated parametric *variety* and speed for both data acquisition and processing as *velocity* complete the fundamental requirements of this big data framework for early AD diagnosis. Brain structural, neurochemical, and behavioral features are extracted from MRI, MRS, and neuropsychological scores, respectively. Subsequently, feature selection and ensemble-based classification are proposed and their outputs are fused based on the combination rule for final accurate classification and validation from clinicians. A multi-modality-based decision framework (BHARAT) for classification of early AD will be immensely helpful.

Keywords: big data framework, Hadoop, Alzheimer's disease, glutathione depletion, structural MRI, MRS, neuropsychological score, ensemble-based classification

OPEN ACCESS

Edited by:
Fabiana Novellino,
Italian National Research Council, Italy

Reviewed by:
Nicola Amoroso,
Università degli Studi di Bari, Italy
James H. Cole,
King's College London,
United Kingdom

***Correspondence:**
Pravat Kumar Mandal
pravat.mandal@gmail.com;
pravat@nbrc.ac.in;
pravat.mandal@florey.edu.au

Specialty section:
This article was submitted to Applied Neuroimaging, a section of the journal Frontiers in Neurology

Received: *21 June 2018*
Accepted: *04 January 2019*
Published: *08 February 2019*

Citation:
Sharma A, Shukla D, Goel T and Mandal PK (2019) BHARAT: An Integrated Big Data Analytic Model for Early Diagnostic Biomarker of Alzheimer's Disease. Front. Neurol. 10:9. doi: 10.3389/fneur.2019.00009

INTRODUCTION

Alzheimer's disease (AD) is a neurodegenerative disorder affecting elderly people and no cure is available to date. Alzheimer's disease is evidenced by cognitive decline and colligated behavioral disruption affecting activities of daily life (1–3). The actual cause of AD is still unknown, but amyloid beta peptide deposition and oxidative stress, specifically depletion of antioxidant glutathione in the hippocampal region (4, 5), are believed to play important roles in AD pathogenesis. Multi-modal imaging techniques such as MRI, MRS, functional MRI (fMRI), and positron emission tomography (PET), are being used extensively to identify early diagnostic biomarkers for AD. The behavioral information derived from various neuropsychological tests such as clinical dementia rating (CDR) (6), mini-mental state examination (MMSE) (6), the functional assessment questionnaire (FAQ) (7), the Hachinski ischemic score (HIS) (8), the geriatric depression scale—short form (GDS-SF) (9), and trail-making test A and B (TMT-A and TMT-B) (10) are useful to aid in AD diagnosis. The heterogeneous and diverse data generated worldwide

from imaging, spectroscopy, and neuropsychology necessitate a common platform for a coherent multi-modal data processing and analysis scheme for the identification of distinctive diagnostic features specific to AD.

To date, machine learning (ML)-based techniques are being used with uni-modal data (structural MRI or fMRI) for early diagnostics of AD research (11–14). Meanwhile, some recent studies show an upgrade from uni-model to multi-model research involving two or more image modalities (MRI, fMRI, Pet etc.) (15–17) and behavioral information from neuropsychological tests (18). However, integration of respective modulation of neuro-chemicals with the imaging information as well as neuropsychological scores has never resulted in a correlation. Hence, there is an urgent need to unify the data diversity for early diagnostic biomarkers for AD.

Big data collections are combinations of multi-modal datasets that are individually manageable, but—as a group—are too large to handle seamlessly and accurately using a single machine. With the growth in data generation, ML faces the challenge of efficiently processing and learning from big data. In this context, the development of advanced tools involving big data analytics (BDA) is the current need for handling enormous volumes of diverse data, which grow with extraordinary velocity. A more comprehensive approach is required that can accommodate the velocity, volume and variety (19) in AD research. "Volume" (19) of data, the first characteristic, has been increasing because of the available size and diversity of heterogeneous data acquired using multi-modalities (e.g., MRI, MRS, and neuropsychological outcomes) with definite protocols. The second big data characteristic, i.e., "Variety" (19), relates to the heterogeneous nature of data generated from diverse data sources. Continuously growing data with exponential and high processing speed implicates "Velocity" (19) as the third important characteristic of the BDA system. As the data volume and variety are constantly increasing there is a need to store and process a large amount of diverse data. Therefore, a popular ecosystem, "Hadoop," is being developed which offers distributed storage and processing at large-scale and is fast and accurate. Hadoop itself presently contains four modules named as follows: "Hadoop common," which supports the other Hadoop modules; "Hadoop Distributed File System" (HDFS), which provide distributed storage; "Hadoop Yet Another Resource Negotiator" (YARN), for job scheduling and cluster resource management; and "Hadoop MapReduce," for parallel processing of large data sets (20).

Comprehending the big data challenges in AD research (21), a new and specific Hadoop (20)-based platform is proposed which incorporates clinical data management, processing, and analysis of the diverse multi-modal imaging, neuro-chemical, and neuropsychological data. This perspective focuses on the available big imaging data generated from multiple modalities such as MRI, MRS, and neuropsychological tests and addresses the current research challenges with possible solutions on the development of a dedicated big data framework for AD research. The proposed novel scheme is a first step toward observation of a new research direction by combining the anatomical, metabolic and cognitive changes, which can provide better understanding of the early onset and progression of AD.

BIG DATA CHALLENGES IN AD RESEARCH

Extensive research has been accomplished over the past few decades in the domain of ML for big data. But challenges remain inherent, some of which include the followings:

- *Large data size:* A major challenge of big data research in AD is to collect, store and standardize the large size of diversified and complex heterogeneous data from distributed sources for further processing and to analyze them at a high velocity. The captured distributed data from different data sources require common and standardized data acquisition protocols, data nomenclature, and data sharing standards for further processing.
- *Feature extraction:* High dimensionality is a common characteristic of big data, especially when using multi-modalities. Feature extraction is used to reduce the dimensionality of data, extracting information that is useful for classification. To date, limited literature is available on extracting features from multiple modalities. Feature selection for the reduction of dimensionality can be achieved using principal component analysis and other similar techniques.
- *Classification:* Selecting the classifiers for specific modality is also a challenging task. Hence, validation for proper benchmark classifier is essential.
- *Noise and missing values:* Sometimes, MRI images, and MRS signals are noisy or contain artifacts. Quality checks should be performed to identify, evaluate, and discard the data from the analysis pipeline. Also, neuropsychological data may contain some missing values. Inclusion of noisy data and missing values may lead to inaccurate models or may lead to overfitting.
- *Security:* Another challenge at a global level for AD research exists for data sharing and security. Data sharing standards should be strictly followed at every level.

PROPOSED BIG DATA ANALYTICS (BDA) FRAMEWORK

BDA framework integrates structured and unstructured data organization, storage, processing, and analyzing a vast volume of complex data. It utilizes data organization, parallel computing, distributed storage techniques, and ML-based algorithms that can deliver fast and scalable data processing. A proposed BDA framework for multi-modal data to classify between healthy old (HO), mild cognitive impairment (MCI), and AD is shown in **Figure 1**. The proposed framework can be broadly partitioned into four major components, namely (1) Data Normalization, (2) Data Management, (3) Data Storage, and (4) Data Processing. This section discusses the details of each of the four components of the proposed Hadoop-based BDA framework for AD classification and its progression. The framework facilitates accommodation of a massive amount of heterogeneous data

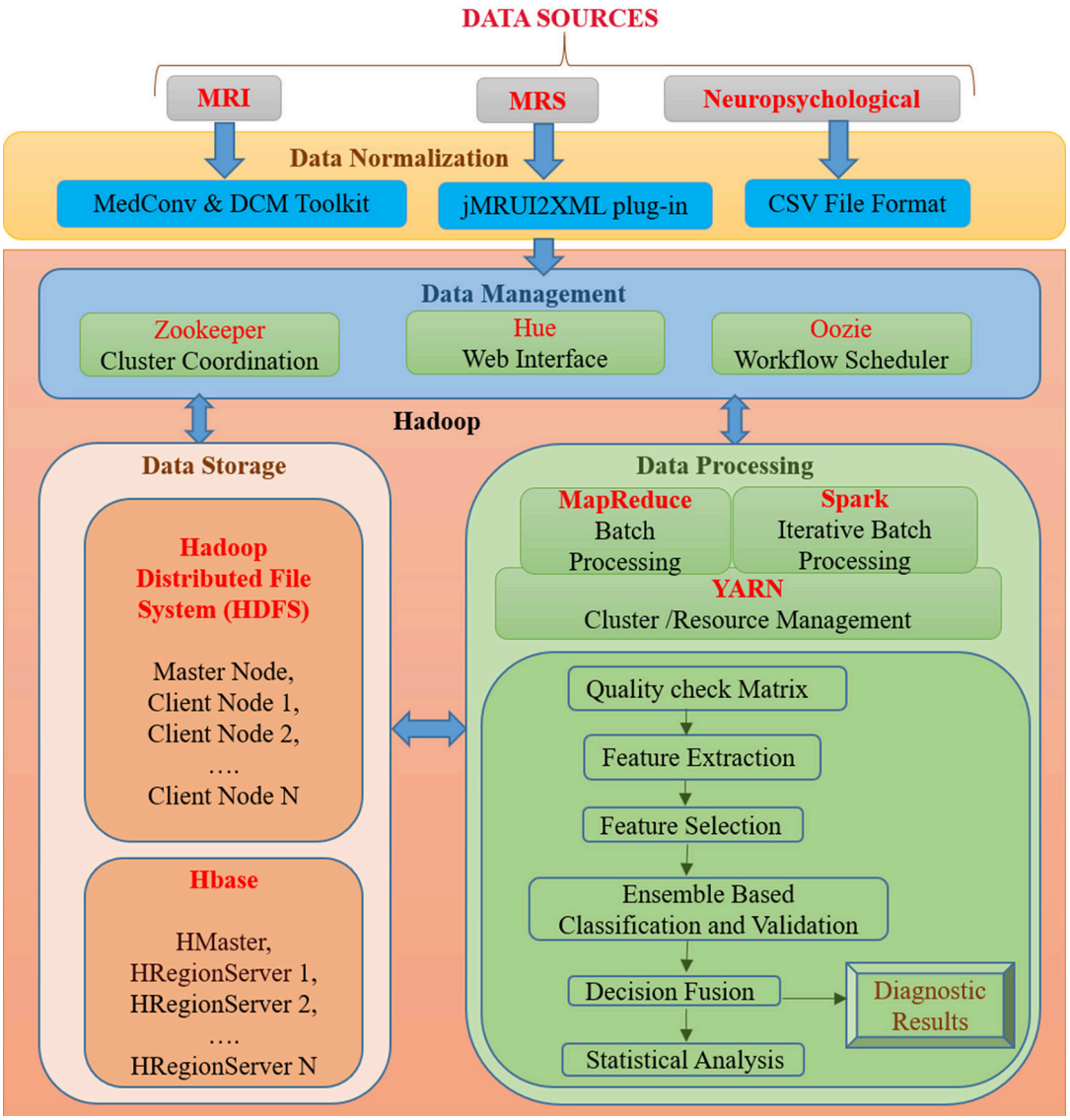

FIGURE 1 | An integrated framework for Big Data Analytics (BHARAT) using Hadoop with four components: Data Normalization, Data Management, Data Storage, and Data Processing. Data Normalization includes conversion of raw data into a suitable format for further processing, which is collected from diverse data sources. Data Management deals with organization and management of data from diverse sources. For example, Zookeeper helps in maintaining synchronization among distributed sources and Hue supports querying and visualization of data. Data storage consists of the HDFS file storage system to store a large amount of data and HBase is a NoSQL database used to read/write data in real time. Data Processing component contains different packages and libraries for processing and analysis of data from different modalities. It performs feature extraction, selection, classification, and decision fusion for accurate classification of data followed by statistical analysis. Diagnostic results are provided as final outcomes and will be further verified from clinician.

followed by data-specific pre-processing, analysis of processed data outcomes, and inference of diagnostic results.

Data Normalization

In the proposed BDA framework, multi-modal (MRI, MRS, and neuropsychological) data originating from distributed sources are ingested in a single platform. The data normalization component deals with the organization of heterogeneous multi-modal neuroimaging data acquired from different modalities, which requires interfaces to accommodate the diversified data in a single platform. In the proposed framework, MRI DICOM images are used. Therefore, in the case of neuroimaging informatics technology initiative (nifti) MRI images, MedCon (22) is used for medical image conversion. DICOM Toolkit (DCMTK) (23) is an assortment of libraries and applications implementing the DICOM standards. It comprises of software for examining, constructing, sending and receiving images over a network connection. For MRS data processing, the jMRUI2XML (24) plugin is used to process the MRS data and then export it to XML format, which can be used for further processing. Neuropsychological scores are uploaded into the file system

in the Comma-Separated Values (CSV) file format usable for processing.

Data Management

The data management component includes tools for organization and user interaction using a front-end and back-end system. Front-end refers to the interface for direct user interaction and accessibility of the system by way of the back end. Along with the front end, the back end deals with storage of raw as well as processed data. It also implements responses to the front end. Front-end functionality consists of the Hadoop user experience (Hue)[1], Apache Zookeeper (25) and Oozie (26) for interface, coordination and scheduling. Hadoop user experience (HUE) provides a web interface for Hadoop for accessing, querying, and visualizing data. This interface stands between a large amount of warehouse and other tools such as HBase, YARN, Oozieetc. It features file browsers for HBase (27) and HDFS (28), and a job browser for YARN (29). It works in coordination with Oozie (26), YARN (29), HBase, HDFS, and many other big data tools. Zookeeper helps in maintaining synchronization among distributed sources and maintains configuration information. It is also able to handle partial network failures (25). Oozie is a workflow scheduler for Hadoop jobs that specifies a sequence of operations and coordinates between them to complete the job (26). Back-end functionality consists of the HDFS and HBase. The front and back ends jointly support in developing a complete framework composed of a web interface for input from diverse data sources and user interaction followed by storing input, processing and analyzing it.

Data Storage

The data storage component is essential for organizing structured and unstructured data acquired from different modalities. Storage facility is provided by both HDFS and HBase. Hadoop Distributed File System (HDFS) is developed to store a large amount of data across different nodes of commodity hardware. It has master-slave architecture comprised of data nodes (slave node) wherein each stores blocks of data, fetches upon requirement, and acknowledges back to the name node (master node) (28). Metadata (data about data) storage is also a critical element for storage. In the data node actual data is stored and the name node stores the metadata, including file location, block size, file permission, etc. In case of any node failure, it has built-in fault tolerance mechanism. The main drawback of HDFS is that it operates on a write once read many (WORM) pattern. Therefore, if changes are required even on a single data point, the whole file must be rewritten. HBase is a non-relational, referred to as Not only SQL (NoSQL), database that provides quick random access to a large amount of structured data. HBase also supports structured, unstructured as well as semi-structured data. Data in HBase is stored in columns by sorting them according to key value pairs. It also contains cryptographic software to provide data security. HBase provides a library and runtime environment within the HBase region server and master processes for executing user code (30).

[1]http://gethue.com/

Data Processing

Data processing includes quality checks, feature extraction, selection, and decision incorporation. Subsequently, these features are used for classification of subjects into HO, MCI, and AD; followed by statistical analysis and verification. Each component of this layer is further discussed below.

MapReduce, Spark, and YARN

The proposed framework classifies subject categories between HO, MCI, and AD using data from three different modalities. Such high-dimensional datasets have problems with storage, analysis, and visualization. MapReduce is a reliable and fault-tolerant framework used to process large amounts of data in parallel on large clusters (31). MapReduce has two functional phases: Map and Reduce. Map organizes raw data into key-value pairs and Reduce processes data in parallel. Apache Spark's MLlib machine learning library is used for feature extraction, dimensionality reduction, classification, and basic statistics (32). MLlib relies on iterative batch processing of Spark. Spark supports iterative processing and improves speed by utilizing in-memory computation (33). YARN helps in job-scheduling and cluster resource management. It also handles and schedules resource requests from the client to run an application and helps in executing the process.

Quality Check Matrix

The quality of the data check was performed before starting the processing of multi-modality data. Further, the framework also takes care of missing values from data to avoid overfitting.

Feature Extraction

Feature extraction is used to extract distinctive and disease-specific features from the image. For MRI data, structural statistical features will be extracted which consist of statistical information from regions of interest (ROI) specific to the AD disease process for AD patients. Statistical features include entropy, histogram-based features like mean and median, texture information of AD-related brain regions like the hippocampus, frontal cortices, etc. In MRS, spectral features representing metabolic information of ROI are extracted in the form of neurochemical content peak area. Neuropsychological data contain scores like MMSE (6), CDR, GDS-SF (9), HIS (8), FAQ (7), and TMT-A and TMT-B (10).

Feature Selection

Features extracted from MRI, MRS, and neuropsychological data are still high-dimensional data for classification. Principle component analysis (PCA) (34) from the ML library is used to reduce the dimension of features by obtaining the set of principal values. The idea of PCA can be extended to high-dimensional space for maximizing variance using the kernel trick.

Ensemble Based Classification and Decision Fusion

Our goal for using multi-modality is to improve the accuracy of the classification of AD patients compared to the decision made by using only one source of data. Therefore, ensemble-based classifiers and their decision fusion approach are proposed for accurate automated classification (35). The concept of using

the ensemble approach for data fusion is that a separate classifier is used to train each modality that comes from different source. Further, a decision made by an individual classifier will be combined according to the appropriate combination rule. We can use the sum rule to obtain data fusion to improve the diagnostic performance.

Statistical Verification

The accuracy of disease diagnosis is important as it has a direct impact on patient treatment. Therefore, statistical analysis of classification accuracy will be conducted to validate the results of the proposed framework. Parameters for statistical analysis include sensitivity, specificity, classification accuracy, and receiver operating characteristics (ROC) (36–38). Diagnostic results are verified from clinicians.

DISCUSSION

To date, AD pathogenesis and effective diagnostic intervention remain unclear. However, it is believed that the available solution is to control its progression from MCI to AD. Early diagnostic biomarkers originating from the combined analysis of the information derived from multi-modal data (MRI, MRS, and neuropsychological) can provide insights to the actual cause of AD. This will finally lead to therapeutic interventions to be followed by clinical trials.

To identify diagnostic AD biomarkers for a large amount of diversified data with the help of accurate feature extraction and classification, a new multi-modal BDA system framework is now proposed. The present BDA framework is designed for collecting, storing, organizing, and analyzing the multi-modal big data.

Big data framework with Hadoop provides an integration of various modalities at one platform. The proposed BDA framework facilitates to normalize and preprocess raw MRI, MRS, and neuropsych data into a suitable format that can be used for further processing. The pre-processed big data will be managed and stored using Hadoop. For improving speed and resource management, the MapReduce programming model and YARN resource manager will be used. Classification of subjects into specific class (HO, MCI, and AD) using neurochemical information from MRS data along with anatomical details of MRI data and neuropsychological data, is the main goal of this study. Feature extraction from a distinct modality is an important step; therefore, new feature extraction techniques are proposed for MRI as well MRS data. For dimensionality reduction of the extracted features, variants of PCA are proposed which contain maximum variance among features. For each modality a different classifier is used, and the decision of each classifier will be fused to get final diagnostic results. Statistical analysis is performed with Spark libraries for validation (39, 40).

Our focus is not only on best classification performance using multi-modality data, but also to determine complimentary information of these modalities with an ensemble-based classifier.

We would like to emphasize that BDA for early diagnostics from various modalities at present are only based on MRI images of patients. The neurochemical-like antioxidant glutathione depletion analysis from brain hippocampal regions are extremely sensitive and specific, with more than 92% sensitivity and 94% specificity (5). This perspective brings these novel features to be included, which are close to the disease process and present a realistic approach.

We would also like to indicate that alternative approaches are available. There are equally promising BDA in Alzheimer's disease: Google BigQuery, Presto, Hydra, and Pachyderm. These alternative platforms compared to Hadoop hold huge promise in BDA for Alzheimer's disease in the coming years. To the best of our knowledge, we have not come across any manuscript where this type of scheme is proposed. We are aware that various research groups have started working in this important and challenging area.

We have already developed a prototype based on the scheme presented in **Figure 1** and it is operational for actual data analysis on a smaller scale. We have tested this scheme involving 128 MRI images, 128 MRS data points, and 128 neuro-psychological data points (scores) in a Scalable Hadoop cluster consisting of two nodes with 36 + 2 cores. The operation takes around 5 min to process these pilot data (MRI, MRS, and neuropsychological) in the PySpark toolbox using different deep-learning libraries along with tensor flow.

CONCLUSIONS

Large-scale data analysis using brain imaging, metabolic, and neuropsychological scores provides information about disease progression and identifies early diagnostic biomarkers. Hence, conceptualization of BIG analytics using three critical points of information is an important step and it will likely to provide much contribution in the development of a working BDA framework, where medical physicists, clinicians, and engineers will work hand-in-hand to advance an effective tool for early diagnosis or prediction of AD.

AUTHOR CONTRIBUTIONS

PKM conceptualized the idea, wrote the manuscript, contributed to the discussion, literature search, and figure modification, and proofread the manuscript. AS was involved in writing the manuscript, literature search, figure preparation and modification, participated in discussion, and proofread of the manuscript. DS and TG contributed equally to the literature search, manuscript preparation, participated in discussion, figure preparation, modification, and proofread the manuscript.

FUNDING

Tata Innovation Award (to PKM) (Ministry of Science and Technology, Government of India). (Award No. BT/HRD/01/05/2015).

DEDICATION

PKM dedicates this manuscript in honor of his parents (Mr. Bhadreswar Mandal & Mrs. Kalpana Mandal) and volunteers (the elderly, MCI and AD patients who participated in various research studies in the NINS laboratory).

ACKNOWLEDGMENTS

PKM, (Principal Investigator) is thankful for financial support from the Tata Innovation Fellowship (Ministry of Science and Technology, Govt. of India). We thank lab members Dr. Praful P. Pai (Senior R&D Engineer), Mr. Jayakrishnan (R&D engineer) for discussion, and Ms. Radhika Shivhare (Senior R&D engineer) for proofreading.

REFERENCES

1. Wilcock GK, Esiri MM, Bowen DM, Smith CC. Alzheimer's disease. Correlation of cortical choline acetyltransferase activity with the severity of dementia and histological abnormalities. *J Neurol Sci.* (1982) 57:407–17. doi: 10.1016/0022-510X(82)90045-4
2. Braak E, Griffing K, Arai K, Bohl J, Bratzke H, Braak H. Neuropathology of Alzheimer's disease: what is new since A. Alzheimer? *Eur Arch Psychiatry Clin Neurosci.* (1999) 249:S14–22.
3. Cummings JL, Cole G. Alzheimer disease. *JAMA* (2002) 287:2335–8. doi: 10.1001/jama.287.18.2335
4. Mandal PK, Tripathi M, Sugunan S. Brain oxidative stress: detection and mapping of anti-oxidant marker 'Glutathione' in different brain regions of healthy male/female, MCI and Alzheimer patients using non-invasive magnetic resonance spectroscopy. *Biochem Biophys Res Commun.* (2012) 417:43–8. doi: 10.1016/j.bbrc.2011.11.047
5. Mandal PK, Saharan S, Tripathi M, Murari G. Brain glutathione levels–a novel biomarker for mild cognitive impairment and Alzheimer's disease. *Biol Psychiatry* (2015) 78:702–10. doi: 10.1016/j.biopsych.2015.04.005
6. Lobo A, Ezquerra J, Gómez BF, Sala J, Seva DA. Cognocitive mini-test (a simple practical test to detect intellectual changes in medical patients). *Actas Luso Esp Neurol Psiquiatr Cienc Afines* (1979) 7:189–202.
7. Pfeffer R, Kurosaki T, Harrah C Jr, Chance J, Filos S. Measurement of functional activities in older adults in the community. *J Gerontol.* (1982) 37:323–9. doi: 10.1093/geronj/37.3.323
8. Rosen WG, Terry RD, Fuld PA, Katzman R, Peck A. Pathological verification of ischemic score in differentiation of dementias. *Ann Neurol.* (1980) 7:486–8. doi: 10.1002/ana.410070516
9. Yesavage JA, Brink TL, Rose TL, Lum O, Huang V, Adey M, et al. Development and validation of a geriatric depression screening scale: a preliminary report. *J Psychiatr Res.* (1982) 17:37–49. doi: 10.1016/0022-3956(82)90033-4
10. Reitan RM. Validity of the Trail Making Test as an indicator of organic brain damage. *Percept Motor Skills* (1958) 8:271–6. doi: 10.2466/pms.1958.8.3.271
11. Whitwell JL, Vemuri P. Assessing subtle structural changes in Alzheimer's disease patients. *Methods Mol Biol.* (2011) 711:535–50. doi: 10.1007/978-1-61737-992-5_27
12. Diciotti S, Ginestroni A, Bessi V, Giannelli M, Tessa C, Bracco L, et al. Identification of mild Alzheimer's disease through automated classification of structural MRI features. *Conf Proc IEEE Eng Med Biol Soc.* (2012) 2012:428–31. doi: 10.1109/EMBC.2012.6345959
13. Hojjati SH, Ebrahimzadeh A, Khazaee A, Babajani-Feremi A, Alzheimer's Disease Neuroimaging Initiative. Predicting conversion from MCI to AD using resting-state fMRI, graph theoretical approach and SVM. *J Neurosci Methods* (2017) 282:69–80. doi: 10.1016/j.jneumeth.2017.03.006
14. Khazaee A, Ebrahimzadeh A, Babajani-Feremi A, Alzheimer's Disease Neuroimaging Initiative. Classification of patients with MCI and AD from healthy controls using directed graph measures of resting-state fMRI. *Behav Brain Res.* (2017) 322(Pt B):339–50. doi: 10.1016/j.bbr.2016.06.043
15. Kim J, Lee B. Identification of Alzheimer's disease and mild cognitive impairment using multimodal sparse hierarchical extreme learning machine. *Hum Brain Mapp.* (2018) 39:3728–41 doi: 10.1002/hbm.24207
16. Mandal PK, Shukla D. Brain metabolic, structural, and behavioral pattern learning for early predictive diagnosis of Alzheimer's disease. *J Alzheimers Dis.* (2018) 63:935–9. doi: 10.3233/JAD-180063
17. Rondina JM, Ferreira LK, de Souza Duran FL, Kubo R, Ono CR, Leite CC, et al. Selecting the most relevant brain regions to discriminate Alzheimer's disease patients from healthy controls using multiple kernel learning: a comparison across functional and structural imaging modalities and atlases. *Neuroimage Clin.* (2018) 17:628–41. doi: 10.1016/j.nicl.2017.10.026
18. Gurevich P, Stuke H, Kastrup A, Stuke H, Hildebrandt H. Neuropsychological testing and machine learning distinguish Alzheimer's disease from other causes for cognitive impairment. *Front Aging Neurosci.* (2017) 9:114. doi: 10.3389/fnagi.2017.00114
19. Laney D. *3-D Data Management: Controlling Data Volume, Velocity, and Variety*. (2001). Available online at: https://blogs.gartner.com/doug-laney/files/2012/01/ad949-3D-Data-Management-Controlling-Data-Volume-Velocity-and-Variety.pdf
20. Hadoop A. "Apache hadoop" (2011). Available online at: https://hadoop.apache.org/
21. Fan J, Han F, Liu H. Challenges of big data analysis. *Natl Sci Rev.* (2014) 1:293–314. doi: 10.1093/nsr/nwt032
22. Nolf EX, Voet T, Jacobs F, Dierckx R, Lemahieu I. An open-source medical image conversion toolkit. *Eur J Nucl Med.* (2003) 30(Suppl. 2):S246. doi: 10.1007/s00259-003-1284-0
23. Eichelberg M, Riesmeier J, Wilkens T, Hewett AJ, Barth A, Jensch P. Ten years of medical imaging standardization and prototypical implementation: the DICOM standard and the OFFIS DICOM toolkit (DCMTK). In: *Medical Imaging 2004: PACS and Imaging Informatics: International Society for Optics and Photonics*. San Diego, CL (2004). p. 57–69.
24. Mocioiu V, Ortega-Martorell S, Olier I, Jablonski M, Starcukova J, Lisboa P, et al. From raw data to data-analysis for magnetic resonance spectroscopy–the missing link: jMRUI2XML. *BMC Bioinformatics* (2015) 16:378. doi: 10.1186/s12859-015-0796-5
25. Hunt P, Konar M, Junqueira FP, Reed B. ZooKeeper: wait-free coordination for internet-scale systems. In: *USENIX Annual Technical Conference*. Boston, MA (2010).
26. Islam M, Huang AK, Battisha M, Chiang M, Srinivasan S, Peters C, et al. Oozie: towards a scalable workflow management system for hadoop. In: *Proceedings of the 1st ACM SIGMOD Workshop on Scalable Workflow Execution Engines and Technologies*. Scottsdale, AZ: ACM (2012). 4 p.
27. George L. *HBase: The Definitive Guide: Random Access to Your Planet-Size Data*. O'Reilly Media, Inc. (2011).
28. Borthakur D. *HDFS Architecture Guide*. Hadoop Apache Project 53 (2008).
29. Vavilapalli,VK, Murthy AC, Douglas C, Agarwal S, Konar M, Evans R, et al. Apache hadoop yarn: yet another resource negotiator. In: *Proceedings of the 4th Annual Symposium on Cloud Computing*. Santa Clara, CL: ACM (2013). 5 p.
30. White T. *Hadoop: The Definitive Guide*. Sebastopol, CL: O'Reilly Media, Inc. (2012).
31. Dean J, Ghemawat S. MapReduce: simplified data processing on large clusters. In: *Proceedings of the 6th Conference on Symposium on Opearting Systems Design and Implementation* .Vol. 6. San Francisco, CA: USENIX Association (2004).
32. Meng X, Bradley J, Yavuz B, Sparks E, Venkataraman S, Liu D, et al. Mllib: machine learning in apache spark. *J Mach Learn Res.* (2016) 17:1235–41.
33. Zaharia M, Xin RS, Wendell P, Das T, Armbrust M, Dave A, et al. Apache spark: a unified engine for big data processing. *Commun ACM* (2016) 59:56–65. doi: 10.1145/2934664
34. Wold S, Esbensen K, Geladi P. Principal component analysis. *Chemometr Intell Lab Syst.* (1987) 2:37–52. doi: 10.1016/0169-7439(87)80084-9
35. Rokach L. Ensemble-based classifiers. *Artif Intell Rev.* (2010) 33:1–39. doi: 10.1007/s10462-009-9124-7
36. Doraiswamy PM, Charles HC, Krishnan KRR. Prediction of cognitive decline in early Alzheimer's disease. *Lancet* (1998) 352:1678. doi: 10.1016/S0140-6736(05)61449-3

37. Streiner DL, Cairney J. What's under the ROC? An introduction to receiver operating characteristics curves. *Can J Psychiatry* (2007) 52:121–8. doi: 10.1177/070674370705200210
38. Lalkhen AG, McCluskey A. Clinical tests: sensitivity and specificity. *Contin Educ Anaesth Crit Care Pain* (2008) 8:221–3. doi: 10.1093/bjaceaccp/mkn041
39. Kohavi, R. (1995). A study of cross-validation and bootstrap for accuracy estimation and model selection. In: *Ijcai*. Montreal, QC. p. 1137–45.
40. Shanahan JG, Dai L. Large scale distributed data science using apache spark. In: *Proceedings of the 21th ACM SIGKDD International Conference on Knowledge Discovery and Data Mining*. ACM (2015). p. 2323–4.

Conflict of Interest Statement: The authors declare that the research was conducted in the absence of any commercial or financial relationships that could be construed as a potential conflict of interest.

frontiers in Neurology

MINI REVIEW
published: 27 February 2018
doi: 10.3389/fneur.2018.00092

Understanding the Physiopathology Behind Axial and Radial Diffusivity Changes—What Do We Know?

Pawel J. Winklewski[1,2,3], Agnieszka Sabisz[3], Patrycja Naumczyk[4], Krzysztof Jodzio[4], Edyta Szurowska[3] and Arkadiusz Szarmach[3]*

[1] Department of Human Physiology, Medical University of Gdańsk, Gdańsk, Poland, [2] Department of Clinical Anatomy and Physiology, Pomeranian University in Słupsk, Słupsk, Poland, [3] 2-nd Department of Radiology, Medical University of Gdańsk, Gdańsk, Poland, [4] Institute of Psychology, University of Gdańsk, Gdańsk, Poland

The use of the diffusion tensor imaging (DTI) is rapidly growing in the neuroimaging field. Nevertheless, rigorously performed quantitative validation of DTI pathologic metrics remains very limited owing to the difficulty in co-registering quantitative histology findings with magnetic resonance imaging. The aim of this review is to summarize the existing state-of-the-art knowledge with respect to axial ($\lambda_{\parallel}$) and radial ($\lambda_{\perp}$) diffusivity as DTI markers of axonal and myelin damage, respectively. First, we provide technical background for DTI and briefly discuss the specific organization of white matter in bundles of axonal fibers running in parallel; this is the natural target for imaging based on diffusion anisotropy. Second, we discuss the four seminal studies that paved the way for considering axial ($\lambda_{\parallel}$) and radial ($\lambda_{\perp}$) diffusivity as potential *in vivo* surrogate markers of axonal and myelin damage, respectively. Then, we present difficulties in interpreting axial ($\lambda_{\parallel}$) and radial ($\lambda_{\perp}$) diffusivity in clinical conditions associated with inflammation, edema, and white matter fiber crossing. Finally, future directions are highlighted. In summary, DTI can reveal strategic information with respect to white matter tracts, disconnection mechanisms, and related symptoms. Axial ($\lambda_{\parallel}$) and radial ($\lambda_{\perp}$) diffusivity seem to provide quite consistent information in healthy subjects, and in pathological conditions with limited edema and inflammatory changes. DTI remains one of the most promising non-invasive diagnostic tools in medicine.

Keywords: diffusion tensor imaging, axial diffusivity, radial diffusivity, myelin dysfunction, axonal injury

OPEN ACCESS

Edited by:
Lars Ersland, Haukeland University Hospital, Norway

Reviewed by:
Gerardo Morfini, University of Illinois at Chicago, United States
Rodolfo Gabriel Gatto, University of Illinois at Chicago, United States

****Correspondence:***
Pawel J. Winklewski
pawelwinklewski@wp.pl

Specialty section:
This article was submitted to Neurodegeneration, a section of the journal Frontiers in Neurology

Received: *01 December 2017*
Accepted: *09 February 2018*
Published: *27 February 2018*

Citation:
Winklewski PJ, Sabisz A, Naumczyk P, Jodzio K, Szurowska E and Szarmach A (2018) Understanding the Physiopathology Behind Axial and Radial Diffusivity Changes—What Do We Know? Front. Neurol. 9:92. doi: 10.3389/fneur.2018.00092

INTRODUCTION

The number of studies using diffusion tensor imaging (DTI) has grown exponentially. A search for the term "diffusion tensor imaging" yields 13,841 records in PubMed. This is not surprising as DTI represent a highly promising method for characterizing microstructural evolution in neuropathology and treatment (1).

For instance, DTI allows developmental changes in the prefrontal cortex to be tracked. It is believed that brain maturation is associated with augmented myelination, organization, and integrity of frontal white matter; this is confirmed by DTI indices, such as fractional anisotropy, mean diffusivity, radial diffusivity ($\lambda_{\perp}$), and axial diffusivity ($\lambda_{\parallel}$). Therefore, DTI provides a tool to highlight patterns associated with the developmental time course of the frontal structural integrity, which correlates with the improvements in higher level cognitive functions taking place between adolescence and early adulthood (2). Interestingly, DTI studies reveal some consistent patterns in subjects exhibiting antisocial behavior. In particular, adult antisocial behavior was shown to be associated with greater

diffusivity within several white matter tracts, including the inferior fronto-occipital fasciculus, uncinate fasciculus, cingulum, thalamic radiations, corticospinal tract, and corpus callosum (3).

At the same time, a clinical meta-analysis in subjects with mild-traumatic brain injury produced conflicting results. This large review, consisting of 86 studies, concluded that "DTI is sensitive to a wide range of group differences in diffusion metrics, but currently lacks the specificity necessary for meaningful clinical application" (4). There is a clear lack of consensus among the experts about the use of DTI indices in a specific region of the brain as biomarkers for post-concussion syndrome, because no consistent trends for DTI variables in these subjects have been defined (5). On the contrary, in subjects suffering from cerebral small vessel disease, associations between DTI parameters and cognition have been confirmed in a multicenter study (6).

When reviewing the DTI studies it is quite striking that rigorous quantitative validation of DTI pathologic metrics remains very limited, most likely due to the difficulty in co-registering quantitative histopathology data with magnetic resonance imaging (MRI). It seems obvious that heterogenic pathologies within the brain white matter, including changes, such as brain edema and the inflammatory response, can potentially affect the consistency of DTI metrics. The aim of this review is to summarize the existing state-of-the-art knowledge with respect to axial ($\lambda_\parallel$) and radial ($\lambda_\perp$) diffusivity as DTI markers of axonal and myelin damage, respectively.

TECHNICAL CONSIDERATIONS

The principles of diffusion-weighted MRI were first described in the mid-1980s (7–9); they were based on the concept of MRI imaging combined with bipolar magnetic field gradient pulses that were introduced earlier to encode molecular diffusion effects on the spin-echo experiment (10). In ideal conditions, diffusion can be considered a truly three-dimensional process. However, in biological materials like tissues, molecular mobility may be constrained or facilitated in particular directions. Such anisotropy results from the presence of obstacles that influence molecular movement. The MRI signal is generated from water molecules by combining radiofrequency pulses with magnetic field gradients. Importantly, only molecular movements occurring within the direction of the gradient pulses are encoded in MRI generated signal. Consequently, the effect of diffusion anisotropy is easily measured by alternating the direction of the gradient pulses and observing variations in diffusivity parameters in the three planes. This feature makes diffusion-weighted MRI unique and distinguishes it from routine T1 or T2 weighted images (11).

Optimization of MRI sequences and fine tuning of the processing and display of recorded MRI signals allows for the full extraction of diffusion anisotropy effects, and thus, provides details on tissue microstructure. This more rigorous and elaborated diffusion-weighted MRI technique is named DTI (12, 13). The DTI matrix is obtained from a series of diffusion-weighted images in various gradient directions. The three diffusivity parameters (λ_1, λ_2, and λ_3), are generated by matrix diagonalization. Diffusivities are scalar indices describing water diffusion in a specific voxels (the smallest volumetric elements in the image) associated with the geometry of white matter tracts (14, 15). The diffusivities (λ_1, λ_2, and λ_3) obtained by DTI matrix diagonalization can be delimitated into parallel (λ_1) and perpendicular (λ_2 and λ_3) components to the axonal tract (16–18). Axial diffusivity, $\lambda_\parallel \equiv \lambda_1 > \lambda_2, \lambda_3$, describes the mean diffusion coefficient of water molecules diffusing parallel to the tract within the voxel of interest. Similarly, radial diffusivity, $\lambda_\perp \equiv (\lambda_2 + \lambda_3)/2$, can be defined as the magnitude of water diffusion perpendicular to the tract (19, 20). Fractional anisotropy in brain measures the total magnitude of water directional movement along the axonal fibers (16), while mean diffusivity is a measure of mean diffusion of each direction. Therefore, fractional anisotropy may be enhanced in situations of facilitated parallel diffusivity, restricted perpendicular diffusivity, or as a result of combination of both factors (21).

White matter in the brain, organized in bundles of axonal fibers running in parallel, is the natural target for imaging based on diffusion anisotropy. In principle, diffusion along the fibers should be faster than in the perpendicular direction. Based on the assumption that the direction of the fastest diffusion indicates the overall orientation of the fibers, color-coded maps of white matter tracts in the brain are created [**Figure 1** (22)]. A non-invasive method to objectively quantify white matter abnormalities greatly support studies aiming at clarification of mechanisms of damage, matching pathology with neurologic function, and assessing therapeutic interventions.

EARLY EXPERIMENTAL STUDIES

White matter impairment leading to neurological disorders can be categorized according to myelin abnormality (demyelination), axonal injury, or a combination of both (23, 24). There are several animal experimental models that allow for at least partial differentiation of these processes. One such model, congenitally dysmyelinated Shiverer mutant mice, was used by Song et al. (19) in his first study on radial ($\lambda_\perp$) and axial ($\lambda_\parallel$) diffusivity. Radial diffusivity ($\lambda_\perp$) was significantly increased, while axial diffusivity ($\lambda_\parallel$) was not altered in congenitally dysmyelinated shiverer

FIGURE 1 | Example of maps computed from diffusion tensor imaging of the brain: **(A)** mean diffusivity, **(B)** axial diffusivity ($\lambda_\parallel$), **(C)** radial diffusivity ($\lambda_\perp$), and **(D)** fractional anisotropy.

mutant mice, as compared to wild-type mice (19), suggesting that radial diffusivity ($\lambda_\perp$) may represent a potential non-invasive marker of myelin disintegration.

In a second study, Song et al. (20) used a mouse model of retinal ischemia. This model is characterized by acute inner retinal degeneration (25, 26) with initial axonal degeneration in the optic nerve, and secondary myelin fragmentation following retinal degeneration (27). Song et al. (20) observed distinct evolution patterns of axial ($\lambda_\parallel$) and radial ($\lambda_\perp$) diffusivity during the progression of optic nerve degeneration. Axial diffusivity ($\lambda_\parallel$) diminished in the injured optic nerve by day 3 following ischemia, while change in radial diffusivity ($\lambda_\perp$) between the injured optic nerves and control nerves was not detected until day 5. Radial diffusivity ($\lambda_\perp$) reached its minimal value on day 5, and remained on this level on day 7 after ischemia. Importantly, this longitudinal DTI examination of the optic nerve was positively linked with neurofilament and myelin basic protein immunostaining (28) results at day 3 (axonal degeneration) and 7 (myelin fragmentation) after the injury.

The notion that demyelination might be associated with a marked increase in radial diffusivity ($\lambda_\perp$), and modest often insignificant changes in axial diffusivity ($\lambda_\parallel$), was further reinforced by the third seminal study of Song et al. (29). In this study, the cuprizone model, which is characterized by consistent demyelination of the corpus callosum in mouse brains, was used. Demyelination after several weeks of diet, including cuprizone (neurotoxicant that chelates copper) is extensive, yet can be reversed if the mice are back to normal chow (30–32). The axonal's damage time course was clearly different from the radial diffusivity time course, demonstrating that radial diffusivity ($\lambda_\perp$) recognizes demyelination as distinct from axonal damage. However, although changes in axial diffusivity measured at the initial stage of cuprizone administration suggested acute axonal damage in white matter, the diminished axial diffusivity ($\lambda_\parallel$) did not reach statistical significance (29). The uncertainty about the potential of axial diffusivity ($\lambda_\parallel$) as a marker of axon damage was further clarified in the study by Sun et al. (33), from the same group using the same cuprizone mouse model. Biweekly *in vivo* DTI examinations showed a transient decrease in axial diffusivity ($\lambda_\parallel$) in the corpus callosum after 2–6 weeks of cuprizone administration, while immunostaining for non-phosphorylated neurofilaments demonstrated corresponding axonal damage after 4 weeks of treatment.

In summary, in four seminal studies, Song and colleagues demonstrated that axial ($\lambda_\parallel$) and radial ($\lambda_\perp$) diffusivity may be useful *in vivo* surrogate markers of axonal and myelin damage, respectively, in selected mouse experimental models of white matter abnormalities.

CRITIQUE OF THE METHOD

Interestingly, when a synthetic model of crossing fibers is used, the three diffusivities (λ_1, λ_2, and λ_3) may not detect the same underlying structural characteristics in particular datasets, because orientation of the related principal eigenvector (a characteristic vector whose direction does not change in the linear transformation and has got the largest magnitude) may differ (34). According to these authors, axial ($\lambda_\parallel$) and radial ($\lambda_\perp$) diffusivities, i.e., the water diffusion coefficient parallel and perpendicular to the axons, may provide an acceptable approximation if the voxel includes a healthy fiber bundle determining the diffusion characteristic of the voxel. However, if the signal-to-noise ratio is low, if crossing fibers are present, or if pathology causes a decrease in anisotropy, such an approach can lead to misinterpretation of the results (35). This is an important statement as the latter situation occurs within brain lesions, characteristic, for instance, of multiple sclerosis (36).

Inflammation, often present in diseases associated with white matter impairment, poses another difficulty for the interpretation of DTI signals (37). In a cuprizone experimental mouse model, it has been shown that axial diffusivity ($\lambda_\parallel$) values were diminished in the beginning of demyelination process in corpus callosum regions characterized by nonuniform axonal edema, beads, varicosities parallel to the axon segments, and microglia/macrophage activation. In the same animals, axial diffusivity ($\lambda_\parallel$) was not decreased during prolonged demyelination, in which axonal atrophy was evident. The radial diffusivity ($\lambda_\perp$) values generally were enhanced in chronically demyelinated corpus callosum voxels, but in regions with extensive axonal edema and prominent inflammatory cell presence, radial diffusivity ($\lambda_\perp$) did not change, likely because of reduced intra-axonal water diffusivity following injury and/or the enhanced restriction related to the presence of infiltrating cells (38).

A combination of oligodendrocyte apoptosis and the development of vasogenic edema could also result in enhanced diffusivity across the axons, leading to discrepancies between radial diffusivity ($\lambda_\perp$) and the histological picture (39). Thus, DTI-derived radial diffusivity ($\lambda_\perp$) may not be specific to myelin integrity and may actually reflect both myelin integrity and extra-axonal water content (40–42). Finally, cerebrospinal fluid contamination represents another challenge. Cheng et al. (43) proposed a combination of the DTI technique and a FLAIR $b = 0$ image to suppress cerebrospinal fluid partial volume effects and improve white matter fiber tractography.

Summing up, experimental studies from different pathogenic events: acute injury (ischemia, trauma), short term/progressive injury (cuprizone model), and congenial and long-term chronic injury (Shivered mice) are part of different cellular responses which can result in different DTI scalars anomalies (**Table 1**). In addition, some of the acute processes (trauma), include complex acute multicellular processes (inflammation) and chronic processes (scarring) which could radically change the white matter matrix structure and temporal course of the DTI parameters. Moreover, trophic iteration between neuronal and glial cell populations in the nervous tissue should be taken into consideration. The pathological changes occurring in one population may defectively alter another cell group and affect axial ($\lambda_\parallel$) and radial ($\lambda_\perp$) diffusivity.

CLINICAL ASPECTS OF AXIAL AND RADIAL DIFFUSIVITY

Pathophysiological changes in multiple sclerosis encompass the dynamic evolution of inflammation, axonal injury, and myelin

TABLE 1 | Summary of findings from specific experimental reports cited in the review.

Experimental model/disease	Axial diffusivity ($\lambda_{\parallel}$)	Radial diffusivity ($\lambda_{\perp}$)	Histopathological correlation	Reference
Congenitally demyelinated Shiverer mutant mice	Not changed	Increased	Yes, for axial (no axon damage—no $\lambda_{\parallel}$ change) and radial (demyelination) diffusivity	(19)
Mouse model of retinal ischemia	Decreased by day 3 after ischemia	Decreased on day 5 and present on day 7 after ischemia	Yes, at day 3 (axonal degeneration) and 7 (myelin fragmentation) after the injury	(20)
Mouse cuprizone model of experimental demyelination and myelination of corpus callosum	Tendency to decrease, but not reached statistical significance	Increased	Yes, for radial diffusivity (demyelination), only tendency for axial diffusivity (axon damage)	(29)
Mouse cuprizone model of experimental demyelination and myelination of corpus callosum	Decreased	Increased	Yes, for both axial (axon damage) and radial (demyelination)	(33)
Mathematical modeling			No, if the signal-to-noise ratio is low, if crossing fibers are present, or if pathology causes a decrease in anisotropy	(34, 35)
Rat model of liposaccharide injection into the corpus callosum		Increased	No, radial diffusivity increase due to vasogenic edema	(37)
Mouse cuprizone model of experimental demyelination and myelination of corpus callosum	Decreased	Increased	No, axial diffusivity did not correlate with axonal atrophy; did not correlate with myelin loss or astrogliosis	(38)
Mouse model of acute spinal cord injury	Increased	Increased	Good correlation in the epicenter and remotely to the changes, axial and radial diffusivity impacted by vasogenic edema	(39)
Mathematical modeling			Cellularity decrease axon diffusivity, have a limited impact on radial diffusivity; vasogenic edema increases radial diffusivity	(42)

loss, which creates a particularly challenging situation for imaging with axial ($\lambda_{\parallel}$) and radial ($\lambda_{\perp}$) diffusivity. The timing of inflammation relative to tissue injury is not always known. In addition to the temporal aspect, the pathology in multiple sclerosis is also complex and variable, with axon and myelin injury strongly interlinked. Nevertheless, Oh et al. (44, 45) demonstrated that fractional anisotropy, mean diffusivity, and radial diffusivity ($\lambda_{\perp}$) could efficiently discriminate multiple sclerosis patients with high and low disability levels. Fractional anisotropy was diminished, mean diffusivity increased, and radial diffusivity ($\lambda_{\perp}$) enhanced in subjects with high disability, as compared with low disability, demonstrating good reproducibility.

Kronlage et al. (46) demonstrated that fractional anisotropy and radial diffusivity ($\lambda_{\perp}$) correlated strongly with electrophysiological markers of demyelination, whereas axial diffusivity ($\lambda_{\parallel}$) did not correlate with markers of axonal neuropathy in subjects with chronic inflammatory demyelinating polyneuropathy. In another study, axial diffusivity ($\lambda_{\parallel}$) and fractional anisotropy showed a significant correlation with axonal integrity, whereas radial diffusivity ($\lambda_{\perp}$) was related to myelin compactness in an animal model of closed head traumatic brain injury (47). In this study, fractional anisotropy was sensitive to astrogliosis in the gray matter, whereas mean diffusivity was associated with augmented cellularity.

Interestingly, Naismith et al. (48) demonstrated that in remote optic neuritis (commonly one of the first manifestations of multiple sclerosis), radial diffusivity ($\lambda_{\perp}$) may discriminate visual outcomes. White matter tracts consisting of parallel axons tightly packed with myelin are anisotropic, or directional, to the diffusion of water. Chronic injury associated with demyelination and axons loss leads to reduced anisotropy. As a consequence diffusion perpendicular to the white matter tract (analogous to $\lambda_{\perp}$) augments, overall diffusivity (mean diffusivity) increases, and tissue directionality diminishes. At the same time, within the human central nervous system, pathologic changes from the acute to the chronic stage result in axial diffusivity ($\lambda_{\parallel}$) becoming less informative over time. As myelin debris is cleared, inflammation and edema diminish, demyelinated axons are less tightly packed, and the widening interstitial space dilutes the ability of DTI to detect and measure anisotropic diffusion ($\lambda_{\parallel}$) within axons. Thus, the correlation between axial diffusivity and visual outcomes in subjects with remote optic neuritis was very modest (48).

To summarize, in cases of axon and myelin injury associated with inflammation and increased cellularity, DTI tends to underestimate the extent of demyelination, while at the same time, may exaggerate the extent of the axonal injury. The final outcome is undervalued radial diffusivity ($\lambda_{\perp}$) and overvalued axial diffusivity ($\lambda_{\parallel}$). In turn, in chronic diseases associated with intensive axonal loss, the increased isotropic diffusion seems to enhance both radial ($\lambda_{\perp}$) and axial diffusivity ($\lambda_{\parallel}$). Consequently, DTI can no longer provide sufficient reliability in terms of underlying pathologies when inflammation, axonal loss, axonal injury, and demyelination coexist.

FUTURE PROSPECTS

Song and colleagues have proposed a new methodology called diffusion basis spectrum imaging (DBSI) to address the DTI inaccuracies with respect to radial ($\lambda_{\perp}$) and axial diffusivity ($\lambda_{\parallel}$). Phantom tests and *in vivo* experiments using cuprizone-treated mice suggest that DBSI might be capable of quantifying the extent of augmented cellularity and vasogenic edema, constituting a reliable marker of inflammation. Moreover, DBSI seems to improve the quantification of axial ($\lambda_{\parallel}$) and radial ($\lambda_{\perp}$) diffusivity, which distinguishes and reflects axonal versus myelin injury (40).

The DBSI model proposed by the Song research group has been validated in several animal and human studies, as reviewed by Cross and Song (49). The possible limitation of the reviewed research describing the interdependencies between axial ($\lambda_{\parallel}$) versus radial ($\lambda_{\perp}$) diffusivity, and axonal versus myelin injury (respectively), is that most of the discussed studies originated from one site. In particular, replication of DBSI-derived data is yet to be published. Animal models of neurodegenerative diseases featuring fluorescently labeled axons (50) represent another option to correlate axonal pathology to specific alterations in axial and radial diffusivities. Further development of DTI technology, including DBSI and other concepts (such as specific animal models), may enormously advance our understanding of underlying pathologies in several central nervous disorders.

Diffusion tensor imaging can reveal strategic information with respect to white matter tracts, disconnection mechanisms, and related symptoms. Axial ($\lambda_{\parallel}$) and radial ($\lambda_{\perp}$) diffusivity seem to provide quite consistent information in healthy subjects, and in pathological conditions with limited edema and inflammatory changes. DTI remains one of the most promising non-invasive diagnostic tools in medicine.

AUTHOR CONTRIBUTIONS

PW and AS drafted and wrote the manuscript. PN, KJ, ES, and AS commented and revised the manuscript. All authors have read and approved the final version of the manuscript.

ACKNOWLEDGMENTS

We would like to thank Agata Majewska for the excellent technical support, including preparation of figures.

FUNDING

AS and PW are supported by the Polish National Science Centre (NCN) grant numbers 2017/01/X/NZ5/00909 and 2017/01/X/NZ4/00779, respectively.

REFERENCES

1. Alexander AL, Lee JE, Lazar M, Field AS. Diffusion tensor imaging of the brain. *Neurotherapeutics* (2007) 4:316–29. doi:10.1016/j.nurt.2007.05.011
2. Sousa SS, Amaro E Jr, Crego A, Gonçalves ÓF, Sampaio A. Developmental trajectory of the prefrontal cortex: a systematic review of diffusion tensor imaging studies. *Brain Imaging Behav* (2017). doi:10.1007/s11682-017-9761-4
3. Waller R, Dotterer HL, Murray L, Maxwell AM, Hyde LW. White-matter tract abnormalities and antisocial behavior: a systematic review of diffusion tensor imaging studies across development. *Neuroimage Clin* (2017) 14:201–15. doi:10.1016/j.nicl.2017.01.014
4. Asken BM, DeKosky ST, Clugston JR, Jaffee MS, Bauer RM. Diffusion tensor imaging (DTI) findings in adult civilian, military, and sport-related mild traumatic brain injury (mTBI): a systematic critical review. *Brain Imaging Behav* (2017). doi:10.1007/s11682-017-9708-9
5. Khong E, Odenwald N, Hashim E, Cusimano MD. Diffusion tensor imaging findings in post-concussion syndrome patients after mild traumatic brain injury: a systematic review. *Front Neurol* (2016) 7:156. doi:10.3389/fneur.2016.00156
6. Croall ID, Lohner V, Moynihan B, Khan U, Hassan A, O'Brien JT, et al. Using DTI to assess white matter microstructure in cerebral small vessel disease (SVD) in multicentre studies. *Clin Sci* (2017) 131:1361–73. doi:10.1042/CS20170146
7. Merboldt KD, Hanicke W, Frahm J. Self-diffusion NMR imaging using stimulated echoes. *J Magn Reson* (1985) 64:479–86.
8. Taylor DG, Bushell MC. The spatial mapping of translational diffusion coefficients by the NMR imaging technique. *Phys Med Biol* (1985) 30:345–9. doi:10.1088/0031-9155/30/4/009
9. Le Bihan D, Breton E, Lallemand D, Grenier P, Cabanis E, Laval-Jeantet M. MR imaging of intravoxel incoherent motions: application to diffusion and perfusion in neurologic disorders. *Radiology* (1986) 161:401–7. doi:10.1148/radiology.161.2.3763909
10. Stejskal EO, Tanner JE. Spin diffusion measurements: spin echoes in the presence of a time-dependent field gradient. *J Chem Phys* (1965) 42:288–92. doi:10.1063/1.1695690
11. Le Bihan D, Mangin JF, Poupon C, Clark CA, Pappata S, Molko N, et al. Diffusion tensor imaging: concepts and applications. *J Magn Reson Imaging* (2001) 13:534–46. doi:10.1002/jmri.1076
12. Basser PJ, Mattiello J, Le Bihan D. Estimation of the effective self-diffusion tensor from the NMR spin echo. *J Magn Reson* (1994) 103:247–54. doi:10.1006/jmrb.1994.1037
13. Basser PJ, Mattiello J, Le Bihan D. MR diffusion tensor spectroscopy and imaging. *Biophys J* (1994) 66:259–67. doi:10.1016/S0006-3495(94)80775-1
14. Pierpaoli C, Basser PJ. Toward a quantitative assessment of diffusion anisotropy. *Magn Reson Med* (1996) 36:893–906; Erratum in *Magn Reson Med* (1997);37:972. doi:10.1002/mrm.1910360612
15. Basser PJ, Pierpaoli C. A simplified method to measure the diffusion tensor from seven MR images. *Magn Reson Med* (1998) 39:928–34. doi:10.1002/mrm.1910390610
16. Basser PJ. Inferring microstructural features and the physiological state of tissues from diffusion-weighted images. *NMR Biomed* (1995) 8:333–44. doi:10.1002/nbm.1940080707
17. Xue R, van Zijl PC, Crain BJ, Solaiyappan M, Mori S. In vivo three-dimensional reconstruction of rat brain axonal projections by diffusion tensor imaging. *Magn Reson Med* (1999) 42:1123–7. doi:10.1002/(SICI)1522-2594(199912)42:6<1123::AID-MRM17>3.0.CO;2-H
18. Basser PJ, Pajevic S, Pierpaoli C, Duda J, Aldroubi A. In vivo fiber tractography using DT-MRI data. *Magn Reson Med* (2000) 44:625–32. doi:10.1002/1522-2594(200010)44:4<625::AID-MRM17>3.0.CO;2-O
19. Song SK, Sun SW, Ramsbottom MJ, Chang C, Russell J, Cross AH. Dysmyelination revealed through MRI as increased radial (but unchanged axial) diffusion of water. *Neuroimage* (2002) 17:1429–36. doi:10.1006/nimg.2002.1267
20. Song SK, Sun SW, Ju WK, Lin SJ, Cross AH, Neufeld AH. Diffusion tensor imaging detects and differentiates axon and myelin degeneration in mouse optic nerve after retinal ischemia. *Neuroimage* (2003) 20:1714–22. doi:10.1016/j.neuroimage.2003.07.005
21. Scholz J, Tomassini V, Johansen-Berg H. Individual differences in white matter microstructure in the healthy brain. 2nd ed. In: Johansen-Berg H, Behrens TEJ, editors. *Diffusion MRI*. San Diego: Elsevier Inc (2014). p. 301–16.

22. Douek P, Turner R, Pekar J, Patronas NJ, Le Bihan D. MR color mapping of myelin fiber orientation. *J Comput Assist Tomogr* (1991) 15:923–9. doi:10.1097/00004728-199111000-00003
23. McGavern DB, Murray PD, Rodriguez M. Quantitation of spinal cord demyelination, remyelination, atrophy, and axonal loss in a model of progressive neurologic injury. *J Neurosci Res* (1999) 58:492–504. doi:10.1002/(SICI)1097-4547(19991115)58:4<492::AID-JNR3>3.0.CO;2-P
24. Perry VH, Anthony DC. Axon damage and repair in multiple sclerosis. *Philos Trans R Soc Lond B Biol Sci* (1999) 354:1641–7. doi:10.1098/rstb.1999.0509
25. Kawai SI, Vora S, Das S, Gachie E, Becker B, Neufeld AH. Modeling of risk factors for the degeneration of retinal ganglion cells after ischemia/reperfusion in rats: effects of age, caloric restriction, diabetes, pigmentation, and glaucoma. *FASEB J* (2001) 15:1285–7. doi:10.1096/fj.00-0666fje
26. Rosenbaum DM, Rosenbaum PS, Singh M, Gupta G, Gupta H, Li B, et al. Functional and morphologic comparison of two methods to produce transient retinal ischemia in the rat. *J Neuroophthalmol* (2001) 21:62–8. doi:10.1097/00041327-200103000-00015
27. Adachi M, Takahashi K, Nishikawa M, Miki H, Uyama M. High intraocular pressure-induced ischemia and reperfusion injury in the optic nerve and retina in rats. *Graefes Arch Clin Exp Ophthalmol* (1996) 234:445–51. doi:10.1007/BF02539411
28. Kim GM, Xu J, Song SK, Yan P, Ku G, Xu XM, et al. Tumor necrosis factor receptor deletion reduces nuclear factor-kappa B activation, cellular inhibitor of apoptosis protein 2 expression, and functional recovery after traumatic spinal cord injury. *J Neurosci* (2001) 21:6617–25.
29. Song SK, Yoshino J, Le TQ, Lin SJ, Sun SW, Cross AH, et al. Demyelination increases radial diffusivity in corpus callosum of mouse brain. *Neuroimage* (2005) 26:132–40. doi:10.1016/j.neuroimage.2005.01.028
30. Matsushima GK, Morell P. The neurotoxicant, cuprizone, as a model to study demyelination and remyelination in the central nervous system. *Brain Pathol* (2001) 11:107–16. doi:10.1111/j.1750-3639.2001.tb00385.x
31. Armstrong RC, Le TQ, Frost EE, Borke RC, Vana AC. Absence of fibroblast growth factor 2 promotes oligodendroglial repopulation of demyelinated white matter. *J Neurosci* (2002) 22:8574–85.
32. Stidworthy MF, Genoud S, Suter U, Mantei N, Franklin RJ. Quantifying the early stages of remyelination following cuprizoneinduced demyelination. *Brain Pathol* (2003) 13:329–39. doi:10.1111/j.1750-3639.2003.tb00032.x
33. Sun SW, Liang HF, Trinkaus K, Cross AH, Armstrong RC, Song SK. Noninvasive detection of cuprizone induced axonal damage and demyelination in the mouse corpus callosum. *Magn Reson Med* (2006) 55:302–8. doi:10.1002/mrm.20774
34. Wheeler-Kingshott CA, Cercignani M. About "axial" and "radial" diffusivities. *Magn Reson Med* (2009) 61:1255–60. doi:10.1002/mrm.21965
35. Wheeler-Kingshott CA, Ciccarelli O, Schneider T, Alexander DC, Cercignani M. A new approach to structural integrity assessment based on axial and radial diffusivities. *Funct Neurol* (2012) 27:85–90.
36. Rovaris M, Agosta F, Pagani E, Filippi M. Diffusion tensor MR imaging. *Neuroimaging Clin N Am* (2009) 19:37–43. doi:10.1016/j.nic.2008.08.001
37. Lodygensky GA, West T, Stump M, Holtzman DM, Inder TE, Neil JJ. In vivo MRI analysis of an inflammatory injury in the developing brain. *Brain Behav Immun* (2010) 24:759–67. doi:10.1016/j.bbi.2009.11.005
38. Xie M, Tobin JE, Budde MD, Chen CI, Trinkaus K, Cross AH, et al. Rostrocaudal analysis of corpus callosum demyelination and axon damage across disease stages refines diffusion tensor imaging correlations with pathological features. *J Neuropathol Exp Neurol* (2010) 69:704–16. doi:10.1097/NEN.0b013e3181e3de90
39. Kim JH, Loy DN, Liang HF, Trinkaus K, Schmidt RE, Song SK. Noninvasive diffusion tensor imaging of evolving white matter pathology in a mouse model of acute spinal cord injury. *Magn Reson Med* (2007) 58:253–60. doi:10.1002/mrm.21316
40. Wang Y, Wang Q, Haldar JP, Yeh FC, Xie M, Sun P, et al. Quantification of increased cellularity during inflammatory demyelination. *Brain* (2011) 134:3590–601. doi:10.1093/brain/awr307
41. Wang X, Cusick MF, Wang Y, Sun P, Libbey JE, Trinkaus K, et al. Diffusion basis spectrum imaging detects and distinguishes coexisting subclinical inflammation, demyelination and axonal injury in experimental autoimmune encephalomyelitis mice. *NMR Biomed* (2014) 27:843–52. doi:10.1002/nbm.3129
42. Chiang CW, Wang Y, Sun P, Lin TH, Trinkaus K, Cross AH, et al. Quantifying white matter tract diffusion parameters in the presence of increased extra-fiber cellularity and vasogenic edema. *Neuroimage* (2014) 101:310–9. doi:10.1016/j.neuroimage.2014.06.064
43. Cheng YW, Chung HW, Chen CY, Chou MC. Diffusion tensor imaging with cerebrospinal fluid suppression and signal-to-noise preservation using acquisition combining fluid-attenuated inversion recovery and conventional imaging: comparison of fiber tracking. *Eur J Radiol* (2011) 79:113–7. doi:10.1016/j.ejrad.2009.12.032
44. Oh J, Zackowski K, Chen M, Newsome S, Saidha S, Smith SA, et al. Multiparametric MRI correlates of sensorimotor function in the spinal cord in multiple sclerosis. *Mult Scler* (2013) 19:427–35. doi:10.1177/1352458512456614
45. Oh J, Saidha S, Chen M, Smith SA, Prince J, Jones C, et al. Spinal cord quantitative MRI discriminates between disability levels in multiple sclerosis. *Neurology* (2013) 80:540–7. doi:10.1212/WNL.0b013e31828154c5
46. Kronlage M, Pitarokoili K, Schwarz D, Godel T, Heiland S, Yoon MS, et al. Diffusion tensor imaging in chronic inflammatory demyelinating polyneuropathy: diagnostic accuracy and correlation with electrophysiology. *Invest Radiol* (2017) 52:701–7. doi:10.1097/RLI.0000000000000394
47. Tu TW, Williams RA, Lescher JD, Jikaria N, Turtzo LC, Frank JA. Radiological-pathological correlation of diffusion tensor and magnetization transfer imaging in a closed head traumatic brain injury model. *Ann Neurol* (2016) 79:907–20. doi:10.1002/ana.24641
48. Naismith RT, Xu J, Tutlam NT, Trinkaus K, Cross AH, Song SK. Radial diffusivity in remote optic neuritis discriminates visual outcomes. *Neurology* (2010) 74:1702–10. doi:10.1212/WNL.0b013e3181e0434d
49. Cross AH, Song SK. A new imaging modality to non-invasively assess multiple sclerosis pathology. *J Neuroimmunol* (2017) 304:81–5. doi:10.1016/j.jneuroim.2016.10.002
50. Gatto RG, Chu Y, Ye AQ, Price SD, Tavassoli E, Buenaventura A, et al. Analysis of YFP(J16)-R6/2 reporter mice and postmortem brains reveals early pathology and increased vulnerability of callosal axons in Huntington's disease. *Hum Mol Genet* (2015) 24:5285–98. doi:10.1093/hmg/ddv248

Conflict of Interest Statement: The authors declare that the research was conducted in the absence of any commercial or financial relationships that could be construed as a potential conflict of interest.

frontiers in Neuroscience

REVIEW
published: 30 August 2018
doi: 10.3389/fnins.2018.00612

Parkinson's Disease: Biomarkers, Treatment, and Risk Factors

*Fatemeh N. Emamzadeh[1] and Andrei Surguchov[2]**

[1] Division of Biomedical and Life Sciences, Faculty of Health and Medicine, University of Lancaster, Lancaster, United Kingdom, [2] Department of Neurology, Kansas University Medical Center, Kansas City, KS, United States

Parkinson's disease (PD) is a progressive neurodegenerative disorder caused mainly by lack of dopamine in the brain. Dopamine is a neurotransmitter involved in movement, motivation, memory, and other functions; its level is decreased in PD brain as a result of dopaminergic cell death. Dopamine loss in PD brain is a cause of motor deficiency and, possibly, a reason of the cognitive deficit observed in some PD patients. PD is mostly not recognized in its early stage because of a long latency between the first damage to dopaminergic cells and the onset of clinical symptoms. Therefore, it is very important to find reliable molecular biomarkers that can distinguish PD from other conditions, monitor its progression, or give an indication of a positive response to a therapeutic intervention. PD biomarkers can be subdivided into four main types: clinical, imaging, biochemical, and genetic. For a long time protein biomarkers, dopamine metabolites, amino acids, etc. in blood, serum, cerebrospinal liquid (CSF) were considered the most promising. Among the candidate biomarkers that have been tested, various forms of α-synuclein (α-syn), i.e., soluble, aggregated, post-translationally modified, etc. were considered potentially the most efficient. However, the encouraging recent results suggest that microRNA-based analysis may bring considerable progress, especially if it is combined with α-syn data. Another promising analysis is the advanced metabolite profiling of body fluids, called "metabolomics" which may uncover metabolic fingerprints specific for various stages of PD. Conventional pharmacological treatment of PD is based on the replacement of dopamine using dopamine precursors (levodopa, L-DOPA, L-3,4 dihydroxyphenylalanine), dopamine agonists (amantadine, apomorphine) and MAO-B inhibitors (selegiline, rasagiline), which can be used alone or in combination with each other. Potential risk factors include environmental toxins, drugs, pesticides, brain microtrauma, focal cerebrovascular damage, and genomic defects. This review covers molecules that might act as the biomarkers of PD. Then, PD risk factors (including genetics and non-genetic factors) and PD treatment options are discussed.

Keywords: Parkinson's disease, biomarkers, α-synuclein, microRNAs, orexin

OPEN ACCESS

Edited by:
Lars Ersland, Haukeland University Hospital, Norway

Reviewed by:
Nicola B. Mercuri, Università degli Studi di Roma Tor Vergata, Italy
Yannick Vermeiren, University of Antwerp, Belgium

***Correspondence:**
Andrei Surguchov
asurguchov@kumc.edu

Specialty section:
This article was submitted to Neurodegeneration, a section of the journal Frontiers in Neuroscience

Received: *07 May 2018*
Accepted: *13 August 2018*
Published: *30 August 2018*

Citation:
Emamzadeh FN and Surguchov A (2018) Parkinson's Disease: Biomarkers, Treatment, and Risk Factors. Front. Neurosci. 12:612. doi: 10.3389/fnins.2018.00612

Abbreviations: 8-OHdG, 8-hydroxy-2′-deoxyguanosine; BBB, blood–brain barrier; CSF, cerebrospinal fluid; DBS, deep brain stimulation; DLBs, dementia with Lewy bodies; GBA, acid β-glucocerebrosidase; HDLs, high density lipoproteins; LBs, Lewy bodies; LDLs, low density lipoproteins; L-dopa, levodopa; LRRK2, leucine-rich repeat kinase 2; MAOA, monoamine oxidase A; MAOB, monoamine oxidase B; MAPKs, mitogen-activated protein kinases; MAPT, microtubule-associated protein tau; MPTP, 1-methyl-4-phenyl-1,2,3,6 tetrahydropyridine; PD, Parkinson's disease; PDD, Parkinson's disease dementia; PEA, β-phenylethylamine; PINK1, PTEN-induced putative kinase 1; SN, substantia nigra; TBP, TATA box-binding protein; TH, tyrosine hydroxylase; VLDLs, very low density lipoproteins.

INTRODUCTION

Parkinson's disease is the second most common neurodegenerative disease characterized by a progressive loss of dopaminergic neurons in the SN pars compacta. In PD, there is a long latency between the first damage to cells in at-risk nuclei of the nervous system, and the onset of clinical symptoms. The symptoms and signs of PD usually do not develop until 70–80% of dopaminergic neurons have already been lost (El-Agnaf et al., 2006). Thus, identifying patients in the period between the presumed onset of dopaminergic cell loss and the appearance of clinical parkinsonism may be of major importance for the development of effective neuroprotective treatment strategies (Berendse et al., 2001). Staining of LBs, the pathological hallmark of PD, to identify affected neurons throughout the nervous system, revealed six neuropathological stages of this disease based on the localization of the involved brain regions (Braak et al., 2003). Examination of brain samples from hundreds of PD patients revealed that the pathological process was relatively uniform. The pathology in the first stage begins in the lower medulla oblongata, specifically the dorsal motor nucleus of the vagal nerve, and the anterior olfactory structures. In stage 2, lesions in the dorsal motor nucleus worsen, inclusions develop in the lower raphe nuclei, and Lewy neurites can be observed in the locus ceruleus. In stage three the SN is affected. In stage four, lesions appear in the cortex, specifically in the temporal mesocortex. In stage five, the pathology appears in the adjoining temporal neocortical fields, while in stage six cortical involvement is clearly seen. Importantly, cognitive status correlates with the neuropathological stage (Braak et al., 2003). It is also essential to find reliable molecular biomarkers that can distinguish PD from other conditions, monitor its progression, or give an indication of a positive response to therapeutic intervention (Siderowf et al., 2018). α-Synuclein (α-Syn) aggregates are assumed to be harmful to dopaminergic neurons in the SN, and their formation may trigger the transmission of toxic α-syn from affected cells to other adjacent cells, resulting in a cascade of LBs formation and, subsequently, cell death (Angot and Brundin, 2009; Steiner et al., 2018). This promotes further dopaminergic cell loss caused by the spread of pathogenic forms of α-syn to neighboring cells (Luk et al., 2012). The transmission of α-syn between cells can be a normal pathway. However, in a stress condition, the aggregation of α-syn may be initiated within the receiver cells, where pre-aggregated α-syn acts as a 'seed' inducing more aggregation of soluble α-syn in a 'prion-like' fashion (Bernis et al., 2015). Furthermore, because α-syn aggregates are normally cleared by the proteasome system or by the lysosomes, any defect in clearance mechanisms could cause the spread of PD pathology as undigested toxic α-syn transmits to other cells. In accordance with this concept lysosomal inhibition enhances the amount of insoluble α-syn, leading to the elevated release of exosomes containing toxic α-syn (Luk et al., 2012). In healthy neurons unwanted proteins are cleared via an exosome mediated pathway, thus explaining why α-syn can be released from neurons in normal conditions, while any cellular or environmental problem that leads to higher α-syn secretion can be harmful to neurons and can be transmitted to other adjacent cells. There is a hypothesis that the accumulation of α-syn in PD patients begins in the enteric nervous system that is in nerves in the upper gastrointestinal tract (GI). α-Syn produced in GI is spread through vagus to the brain, suggesting a significant role of gut-brain axis in PD development (Liddle, 2018). Therefore, monitoring PD occurrence, diagnosis of early stage of this disease, ability to distinguish it from other parkinsonian syndromes, monitoring of its response to treatment and progression all require the identification of reliable biomarkers. After many years of disease PD can eventually evolve into PDD. The methods of diagnostics and distinctions between PD, PDD, and DLB are described in a recent comprehensive review (McKeith et al., 2017)

NEUROCHEMICAL BIOMARKERS

Orexin

Orexin, also known as hypocretin, is a neuropeptide hormone expressed by a small number of neurons of the dorsolateral hypothalamus. Orexin is secreted by the lateral and posterior neurons of the hypothalamus. The hormone regulates many physiological functions, such as the sleep-wake cycle (Hagan et al., 1999), cardiovascular responses, heart rate, and hypertension (Imperatore et al., 2017). PD patients usually suffer from narcolepsy due to the loss of hypocretin neurons in the hypothalamus. The concentration of orexin A is lower in PD patients than in healthy individuals, and the level of orexin is related to the severity of the disease. The more severe is the disease, the higher loss of hypocretin neurons and the lower orexin levels in the CSF are observed (Fronczek et al., 2007). In the late stages of PD, decreased orexin levels may be responsible for daytime sleepiness (Wienecke et al., 2012). In narcolepsy of PD patients elevated levels of glial fibrillary acidic protein (GFAP) in the CSF seem to be causative for the reduction of orexin levels (Takahashi et al., 2015) pointing to GFAP as another potential biomarker. GFAP is an intermediate filament protein of the cytoskeleton that is expressed mostly in astrocytes. Hypophosphorylation and overexpression of GFAP often occur in PD patients, suggesting that these alterations in astrocytes are associated with the pathogenesis of PD (Clairembault et al., 2014). Astrocytes may be involved in the progression of PD by the production of pro-inflammatory cytokines that damage dopaminergic neurons (Rappold and Tieu, 2010). Therefore, PD can be identified by elevated levels of GFAP as an astroglial marker.

8-Hydroxy-2′-Deoxyguanosine

Reactive oxygen species (ROS) species (such as O_2-, H_2O_2, and·OH) can damage biological molecules basically through irreversible reactions causing degenerative processes associated with aging. One of the DNA lesions caused by ROS is an oxidized form of 8-hydroxyguanine (8-OHG) known as 8-OHdG which can be used as a biomarker of DNA damage (Shigenaga et al., 1989). Likewise, an increase in 8-OHdG serum levels has been measured in PD patients compared to the normal individuals. CSF 8-OHdG levels are also higher in PD patients than in

normal cases, but the difference is not as significant as serum levels. Therefore, 8-OHdG could be developed as a potential biomarker for PD (Kikuchi et al., 2002). It has been shown in the rat model that PD stage is directly related to urinary 8-OHdG level, suggesting that it can be used as a severity biomarker for PD (Kikuchi et al., 2011). However, it should be remembered that 8-OHdG is a marker of oxidative DNA damage, but not of progression of PD, so its specificity is limited (Simon et al., 2015).

Peripheral Proteasomes and Caspase Activity

Proteasomes are large protein complexes responsible for degrading and elimination of unwanted and misfolded proteins and therefore are important for cell survival. Damaged proteins that are tagged with ubiquitin molecules by ubiquitin ligase, trigger the ATP-dependent proteolytic activity of the proteasome (Lodish et al., 2004). In PD, the accumulation of proteins within the neurons leads to the formation of pathological intracellular inclusions called LBs. Proteasome dysfunction may be involved in the formation of protein aggregates and associated with LBs (Bentea et al., 2017). In PD mutations disturbing proteasome activity may lead to the accumulation of aggregated α-syn (Shadrina et al., 2010; Ciechanover and Kwon, 2015). In some PD cases, mitochondrial deficiency causes the production of more ROS and higher α-syn oxidation leading to increased ATP-independent proteasomal activity and higher α-syn oligomerization. Depletion of ATP levels in this case inhibits 26S proteasome, but 20S complex still remains active and degrades oxidized α-syn (Martins-Branco et al., 2012). In advanced PD, the severity and duration of PD correlate with reduced proteasome 20S activity and increased caspase 3 activity. The activation of caspase and thus initiation of apoptosis is the main reason of proteasome 20S activity reduction. Therefore, these proteasome and caspase components may be also considered as potential PD biomarkers (Blandini et al., 2006).

Dopamine, Dopamine Receptor, and Dopamine Transporter Activity

A catecholamine neurotransmitter dopamine is secreted by the SN, hypothalamus and some other regions of the brain. TH synthesizes the dopamine precursor (L-DOPA) that is converted to dopamine by L-aromatic amino acid decarboxylase (AADC). In the brain, dopamine is used as the precursor of noradrenaline (norepinephrine) and adrenaline (epinephrine). Loss of dopaminergic neurons in the midbrain and SN of PD brains leads to the reduction of dopamine levels (Obeso et al., 2008). The dopamine transporter (DAT) controls dopamine levels by facilitating its reuptake back to the cytosol. However, free dopamine is toxic for neurons, since its oxidation creates poisonous reactive quinones. Therefore, the vesicular monoamine transporter 2 (VMAT2) stores excess dopamine in vesicles. Thus, any change in dopamine or DAT levels may be an indicator of PD. Moreover, dopamine activates five types of receptors (D1R–D5R) and the severity of PD is related to the decreased expression of the dopamine type 3 receptor (D3R), leading to more severe symptoms because of reduced dopamine signals (Nagai et al., 1996). Therefore, D3R can be also considered as a potential biomarker for PD (Caronti et al., 2001).

Recent studies have point to 3-methoxy-4-hydroxyphenylglycol (MHPG) as a valuable biomarker to distinguish several forms of neurodegenerative diseases. This biogenic amine and norepinephrine's metabolite passes the BBB, and analysis of its level in serum and CSF may be helpful to determine cognitive staging in PD, distinguish PD from non-PD controls, DLB versus AD, etc. (Vermeiren and De Deyn, 2017; van der Zee et al., 2018). This method is promising, since the locus coeruleus becomes affected in an earlier stage than the SN by α-syn.

In another recent article a preclinical phase of PD is identified by analysis of dopamine metabolites in CSF. Low CSF concentrations of 3,4-dihydroxyphenylacetic acid (DOPAC) and DOPA identify pre-clinical PD in at-risk healthy individuals (Goldstein et al., 2018).

Catecholamine neurons are not abundant in the nervous system, and their vulnerability in PD and related diseases (Goldstein et al., 2018) is not explained. A concept of autotoxicity assumes intrinsic cytotoxicity of catecholamines in cells in which it is produced. According to a recent theory, PD might develop when 3,4-dihydroxyphenylacetaldehyde (DOPAL) oligomerizes and aggregates α-syn, providing a link between synucleinopathy and catecholamine neuron loss in LBD (Goldstein et al., 2018).

According to the "catecholaldehyde hypothesis" for the pathogenesis of PD, long-term increased build-up of DOPAL, the catecholaldehyde metabolite of dopamine, causes or contributes to the eventual death of dopaminergic neurons. LBs, a neuropathological hallmark of PD, contain precipitated α-syn. Bases for the tendency of α-syn to precipitate in the cytoplasm of catecholaminergic neurons have also been mysterious. Since DOPAL potently oligomerizes and aggregates α-syn, the catecholaldehyde hypothesis provides a link between synucleinopathy and catecholamine neuron loss in Lewy body diseases. The concept developed here is that DOPAL and α-syn are nodes in a complex nexus of interacting homeostatic systems.

α-Synuclein

α-Synuclein, which is found in an aggregated and fibrillar form, has attracted considerable attention as a potential molecular biomarker of PD. (Emamzadeh, 2016). Human α-syn is predominantly expressed in the brain in the neocortex, hippocampus, SN, thalamus and cerebellum, and is found in LBs (Surguchov, 2015). It is encoded by the SNCA gene that consists of six exons ranging in size from 42 to 1,110 bp (McLean et al., 2000; Yu et al., 2007). As noted above, the predominant form of α-syn is the full-length protein, but other shorter isoforms have been described. Importantly, C-terminal truncation of α-syn induces aggregation, suggesting that C-terminal modifications might be involved in the pathology of α-syn (Venda et al., 2010). Changes in the levels of α-syn have been reported in CSF and plasma of PD patients compared to control individuals (Hong et al., 2010). Recent evidence suggests that α-syn can be secreted into the extracellular space of the brain and spread the pathology of PD by propagating in a prion-like fashion (Masuda-Suzukake et al., 2013). This extracellular form of the

protein can also be found in human body fluids, including blood and CSF (Mollenhauer et al., 2011). The gradual spread of α-syn pathology leads to a high concentration of extracellular α-syn that can potentially damage healthy neurons. Moreover, recent biomarker studies have shown changes in the level of α-syn in blood plasma from patients with PD (Li et al., 2007; Foulds et al., 2011), suggesting that α-syn might cross the BBB. Later, radiolabeled α-syn was traced in the bidirectional path from blood to the CNS and vice versa (Sui et al., 2014). Therefore, α-syn can be considered as a potential biomarker for PD.

Apolipoprotein A1 (ApoA1)

ApoA1 is a 28 AA apolipoprotein with ∼28 kDa molecular weight which is the main constituent of HDL particles (Brewer et al., 1983). This apolipoprotein is synthesized mostly by the liver and the small intestine and is responsible for gathering extra cholesterol from cells. ApoA1 in cooperation with apoE participates in lipid transport in the brain (Emamzadeh, 2017). ApoA1 together with another apolipoprotein, apoE are responsible for lipid transportation in the brain. Lower levels of one isoform of apoA1 and tetranectin are reported in the CSF of PD patients, suggesting that apoA1 is a potential biomarker for PD (Wang et al., 2010; Swanson et al., 2015). ApoA1 cannot be secreted from neurons, but as the main component of HDL, it is required for cholesterol transportation to the brain. Therefore, it possibly passes through the BBB and contribute to the protective roles of HDL. In PD, lower level of apoA1 means less efficient HDL and reduced brain cholesterol homeostasis and function (Vitali et al., 2014).

RNA-Based PD Biomarkers

Recent investigation of microRNAs (miRNAs) in PD point to their emerging role as potential PD biomarkers, especially due to their presence in CSF and peripheral circulation both free and in exosomes. miRNAs are small 21–24 nucleotide non-coding RNAs that regulate gene expression post-transcriptionally. Due to their ability to cross the BBB miRNAs have a high potential as convenient PD biomarkers. In a recent study Dos Santos et al. (2018) analyzed miRNA expression profile using next generation sequencing (NGS) in the CSF of early stage PD patients and controls. The authors have identified a miRNA-based biomarker panel for the early diagnosis of PD, including the five best ranking variables (Let-7f-5p, miR-125a-5p, miR-151a-3p, miR-27a-3p and miR-423-5p). The analysis showed high predictive value with 90% diagnostic sensitivity. Inclusion of α-syn in the analysis further improves robustness of a miRNA-based panel. Several other teams confirmed that microRNAs may be used as new PD biomarkers suggesting a breakthrough for novel diagnostic and therapeutic approaches to this disease (Arshad et al., 2017; Vitali et al., 2018). Several other biomarkers are under investigation in a number of Medical Centers, the information about which can be found on the website: https://clinicaltrials.gov/ct2/results?cond=Parkinson$+$Disease&term=biomarker&cntry=&state=&city=&dist=.

METABOLITE PROFILING

Metabolic profiling of human tissues and/or biological fluids mirrors the complex interaction of genes, proteins and the environment of an individual. Proton (1H) and phosphorus (31P) magnetic resonance spectroscopy (MRS) are non-invasive imaging techniques that have been used to the study metabolites involved in energy metabolism, including ATP, lactate, creatine and other low molecular weight metabolite (Havelund et al., 2017). Significant alterations in metabolites have been described in PD patients and in animal models, including rise of lactate in striatum (Henchcliffe et al., 2008) and decrease of *N*-acetylaspartate/creatine ratios in advanced PD (Seraji-Bozorgzad et al., 2015). Alterations in alanine, branched-chain amino acids and fatty acid metabolism point to mitochondrial dysfunction in PD (Havelund et al., 2017).

NEUROIMAGING BIOMARKERS

Today's technology is able to detect brain's abnormalities in PD patients using imaging techniques, such as transcranial B-mode sonography (TCS), susceptibility-weighted imaging (SWI), diffusion weighted imaging (DWI) (Chung et al., 2009), positron emission tomography (PET) scan and, single-photon emission computed tomography (SPECT) scan.

Transcranial B-Mode Sonography (TCS)

Transcranial B-mode sonography monitors the blood flow velocity of brain's vessels by measuring the frequency of ultrasounds waves and their echoes. This inexpensive and reliable method shows the higher echogenicity of the SN in PD brains compared to normal group that possibly occurs due to increased iron and gliosis levels in SN of PD patients (Skoloudík et al., 2014). The increased iron level in PD can be due to either alternation or malfunction of the BBB. In PD the increase in the number of iron-transferring receptors including both transferrin receptors of BBB and iron-binding receptors of neurons can lead to accumulation of iron in SN (Hare et al., 2013).

Magnetic Resonance Imaging (MRI)

Diffusion weighted imaging is a form of MRI that measures the rate of water diffusion through a tissue to determine the structural details of that tissue. The higher measured diffusivity means the greater mobility of water molecules that can be due to the death of cells and the reduction of the region volume. This technique can differentiate PD from multiple system atrophy (MSA) in the early stage, while the clinical symptoms of these disorders are similar. In particular, the higher diffusivity of water in middle cerebellar peduncles in MSA patients in comparison to PD patients has been reported using DWI (Chung et al., 2009). DWI can also differentiate patients with progressive supranuclear palsy (PSP) from PD patients by detecting abnormalities in basal ganglia (Seppi et al., 2003). More traditional MRI methods, such as high-resolution 3-Tesla T1-weighted MRI can also detect the reduced volume of caudate and

putamen in PD patients in compared to controls (Saeed et al., 2017).

Single-Photon Emission Computed Tomography (SPECT) Scan

Both PET and SPECT scans can detect the early onset of PD and loss of dopaminergic neurons using radiotracers and computer techniques to generate 3D images. The majority of radiotracers are non-invasive radiopharmaceuticals with a short lifetime that usually decay soon after the imaging is complete. Moreover, the 3D images of PET and SPECT scans reveal function of an organ, whereas MRI can only monitor the anatomy and structure (Histed et al., 2012).

The SPECT scan radiotracers have a longer life-time in comparison to PET radiotracers. They mostly are ^{123}iodine (^{123}I) and ^{99m}technetium (^{99m}Tc) that emit gamma rays. The DAT-SPECT imaging can monitor degeneration of presynaptic terminals in dopaminergic neurons by visualizing DAT quantity. This method is a good way to diagnose reduction of DAT in the brain, and importantly it can't distinguish PD and other Parkinsonian Syndromes. The DAT gamma-emitting ligands, such as ^{123}I-iometopane (^{123}I-β-CIT), ^{123}I-ioflupane (^{123}I-FP-CIT), ^{123}I-altropane (^{123}I-IPT) are the most common DAT-density SPECT tracers. These ligands are derivatives of tropane and dopamine reuptake inhibitors that target DAT (Wang et al., 2012; Brooks, 2016).

Single-photon emission computed tomography also employs dopamine D2 receptor radioligands that are dopamine antagonists. They include ^{123}I-iodobenzamide (^{123}I-IBZM) (Reiche et al., 1995), ^{123}I-IBF (Sasaki et al., 2003), and ^{123}I-epidepride (Pirker et al., 1997). ^{123}I-2′-iodospiperone (2′-ISP) is also used in some studies to monitor D2 dopamine receptors. Although this radiotracer can distinguish between PD and other form of parkinsonism due to the pattern of its uptake in basal ganglia, it produces a high imaging background and needs to be modified to improve its performance (Yonekura et al., 1995).

The number of vesicular acetylcholine transporter (VAChT) can be monitored by SPECT radiotracers as an approach for PD early diagnosis. Acetylcholine (ACh) is a neurotransmitter that is in balance with dopamine in healthy people. The death of dopaminergic neurons and reduction of dopamine levels in PD are associated with increased Ach. ^{123}I-iodobenzovesamicol (^{123}I-IBVM) binds to VAChT and reveals the density of acetylcholine containing vesicles. Reduction of VAChT in parietal and occipital lobes in PD patients without dementia and reduced VAChT in all lobes of the cerebral cortex in PD patients with dementia has been established by this SPECT radiotracer (Niethammer et al., 2012).

^{123}I-metaiodobenzylguanidine (^{123}I-MIBG) is another radiotracer that can distinguish between PD and MSA (Goldstein, 2001). The heart-to-mediastinum ration of ^{123}I-MIBG uptake is impaired in idiopathic PD patients, but not in patients with MSA. PET/CT scanning of these PD patients illustrated also decreased FP-CIT striatal uptake (Oh et al., 2015). MIBG scintigraphy allows to distinguish not only between PD versus MSA, but also between PD and DLB (Goldstein, 2001, 2013).

Positron Emission Tomography (PET) Scan

The PET scan radiotracers emit electron anti-particles (positrons) that are positively charged with the same mass as an electron. The presence of presynaptic DAT in dopaminergic neurons of striatum and SN can be assessed with ^{18}F and/or ^{11}C radiolabeled dopamine analogs. These DAT radioligands include ^{18}F-dopamine (^{18}F-dopa) (Ibrahim et al., 2016), ^{18}F-FE-PE2I (Fazio et al., 2015), ^{18}F-β-CFT (Rinne et al., 1999), ^{18}F-LBT999 (Arlicot et al., 2017), and^{11}C-methylphenidate. The VMAT2 quantification is also possible by using either ^{11}C or ^{18}F radiolabeled dihydrotetrabenazine (DTBZ) (Tong et al., 2008; Lin et al., 2013). Because of dopaminergic cell loss and subsequent loss of VMAT2, the PET signal of radiolabeled DTBZ is lower in PD patients than in controls. Both DAT and VMAT2 radioligands can detect the early signs of dopaminergic damage, although PD may not be differentiated from atypical Parkinsonism with dopaminergic dysfunction. ^{11}C-MP4A is another PET radiotracer that monitors the level of acetylcholinesterase (AChE) activity. AChE hydrolyses deactivates Ach and terminates the signal. Impairment of cholinergic system and reduction of cortical AChE has been assessed by ^{11}C-MP4A-PET scan. AChE activity reduces more in PDD than in PD, indicating that cholinergic dysfunction is correlated with dementia in PD (Bohnen et al., 2006).

PARKINSON'S DISEASE TREATMENT

The development of neuroprotective drugs for PD is an important unmet medical need, since this disease progressively impair the patients' quality of life and functionality in activities of daily living. The identification of new therapeutic targets is therefore of great importance. Although different medications and therapies for controlling PD symptoms are currently available, no cure for PD exists. The development of treatments for PD, based on patients' symptoms and needs, vary from different medications to rehabilitation or even surgery. PD includes different clinical entities observed in several studies investigating the existence of PD subtypes. A cluster analysis permits to identify distinct PD subtypes according to the relevance of both motor and non-motor symptoms and select therapeutic approach according to cluster symptoms presentation (Lauretani et al., 2014).

MEDICATIONS

The most common therapy for PD includes different commercially available medications that treat the lack of dopamine in the SN. These medications can temporarily alleviate PD symptoms in different ways by enhancing dopamine level, mimicking the role of dopamine or inhibiting dopamine

oxidative metabolism, which leads to the generation of reactive oxygen species (ROS) (Goldenberg, 2008). Formation of protein aggregates that lead to neuronal cell death is another important target for PD treatment. Among different PD medications, levodopa (L-dopa, L-3,4-dihydroxyphenylalanine) is an effective drug. Levodopa is the immediate metabolic precursor of dopamine which is produced by TH from L-tyrosine. In the dopaminergic neurons, dopa-decarboxylase converts levodopa into dopamine. The orally taken levodopa can be decarboxylated in peripheral sites before reaching the CNS. Therefore, levodopa is available in combination with carbidopa or benserazide that are peripheral inhibitors of Dopa decarboxylase, but do not pass through the BBB. Unchanged levodopa in the presence of decarboxylase peripheral inhibitors can penetrate into the CNS and is used as a precursor of dopamine (Goldenberg, 2008).

Levodopa, is more efficiently transformed into DA after vesicle storage by the serotonergic neurons, rather than the dopaminergic ones of the nigrostriatal system. Since the serotonergic distribution throughout the brain is very different than the dopaminergic one, this causes the well-known side effects of L-DOPA therapy and reduces its efficiency as a drug (De Deurwaerdère et al., 2017).

Sinemet was the first brand of carbidopa/levodopa combination in the pharmaceutical market (Scriabine, 1999). Rytary and duopa are two newly approved medications for PD by the Food and Drug Administration (FDA). Xadago (safinamide) is recently approved medication for PD patients who do not benefit from levodopa/carbidopa. Rytary is manufactured by Impax Laboratories as an oral capsule containing carbidopa-levodopa together with entacapone to prolong its effects. Doupa produced by AbbVie Company is used for the treatment of motor fluctuations in advanced PD. Doupa is an enteral gel made of levodopa-carbidopa that is pumped to patient intestines (Olanow et al., 2014).

A group of dopamine agonists are agents that bind to the dopaminergic post-synaptic receptors and trigger the same signal as dopamine itself. This group include pergolide, pramipexole dihydrochloride, ropinirole hydrochloride, rotigotine, and apomorphine hydrochloride (Jankovic and Aguilar, 2008).

Inhibitors of MAOB – selegiline and rasagiline are also available as PD medications. Monoamine oxidase isoforms, including MAOA and MAOB, located on the outer membrane of mitochondria are involved in the oxidative deamination of biogenic amines, such as neurotransmitters and xenobiotic amines, e.g., 1-methyl-4-phenyl-1,2,3,6-tetrahydropyridine (MPTP) (Bach et al., 1988). The MAOs have a significant effect on the course of PD, because they are involved in the metabolism of dopamine. Oxidative metabolism of dopamine in the dopaminergic cells of SN by MAOs leads to ROS generation, oxidative damage and cell death (Reiter, 1995). Moreover, MAOB catalyzes the conversion of MPTP into 1-methyl-4-phenylpyridine (MPP+) which is responsible for parkinsonism in intravenous drug users (Langston, 1996). Selegiline and rasagiline can protect neurons against oxidative damage induced by dopamine metabolites diminishing MAOB activity. Moreover, several substances, such as entacapone and tolcapone that inhibit catechol-*o*-methyl transferase (COMT) are available as alternative PD medications. These two medications block the conversion of levodopa into methylated levodopa. Therefore, inhibition of COMT activity by these medications can extend the existence of functional levodopa preventing its degradation (Goldenberg, 2008).

Additionally, some other chemicals can be considered as potential PD medicines. Rapamycin can be a useful treatment for PD as an up-regulator of autophagy. Rapamycin induces autophagy in cells by inhibition of a specific kinase activity called mTOR. Autophagy is a potential target for PD treatment, since it initiates the clearance of protein aggregates and inhibits apoptosis (Hochfeld et al., 2013). Adenosine A2A receptor antagonists, such as caffeine also reduces the risk of PD. Transgenic mice with mutant α-syn and deleted adenosine A2A receptor genes are protected against PD. Thus, A2A receptor antagonists are potential candidates for prevention and treatment of PD (Kachroo and Schwarzschild, 2012).

Formation of protein aggregates that leads to neuronal cell death is a promising target for PD treatment. In January 2015, Neuropore Therapies has announced phase I clinical trial of a new drug, NPT200-11 (UCB-1332) that inhibits oligomerization of α-syn (Oertel, 2017). Another potential drug modulating the aggregation of α-syn blocking or reducing the conversion of monomers to oligomers or later on to fibrils is ANLE138b (Levin et al., 2014). Several promising compounds are under development and/or in preclinical testing that may enhance autophagy of α-syn. Recent screening of compounds protecting cells from α-syn induced neurodegeneration identified a non-selective phosphodiesterase (PDE) inhibitor dipyridamole. Importantly, PDE1 inhibition also protects dopaminergic neurons from α-syn induced degeneration in mouse SN. PDE inhibitors are currently at preclinical testing (Höllerhage et al., 2017). Another antiaggregation compound – a natural product squalamine displaces α-syn from the surfaces of lipid vesicles, thereby blocking the first steps in its aggregation process. Furthermore, squalamine suppresses the toxicity of α-syn oligomers by inhibiting their interactions with lipid membranes (Perni et al., 2017).

SURGERY

Deep brain stimulation therapy is rarely used for certain types of brain-related disorders including PD, dystonia, obsessive-compulsive disorder and treatment resistant depression (Herrington et al., 2016). When PD symptoms are very severe and medications cannot moderate them, surgery and DBS can be considered as the final options for the treatment. It involves sending electrical impulses to certain parts of the brain (usually SN or globus pallidus, which communicate with the SN) by a neurostimulator device that is a brain implant known as a 'brain pacemaker.' The target area of DBS is usually the subthalamic nucleus (STN). The stimulation of the dorsolateral STN border alongside the surgery can improve its efficiency (Herzog et al., 2004). Later it was found that stimulation of caudal zona incerta (cZI) can be more effective with fewer complications after the surgery (Plaha et al., 2006). Stimulation

of neurons may also lead to neurogenesis and neuroplasticity and thus can improve for a long time motor problems, such as dyskinesia and tremor, and all other levodopa-responsive symptoms, for a long time. However, there are two problems with DBS, namely a 3- to 6-month waiting period required for optimal results and the possibility of brain infection (Bronstein et al., 2011).

GENE THERAPY

The development of gene therapy of PD has made a major progress in a recent decade. Advanced PD does not give a good response to levodopa therapy. Broaden loss of dopaminergic neurons is accompanied by reduction in aromatic amino acid decarboxylase (AADC) levels that converts L-DOPA to dopamine. After successful preclinical studies, adeno-associated viral vectors carrying human AADC gene are recently delivered into putaminal neurons and subthalamic nucleus of PD patients. In this method, sufficient amount of dopamine production can be controlled by taking adequate levodopa dose. Orally taken levodopa can be converted into dopamine by AADC and sooth PD symptoms (Muramatsu et al., 2010). Safety and efficiency of the method have been proven over 4 years by annually PET imaging from patients who received specific dosages of AAV2-hAADC (Mittermeyer et al., 2012). Another target for gene therapy in PD is glutamic acid decarboxylase (GAD) that facilitate production of GABA in GABA-ergic neurons in the subthalamic nucleus. GABA as an inhibitory neurotransmitter regulates muscle tone and improve motor functions (Watanabe et al., 2002). Lack of dopamine in PD causes activation of the subthalamic nucleus and unnecessary muscular responses that GABA by its inhibitory effect can significantly improve. This method can be compared with DBS that by sending electric shocks to subthalamic nucleus reduces its hyperactivity and improve motor impairment (Coune et al., 2012). The human trial of this method was performed by bilateral injection of AAV2-GAD in the subthalamic nucleus of patients with advanced PD. This approach has shown safety and efficiency, although it needs more investigation to be considered as a treatment (LeWitt et al., 2011). Therapeutic effect of glial cell line-derived neurotrophic factor (GDNF) on neuronal function in non-human models of PD encouraged scientists to inject it directly into putamen of PD patients. This surgery helped patients with improved movement, reduced dyskinesia and increased dopamine storage in the putamen (Gill et al., 2003). Therefore, GDNF is a possible option for gene therapy. Neurturin gene is another candidate for PD gene therapy. Neurturin is a neurotrophic factor important for survival and differentiation of dopaminergic neurons (Lin et al., 1993). The human trial of this factor was conducted by bilateral injection of vector AAV2-neurturin (CERE-120) into the putamen biomarkers patients with advanced PD (Bartus et al., 2013). Injected neurturin cannot spread into SN and play its therapeutic role because of vast axonal transport defects in PD patients. Another consequence of this method may be the accumulation of α-syn that leads to downregulation of neurturin expression (Bartus et al., 2014).

NON-GENETIC RISK FACTORS OF PARKINSON DISEASE

Only 10–15% of PD cases are early onset familial PD, while the remaining cases are idiopathic pointing to an important role of non-genetic and environmental factors in PD pathogenesis. Exposure to environmental toxins can cause dopaminergic cell death. The accumulation of heavy metals in the SN enhances the risk of developing PD. The effect of exposure to heavy metals could increase oxidative stress in dopaminergic cells, leading to PD. MAO in the presence of oxygen can mediate dopamine oxidation *in vitro* into 3,4-dihydroxylphenyl-acetaldehyde (DOPAL). DOPAL initiates oligomerization of α-syn into non-fibrillar, SDS-resistant aggregates (Burke, 2003). However, another study has revealed that inhibition of MAO to stop the production of DOPAL is not sufficient to reduce oligomerization of α-syn (Burke, 2003). The auto-oxidation of dopamine to dourmine quinone (DAQ) can also increase both formation and secretion of non-fibrillar α-syn oligomers, thus promoting pathogenic α-syn transmission to adjacent neurons and glia (Lee et al., 2011). Neuromelanin pigment is highly expressed in dopaminergic neurons, preventing oxidative stress related to the accumulation of cytosolic dopamine. On the other hand, dying neurons in PD brains release neuromelanin that activates neuroglia and triggers neuroinflammation (Zucca et al., 2014). Moreover, lipidated neuromelanin can interact with α-syn and trigger its aggregation into the insoluble complex in PD patients (Double and Halliday, 2006).

Genetic polymorphisms of cytochrome P450 2D6 (CYP2D6) – an enzyme involved in metabolizing environmental toxins, are also related to the development of PD. For example, CYP2D6 deficient metabolizers are two times higher at risk of developing PD if they are also exposed to pesticides. Therefore, sufficient levels of CYP2D6 activity are required for the metabolism of pesticides (e.g., organophosphates, atrazine), which are linked to the pathogenesis of PD (Elbaz and Tranchant, 2007).

Reactive oxygen species and thus oxidative stress is also known as a pathological factor in PD. NADPH oxidase-2 enzyme (NOX2) is a membrane-bound oxidase present primarily in phagocytes generating ROS in phagosomes to kill bacteria. NOX2-derived ROS also damages dopaminergic neurons. Dopaminergic neurons in NOX2-knockout mice start to degenerate faster than similar cells in wild-type controls after administration of MPTP (Brieger et al., 2012).

In 1956 two neurologists, Poskanzer and Schwab hypothesized that PD is related to influenza infection (Estupinan et al., 2013). They studied a group of PD patients and revealed that age of disease onset is shifted in the direction of an age group who were born before or during the influenza pandemic in 1918 and mostly had been infected by the flu virus. However, other studies showed that influenza infection can cause PD-like symptoms, but cannot increase the risk of developing PD (Estupinan et al., 2013). Another hypothesis proposes that Toxoplasma gondii, an

intracellular parasite causing toxoplasmosis, may increase the risk of PD. The parasite in the brain infected those areas that are affected in PD, including basal ganglia (Miman et al., 2010), although other studies did not get a similar result (Mahami Oskouei et al., 2016).

GENETIC FORMS AND GENETIC RISK FACTORS OF PD

Although most cases of PD are idiopathic forms of the disease, about 15% of PD patients are recognized as having a first-degree family member with this disease. Recently, the genetic factors and gene loci involving in autosomal dominant and autosomal recessive forms of PD have been discovered due to advanced molecular genetics (Samii et al., 2004; Karimi-Moghadam et al., 2018) (**Tables 1**, **2**). The mutations in several genes, including α-syn, LRRK2, PINK1, Parkin, DJ-1, VPS35 and GBA1 are linked to PD (Zeng et al., 2018). In addition to mutations in these genetic loci, polymorphisms, and trinucleotide repeats are recognized as PD genes, or susceptibility factors for PD (**Table 3**).

EPIGENETIC RISK FACTORS OF PD

Epigenetics refer to chromatin alternations, including DNA methylation and histone post translational modifications that can alter gene expression without changes in DNA sequence. These modifications can be inherited, but environmental factors including nutritional, chemical and physical factors can also affect epigenetics (Surguchov et al., 2017). In sporadic form of PD involvement of environmental factors in initiation and progression of disease emerging an idea that epigenetic plays an important role in PD (Feng et al., 2015). One of the examples of epigenetic mechanism in PD is modification of α-syn gene (SNCA). SNCA has two CpG islands with the first one being located in exon 1 (CpG-1) and the second one (CpG-2) within intron 1. Transcription factors (TFs) GATA and ZSCAN21 bind to the intron 1 CpG-2 island and modulate transcription of α-syn. CpG-2 methylation prevents the binding of the TFs to SNCA and subsequently inhibits the overexpression of α-syn. Interestingly, binding of transcription factors to α-syn (Iwata et al., 2001) and another member of the synuclein family, γ-synuclein (Surgucheva and Surguchov, 2008), has been

TABLE 1 | Autosomal recessive and X-linked genes involved in Parkinson's disease.

Inheritance pattern	Locus	Chr. location	Mutation site in	Involved protein
Autosomal recessive	PARK2/PARKN	6q25.2-q27	*Parkin*	Ubiquitin-protein ligase (Kitada et al., 1988)
	PARK6	1p36	*PINK1*	PTEN-induced putative kinase 1 (Valente et al., 2004)
	PARK7	1p36.23	*DJ1*	Oncogene DJ1 (van Duijn et al., 2001)
	PARK9	1p36	*ATP13A2*	Lysosomal type 5 P-type ATPase (Ramirez et al., 2006)
	PARK14	22q13.1	*PLA2G6*	Phospholipase A2 (Paisan-Ruiz et al., 2009; Shi et al., 2011)
	PARK15	22q12-q13	*FBXO7*	F-BOX only protein 7 (Paisan-Ruiz et al., 2009)
	PARK19	1p32	*DNAJC6*	Putative tyrosine-protein phosphatase auxilin (Koroglu et al., 2013)
	PARK20	21q22	*SYNJ1*	Synaptojanin-1 (Krebs et al., 2013)
X-linked	PARK12	Xq21-q25	*TAF1*	TFIID subunit 1 (Graeber and Muller, 1992)

TABLE 2 | Autosomal dominant genes involved in Parkinson's disease.

Inheritance pattern	Locus	Chr. location	Mutation site	Involved protein
Autosomal dominant	PARK1	4q21	*SNCA*	α-Syn (Xu et al., 2017)
	PARK3	2p13.2	*SPR*	Sepiapterin reductase in BH4 pathway (Karamohamed et al., 2003)
	PARK4	4q21	Triplication of *SNCA*	α-Syn (Singleton et al., 2003)
	PARK5	4p14	*UCHL1*	Ubiquitin C-terminal hydrolase (Leroy et al., 1998)
	PARK8	12q12	*LRRK2*	Leucine-reach repeat kinase 2 (Zimprich et al., 2004)
	PARK11	2q37	*GIGYF2*	GRB10-interacting GYF protein 2 (Lautier et al., 2008; Tan et al., 2009)
	PARK13	2p12	*HTRA2*	HTRA serine peptidase (Strauss et al., 2005; Lin et al., 2011)
	PARK16	1q32	Multiple independent sites?	Unknown (Satake et al., 2009; Li et al., 2011)
	PARK17	16p12.1-q12.1	*VPS35*	Vacuolar protein sorting 35 (Vilariño-Güell et al., 2011)
	PARK18	3q27	*EIF4G1*	Eukaryotic translation initiation factor 4 gamma 1 (Chartier-Harlin et al., 2011)
	PARK21	3q22	*DNAJC13*	DNAJ-domain-bearing protein (Appel-Cresswell et al., 2014; Vilariño-Güell et al., 2014)

TABLE 3 | Susceptibility factors of Parkinson's disease.

Susceptibility factors	Involved gene	Chr. location	Putative function	Phenotype
	GBA	1q21	Acid β-glucocerebrosidase	Gaucher disease (Pulkes et al., 2014)
	MAPT	17q21.1	Microtubule-associated protein tau	Supranuclear palsy, Dementia (Das et al., 2009)
	MC1R	16q24.3	Melanocyte-stimulating hormone receptor	Albinism (Tell-Marti et al., 2015)
	ADH1C	4q23	Alcohol dehydrogenase 1C	Alcohol dependence (Buervenich et al., 2005)
	ADH4	4q22	Alcohol dehydrogenase 4	Alcohol dependence (Buervenich et al., 2000)
	HLA	6p21.3	Major histocompatibility complex	Imamura et al., 2003
	ATXN2	12q24.1	Ataxin-2	Spinocerebellar ataxia 2 (Charles et al., 2007)
	ATXN3	14q21	Ataxin-3	Machado-Joseph disease (Gwinn-Hardy et al., 2001)
	TBP	6q27	TATA box-binding protein	Spinocerebellar ataxia 17 (Wu et al., 2004)
	ATXN8OS	13q21.33	Ataxin-8 opposite strand	Spinocerebellar ataxia 8 (Wu et al., 2004)
	NR4A2	2q24.1	Nuclear receptor subfamily 4 group A member 2 (transcription factor)	Le et al., 2003

described, suggesting that synuclein family members are involved in various complex mechanisms of gene expression regulation. Therefore, their role in PD is not limited to the formation of toxic aggregates, but may be complemented by participation in regulatory processes.

Matsumoto et al. (2010) found that CpGs in SNCA were hypermethylated in controls, but not methylated in PD patients, suggesting that methylation was an epigenetic risk factor for PD that is related to the pathogenesis of α-syn. In PD, demethylated SNCA codes for a high amount of α-syn that may initiate aggregation and promote neurodegeneration. Additionally, the levels of nuclear DNA (cytosine-5′) methyltransferase 1 (DNMT1) in post-mortem PD brains is lower than in control brains. This methylase epigenetically suppresses gene expression by DNA methylation, and its reduced level in PD may be associated with SNCA hypomethylation.

Epigenetic modifications in other genes are also implicated in contributing to PD, including tumor necrosis factor α (TNF-α), PARK16, transmembrane glycoprotein NMB (GPNMB), and syntaxin-1B (STX1B) genes. Hypomethylation of the TNF-α promoter, hypermethylation of a CpG dinucleotide in synphilin-1, STX1B and hypermethylation of multiple CpG sites proximal to GPNMB are all described in PD (Yang et al., 2017). Moreover, the epigenetic changes in mitochondrial DNA (mtDNA) can also trigger PD. Several studies show the hypo-methylation and hyper-hydroxymethylation of mtDNA displacement loop (D-loop) in the SN of PD brains (Iacobazzi et al., 2013; Chuang et al., 2017).

CONCLUSION

Pathology of PD is complex and include a combination of genetics, epigenetics and environmental factors. Current medical, pathological, and experimental data support the Braak hypothesis (Braak et al., 2003) of spatiotemporal spread of PD pathology involving α-syn propagation from the gastrointestinal and olfactory system via transsynaptic cell-to-cell transfer through the vegetative nervous systems to the CNS. Many non-motor symptoms, including sleep disorders, olfactory deficiency, hyposmia (reduced ability to smell and to detect odors), constipation and others may play an important role as successful, future diagnostic to target PD pathology and mechanisms during the initial stages of disease (Reichmann et al., 2016). Important contributing factors to PD are dysfunctions of mitochondria and endoplasmic reticulum, impairment of autophagy and endocytosis, and deregulation of immunity. Despite intensive investigation of PD mechanism the disease is still incurable. Future challenges for physicians and researchers working in the field of PD and similar disorders will be directed to the identification of biomarkers for an early diagnosis of these diseases at preclinical stage. New biomarkers should follow the progression of the disease and determine key metabolomic alterations to identify potential targets for intervention. Future tasks should be also directed to the development and application of preventive measures to stop or reduce disease progression at pre-symptomatic stages and the finding of novel antiparkinsonian drugs with specific neuroprotective effects on the dopaminergic system. In addition to conservative approach based on the identification of new protein biomarkers in blood, plasma and CSF, there is a growing hope that analysis of microRNAs may greatly contribute to early diagnosis of this disease. The development of induced pluripotent stem cell (iPSC) and genome editing technique open new hopes for the treatment of several human diseases, especially genetic disorders. For PD which is predominantly sporadic disease and

a mix of several relatively rare genetic causes these methods gave the opportunity to develop new models and study phenotypes in both genetic and sporadic cases to piece together pathogenic pathways involving their gene products.

AUTHOR CONTRIBUTIONS

FE designed the article contents and wrote the original manuscript. AS revised and edited the manuscript, searched for additional related literature and discussed the writing with FE.

FUNDING

This work was supported by an EC Framework 7 Marie Curie Fellowship Training Network Grant (NEURASYNC) for FE and by VA Merit Review grants 1I01BX000361 and the Glaucoma Foundation grant QB42308 for AS.

ACKNOWLEDGMENTS

FE acknowledges Professor David Allsop for his help and support.

REFERENCES

Angot, E., and Brundin, P. (2009). Dissecting the potential molecular mechanisms underlying alpha-synuclein cell-to-cell transfer in Parkinson's disease. *Parkinsonism Relat. Disord.* 15(Suppl. 3), S143–S147. doi: 10.1016/S1353-8020(09)70802-8

Appel-Cresswell, S., Rajput, A. H., Sossi, V., Thompson, C., Silva, V., McKenzie, J., et al. (2014). Clinical, positron emission tomography, and pathological studies of DNAJC13 p.N855S parkinsonism. *Mov. Disord.* 29, 1684–1687. doi: 10.1002/mds.26019

Arlicot, N., Vercouillie, J., Malherbe, C., Bidault, R., Gissot, V., Maia, S., et al. (2017). PET imaging of dopamine transporter with 18F-LBT999: first human exploration. *J. Nucl. Med.* 58:1276. doi: 10.1111/j.1527-3458.2007.00033.x

Arshad, A. R., Sulaiman, S. A., Saperi, A. A., Jamal, R., Mohamed Ibrahim, N., and Abdul Murad, N. A. (2017). MicroRNAs and target genes as biomarkers for the diagnosis of early onset of Parkinson disease. *Front. Mol. Neurosci.* 10:352. doi: 10.3389/fnmol.2017.00352

Bach, A. W., Lan, N. C., Johnson, D. L., Abell, C. W., Bembenek, M. E., Kwan, S.-W., et al. (1988). cDNA cloning of human liver monoamine oxidase A and B: molecular basis of differences in enzymatic properties. *Proc. Nat. Acad. Sci. U.S.A.* 85, 4934–4938. doi: 10.1073/pnas.85.13.4934

Bartus, R. T., Baumann, T. L., Siffert, J., Herzog, C. D., Alterman, R., Boulis, N., et al. (2013). Safety/feasibility of targeting the substantia nigra with AAV2-neurturin in Parkinson patients. *Neurology* 80, 1698–1701. doi: 10.1212/WNL.0b013e3182904faa

Bartus, R. T., Weinberg, M. S., and Samulski, R. J. (2014). Parkinson's disease gene therapy: success by design meets failure by efficacy. *Mol. Ther.* 22, 487–497. doi: 10.1038/mt.2013.281

Bentea, E., Verbruggen, L., and Massie, A. (2017). The proteasome inhibition model of Parkinson's disease. *J. Parkinsons Dis.* 7, 31–63. doi: 10.3233/JPD-160921

Berendse, H. W., Booij, J., Francot, C. M., Bergmans, P. L., Hijman, R., and Stoof, J. C. (2001). Subclinical dopaminergic dysfunction in asymptomatic Parkinson's disease patients' relatives with a decreased sense of smell. *Ann. Neurol.* 50, 34–41. doi: 10.1002/ana.1049

Bernis, M. E., Babila, J. T., Breid, S., Wüsten, K. A., Wüllner, U., and Tamgüney, G. (2015). Prion-like propagation of human brain-derived alpha-synuclein in transgenic mice expressing human wild-type alpha-synuclein. *Acta Neuropathol. Commun.* 3:75. doi: 10.1186/s40478-015-0254-7

Blandini, F., Sinforiani, E., Pacchetti, C., Samuele, A., Bazzini, E., and Zangaglia, R. (2006). Peripheral proteasome and caspase activity in Parkinson disease and Alzheimer disease. *Neurology* 66, 529–534. doi: 10.1212/01.wnl.0000198511.09968.b3

Bohnen, N. I., Albin, R. L., Koeppe, R. A., Wernette, K. A., Kilbourn, M. R., Minoshima, S., et al. (2006). Positron emission tomography of monoaminergic vesicular binding in aging and Parkinson disease. *J. Cereb. Blood Flow Metab.* 26, 1198–1212. doi: 10.1038/sj.jcbfm.9600276

Braak, H., Del Tredici, K., Rüb, U., de Vos, R. A., Jansen Steur, E. N., and Braak, E. (2003). Staging of brain pathology related to sporadic Parkinson's disease. *Neurobiol. Aging* 24, 197–211. doi: 10.1016/s0197-4580(02)00065-9

Brewer, H. B. Jr., Fairwell, T., Kay, L., Meng, M., Ronan, R., Law, S., et al. (1983). Human plasma proapoA-I: isolation and amino-terminal sequence. *Biochem. Biophys. Res. Commun.* 113, 626–632. doi: 10.1016/0006-291X(83)91772-2

Brieger, K., Schiavone, S., Miller, F. J., and Krause, K. H. (2012). Reactive oxygen species: from health to disease. *Swiss Med. Wkly.* 142:w13659. doi: 10.4414/smw.2012.13659

Bronstein, J. M., Tagliati, M., Alterman, R. L., Lozano, A. M., Volkmann, J., Stefani, A., et al. (2011). Deep brain stimulation for Parkinson disease: an expert consensus and review of key issues. *Arch. Neurol.* 68:165. doi: 10.1001/archneurol.2010.260

Brooks, D. J. (2016). Molecular imaging of dopamine transporters. *Ageing Res. Rev.* 30, 114–121. doi: 10.1016/j.arr.2015.12.009

Buervenich, S., Carmine, A., Galter, D., Shahabi, H. N., Johnels, B., Holmberg, B., et al. (2005). A rare truncating mutation in ADH1C (G78Stop) shows significant association with Parkinson disease in a large international sample. *Arch. Neurol.* 62, 74–78. doi: 10.1001/archneur.62.1.74

Buervenich, S., Sydow, O., Carmine, A., Zhang, Z., Anvret, M., and Olson, L. (2000). Alcohol dehydrogenase alleles in Parkinson's disease. *Mov. Disord.* 15, 813–818. doi: 10.1002/1531-8257(200009)15:5<813::AID-MDS1008>3.0.CO;2-Y

Burke, W. J. (2003). 3,4-dihydroxyphenylacetaldehyde: a potential target for neuroprotective therapy in Parkinson's disease. *Curr. Drug Targets CNS Neurol. Disord.* 2, 143–148. doi: 10.2174/1568007033482913

Caronti, B., Antonini, G., Calderaro, C., Ruggieri, S., Palladini, G., Pontieri, F. E., et al. (2001). Dopamine transporter immunoreactivity in peripheral blood lymphocytes in Parkinson's disease. *Neural. Transm.* 108, 803–807. doi: 10.1007/s007020170030

Charles, P., Camuzat, A., Benammar, N., Sellal, F., Destee, A., Bonnet, A.-M., et al. (2007). Are interrupted SCA2 CAG repeat expansions responsible for parkinsonism? *Neurology* 69, 1970–1975.

Chartier-Harlin, M.-C., Dachsel, J. C., Vilarino-Guell, C., Lincoln, S. J., Lepretre, F., Hulihan, M., et al. (2011). Translation initiator EIF4G1 mutations in familial Parkinson disease. *Am. J. Hum. Genet.* 89, 398–406. doi: 10.1016/j.ajhg.2011.08.009

Chuang, Y. H., Paul, K. C., Bronstein, J. M., Bordelon, Y., Horvath, S., and Ritz, B. (2017). Parkinson's disease is associated with DNA methylation levels in human blood and saliva. *Genome Med.* 9:76. doi: 10.1186/s13073-017-0466-5

Chung, E. J., Kim, E. G., Bae, J. S., Eun, C. K., Lee, K. S., and Oh, M. (2009). Usefulness of diffusion-weighted MRI for differentiation between Parkinson's disease and Parkinson variant of multiple system atrophy. *J. Mov. Disord.* 2, 64–68. doi: 10.14802/jmd.09017

Ciechanover, A., and Kwon, Y. T. (2015). Degradation of misfolded proteins in neurodegenerative diseases: therapeutic targets and strategies. *Exp. Mol. Med.* 47:e147. doi: 10.1038/emm.2014.117

Clairembault, T., Kamphuis, W., Leclair-Visonneau, L., Rolli-Derkinderen, M., Coron, E., Neunlist, M., et al. (2014). Enteric GFAP expression and phosphorylation in Parkinson's disease. *J. Neurochem.* 130, 805–815. doi: 10.1111/jnc.12742

Coune, P. G., Schneider, B. L., and Aebischer, P. (2012). Parkinson's disease: gene therapies. *Cold Spring Harb. Perspect. Med.* 2:a009431. doi: 10.1101/cshperspect.a009431

Das, G., Misra, A. K., Das, S. K., Ray, K., and Ray, J. (2009). Microtubule-Associated Protein Tau (MAPT) influences the risk of Parkinson's disease among Indians. *Neurosci. Lett.* 460, 16–20. doi: 10.1016/j.neulet.2009.05.031

De Deurwaerdère, P., Di Giovanni, G., and Millan, M. J. (2017). Expanding the repertoire of L-DOPA's actions: a comprehensive review of its functional neurochemistry. *Prog. Neurobiol.* 151, 57–100. doi: 10.1016/j.pneurobio.2016.07.002

Dos Santos, M. C. T., Barreto-Sanz, M. A., Correia, B. R. S., Bell, R., Widnall, C., Perez, L. T., et al. (2018). miRNA-based signatures in cerebrospinal fluid as potential diagnostic tools for early tage Parkinson's disease. *Oncotarget* 9, 17455–17465. doi: 10.18632/oncotarget.24736

Double, K. L., and Halliday, G. M. (2006). New face of neuromelanin. *J. Neural Transm. Suppl.* 70, 119–123. doi: 10.1007/978-3-211-45295-0_19

El-Agnaf, O. M. A., Salem, S. A., Paleologou, K. E., Curran, M. D., Gibson, M. J., Court, J. A., et al. (2006). Detection of oligomeric forms of (-synuclein protein in human plasma as a potential biomarker for Parkinson's disease. *FASEB J.* 20, 419–425. doi: 10.1096/fj.03-1449com

Elbaz, A., and Tranchant, C. (2007). Epidemiologic studies of environmental exposures in Parkinson's disease. *Neurol. Sci.* 262, 37–44. doi: 10.1016/j.jns.2007.06.024

Emamzadeh, F. N. (2016). Alpha-synuclein structure, functions, and interactions. *J. Res. Med. Sci.?* 21:29. doi: 10.4103/1735-1995.181989

Emamzadeh, F. N. (2017). Role of Apolipoproteins and α-Synuclein in Parkinson's disease. *J. Mol. Neurosci.* 62, 344–355. doi: 10.1007/s12031-017-0942-9

Estupinan, D., Nathoo, S., and Okun, M. S. (2013). The demise of Poskanzer and Schwab's influenza theory on the pathogenesis of Parkinson's disease. *Parkinsons Dis.* 2013:167843. doi: 10.1155/2013/167843

Fazio, P., Svenningsson, P., Forsberg, A., Jönsson, E. G., Amini, N., Nakao, R., et al. (2015). Quantitative Analysis of ^{18}F-(E)-N-(3-Iodoprop-2-Enyl)-2β-Carbofluoroethoxy-3β-(4'-Methyl-Phenyl) nortropane binding to the dopamine transporter in Parkinson disease. *J. Nucl. Med.* 56, 714–720. doi: 10.2967/jnumed.114.152421

Feng, Y., Jankovic, J., and Wu, Y. C. (2015). Epigenetic mechanisms in Parkinson's disease. *J. Neurol. Sci.* 349, 3–9. doi: 10.1016/j.jns.2014.12.017

Foulds, P. G., Mitchell, J. D., Parker, A., Turner, R., Green, G., Diggle, P., et al. (2011). Phosphorylated α-synuclein can be detected in blood plasma and is potentially a useful biomarker for Parkinson's disease. *FASEB J.* 25, 4127–4137. doi: 10.1096/fj.10-179192

Fronczek, R., Overeem, S., Lee, S. Y., Hegeman, I. M., van Pelt, J., van Duinen, S. G., et al. (2007). Hypocretin (orexin) loss in Parkinson's disease. *Brain* 130, 1577–1585. doi: 10.1093/brain/awm090

Gill, S. S., Patel, N. K., Hotton, G. R., O'Sullivan, K., McCarter, R., Bunnage, M., et al. (2003). Direct brain infusion of glial cell line-derived neurotrophic factor in Parkinson disease. *Nat. Med.* 9, 589–595. doi: 10.1038/nm850

Goldenberg, M. M. (2008). Medical management of Parkinson's disease. *P T* 33, 590–606.

Goldstein, D. S. (2001). Cardiac sympathetic neuroimaging to distinguish multiple system atrophy from Parkinson disease. *Clin. Auton. Res.* 11, 341–342. doi: 10.1007/BF02292764

Goldstein, D. S. (2013). Sympathetic neuroimaging. *Handb. Clin. Neurol.* 117, 365–370. doi: 10.1016/B978-0-444-53491-0.00029-8

Goldstein, D. S., Holmes, C., Lopez, G. J., Wu, T., and Sharabi, Y. (2018). Cerebrospinal fluid biomarkers of central dopamine deficiency predict Parkinson's disease. *Parkinsonism Relat. Disord.* 50, 108–112. doi: 10.1016/j.parkreldis.2018.02.023

Graeber, M. B., and Muller, U. (1992). The X-linked dystonia-parkinsonism syndrome: clinical and molecular genetic analysis. *Brain Pathol.* 2, 287–295. doi: 10.1111/j.1750-3639.1992.tb00706.x

Gwinn-Hardy, K., Singleton, A., O'Suilleabhain, P., Boss, M., Nicholl, D., Adam, A., et al. (2001). Spinocerebellar ataxia type 3 phenotypically resembling parkinson disease in a black family. *Arch. Neurol.* 58, 296–299. doi: 10.1001/archneur.58.2.296

Hagan, J. J., Leslie, R. A., Patel, S., Evans, M. L., Wattam, T. A., Holmes, S., et al. (1999). Orexin a activates locus coeruleus cell firing and increases arousal in the rat. *Proc. Nat. Acad. Sci. U.S.A.* 96, 10911–10916. doi: 10.1073/pnas.96.19.10911

Hare, D., Ayton, S., Bush, A., and Lei, P. (2013). A delicate balance: iron metabolism and diseases of the brain. *Front. Aging Neurosci.* 18:34. doi: 10.3389/fnagi.2013.00034

Havelund, J. F., Heegaard, N. H. H., Færgeman, N. J. K., and Gramsbergen, J. B. (2017). Biomarker research in Parkinson's disease using metabolite profiling. *Metabolites* 7:E42. doi: 10.3390/metabo7030042

Henchcliffe, C., Shungu, D. C., Mao, X., Huang, C., Nirenberg, M. J., and Jenkins, B. G. (2008). Multinuclear magnetic resonance spectroscopy for in vivo assessment of mitochondrial dysfunction in Parkinson's disease. *Ann. N. Y. Acad. Sci.* 1147, 206–220. doi: 10.1196/annals.1427.037

Herrington, T. M., Cheng, J. J., and Eskandar, E. N. (2016). Mechanisms of deep brain stimulation. *J. Neurophysiol.* 115, 19–38. doi: 10.1152/jn.00281.2015

Herzog, J., Fietzek, U., Hamel, W., Morsnowski, A., Steigerwald, F., and Schrader, B. (2004). Most effective stimulation site in subthalamic deep brain stimulation for Parkinson's disease. *Mov. Disord.* 19, 1050–1054. doi: 10.1002/mds.20056

Histed, S. N., Lindenberg, M. L., Mena, E., Turkbey, B., Choyke, P. L., and Kurdziel, K. A. (2012). Review of functional/ anatomic imaging in oncology. *Nucl. Med. Commun.* 33, 349–361. doi: 10.1097/MNM.0b013e32834ec8a5

Hochfeld, W. E., Lee, S., and Rubinsztein, D. C. (2013). Therapeutic induction of autophagy to modulate neurodegenerative disease progression. *Acta Pharmacol. Sin.* 34, 600–604. doi: 10.1038/aps.2012.189

Höllerhage, M., Moebius, C., Melms, J., Chiu, W. H., Goebel, J. N., Chakroun, T., et al. (2017). Protective efficacy of phosphodiesterase-1 inhibition against alpha-synuclein toxicity revealed by compound screening in LUHMES cells. *Sci. Rep.* 7:11469. doi: 10.1038/s41598-017-11664-5

Hong, Z., Shi, M., Chung, K. A., Quinn, J. F., Peskind, E. R., Galasko, D., et al. (2010). DJ-1 and alpha-synuclein in human cerebrospinal fluid as biomarkers of Parkinson's disease. *Brain* 133, 713–726. doi: 10.1093/brain/awq008

Iacobazzi, V., Castegna, A., Infantino, V., and Andria, G. (2013). Mitochondrial DNA methylation as a next-generation biomarker and diagnostic tool. *Mol. Genet. Metab.* 110, 25–34. doi: 10.1016/j.ymgme.2013.07.012

Ibrahim, N., Kusmirek, J., Struck, A. F., Floberg, J. M., Perlman, S. B., Gallagher, C., et al. (2016). The sensitivity and specificity of F-DOPA PET in a movement disorder clinic. *Am. J. Nucl. Med. Mol. Imaging* 6, 102–109.

Imamura, K., Hishikawa, N., Sawada, M., Nagatsu, T., Yoshida, M., and Hashizume, Y. (2003). Distribution of major histocompatibility complex class II-positive microglia and cytokine profile of Parkinson's disease brains. *Acta Neuropathol.* 106, 518–526. doi: 10.1007/s00401-003-0766-2

Imperatore, R., Palomba, L., and Cristino, L. (2017). Role of Orexin-a in hypertension and obesity. *Curr. Hypertens. Rep.* 19:34. doi: 10.1007/s11906-017-0729-y

Iwata, A., Miura, S., Kanazawa, I., Sawada, M., and Nukina, N. (2001). alpha-Synuclein forms a complex with transcription factor Elk-1. *J. Neurochem.* 77, 239–252. doi: 10.1046/j.1471-4159.2001.t01-1-00232.x

Jankovic, J., and Aguilar, G. (2008). Current approaches to the treatment of Parkinson's disease. *Neuropsychiatr. Dis. Treat.* 4, 743–757. doi: 10.2147/NDT.S2006

Kachroo, A., and Schwarzschild, M. A. (2012). Adenosine A2A receptor gene disruption protects in an α-synuclein model of Parkinson's disease. *Ann. Neurol.* 71, 278–282. doi: 10.1002/ana.22630

Karamohamed, S., DeStefano, A. L., Wilk, J. B., Shoemaker, C. M., Golbe, L. I., Mark, M. H., et al. (2003). A haplotype at the PARK3 locus influences onset age for Parkinson's disease: the GenePD study. *Neurology* 61, 1557–1561. doi: 10.1212/01.WNL.0000095966.99430.F4

Karimi-Moghadam, A., Charsouei, S., Bell, B., and Jabalameli, M. R. (2018). Parkinson disease from mendelian forms to genetic susceptibility: new molecular insights into the neurodegeneration process. *Cell. Mol. Neurobiol.* 38, 1153–1178. doi: 10.1007/s10571-018-0587-4

Kikuchi, A., Takeda, A., Onodera, H., Kimpara, T., Hisanaga, K., Sato, N., et al. (2002). Systemic increase of oxidative nucleic acid damage in Parkinson's disease and multiple system atrophy. *Neurobiol. Dis.* 9, 244–248. doi: 10.1006/nbdi.2002.0466

Kikuchi, Y., Yasuhara, T., Agari, T., Kondo, A., Kuramoto, S., Kameda, M., et al. (2011). Urinary 8-OHdG elevations in a partial lesion rat model of Parkinson's disease correlate with behavioral symptoms and nigrostriatal dopaminergic depletion. *J. Cell. Physiol.* 226, 1390–1398. doi: 10.1002/jcp.22467

Kitada, T., Asakawa, S., Hattori, N., Matsumine, H., Yamamura, Y., Minoshima, S., et al. (1988). Mutations in the parkin gene cause autosomal recessive juvenile parkinsonism. *Nature* 392, 605–608. doi: 10.1038/33416

Koroglu, C., Baysal, L., Cetinkaya, M., Karasoy, H., and Tolun, A. (2013). DNAJC6 is responsible for juvenile parkinsonism with phenotypic variability. *Parkinsonism Relat. Disord.* 19, 320–324. doi: 10.1016/j.parkreldis.2012.11.006

Krebs, C. E., Karkheiran, S., Powell, J. C., Cao, M., Makarov, V., Darvish, H., et al. (2013). The Sac1 domain of SYNJ1 identified mutated in a family with early-onset progressive parkinsonism with generalized seizures. *Hum. Mutat.* 34, 1200–1207. doi: 10.1002/humu.22372

Langston, J. W. (1996). The etiology of Parkinson's disease with emphasis on the MPTP story. *Neurology* 47, 153–160. doi: 10.1212/WNL.47.6_Suppl_3.153S

Lautier, C., Goldwurm, S., Durr, A., Giovannone, B., Tsiaras, W. G., and Pezzoli, G. (2008). Mutations in the GIGYF2 (TNRC15) gene at the PARK11 locus in familial Parkinson disease. *Am. J. Hum. Genet.* 82, 822–833. doi: 10.1016/j.ajhg.2008.01.015

Lauretani, F., Saginario, A., Ceda, G. P., Galuppo, L., Ruffini, L., Nardelli, A., et al. (2014). Treatment of the motor and non-motor symptoms in Parkinson's disease according to cluster symptoms presentation. *Curr. Drug Targets* 15, 943–947.

Le, W., Xu, P., Jankovic, J., Jiang, H., Appel, S. H., Smith, R. G., et al. (2003). Mutations in NR4A2 associated with familial Parkinson disease. *Nat. Genet.* 33, 85–89. doi: 10.1038/ng1066

Lee, H., Baek, S. M., Ho, D., Suk, J., Cho, E., and Lee, S. (2011). Dopamine promotes formation and secretion of non-fibrillar alpha-synuclein oligomers. *Exp. Mol. Med.* 43, 216–222. doi: 10.3858/emm.2011.43.4.026

Leroy, E., Boyer, R., Auburger, G., Leube, B., Ulm, G., Mezey, E., et al. (1998). The ubiquitin pathway in Parkinson's disease. *Nature* 395, 451–452. doi: 10.1038/26652

Levin, J., Schmidt, F., Boehm, C., Prix, C., Bötzel, K., Ryazanov, S., et al. (2014). The oligomer modulator anle138b inhibits disease progression in a Parkinson mouse model even with treatment started after disease onset. *Acta Neuropathol.* 127, 779–780. doi: 10.1007/s00401-014-1265-3

LeWitt, P. A., Rezai, A. R., Leehey, M. A., Ojemann, S. G., Flaherty, A. W., Eskandar, E. N., et al. (2011). AAV2-GAD gene therapy for advanced Parkinson's disease: a double-blind, sham-surgery controlled, randomised trial. *Lancet Neurol.* 10, 309–319. doi: 10.1016/S1474-4422(11)70039-4

Li, D. H., Wang, J., Mao, C. J., Hu, W. D., Xiao, L., Yang, Y. P., et al. (2011). Association of PARK 16 polymorphisms with Parkinson's disease in Han population of Suzhou. *Zhonghua Yi Xue Za Zhi* 91, 296–300. doi: 10.1016/S1474-4422(11)70039-4

Li, Q. X., Mok, S. S., Laughton, K. M., McLean, C. A., Cappai, R., Masters, C. L., et al. (2007). Plasma alpha-synuclein is decreased in subjects with Parkinson's disease. *Exp. Neurol.* 204, 583–588. doi: 10.1016/j.expneurol.2006.12.006

Liddle, R. A. (2018). Parkinson's disease from the gut. *Brain Res.* 1693(Pt B), 201–206. doi: 10.1016/j.brainres.2018.01.010

Lin, C.-H., Chen, M.-L., Chen, G. S., Tai, C.-H., and Wu, R.-M. (2011). Novel variant Pro143Ala in *HTRA2* contributes to Parkinson's disease by inducing hyperphosphorylation of HTRA2 protein in mitochondria. *Hum. Genet.* 130, 817–827. doi: 10.1007/s00439-011-1041-6

Lin, K. J., Weng, Y. H., Hsieh, C. J., Lin, W. Y., Wey, S. P., Kung, M. P., et al. (2013). Brain imaging of vesicular monoamine transporter type 2 in healthy aging subjects by 18F-FP-(+)-DTBZ PET. *PLoS One* 8:e75952. doi: 10.1371/journal.pone.0075952

Lin, L. F., Doherty, D. H., Lile, J. D., Bektesh, S., and Collins, F. (1993). GDNF: a glial cell line-derived neurotrophic factor for midbrain dopaminergic neurons. *Science* 260, 1130–1132. doi: 10.1126/science.8493557

Lodish, H., Berk, A., Matsudaira, P., Kaiser, C. A., Krieger, M., Scott, M. P., et al. (2004). in *Molecular Cell Biology*, 5th Edn, ed. J. Darnell (New York, NY: W.H. Freeman and CO), 66–72.

Luk, K. C., Kehm, V., Carroll, J., Zhang, B., O'Brien, P., Trojanowski, J. Q., et al. (2012). Pathological α-synuclein transmission initiates parkinson-like neurodegeneration in non-transgenic mice. *Science* 16, 949–953. doi: 10.1126/science.1227157

Mahami Oskouei, M., Hamidi, F., Talebi, M., Farhoudi, M., Taheraghdam, A. A., and Kazemi, T. (2016). The correlation between *Toxoplasma gondii* infection and Parkinson's disease: a case-control study. *J. Parasit. Dis.* 40, 872–876. doi: 10.1007/s12639-014-0595-3

Martins-Branco, D., Esteves, A. R., Santos, D., Arduino, D. M., Swerdlow, R. H., and Oliveira, C. R. (2012). Ubiquitin proteasome system in Parkinson's disease: a keeper or a witness? *Exp. Neurol.* 238, 89–99. doi: 10.1016/j.expneurol.2012.08.008

Masuda-Suzukake, M., Nonaka, T., Hosokawa, M., Oikawa, T., Arai, T., Akiyama, H., et al. (2013). Prion-like spreading of pathological α-synuclein in brain. *Brain* 136, 1128–1138. doi: 10.1093/brain/awt037

Matsumoto, L., Takuma, H., Tamaoka, A., Kurisaki, H., Date, H., Tsuji, S., et al. (2010). CpG demethylation enhances alpha-synuclein expression and affects the pathogenesis of Parkinson's disease. *PLoS One* 5:e15522. doi: 10.1371/journal.pone.0015522

McKeith, I. G., Boeve, B. F., Dickson, D. W., Halliday, G., Taylor, J. P., Weintraub, D., et al. (2017). Diagnosis and management of dementia with Lewy bodies: fourth consensus report of the DLB consortium. *Neurology* 89, 88–100. doi: 10.1212/WNL.0000000000004058

McLean, P. J., Kawamata, H., Ribich, S., and Hyman, B. T. (2000). Membrane association and protein conformation of α-synuclein in intact neurons. Effect of Parkinson's disease-linked mutations. *J. Biol. Chem.* 275, 8812–8816. doi: 10.1074/jbc.275.12.8812

Miman, O., Kusbeci, O. Y., Aktepe, O. C., and Cetinkaya, Z. (2010). The probable relation between *Toxoplasma gondii* and Parkinson's disease. *Neurosci. Lett.* 475, 129–131. doi: 10.1016/j.neulet.2010.03.057

Mittermeyer, G., Christine, C. W., Rosenbluth, K. H., Baker, S. L., Starr, P., Larson, P., et al. (2012). Long-term evaluation of a phase 1 study of AADC gene therapy for Parkinson's disease. *Hum. Gene Ther.* 23, 377–381. doi: 10.1089/hum.2011.220

Mollenhauer, B., Locascio, J. J., Schulz-Schaeffer, W., Sixel-Döring, F., Trenkwalder, C., and Schlossmacher, M. G. (2011). α-Synuclein and tau concentrations in cerebrospinal fluid of patients presenting with parkinsonism: a cohort study. *Lancet Neurol.* 10, 230–240. doi: 10.1016/S1474-4422(11)70014-X

Muramatsu, S., Fujimoto, K., Kato, S., Mizukami, H., Asari, S., Ikeguchi, K., et al. (2010). A phase I study of aromatic L-amino acid decarboxylase gene therapy for Parkinson's disease. *Mol. Ther.* 18, 1731–1735. doi: 10.1038/mt.2010.135

Nagai, Y., Ueno, S., Saeki, Y., Soga, F., Hirano, M., and Yanagihara, T. (1996). Decrease of the D3 dopamine receptor mRNA expression in lymphocytes from patients with Parkinson's disease. *Neurology* 46, 791–795. doi: 10.1212/WNL.46.3.791

Niethammer, M., Feigin, A., and Eidelberg, D. (2012). Functional neuroimaging in Parkinson's disease. *Cold Spring Harb. Perspect. Med.* 2:a009274. doi: 10.1101/cshperspect.a009274

Obeso, J. A., Rodríguez-Oroz, M. C., Benitez-Temino, B., Blesa, F. J., Guridi, J., Marin, C., et al. (2008). Functional organization of the basal ganglia: therapeutic implications for Parkinson's disease. *Mov. Disord.* 23, 548–559. doi: 10.1002/mds.22062

Oertel, W. H. (2017). Recent advances in treating Parkinson's disease. *F1000Res.* 6:260. doi: 10.12688/f1000research.10100.1

Oh, J. K., Choi, E. K., Song, I. U., Kim, J. S., and Chung, Y. A. (2015). Comparison of I-123 MIBG planar imaging and SPECT for the detection of decreased heart uptake in Parkinson disease. *J. Neural Transm. (Vienna)* 122, 1421–1427. doi: 10.1007/s00702-015-1409-1

Olanow, C. W., Kieburtz, K., Odin, P., Espay, A. J., Standaert, D. G., Fernandez, H. H., et al. (2014). Continuous intrajejunal infusion of levodopa-carbidopa intestinal gel for patients with advanced Parkinson's disease: a randomised, controlled, double-blind, double-dummy study. *Lancet Neurol.* 13, 141–149. doi: 10.1016/S1474-4422(13)70293-X

Paisan-Ruiz, C., Bhatia, K. P., Li, A., Hernandez, D., Davis, M., Wood, N. W., et al. (2009). Characterization of PLA2G6 as a locus for dystonia-parkinsonism. *Ann. Neurol.* 65, 19–23. doi: 10.1002/ana.21415

Perni, M., Galvagnion, C., Maltsev, A., Meisl, G., Müller, M. B., Challa, P. K., et al. (2017). A natural product inhibits the initiation of α-synuclein aggregation and suppresses its toxicity. *Proc. Natl. Acad. Sci. U.S.A.* 114, E1009–E1017. doi: 10.1073/pnas.1610586114

Pirker, W., Asenbaum, S., Wenger, S., Kornhuber, J., Angelberger, P., Deecke, L., et al. (1997). Iodine-123-epidepride-SPECT: studies in Parkinson's disease, multiple system atrophy and Huntington's disease. *J. Nucl. Med.* 38, 1711–1717.

Plaha, P., Ben-Shlomo, Y., Patel, N. K., and Gill, S. S. (2006). Stimulation of the caudal zona incerta is superior to stimulation of the subthalamic nucleus in improving contralateral parkinsonism. *Brain* 129, 1732–1747. doi: 10.1093/brain/awl127

Pulkes, T., Choubtum, L., Chitphuk, S., Thakkinstian, A., Pongpakdee, S., Kulkantrakorn, K., et al. (2014). Glucocerebrosidase mutations in Thai patients

with Parkinson's disease. *Parkinsonism Relat. Disord.* 20, 986–991. doi: 10.1016/j.parkreldis.2014.06.007

Ramirez, A., Heimbach, A., and Grundemann, J. (2006). Hereditary parkinsonism with dementia is caused by mutations in ATP13A2, encoding a lysosomal type 5 P-type ATPase. *Nat. Genet.* 38, 1184–1191. doi: 10.1038/ng1884

Rappold, P. M., and Tieu, K. (2010). Astrocytes and therapeutics for Parkinson's disease. *Neurotherapeutics* 7, 413–423. doi: 10.1016/j.nurt.2010.07.001

Reiche, W., Grundmann, M., and Huber, G. (1995). Dopamine (D2) receptor SPECT with 123I-iodobenzamide (IBZM) in diagnosis of Parkinson syndrome. *Radiologie* 35, 838–843.

Reichmann, H., Brandt, M. D., and Klingelhoefer, L. (2016). The nonmotor features of Parkinson's disease: pathophysiology and management advances. *Curr. Opin. Neurol.* 29, 467–473. doi: 10.1097/WCO.0000000000000348

Reiter, R. J. (1995). Oxidative processes and antioxidative defense mechanisms in the aging brain. *FASEB J.* 9, 526–533. doi: 10.1096/fasebj.9.7.7737461

Rinne, J., Ruottinen, H., Bergman, J., Haaparanta, M., Sonninen, P., and Solin, O. (1999). Usefulness of a dopamine transporter PET ligand [18F]β-CFT in assessing disability in Parkinson's disease. *J. Neurol. Neurosurg. Psychiatry* 67, 737–741. doi: 10.1136/jnnp.67.6.737

Saeed, U., Compagnone, J., Aviv, R. I., Strafella, A. P., Black, S. E., Lang, A. E., et al. (2017). Imaging biomarkers in Parkinson's disease and Parkinsonian syndromes: current and emerging concepts. *Transl. Neurodegener.* 6:8. doi: 10.1186/s40035-017-0076-6

Samii, A., Nutt, J. G., and Ransom, B. R. (2004). Parkinson's disease. *Lancet* 363, 1783–1793. doi: 10.1016/S0140-6736(04)16305-8

Sasaki, T., Amano, T., Hashimoto, J., Itoh, Y., Muramatsu, K., Kubo, A., et al. (2003). [SPECT imaging using [123I]beta-CIT and [123I]IBF in extrapyramidal diseases]. *No To Shinkei* 55, 57–64.

Satake, W., Nakabayashi, Y., Mizuta, I., Hirota, Y., Ito, C., and Kubo, M. (2009). Genome-wide association study identifies common variants at four loci as genetic risk factors for Parkinson's disease. *Nat. Genet.* 41, 1303–1307. doi: 10.1038/ng.485

Scriabine, A. (1999). "Discovery and development of major drugs currently in use," in *The Pharmaceutical Innovation: Revolutionizing Human Health*, ed. A. Scriabine (Philadelphia: Chemical Heritage Press), 222–223.

Seppi, K., Schocke, M. F., Esterhammer, R., Kremser, C., Brenneis, C., Mueller, J., et al. (2003). Diffusion-weighted imaging discriminates progressive supranuclear palsy from PD, but not from the parkinson variant of multiple system atrophy. *Neurology* 60, 922–927. doi: 10.1212/01.WNL.0000049911.91657.9D

Seraji-Bozorgzad, N., Bao, F., George, E., Krstevska, S., Gorden, V., Chorostecki, J., et al. (2015). Longitudinal study of the substantia nigra in Parkinson disease: a high-field 1 H-MR spectroscopy imaging study. *Mov. Disord.* 30, 1400–1404. doi: 10.1002/mds.26323

Shadrina, M. I., Slominsky, P. A., and Limborska, S. A. (2010). Chapter 6. Molecular Mechanisms of Pathogenesis of Parkinson's disease. *Int. Rev. Cell Mol. Biol.* 281, 229–266. doi: 10.1016/S1937-6448(10)81006-8

Shi, C.-h., Tang, B.-s., Wang, L., Lv, Z.-y., Wang, J., Luo, L.-z., et al. (2011). *PLA2G6* gene mutation in autosomal recessive early-onset parkinsonism in a Chinese cohort. *Neurology* 77, 75–81. doi: 10.1212/WNL.0b013e318221acd3

Shigenaga, M., Gimeno, C. J., and Ames, B. N. (1989). Urinary 8-hydroxy-2'-deoxyguanosine as a biomarker of in vivo oxidative DNA damage. *Proc. Natl. Acad. Sci. U.S.A.* 86, 9697–9701. doi: 10.1073/pnas.86.24.9697

Siderowf, A., Aarsland, D., Mollenhauer, B., Goldman, J. G., and Ravina, B. (2018). Biomarkers for cognitive impairment in Lewy body disorders: status and relevance for clinical trials. *Mov. Disord.* 33, 528–536. doi: 10.1002/mds.27355

Simon, D. K., Simuni, T., Elm, J., Clark-Matott, J., Graebner, A. K., and Baker, L. (2015). Peripheral biomarkers of Parkinson's disease progression and Pioglitazone effects. *J. Parkinsons Dis.* 4, 731–736. doi: 10.3233/JPD-150666

Singleton, A. B., Farrer, M., Johnson, J., Singleton, A., Hague, S., Kachergus, J., et al. (2003). A-synuclein locus triplication causes Parkinson's disease. *Science* 302:841. doi: 10.1126/science.1090278

Skoloudík, D., Jelínková, M., Blahuta, J., Cermák, P., Soukup, T., Bártová, P., et al. (2014). Transcranial sonography of the substantia nigra: digital image analysis. *AJNR Am. J. Neuroradiol.* 35, 2273–2278. doi: 10.3174/ajnr.A4049

Steiner, J. A., Quansah, E., and Brundin, P. (2018). The concept of alpha-synuclein as a prion-like protein: ten years after. *Cell Tissue Res.* 373, 161–173. doi: 10.1007/s00441-018-2814-1

Strauss, K. M., Martins, L. M., Plun-Favreau, H., Marx, F. P., Kautzmann, S., Berg, D., et al. (2005). Loss of function mutations in the gene encoding Omi/HtrA2 in Parkinson's disease. *Hum. Mol. Genet.* 14, 2099–2111. doi: 10.1093/hmg/ddi215

Sui, Y. T., Bullock, K. M., Erickson, M. A., Zhang, J., and Banks, W. A. (2014). Alpha synuclein is transported into and out of the brain by the blood-brain barrier. *Peptides* 62, 197–202. doi: 10.1016/j.peptides.2014.09.018

Surgucheva, I., and Surguchov, A. (2008). Gamma-synuclein: cell-type-specific promoter activity and binding to transcription factors. *J. Mol. Neurosci.* 35, 267–271. doi: 10.1007/s12031-008-9074-6

Surguchov, A. (2015). Intracellular dynamics of synucleins: here, there and everywhere. *Int. Rev. Cell Mol. Biol.* 320, 103–169. doi: 10.1016/bs.ircmb.2015.07.007

Surguchov, A., Surgucheva, I., Sharma, M., Sharma, R., and Singh V. (2017). Pore-forming proteins as mediators of novel epigenetic mechanism of epilepsy. *Front. Neurol.* 8:3. doi: 10.3389/fneur.2017.00003

Swanson, C. R., Berlyand, Y., Xie, S. X., Alcalay, R. N., Chahine, L. M., and Chen-Plotkin, A. S. (2015). Plasma apolipoprotein A1 associates with age at onset and motor severity in early Parkinson's disease patients. *Mov. Disord.* 30, 1648–1656. doi: 10.1002/mds.26290

Takahashi, Y., Kanbayashi, T., Hoshikawa, M., Imanishi, A., Sagawa, Y., Tsutsui, K., et al. (2015). Relationship of orexin (hypocretin) system and astrocyte activation in Parkinson's disease with hypersomnolence. *Sleep Biol. Rhythms* 13, 252–260. doi: 10.1111/sbr.12112

Tan, E.-K., Lin, C.-H., Tai, C.-H., Tan, L. C., Chen, M.-L., and Li, R. (2009). Non-synonymous GIGYF2 variants in Parkinson's disease from two Asian populations. *Hum. Genet.* 126, 425–430. doi: 10.1007/s00439-009-0678-x

Tell-Marti, G., Puig-Butille, J. A., Potrony, M., Badenas, C., Milà, M., and Malvehy, J. (2015). The MC1R melanoma risk variant p.R160W is associated with Parkinson disease. *Ann. Neurol.* 77, 889–894. doi: 10.1002/ana.24373

Tong, J., Wilson, A. A., Boileau, I., Houle, S., and Kish, S. J. (2008). Dopamine modulating drugs influence striatal (+)-[11C]DTBZ binding in rats: VMAT2 binding is sensitive to changes in vesicular dopamine concentration. *Synapse* 62, 873–876. doi: 10.1002/syn.20573

Valente, E. M., Abou-Sleiman, P. M., Caputo, V., Muqit, M. M., Harvey, K., Gispert, S., et al. (2004). Hereditary early-onset Parkinson's disease caused by mutations in PINK1. *Science* 304, 1158–1160. doi: 10.1126/science.1096284

van der Zee, S., Vermeiren, Y., Fransen, E., Van Dam, D., Aerts, T., Gerritsen, M. J., et al. (2018). Monoaminergic markers across the cognitive spectrum of Lewy body disease. *J. Parkinsons Dis.* 8, 71–84. doi: 10.3233/JPD-171228

van Duijn, C. M., Dekker, M. C., Bonifati, V., Galjaard, R. J., Houwing-Duistermaat, J. J., Snijders, P. J., et al. (2001). Park7, a novel locus for autosomal recessive early-onset parkinsonism, on chromosome 1p36. *Am. J. Hum. Genet.* 69, 629–634. doi: 10.1086/322996

Venda, L. L., Cragg, S. J., Buchman, V. L., and Wade-Martins, R. (2010). α-Synuclein and dopamine at the crossroads of Parkinson's disease. *Trends Neurosci.* 33, 559–568. doi: 10.1016/j.tins.2010.09.004

Vermeiren, Y., and De Deyn, P. P. (2017). Targeting the norepinephrinergic system in Parkinson's disease and related disorders: the locus coeruleus story. *Neurochem. Int.* 102, 22–32. doi: 10.1016/j.neuint.2016.11.009

Vilariño-Güell, C., Rajput, A., Milnerwood, A. J., Shah, B., Szu-Tu, C., Trinh, J., et al. (2014). DNAJC13 mutations in Parkinson disease. *Hum. Mol. Genet.* 23, 1794–1801. doi: 10.1093/hmg/ddt570

Vilariño-Güell, C., Wider, C., Ross, O. A., Dachsel, J. C., Kachergus, J. M., and Lincoln, S. J. (2011). VPS35 mutations in Parkinson disease. *Am. J. Hum. Genet.* 89, 162–167. doi: 10.1016/j.ajhg.2011.06.001

Vitali, C., Wellington, C. L., and Calabresi, L. (2014). HDL and cholesterol handling in the brain. *Cardiovasc. Res.* 103, 405–413. doi: 10.1093/cvr/cvu148

Vitali, M. C. T., Barreto-Sanz, M. A., Correia, B. R. S., Bell, R., Widnall, C., Perez, L. T., et al. (2018). miRNA-based signatures in cerebrospinal fluid as potential diagnostic tools for early stage Parkinson's disease. *Oncotarget* 9, 17455–17465. doi: 10.18632/oncotarget.24736

Wang, E. S., Sun, Y., Guo, J. G., Gao, X., Hu, J. W., Zhou, L., et al. (2010). Tetranectin and apolipoprotein A-I in cerebrospinal fluid as potential biomarkers for Parkinson's disease. *Acta Neurol. Scand.* 122, 350–359. doi: 10.1111/j.1600-0404.2009.01318.x

Wang, L., Zhang, Q., Li, H., and Zhang, H. (2012). SPECT molecular imaging in Parkinson's disease. *J. Biomed. Biotechnol.* 2012;412486. doi: 10.1155/2012/412486

Watanabe, M., Maemura, K., Kanbara, K., Tamayama, T., and Hayasaki, H. (2002). GABA and GABA receptors in the central nervous system and other organs. *Int. Rev. Cytol.* 213, 1–47. doi: 10.1016/S0074-7696(02)13011-7

Wienecke, M., Werth, E., Poryazova, R., Baumann-Vogel, H., Bassetti, C. L., Weller, M., et al. (2012). Progressive dopamine and hypocretin deficiencies in Parkinson's disease: is there an impact on sleep and wakefulness? *J. Sleep Res.* 21, 710–717. doi: 10.1111/j.1365-2869.2012.01027.x

Wu, Y. R., Lin, H. Y., Chen, C. M., Gwinn-Hardy, K., Ro, L. S., Wang, Y. C., et al. (2004). Genetic testing in spinocerebellar ataxia in Taiwan: expansions of trinucleotide repeats in SCA8 and SCA17 are associated with typical Parkinson's disease. *Clin. Genet.* 65, 209–214. doi: 10.1111/j.0009-9163.2004.00213.x

Xu, L., Ma, B., Nussinov, R., and Thompson, D. (2017). Familial Mutations May Switch Conformational Preferences in α-Synuclein Fibrils. *ACS Chem. Neurosci.* 8, 837–849. doi: 10.1021/acschemneuro.6b00406

Yang, Z., Wang, X., Yang, J., Sun, M., Wang, Y., and Wang, X. (2017). Aberrant CpG methylation mediates abnormal transcription of MAO-A. *Neurotox. Res.* 31, 334–347. doi: 10.1007/s12640-016-9686-5

Yonekura, Y., Saji, H., Iwasaki, Y., Tsuchida, T., Fukuyama, H., Shimatsu, A., et al. (1995). Initial clinical experiences with dopamine D2 receptor imaging by means of 2'-iodospiperone and single-photon emission computed tomography. *Ann. Nucl. Med.* 9, 131–136. doi: 10.1007/BF03165039

Yu, S., Li, X., Liu, G., Han, J., Zhang, C., Li, Y., et al. (2007). Extensive nuclear localization of α-synuclein in normal rat brain neurons revealed by a novel monoclonal antibody. *Neuroscience* 145, 539–555. doi: 10.1016/j.neuroscience.2006.12.028

Zeng, X. S., Geng, W. S., Jia, J. J., Chen, L., and Zhang, P. P. (2018). Cellular and molecular basis of neurodegeneration in Parkinson disease. *Front. Aging Neurosci.* 10:109. doi: 10.3389/fnagi.2018.00109

Zimprich, A., Biskup, S., Leitner, P., Lichtner, P., Farrer, M., Lincoln, S., et al. (2004). Mutations in LRRK2 cause autosomal-dominant parkinsonism with pleomorphic pathology. *Neuron* 44, 601–607. doi: 10.1016/j.neuron.2004.11.005

Zucca, F. A., Basso, E., Cupaioli, F. A., Ferrari, E., Sulzer, D., Casella, L., et al. (2014). Neuromelanin of the human substantia nigra: an update. *Neurotox. Res.* 25, 13–23. doi: 10.1007/s12640-013-9435-y

Conflict of Interest Statement: The authors declare that the research was conducted in the absence of any commercial or financial relationships that could be construed as a potential conflict of interest.

frontiers in Neurology

REVIEW
published: 07 September 2018
doi: 10.3389/fneur.2018.00750

Driving Ability in Alzheimer Disease Spectrum: Neural Basis, Assessment, and Potential Use of Optic Flow Event-Related Potentials

Takao Yamasaki[1,2]* *and Shozo Tobimatsu*[1]

[1] Department of Clinical Neurophysiology, Neurological Institute, Graduate School of Medical Sciences, Kyushu University, Fukuoka, Japan, [2] Department of Neurology, Minkodo Minohara Hospital, Fukuoka, Japan

Driving requires multiple cognitive functions including visuospatial perception and recruits widespread brain networks. Recently, traffic accidents in dementia, particularly in Alzheimer disease spectrum (ADS), have increased and become an urgent social problem. Therefore, it is necessary to develop the objective and reliable biomarkers for driving ability in patients with ADS. Interestingly, even in the early stage of the disease, patients with ADS are characterized by the impairment of visuospatial function such as radial optic flow (OF) perception related to self-motion perception. For the last decade, we have studied the feasibility of event-related potentials (ERPs) in response to radial OF in ADS and proposed that OF-ERPs provided an additional information on the alteration of visuospatial perception in ADS (1, 2). Hence, we hypothesized that OF-ERPs can be a possible predictive biomarker of driving ability in ADS. In this review, the recent concept of neural substrates of driving in healthy humans are firstly outlined. Second, we mention the alterations of driving performance and its brain network in ADS. Third, the current status of assessment tools for driving ability is stated. Fourth, we describe ERP studies related to driving ability in ADS. Further, the neural basis of OF processing and OF-ERPs in healthy humans are mentioned. Finally, the application of OF-ERPs to ADS is described. The aim of this review was to introduce the potential use of OF-ERPs for assessment of driving ability in ADS.

Keywords: Alzheimer disease spectrum, radial optic flow perception, event-related potentials, driving ability, Alzheimer's disease, mild cognitive impairment

OPEN ACCESS

Edited by:
Pravat K. Mandal, National Brain Research Centre (NBRC), India

Reviewed by:
Deepika Shukla, National Brain Research Centre (NBRC), India
Jordi A. Matias-Guiu, Hospital Clínico San Carlos, Spain

***Correspondence:**
Takao Yamasaki
yamasa@neurophy.med.kyushu-u.ac.jp

Specialty section:
This article was submitted to Applied Neuroimaging, a section of the journal Frontiers in Neurology

Received: *01 June 2018*
Accepted: *17 August 2018*
Published: *07 September 2018*

Citation:
Yamasaki T and Tobimatsu S (2018) Driving Ability in Alzheimer Disease Spectrum: Neural Basis, Assessment, and Potential Use of Optic Flow Event-Related Potentials. Front. Neurol. 9:750. doi: 10.3389/fneur.2018.00750

INTRODUCTION

Driving is a complicated skill that needs to integrate multiple cognitive, perceptual and motor abilities (3), and is supported by widely distributed brain network responsible for these complex processes (4–8). The driving ability can be disturbed by a decline in these brain networks due to normal aging and cognitive impairment such as dementia (3, 9–11). In recent years, the number of individuals with dementia is steadily increasing due to aging of the population (12). Under such circumstances, traffic accidents in individuals with dementia have increased and become an urgent social problem (11).

Among dementia, Alzheimer's disease (AD) is the most common (12). AD progresses on a spectrum with three stages, so-called, "AD spectrum (ADS)" (13); (1) preclinical AD (14), (2) mild cognitive impairment (MCI) due to AD (15), and (3) AD dementia (16). AD dementia is

characterized by the impairment of short-term episodic memory, orientation, visuospatial function, language and executive function (12). The major neuropathological hallmarks of AD are deposition of β amyloid (senile plaques) and accumulation of neurofibrillary tangles, which cause a series of toxic events that result in synaptic dysfunction, neuronal loss and brain atrophy (12). Overall, multiple cognitive function associated with distributed brain network are impaired due to the AD pathology, resulting in the decline of driving ability in patients with AD.

There are various methods to assess driving ability, which include on-road test, driving simulation, and neuropsychological tests. However, recent systematic review and meta-analysis on these methods have demonstrated a lack of consistency of the findings among the studies though the several cognitive tests are considered to be the predictors of driving performance in AD patients (3, 17). So far, there have been no tests sufficient to determine driving safety, so it is necessary to establish a reliable method that can accurately evaluate driving ability in ADS. Interestingly, visuospatial dysfunction is often an early symptom even in the early stage of ADS (18, 19). Specifically, psychophysical studies demonstrated that AD patients exhibited selective elevation of motion coherence thresholds for radial optic flow (OF) motion which was related to self-motion perception (20), compared with those of coherent horizontal (HO) motion and static forms (19). In addition, the impaired OF perception was correlated with poor performance of the spatial navigation test (19). These findings suggest that the deficits of OF perception is responsible for the impairment of spatial navigation including the driving performance in AD patients. Some patients with MCI also exhibited selective impairment of coherent OF motion perception (18).

Event-rerated potentials (ERPs) are a pertinent tool to assess the visual function as well as dysfunction in humans because ERPs are non-invasive, objective, rapid, repeatable with the low cost. ERPs are also characterized by excellent temporal resolution ($<$ 1 ms) and can measure neural activity directly compared with functional magnetic resonance imaging (fMRI) (21, 22). Therefore, radial OF-ERPs may be a neural biomarker for decline of driving performance in ADS.

In this review, we first outline the neural basis of driving ability in healthy humans. Second, we describe the alterations of performance and associated brain function for driving in ADS. Third, we refer to current status of the assessment tests for driving and its problems. Fourth, ERP studies related to driving ability in ADS are stated. Further, we mention the neural basis of OF perception and findings of OF-related ERPs in healthy humans. Finally, we introduce the potential use of OF-ERPs for assessing driving ability of ADS. The aim of this review was to stress the feasibility of neurophysiological evaluation of OF perception that can be a neural biomarker for altered driving ability in ADS.

NEURAL BASIS OF DRIVING ABILITY IN HEALTHY INDIVIDUALS

Driving requires the coordination of multiple cognitive functions and recruitment of associated multiple brain regions. Several fMRI studies on various driving tasks have demonstrated the activation of widespread brain network including occipital, parietal, frontal, motor and cerebellar regions and others to maintain safe driving (4–8). **Figure 1** shows an example of activated brain regions while driving in a recent fMRI study (4). In their study, during driving only condition, the occipital activations were observed in the inferior, superior and middle occipital gyri and lingual gyrus. The activated areas of parietal lobe were superior and inferior parietal lobe, postcentral gyrus, and precuneus. The activations of frontal regions consisted of the inferior, middle and superior frontal gyri and precentral gyrus. The superior and middle temporal gyri were the activated areas of temporal regions. The activations of the cerebellum included the uvular, declive, and cerebellar tonsil. In addition, the limbic region such as cingulate gyrus, sub-lobar region including insula and lentiform nucleus were activated (4).

During driving, occipital and parietal regions plays a crucial role in visuospatial perception and attention to visual motion and fixed landmarks during vehicle movement. The frontal region is important for the executive function, working memory, processing thoughts, and decision-making. The motor and cerebellar regions engage in fine-control and action planning during movement execution (4–8). Furthermore, the recruitment of these brain regions is changeable but not uniform while driving. For instance, during distracted driving, brain activations shift the posterior regions to the frontal regions, particularly in the prefrontal areas (6). Taken together, because brain networks related to driving are broadly distributed, they may be susceptible to brain disorder such as ADS which shows extensive brain damage.

ALTERED DRIVING PERFORMANCE IN ADS

Older drivers are at higher risk for traffic accidents such as crashes, injuries and deaths than other age groups (11). Further, individuals with AD dementia have an increased risk of traffic accidents compared to healthy older drivers (11). Severity of decline in driving performance was correlated with a degree of cognitive impairment in AD dementia (23). Individuals with MCI also had significantly more errors (collisions, center line crossings, road edge excursions, stop sign missed, speed limit exceedance) compared with healthy control drivers (10). MCI is classified into two types: amnestic MCI (aMCI) (with memory impairment) and non-aMCI (without memory impairment) (24). MCI is further classified into single-domain MCI (with impairment in single cognitive domain) and multiple-domain MCI (with impairment in multiple cognitive domain) (24). Patients with multiple-domain aMCI have the two or more impairments of memory, attention, viusospatial function, and executive function. Comparing multiple-domain aMCI with single-domain aMCI, the former demonstrates greater driving difficulty compared with the latter and healthy controls (10). Since all these cognitive functions are important for driving performance, multiple-domain aMCI may exhibit a greater driving difficulty than single-domain aMCI.

A single-photon emission computed tomography (SPECT) study has demonstrated that severity of impaired driving

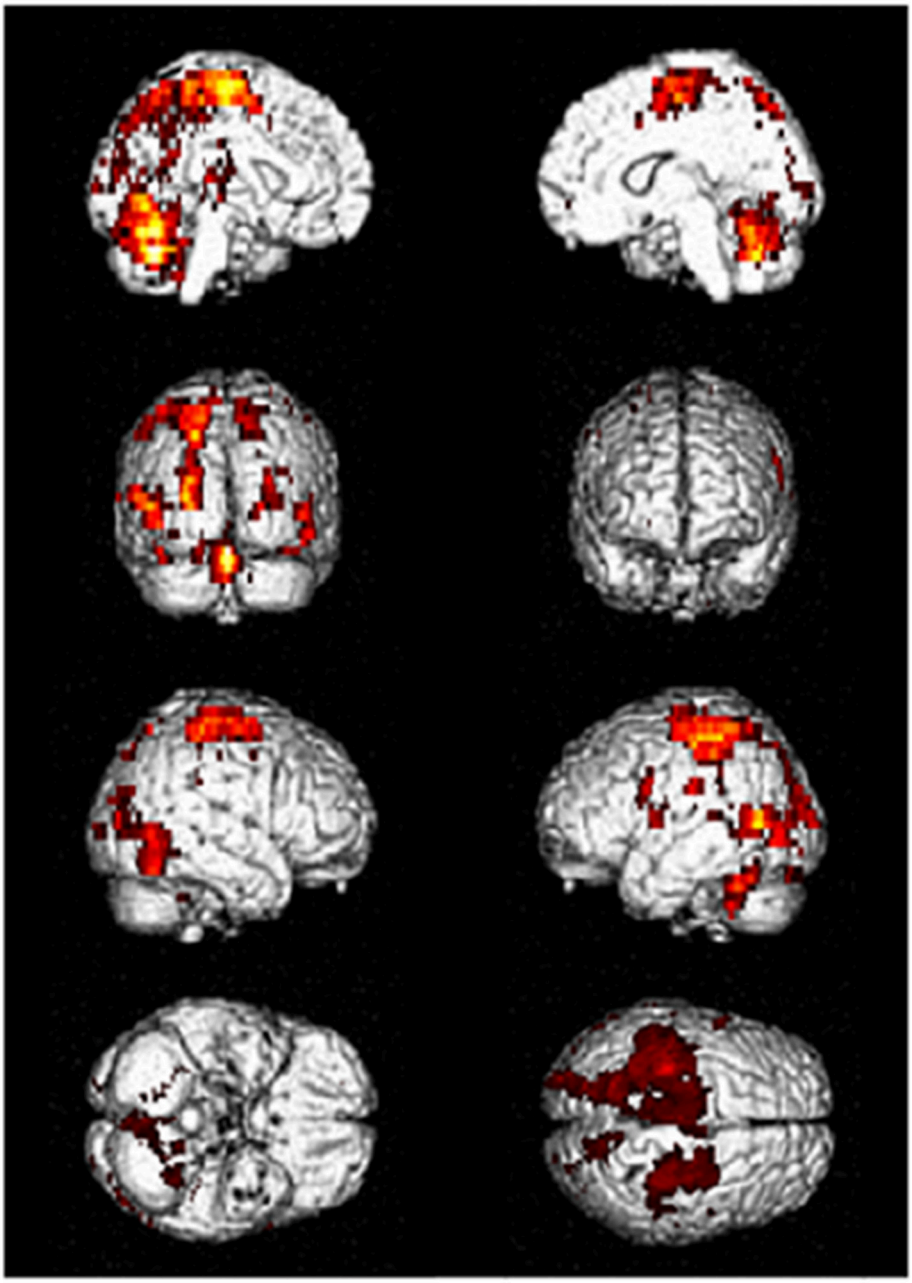

FIGURE 1 | Activated brain regions during driving in fMRI. Distributed brain networks including occipital, parietal, frontal, motor, and cerebellar regions are mainly activated while driving only task. fMRI, functional magnetic resonance imaging. [Modified from (4), licensed under Creative Commons].

performance is significantly correlated with the changes of cerebral blood flow in the temporo-parietal regions in early stage of AD (25). A positron emission tomography (PET) study showed that the executive functioning was correlated with metabolism in the temporo-parietal regions, which was impaired in early stage of AD (26). Neuropsychological studies also reported a significant relationship between driving performance and visuospatial perceptual ability in AD (17). These findings indicate that the hypoperfusion or hypometabolism of temporo-parietal regions reflects the impairments of visuospatial perception and executive function, which result in impaired driving performance in early stage of AD. Moreover, with increased severity of driving impairment, the perfusion of frontal region was also reduced in addition to temporo-parietal regions in SPECT (25). The AD pathology is observed in the temporo-parietal regions in the early stage of the disease while

that pathology spread into the frontal regions in the later stage (27). Therefore, the impairment of executive function involving the frontal regions can be more correlated with the driving impairment for the late stage of AD. Interestingly, a recent PET study have revealed that driving risk is strongly correlated with accumulation of amyloid even in the preclinical stage of AD (28). In another study using tau and amyloid PET, participants at Stage 2 [amyloid (+) and tau (+)] of preclinical AD (14) were more likely to receive a marginal/fail rating compared to participants at Stage 0 [amyloid (-) and tau (-)] or 1 [amyloid (+) and tau (-)] (11, 14). This finding suggests that individuals with preclinical AD (Stage 2) may already decline in driving skills.

Overall, the driving performance is gradually worsening along with the course of ADS from preclinical AD to AD dementia. These alterations of driving performance seem to be induced by the progression of AD pathology. In particular, the early pathological change in the posterior temporo-parietal regions associated with visuospatial function (OF perception) may be responsible for the impaired driving in the early stage of ADS.

ASSESSMENT TOOLS FOR DRIVING ABILITY IN ADS

Various methods including on-road test, driving simulation and neuropsychological tests have been used for evaluating driving ability (3, 17, 29). The on-road test is the gold standard for assessing fitness to drive, but it requires much time for patients. There is also a need for someone who is proficient in the judgment. The driving simulation is similar to the on-road test, but it is expensive. Therefore, these two tests cannot be routinely performed at the medical clinics. For this reason, neuropsychological tests are commonly used. Neuropsychological tests can evaluate various aspects of brain function including attention, executive function and visuospatial abilities known to be impaired in patients with ADS. For example, the following tests are frequently used; the Mini-Mental State Examination (MMSE) for memory, attention and language skill, the Trail Making Test Part A and B (TMT-A and -B) for cognitive flexibility, Drawing test for visuo-constructive ability, and Maze test for visual orientation (29). However, these neuropsychological examinations, especially when doing multiple tests, require a long time to perform, so that patients often get tired. Characteristics with some pros and cons of these assessment tools are briefly summarized in **Table 1**.

There have been many studies that investigate the usefulness of above mentioned tests as predictors of driving ability (3, 17, 29). However, a recent systematic review (17) demonstrated a lack of consistency in the findings, with some studies showing a relationship between cognitive test and driving performance for individuals with AD, whereas others did not. Further, this review suggested that deficits in a single cognitive ability were not a reliable predictor of driving performance. In contrast, a composite battery that assessed the multiple cognitive domains required to be an efficient driver was the best predictor of driving performance in individuals with AD (17). Another study compared the predictive value of the three types of assessment such as clinical interview, neuropsychological test battery (including multiple tests) and driving simulation (29). They found that neuropsychological assessment provided the best prediction of fitness to drive. Clinical interviews were less objective and less standardized than neuropsychological

TABLE 1 | Assessment tools for driving ability in ADS.

Assessment tools	Characteristics	Pros	Cons
On-road test	- Gold standard - Evaluate driving abilities using actual vehicle by a trained expert	- Close to driving in the natural environment	- Expensive - Limited availability - Need a trained expert - Long time to perform - Cannot examine the driving ability under hazardous conditions
Driving simulators	- Mimic real-world driving using a front monitor, a handle, an accelerator, a brake pedal, etc. which resemble an actual vehicle	- Wide range of test conditions (e.g., night and day, different weather conditions, or road environments) - Especially, we can safely examine the driving performance under hazardous conditions	- Expensive - Limited availability
Neuropsychological tests	- Assess various cognitive functions indispensable for driving (e.g., attention, executive function and visuospatial abilities, etc)	- Widely available - Multiple options for standardized measures	- Long time to perform - Need a trained expert
ERPs	- Directly measure neural activity from scalp electrodes while watching OF stimuli in the case of OF-ERPs	- Widely available - Non-invasive - Inexpensive - Short time to perform - Easy to use	- Currently not standardization for driving assessment

ERPs, event-related potentials; OF, optic flow.

tests and driving simulation. Driving simulation is also not sufficiently predictive if used alone. However, combining all three types of assessments yielded the best prediction for fitness to drive in patients with AD (29). Other systematic review and meta-analysis have demonstrated that executive function, attention, visuospatial function and global cognition revealed by neuropsychological tests may be predictive of driving performance in patients with MCI and AD. Specifically, TMT-A and -B and Maze test emerged as the best single predictors of driving performance though there were variability and inconsistencies. On-road and simulator assessments have yielded inconsistent results in terms of the safety to drive in patients with MCI and AD (3).

From the results of these studies, there has been no single test sufficient to determine driving safety in patients with MCI and AD though the combined use of these tests is somewhat useful. Accordingly, it is necessary to establish an objective method that can be performed easily, in a short time, at a low cost, but has high reliability. Note that ERPs have all such features, therefore, ERPs are suitable for evaluating driving ability in ADS. In the following section, we describe ERP researches on driving evaluation in ADS.

ASSESSMENT OF DRIVING ABILITY IN ADS USING ERPS

ERPs are electrical potential generated by the brain time-locked to a sensory, cognitive, or motor event and provide a powerful, non-invasive technique with superb temporal resolution, for studying the brain's synaptic function (30–32). In general, early ERP components (< 200 ms) reflect sensory processes as they depend mainly on the physical parameters of the stimulus, so-called exogenous component. Conversely, later ERP components (> 200 ms) are relatively more dependent on the mental operations performed on the stimuli as well as on non-sensory factors such as predictability, higher perceptual and semantic features, so-called endogenous component.

ERPs have been extensively used for functional evaluation of brain in ADS (30–32). The P300 component (around at 300–500 ms) elicited by an oddball paradigm has been most studied in ADS as the convenient measure of the cognitive dysfunction. In general, early sensory components at around 50–100 ms are relatively spared whereas potentials starting around 200 ms and beyond are more consistently abnormal even in the early stage of AD and MCI. Thus, ERPs may reveal neurophysiological changes related to the expansion of the neocortical association areas of AD pathology (32).

For the ERP research on driving, the P300 cognitive component is often used as an index of driving performance in healthy individuals (33–36). However, there have been no P300-ERP studies on driving ability in ADS. To our knowledge, only two ERP studies used N200 component for the driving ability of AD (37, 38) (**Table 2**). In a study of (37), ERPs were recorded in young and older normal controls, and early AD patients while participants viewed real-world videos and dot motion stimuli (OF) simulating self-movement scenes. In both stimulus conditions, N200 latencies were delayed by aging whereas AD patients exhibited the diminished N200 amplitude. In addition, AD patients were uniquely unresponsive to increments in motion speed. Since OF is crucial for speed judgments and braking during vehicular navigation, the authors proposed that the AD unresponsiveness to accelerations might reveal some of the mechanism involved in their driving impairment and potentially help identify high-risk individuals at earlier stage. In another study (abstract form) (38), early AD patients and older normal control took a virtual reality driving evaluation that incorporates multiple cognitive, visual and motor tests. OF-ERPs were also recorded. Compared to older normal control, AD patients had significantly lower driving scores and smaller N200 amplitudes. Furthermore, there was a highly significant correlation between driving scores and N200 amplitudes. The authors concluded that significant correlations between vehicular driving scores and N200 amplitudes supported the role of extrastriate cortical dysfunction in impaired driving capacity and that the potential use of ERPs as screening tools for selective functional impairments and as biomarkers of AD.

These two studies (37, 38) suggest that OF-ERPs (sensory N200 component) may be useful for evaluation of driving ability in AD. However, it remains unknown whether the N200 component is the best predictor of driving ability in AD, and whether or not OF-ERPs can be an index of driving ability even in aMCI. For the last decade, we have been studying the feasibility of sensory ERPs in response to radial OF in aMCI and AD and proposed that OF-ERPs provided an additional information on the alteration of visuospatial perception in ADS (1, 2). The visuospatial deficits (impaired OF perception) related to the posterior temporo-parietal dysfunction play a key role in the navigational or driving impairment in ADS (18, 19, 25). Hence, we hypothesized that sensory ERPs elicited by OF but not P300 cognitive ERPs could be a neural biomarker in driving impairment even in the early stage of ADS. In the following section, we describe neural basis of OF processing in healthy humans and the potential use of OF-ERPs as a driving evaluation method.

NEURAL BASIS OF OF PERCEPTION IN HEALTHY HUMANS

When we move through our environment with walking or cars, the radial pattern of OF is produced at the retina (**Figure 2A**). The ability of visual motion system that analyzes OF is biologically important because it provides visual cues that can be used to perceive the direction of self-motion, to guide locomotion and to avoid obstacles (20, 39). Thus, the drivers must analyze radial OF information continuously to control his/her vehicle during driving, so that the OF processing is indispensable for safe driving.

In humans, there are two functionally and anatomically segregated visual pathways: the ventral and dorsal pathways (**Figure 3**) (21, 22, 42). Both pathways begin in the retina and project to the primary visual cortex (V1). After V1, the ventral

TABLE 2 | ERP studies on driving ability in ADS.

References	Participants	Study design and protocol	Outcome measure	Summary of main findings
Fernandez and Duffy (2012) (37)	- [OF (dot motion)] - Early AD *(n = 15; age, 78.6 ± 8.0)* - Older normal control *(n = 16; age, 76.2 ± 10.0)* - Young normal control *(n = 12; age, unknown)* [Real-world video motion stimuli] - Early AD *(n = 6; age, 73.2 ± 6.3)* - Older normal control *(n = 5; age, 70.6 ± 6.4)* - Young normal control *(n = 9; age, 29.33 ± 8.5)*	- Cross-sectional study - ERPs evoked by OF (dot motion) (Changes of coherence and speed) - ERPs evoked by real-world video motion stimuli (Changes of coherence and speed)	- N200 amplitude and latency	- Diminished N200 amplitude in early AD - Increasing speed elicits smaller N200 amplitudes in early AD
Fernandez-Romero and Cox (2016) (38) (abstract form)	- Early AD *(n = unknown; age, unknown)* - Older normal control *(n = unknown; age, unknown)*	- Cross-sectional study - ERPs evoked by OF - Virtual reality driving evaluation	- N200 amplitude and latency - Multiple cognitive, visual and motor tests	- Smaller N200 amplitude in early AD - Lower driving score in early AD - Significant correlations between vehicular driving scores and N200 amplitudes
Yamasaki et al (1)	- aMCI *(n = 18; age, 72.4 ± 6.9)* - Early AD *(n = 18; age, 75.5 ± 5.7)* - Older normal control *(n = 18; age, 71.8 ± 4.1)* - Young normal control *(n = 18; age, 28.2 ± 5.1)*	- Cross-sectional study - ERPs evoked by OF and HO (dot motion)	- N170 and P200 amplitudes and latencies	- Prolonged latency of OF-specific P200 in aMCI - Prolonged latencies of N170 and P200 in early AD - Significant correlation between OF-specific P200 latency and MMSE score
Yamasaki et al (2)	- aMCI *(n = 15; age, 74.4 ± 4.4)* - Older normal control *(n = 15; age, 73.5 ± 4.5)* - Young normal control *(n = 15; age, 27.9 ± 5.0)*	- Cross-sectional study - ERPs evoked by OF (dot motion), faces, words, chromatic and achromatic gratings	- N170 and P200 amplitudes and latencies for OF - N170 amplitudes and latencies for faces and words - N120 amplitude and latency for chromatic gratings - Steady-state response for achromatic gratings	- Prolonged N170 and P200 latencies for OF in aMCI - Prolonged N170 latencies for faces and words in aMCI - Normal N120 for chromatic gratings in aMCI - Normal steady-state response for achromatic gratings in aMCI - Significant correlations between N170 latency for OF and LM WMS-R scores, and between P200 amplitude for OF and LM WMS-R scores - High AUC in N170 and P200 latencies for OF in ROC analysis

aMCI, amnestic mild cognitive impairment; AD, Alzheimer's disease; ERPs, event-related potentials; OF, optic flow; MMSE, Mini-Mental State Examination; LM WMS-R, logical memory in Wechsler Memory Scale-Revised; ROC, receiver operating characteristic; AUC, area under the curve.

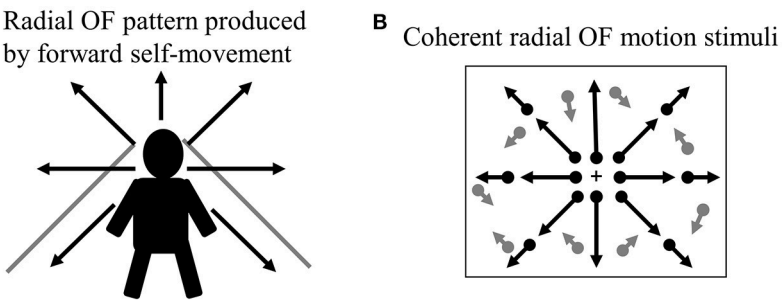

FIGURE 2 | Radial OF motion. **(A)** When we move through our environment, radial OF pattern is produced by forward self-movement. **(B)** Coherent radial OF motion stimuli used in our study. We can create radial OF motion stimuli easily using random dots. Dots radiate from the focus of expansion, which corresponds to the observer's direction of heading. OF, optic flow.

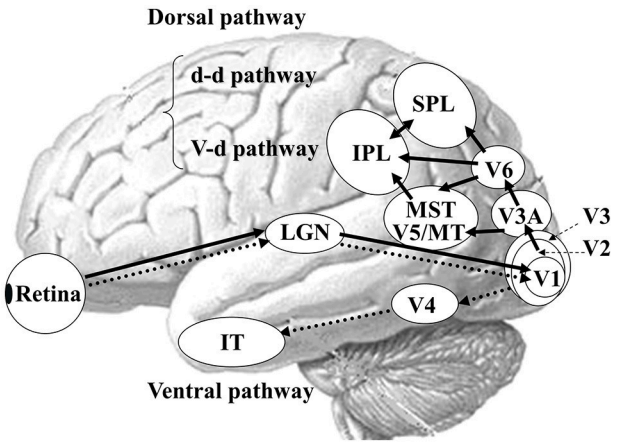

FIGURE 3 | Parallel visual pathways in humans. There are two major parallel streams: ventral and dorsal pathways in humans. Detailed functions of the two streams are provided in the text (see section Neural Basis of OF Perception in Healthy Humans). A recent study has revealed the importance of interconnection between IPL and SPL for OF processing (40) so that we modified this figure considering this point. d-d pathway, dorso-dorsal pathway; v-d pathway, ventro-dorsal pathway; LGN, lateral geniculate nucleus; MT, middle temporal area; MST, medial superior temporal area; IPL, inferior parietal lobule, SPL, superior parietal lobule; IT, inferior temporal cortex. [Modified from (41), Copyright (2012) with permission from IOS press].

stream is important for form and color perception, projecting to V4 and the inferior temporal (IT) cortex. In contrast, the dorsal stream is responsible for motion perception, connecting to V5/middle temporal (MT)+ (V5/MT and medial superior temporal area [MST]), V6 and the posterior parietal cortex (21). The dorsal stream also comprises two distinct functional flows; the dorso-dorsal (d-d) and ventro-dorsal (v-d) streams (43). The d-d stream consists of V6 and the superior parietal lobule (SPL) while the v-d stream involves V5/MT and the inferior parietal lobule (IPL). From the concept of such visual processing mechanism, the OF perception is mainly processed by the dorsal stream.

Primate studies have reported a number of cortical areas that selectively respond to OF, including the dorsal part of the MST (44), the ventral intraparietal area (VIP) (45), area 7a (46) as well as area PEc (47). Conversely, V5/MT neurons do not show such specific selectivity (48). In humans, several OF selective areas have been identified by neuroimaging studies within the dorsal streams (49–57). These OF selective areas contain visual areas such as MST and V6, multisensory areas such as the VIP, the precuneus motion area (PcM) and cingulate sulcus visual area, and vestibular areas such as the putative area 2v (p2v) and parieto-insular vestibular cortex (PIVC). A recent fMRI study have demonstrated that the posterior-insular cortex (PIC) area plays an important role in the integration of visual and vestibular stimuli for the perception of self-motion while the PIVC is selectively responsive to vestibular stimulation (58, 59). Overall, the VIP, PcM and p2V are located within the d-d stream (SPL) while the v-d stream (IPL) consists of PIC (40).

OF-ERPS IN HEALTHY HUMANS

In order to compare OF processing with HO processing in healthy humans, we recorded ERPs for coherent OF and HO motion stimuli in healthy young subjects by using a high-density EEG system (60) (**Figures 2B**, **4**). We used coherent motion stimuli as the visual stimuli, which consisted of 400 white square dots randomly distributed on a black background. The white dots moved at a velocity of 5.0°/s. Two types of motion stimuli (OF and HO) were used. OF stimuli contained dots that moved in a radial outward pattern while HO contained dots that moved leftward or rightward. The coherent level was 90% in both stimuli. Both stimuli had the same dot density, luminance, contrast and average dot speed. Random motion (RM) was used as a baseline condition. The OF and HO stimuli were presented for 750 ms, with the presentation of RM for 1,500–3,000 ms alternately. The N170 [analogous to N200 in previous ERP studies (37, 38), about 170 ms] and P200 (about 200 ms) were recorded as major components. We analyzed the peak latencies, amplitudes, scalp distribution and the sources in both components.

The N170 was distributed over occipito-temporal regions in response to both OF and HO stimuli. The distribution of the OF-N170 extended further into the parietal region compared with those of HO-N170 (**Figure 4B**). The OF-N170 amplitude was significantly larger and its latency was significantly shorter than those of HO-N170 (**Figure 4A**). Exact low resolution brain electromagnetic tomography (eLORETA) analysis of the N170 revealed that the current density was significantly elevated over the occipito-temporal areas including V5/MT+ in response to both stimuli compared with RM baseline (**Figure 5A**). These findings were consistent with those of minimum-norm estimate (MNE) of visual evoked magnetic fields (VEFs) (61). A direct comparison between OF and HO stimuli revealed no significant difference in the current density of the N170. Current density estimation with eLORETA in ERPs and MNE in VEFs provided strong evidence that the generator source of the N170 was located in V5/MT+ for both stimuli. Therefore, the N170 constitutes a non-specific motion component derived from an area close to V5/MT+. However, OF stimuli elicited an N170 with a higher amplitude and shorter latency, compared with HO (**Figure 4A**), which may reflect a higher activity of V5/MT+ during OF processing. Alternatively, V5/MT+ can be subdivided into V5/MT and MST (50, 62). V5/MT neurons respond to both OF and HO stimuli (48), whereas MST selectively responds to OF (44, 46). Thus, the selective activation of MST neurons may contribute to the higher amplitude and shorter latency of the OF-N170 response.

The P200 component exhibited distinct characteristics between OF and HO. The OF-P200 was distributed over the parieto-central region (**Figure 4**). HO stimulus also evoked an observable P200, but its topography was limited to the central region (**Figure 4**). The P200 amplitude was significantly larger for OF compared with HO stimuli. Similarly, the latency of OF-P200 was significantly faster compared with that of HO-P200 (**Figure 4A**). Regarding the parietal OF-P200, the current density was significantly elevated in the IPL (**Figure 5B**, top

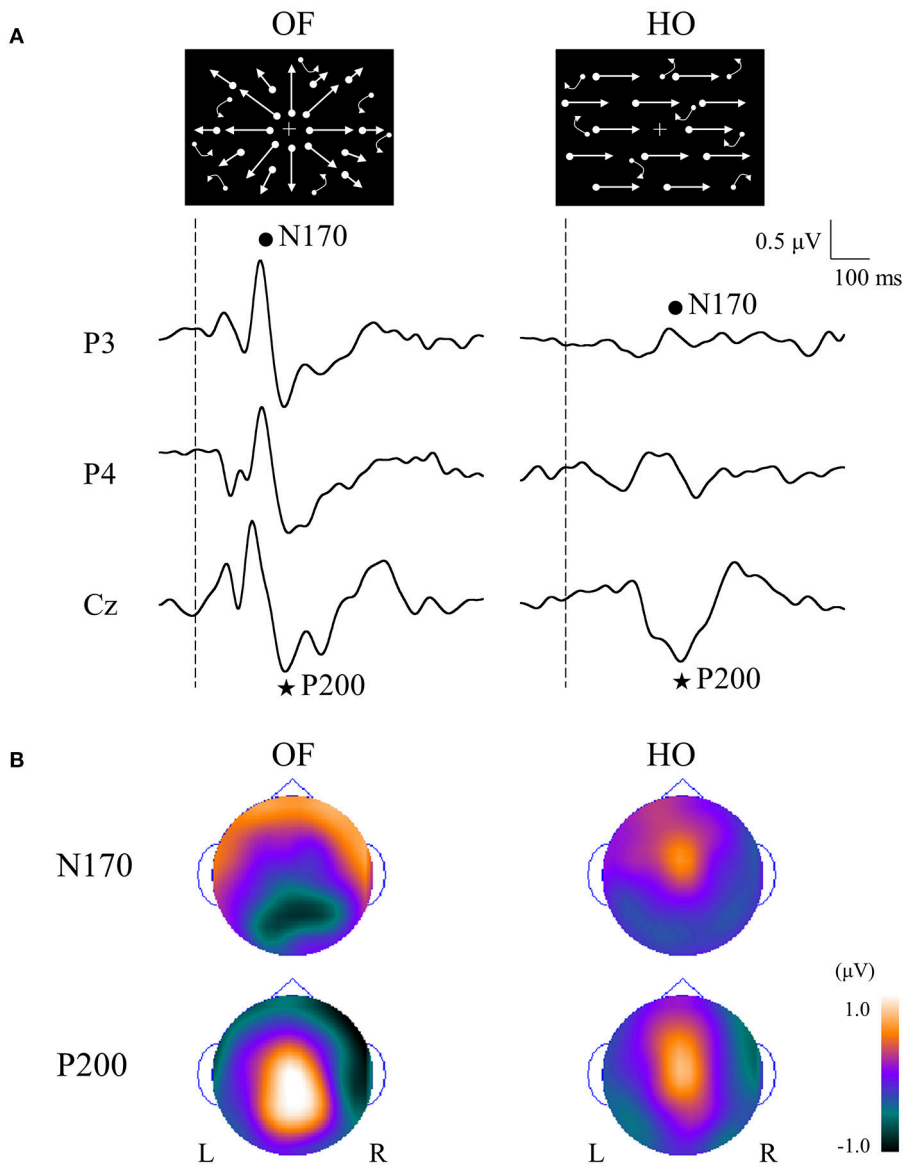

FIGURE 4 | ERPs in response to coherent OF and HO motion stimuli and their scalp topography in healthy subjects. **(A)** It is evident that the N170 and P200 are distinct motion-related components. The N170 component was distributed over occipito-temporal areas regardless of the stimulus type, extending further to the parietal region in the OF condition only. **(B)** The P200 component in response to OF stimuli was distributed over the parieto-central region while that of HO was distributed over the central region. The color bar represents the amplitude value (red = positive, blue = negative). Please note that this figure was presented at 2009 International Symposium on Early Detection and Rehabilitation Technology of Dementia. December 11–12, 2009, Okayama, Japan. ERPs, event-related potentials; HO, horizontal motion.

row). In contrast, for the central HO-P200, the current density was distributed over the SPL (**Figure 5B**, middle row). A direct comparison revealed that the current density of the IPL in response to OF stimuli compared with HO stimuli was significantly elevated (red color). Conversely, the current density of SPL was significantly elevated in HO compared with OF (blue color) (**Figure 5B**, bottom row). Overall, these findings suggest that the parietal OF-P200 is functionally coupled with the IPL (the v-d stream) and that it is the OF-specific component. Conversely, the central HO-P200 is related to the SPL (the d-d stream) (60). These functional dissociations between IPL (OF perception) and SPL (HO perception) were consistent with our fMRI study (41). Therefore, we propose that different spatio-temporal processing is driven by these motion stimuli within the two distinct dorsal streams in humans. From these findings, it is likely that ERPs with coherent OF and HO motion are useful for functional evaluation of the dorsal stream. More specifically, OF-related ERPs (OF-N170 and OF-P200 components) are

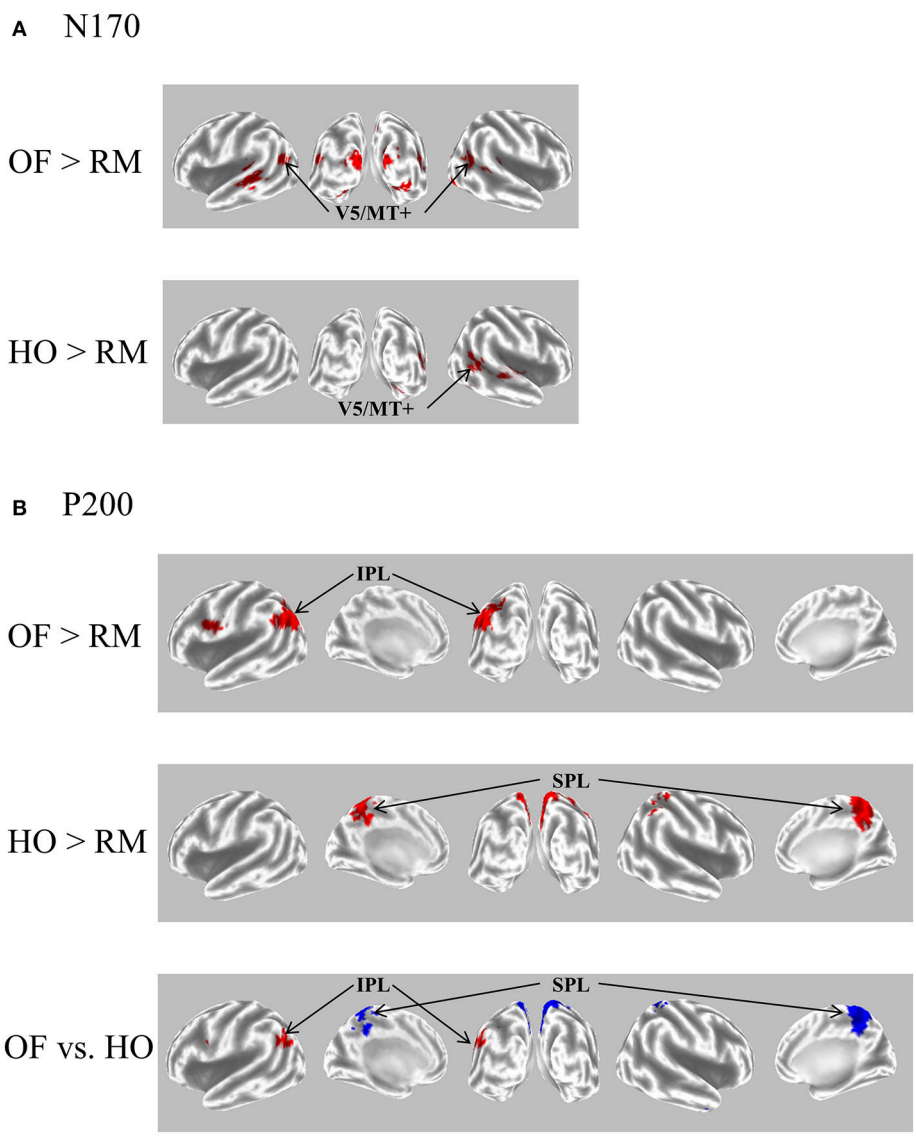

FIGURE 5 | eLORETA-based statistical nonparametric maps for a comparison between OF and HO in GFP peaks of N170 and P200. **(A)** The current density of N170 was significantly elevated over the occipito-temporal areas including V5/MT+ in both stimulus conditions. **(B)** The current density of the parietal P200 for OF was significantly elevated in the left IPL (BA 39/40). Conversely, there was a significant elevation of the current density of the central P200 for HO in the bilateral SPL (BA 7). In the figure at the bottom, red and blue mean OF and HO, respectively. Please note that this figure was presented at 2009 International Symposium on Early Detection and Rehabilitation Technology of Dementia. December 11–12, 2009, Okayama, Japan. eLORETA, exact low resolution brain electromagnetic tomography; GFP, global field power; RM, random motion.

considered to be able to identify subtle changes of visuospatial function (OF perception) associated with driving ability in individuals.

OF-ERPS IN ADS

To examine whether we can detect the impairment of OF perception in aMCI and AD, ERPs for OF and HO were recorded in patients with aMCI and AD, and in healthy old and young adults (1) (**Table 2**). aMCI was defined according to the criteria of Petersen (24). The patients with AD met the criteria for probable AD according to NINCDS-ADRDA (63). Neuropsychological tests including MMSE and the Clinical Dementia Rating (CDR) were performed. Regarding ERPs, visual stimuli and analysis were same as the former study in healthy young subjects (60). There was no significant difference in both OF-N170 and HO-N170 responses between aMCI patients and healthy old adults (**Figure 6**). In contrast, the latency of OF-P200 was significantly prolonged in aMCI patients compared with healthy old adults (**Figure 6**). Therefore, within the dorsal stream, the v-d stream (IPL) related to OF perception, but not the d-d stream (SPL) associated with HO perception, is selectively impaired in aMCI

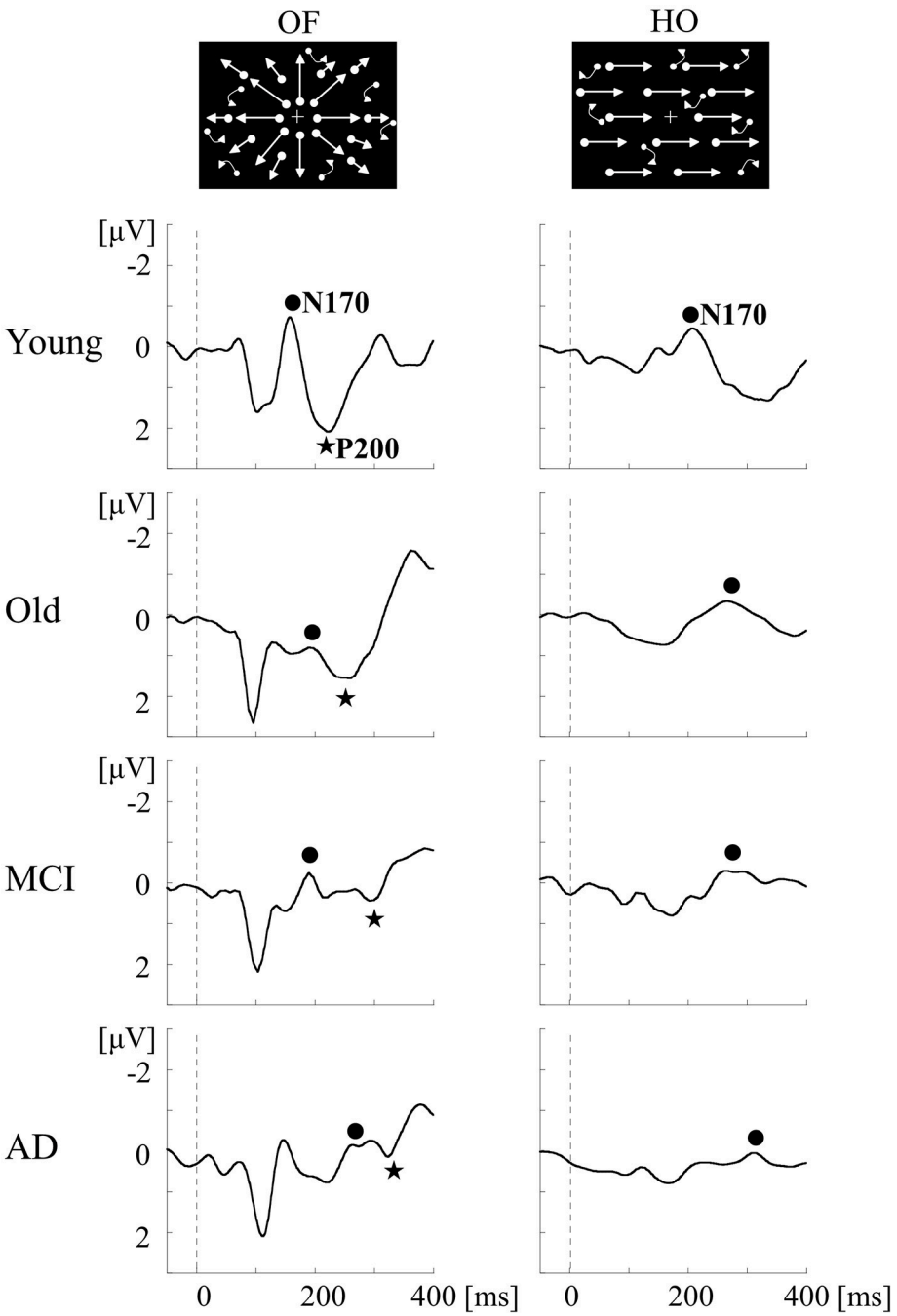

FIGURE 6 | ERPs in response to coherent OF and HO motion stimuli in the MCI, AD and healthy control groups. MCI patients exhibit more prolongation of P200 latency for OF than healthy elderly adults, but no prolongation of N170 latency for both stimuli. AD patients show a prolongation of both N170 and P200 latencies compared with other groups. MCI, mild cognitive impairment. [Modified from (64), Copyright (2012) with permission from IEEE].

patients. On the other hand, AD patients showed a prolongation of N170 and P200 latencies for both OF and HO stimuli compared with healthy old adults and aMCI patients (**Figure 6**). Our results indicate that aMCI patients exhibit a selective impairment of OF perception related to the higher-level of dorsal stream (v-d stream including IPL). Conversely, AD patients show the impairments of both OF and HO perception associated with the distributed higher-level dorsal stream (both v-d and d-d streams including IPL, SPL and V5/MT+). These findings were consistent with the spread of AD pathology following disease progression (1, 64). Thus, we can detect the impairment of OF perception even in patients with aMCI by using OF-ERPs.

We further recorded ERPs to multimodal visual stimuli (chromatic and achromatic gratings, faces, kanji and kana words and OF motion) in aMCI patients, healthy old and young adults (2) (**Table 2**). Inclusion criteria for aMCI patients and healthy old adults followed the criteria of the Japanese Alzheimer's Disease Neuroimaging Initiative (65). These criteria were based on several neuropsychological tests: MMSE, CDR, Geriatric Depression Scale and the logical memory test (delayed recall) of the Wechsler Memory Scale-Revised (WMS-R). Multimodal visual stimuli were optimized to activate elements of each visual stream separately. The OF stimulus was same as the former studies (1, 60). ERP responses to lower (V1) level stimuli (chromatic and achromatic gratings) were not significantly differed between aMCI patients and healthy old adults. Conversely, ERP latencies for higher-ventral (faces and kanji words) and higher-dorsal (kana words and OF motion) were significantly prolonged in aMCI patients. Interestingly, OF-related ERPs were significantly correlated with the logical memory test (delayed recall) of the WMS-R (OF-N170 latency, $r = -0.507$; OF-P200 amplitude, $r = 0.493$) (**Figure 7A**). Furthermore, the receiver operating characteristic (ROC) analysis exhibited that the highest area under the curve (AUC) was observed for OF-ERP latencies (OF-N170 latency, AUC = 0.856; OF-P200 latency, AUC = 0.831) (**Figure 7B**). This suggests that OF-ERPs have the best distinguishing ability between aMCI and healthy old adults.

A POTENTIAL USE OF OPTIC FLOW-ERPS IN ASSESSING DRIVING ABILITY IN ADS

Overall, in our ERP studies (1, 2), OF-related visuospatial perception indispensable for driving was associated with cognitive function in ADS. As previously mentioned, severity of decline in driving ability was correlated with the degree of cognitive function (23) or visuospatial function (17). Therefore, we assume that OF-ERPs can detect early signs of decline in driving ability in patients with ADS.

In support of our view that altered OF-related visuospatial perception is associated with the driving disability in ADS, Vilhelmsen et al. (66) found that the latency of N2 (analogous to N170 in our study) increased as the speed of OF-motion increased (driving speeds 25, 50, and 75 km/h) in healthy young subjects. They supposed that the subjects perceived the OF stimulus with higher speeds as more complex than that of the lower speeds, which resulted in the increased N2 latency. Healthy individuals can handle our OF stimulus easily but the damaged ADS brain may need more effort because of an excessive

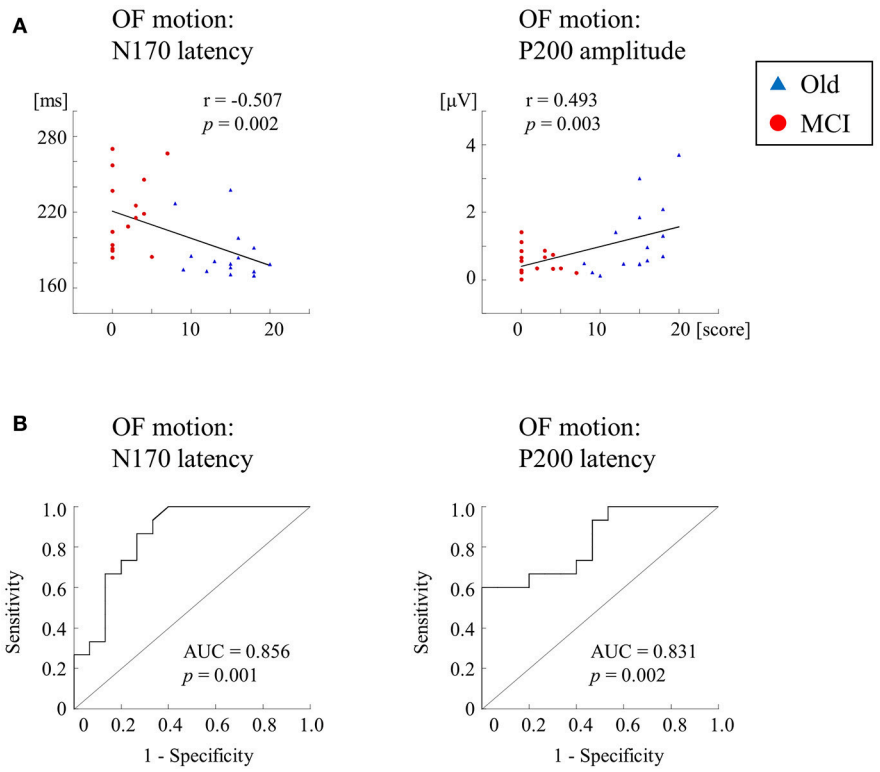

FIGURE 7 | Correlation and ROC analyses. **(A)** Correlation of ERPs with delayed LM WMS-R scores. ERPs for OF motion stimuli are significantly correlated with delayed LM WMS-R scores. **(B)** The results of ROC curve analysis for discriminability of ERP components. The N170 and P200 latencies for OF motion have AUCs ≥ the threshold of 0.7 for acceptable discrimination. Please note that AD group was not recruited in this study [Modified from (1), Copyright (2016) with permission from IOS press]. LM WMS-R, logical memory in Wechsler Memory Scale-Revised; ROC, receiver operating characteristic; AUC, area under the curve.

load for the visuospatial processing system. This interpretation may explain the delayed N170 and P200 latencies in our study (1, 2).

Based on ERP findings of our (1, 2) and other groups (37, 38), OF-ERPs (both N170 and P200 components) may be useful for evaluation of driving ability in aMCI and AD patients. However, it should be kept in mind that the relationship between OF-ERPs and the performance of on-road and driving simulator tests has not established. In addition, we have not yet determined the reference values of OF-ERPs (amplitude and latency) on driving ability. Thus, in the near future, we will perform a large-scale longitudinal ERP study for determining the relationship between driving ability and OF perception in a wide range of ADS. By doing so, we can assess driver's aptitude to prevent the traffic accidents in patients with ADS. Meanwhile, we are currently trying to develop the simple and reliable touch panel-type assessment system of driving ability using radial OF stimuli (measuring OF-detection threshold) (https://kaken.nii.ac.jp/en/grant/KAKENHI-PROJECT-17K09801/). This system may be useful for driving performance evaluation, which is much simpler than ERPs.

CONCLUSIONS

To maintain safe driving, widespread brain networks including occipital, parietal, frontal, motor and cerebellar regions are recruited. These brain networks are vulnerable in ADS pathology that shows extensive neocortical brain damage. In ADS, the driving ability continues to gradually decline accompanied by the course of AD pathology. Especially, the early pathological change in the posterior temporo-parietal regions related to OF perception is responsible for the impaired driving in the early stage of ADS. Although various methods including on-road test, driving simulation and neuropsychological tests are used for evaluating driving ability, there is no single test sufficient to determine driving safety in ADS patients. Conversely, ERPs are non-invasive and objective method that can be performed easily, in a short time, at a low cost, but has high reliability. Based on previous and our ERP studies, OF-ERPs can be an indicative neural biomarker for assessing the decline of driving ability in ADS.

AUTHOR CONTRIBUTIONS

All authors listed have made a substantial, direct and intellectual contribution to the work, and approved it for publication.

FUNDING

This study was partly supported by the following grants: JSPS KAKENHI Grant Number JP17K09801 to TY, and Grant from the Research on Innovative Areas (No.15H05875) from the Ministry of Education, Culture, Sports, Science, and Technology to ST.

ACKNOWLEDGMENTS

We wish to thank Drs. Yasumasa Ohyagi (Department of Neurology and Geriatric Medicine, Ehime University), Junichi Kira (Department of Neurology, Kyushu University) and Shigenobu Kanba (Department of Neuropsychiatry, Kyushu University) for their research assistance.

REFERENCES

1. Yamasaki T, Goto Y, Ohyagi Y, Monji A, Munetsuna S, Minohara M, et al. Selective impairment of optic flow perception in amnestic mild cognitive impairment: evidence from event-related potentials. *J Alzheimers Dis.* (2012) 28:695–708. doi: 10.3233/JAD-2011-110167
2. Yamasaki T, Horie S, Ohyagi Y, Tanaka E, Nakamura N, Goto Y, et al. A potential VEP biomarker for mild cognitive impairment: evidence from selective visual deficit of higher-level dorsal pathway. *J Alzheimers Dis.* (2016) 53:661–76. doi: 10.3233/JAD-150939
3. Hird MA, Egeto P, Fischer CE, Naglie G, Schweizer TA. A systematic review and meta-analysis of on-road simulator and cognitive driving assessment in Alzheimer's disease and mild cognitive impairment. *J Alzheimers Dis.* (2016) 53:713–29. doi: 10.3233/JAD-160276
4. Choi MH, Kim HS, Yoon HJ, Lee JC, Baek JH, Choi JS, et al. Increase in brain activation due to sub-tasks during driving: fMRI study using new MR-compatible driving simulator. *J Physiol Anthropol.* (2017) 36:11. doi: 10.1186/s40101-017-0128-8
5. Just MA, Keller TA, Cynkar J. A decrease in brain activation associated with driving when listening to someone speak. *Brain Res.* (2008) 1205:70–80. doi: 10.1016/j.brainres.2007.12.075
6. Schweizer TA, Kan K, Hung Y, Tam F, Naglie G, Graham SJ. Brain activity during driving with distraction: an immersive fMRI study. *Front Hum Neurosci.* (2013) 7:53. doi: 10.3389/fnhum.2013.00053
7. Spiers HJ, Maguire EA. Neural substrates of driving behaviour. *Neuroimage* (2007) 36:245–55. doi: 10.1016/j.neuroimage.2007.02.032
8. Uchiyama Y, Ebe K, Kozato A, Okada T, Sadato N. The neural substrates of driving at a safe distance: a functional MRI study. *Neurosci Lett.* (2003) 352:199–202. doi: 10.1016/j.neulet.2003.08.072
9. Allison S, Babulal GM, Stout SH, Barco PP, Carr DB, Fagan AM, et al. Alzheimer disease biomarkers and driving in clinically normal older adults: role of spatial navigation abilities. *Alzheimer Dis Assoc Disord.* (2018) 32:101–6. doi: 10.1097/WAD.0000000000000257
10. Hird MA, Vesely KA, Fischer CE, Graham SJ, Naglie G, Schweizer TA. Investigating simulated driving errors in amnestic single- and multiple-domain mild cognitive impairment. *J Alzheimers Dis.* (2017) 56:447–52. doi: 10.3233/JAD-160995
11. Roe CM, Babulal GM, Mishra S, Gordon BA, Stout SH, Ott BR, et al. Tau and amyloid positron emission tomography imaging predict driving performance among older adults with and without preclinical Alzheimer's disease. *J Alzheimers Dis.* (2018) 61:509–13. doi: 10.3233/JAD-170521
12. Alzheimer's Association. 2018 Alzheimer's disease facts and figures. *Alzheimers Dement.* (2018) 14:367–429. doi: 10.1016/j.jalz.2018.02.001
13. Petersen RC. New clinical criteria for the Alzheimer's disease spectrum. *Minn Med.* (2012) 95:42–5.
14. Sperling RA, Aisen PS, Beckett LA, Bennett DA, Craft S, Fagan AM, et al. Toward defining the preclinical stages of Alzheimer's disease: recommendations from the National Institute on Aging-Alzheimer's Association workgroups on diagnostic guidelines for Alzheimer's disease. *Alzheimers Dement.* (2011) 7:280–92. doi: 10.1016/j.jalz.2011.03.003
15. Albert MS, DeKosky ST, Dickson D, Dubois B, Feldman HH, Fox NC, et al. The diagnosis of mild cognitive impairment due to Alzheimer's disease: recommendations from the National Institute on Aging-Alzheimer's

Association workgroups on diagnostic guidelines for Alzheimer's disease. *Alzheimers Dement.* (2011) 7:270–9. doi: 10.1016/j.jalz.2011.03.008
16. McKhann GM, Knopman DS, Chertkow H, Hyman BT, Jack CRJr, Kawas CH, et al. The diagnosis of dementia due to Alzheimer's disease: recommendations from the national institute on aging-alzheimer's association workgroups on diagnostic guidelines for alzheimer's disease. *Alzheimers Dement.* (2011) 7:263–9. doi: 10.1016/j.jalz.2011.03.005
17. Bennett JM, Chekaluk HE, Batchelor J. Cognitive tests and determining fitness to drive in dementia: a systematic review. *J Am Geriatr Soc.* (2016) 64:1904–17. doi: 10.1111/jgs.14180
18. Mapstone M, Steffenella TM, Duffy CJ. A visuospatial variant of mild cognitive impairment: getting lost between aging and AD. *Neurology* (2003) 60:802–8. doi: 10.1212/01.WNL.0000049471.76799.DE
19. Tetewsky SJ, Duffy CJ. Visual loss and getting lost in Alzheimer's disease. *Neurology* (1999) 52:958–65.
20. Gibson JJ. *The Perception of the Visual World.* Boston, MA: Houghton Mifflin (1950).
21. Tobimatsu S, Celesia GG. Studies of human visual pathophysiology with visual evoked potentials. *Clin Neurophysiol.* (2006) 117:1414–33. doi: 10.1016/j.clinph.2006.01.004
22. Yamasaki T, Tobimatsu S. Electrophysiological assessment of the human visual system. In: Harris JM, Scott J, editors. *Neuroscience Research Progress, Visual Cortex: Anatomy, Functions and Injuries.* New York, NY: Nova Science Publishers (2012). p. 37–67.
23. Ott BR, Heindel WC, Papandonatos GD, Festa EK, Davis JD, Daiello LA, et al. A longitudinal study of drivers with Alzheimer disease. *Neurology* (2008) 70:1171–8. doi: 10.1212/01.wnl.0000294469.27156.30
24. Petersen RC. Mild cognitive impairment as a diagnostic entity. *J Intern Med.* (2004) 256:183–94. doi: 10.1111/j.1365-2796.2004.01388.x
25. Ott BR, Heindel WC, Whelihan WM, Caron MD, Piatt AL, Noto RB. A single-photon emission computed tomography imaging study of driving impairment in patients with Alzheimer's disease. *Dement Geriatr Cogn Disord.* (2000) 11:153–60. doi: 10.1159/000017229
26. Matías-Guiu JA, Cabrera-Martín MN, Valles-Salgado M, Pérez-Pérez A, Rognoni T, Matías-Guiu J, et al. Neural basis of cognitive assessment in Alzheimer disease, amnestic mild cognitive impairment, and subjective memory complaints. *Am J Geriatr Psychiatry* (2017) 25:730–40. doi: 10.1016/j.jagp.2017.02.002
27. Braak H, Braak E. Neuropathological stageing of Alzheimer-related changes. *Acta Neuropathol.* (1991) 82:239–59. doi: 10.1007/BF00308809
28. Ott BR, Jones RN, Noto RB, Yoo DC, Snyder PJ, Bernier JN, et al. Brain amyloid in preclinical Alzheimer's disease is associated with increased driving risk. *Alzheimers Dement.* (2017) 6:136–42. doi: 10.1016/j.dadm.2016.10.008
29. Piersma D, Fuermaier AB, de Waard D, Davidse RJ, de Groot J, Doumen MJ, et al. Prediction of fitness to drive in patients with Alzheimer's dementia. *PLoS ONE* (2016) 11:e0149566. doi: 10.1371/journal.pone.0149566
30. Horváth A, Szucs A, Csukly G, Sákovics A, Stefanics G, Kamondi A. EEG and ERP biomarkers of Alzheimer's disease: a critical review. *Front Biosci.* (2018) 23:183–220. doi: 10.2741/4587
31. Scally B, Calderon PL, Anghinah R, Parra MA. Event-related potentials in the continuum of Alzheimer's disease: would they suit recent guidelines for preclinical assessment? *J Clin Diagn Res.* (2016) 4:127. doi: 10.4172/2376-0311.1000127
32. Olichney JM, Yang JC, Taylor J, Kutas M. Cognitive event-related potentials: biomarkers of synaptic dysfunction across the stages of Alzheimer's disease. *J Alzheimers Dis.* (2011) 26:215–28. doi: 10.3233/JAD-2011-0047
33. Ou B, Wu C, Zhao G, Wu J. P300 amplitude reflects individual differences of navigation performance in a driving task. *Int J Ind Ergon.* (2012) 42:8–16. doi: 10.1016/j.ergon.2011.11.006
34. Ebe K, Itoh K, Kwee IL, Nakada T. Covert effects of "one drink" of alcohol on brain processes related to car driving: an event-related potential study. *Neurosci Lett.* (2015) 593:78–82. doi: 10.1016/j.neulet.2015.03.020
35. Chai J, Qu W, Sun X, Zhang K, Ge Y. Negativity bias in dangerous drivers. *PLoS ONE* (2016) 11:e0147083. doi: 10.1371/journal.pone.0147083
36. Solís-Marcos I, Galvao-Carmona A, Kircher K. Reduced attention allocation during short periods of partially automated driving: an event-related potentials study. *Front Hum Neurosci.* (2017) 11:537. doi: 10.3389/fnhum.2017.00537
37. Fernandez R, Duffy CJ. Early Alzheimer's disease blocks responses to accelerating self-movement. *Neurobiol Aging* (2012) 33:2551–60. doi: 10.1016/j.neurobiolaging.2011.12.031
38. Fernandez-Romero R, Cox DJ. Impaired driving capacity in early stage Alzheimer's is associated with decreased cortical responsiveness to simulated self-movement. *Alzheimers Dement.* (2016) 12:882. doi: 10.1016/j.jalz.2016.06.1824
39. Warren WH, Hannon DJ. Direction of self-motion is perceived from optic flow. *Nature* (1988) 336:162–3. doi: 10.1038/336162a0
40. Uesaki M, Takemura H, Ashida H. Computational neuroanatomy of human stratum proprium of interparietal sulcus. *Brain Struct Funct.* (2018) 223:489–507. doi: 10.1007/s00429-017-1492-1
41. Yamasaki T, Horie S, Muranaka H, Kaseda Y, Mimori Y, Tobimatsu S. Relevance of *in vivo* neurophysiological biomarkers for mild cognitive impairment and Alzheimer's disease. *J Alzheimers Dis.* (2012) 31:S137–54. doi: 10.3233/JAD-2012-112093
42. Livingstone M, Hubel D. Segregation of form, color, movement, and depth: anatomy, physiology, and perception. *Science* (1988) 240:740–9. doi: 10.1126/science.3283936
43. Rizzolatti G, Matelli M. Two different streams form the dorsal visual system: anatomy and functions. *Exp Brain Res.* (2003) 153:146–57. doi: 10.1007/s00221-003-1588-0
44. Tanaka K, Saito H. Analysis of motion of the visual field by direction, expansion/contraction and rotation cells in the dorsal part of the medial superior temporal area of the macaque monkey. *J Neurophysiol.* (1989) 62:642–56. doi: 10.1152/jn.1989.62.3.642
45. Zhang T, Heuer HW, Britten KH. Parietal area VIP neuronal responses to heading stimuli are encoded in head-centered coordinates. *Neuron* (2004) 42:993–1001. doi: 10.1016/j.neuron.2004.06.008
46. Siegel RM, Reid HL. Analysis of optic flow in the monkey parietal 7a. *Cereb Cortex* (1997) 7:327–46. doi: 10.1093/cercor/7.4.327
47. Raffi M, Squatrito S, Maioli MG. Neuronal responses to optic flow in the monkey parietal area PEc. *Cereb Cortex* (2002) 12:639–46. doi: 10.1093/cercor/12.6.639
48. Lagae L, Maes H, Raiguel S, Xiao DK, Orban GA. Responses of macaque STS neurons to optic flow components: a comparison of MT and MST. *J Neurophysiol.* (1994) 71:1597–626. doi: 10.1152/jn.1994.71.5.1597
49. de Jong BM, Shipp S, Skidmore B, Frackowiak RS, Zeki S. The cerebral activity related to the visual perception of forward motion in depth. *Brain* (1994) 117:1039–54. doi: 10.1093/brain/117.5.1039
50. Morrone MC, Tosetti M, Montanaro D, Fiorentini A, Cioni G, Burr DC. A cortical area that responds specifically to optic flow, revealed by fMRI. *Nat Neurosci.* (2000) 12:1322–8. doi: 10.1038/81860
51. Peuskens H, Sunaert S, Dupont P, Van Hecke P, Orban GA. Human brain regions involved in heading estimation. *J Neurosci.* (2001) 21:2451–61. doi: 10.1523/JNEUROSCI.21-07-02451.2001
52. Ptito M, Kupers R, Faubert J, Gjedde A. Cortical representation of inward and outward radial motion in man. *Neuroimage* (2001) 14:1409–15. doi: 10.1006/nimg.2001.0947
53. Wunderlich G, Marshall JC, Amunts K, Weiss PH, Mohlberg H, Zafieris O, et al. The importance of seeing it coming: a functional magnetic resonance imaging study of motion-in-depth towards the human observer. *Neuroscience* (2002) 112:535–40. doi: 10.1016/S0306-4522(02)00110-0
54. Cardin V, Smith AT. Sensitivity of human visual and vestibular cortical regions to egomotion-compatible visual stimulation. *Cereb Cortex* (2010) 20:1964–73. doi: 10.1093/cercor/bhp268
55. Biagi L, Crespi SA, Tosetti M, Morrone MC. BOLD response selective to flow-motion in very young infants. *PLoS Biol.* (2015) 13:e1002260. doi: 10.1371/journal.pbio.1002260
56. Uesaki M, Ashida H. Optic-flow selective cortical sensory regions associated with self-reported states of vection. *Front Psychol.* (2015) 6:775. doi: 10.3389/fpsyg.2015.00775
57. Wada A, Sakano Y, Ando H. Differential responses to a visual self-motion signal in human medial cortical regions revealed by wide-view stimulation. *Front Psychol.* (2016) 7:309. doi: 10.3389/fpsyg.2016.00309

58. Frank SM, Baumann O, Mattingley JB, Greenlee MW. Vestibular and visual responses in human posterior insular cortex. *J Neurophysiol.* (2014) 112:2481–91. doi: 10.1152/jn.00078.2014
59. Frank SM, Wirth AM, Greenlee MW. Visual-vestibular processing in the human Sylvian fissure. *J Neurophysiol.* (2016) 116:263–71. doi: 10.1152/jn.00009.2016
60. Yamasaki T, Tobimatsu S. Motion perception in healthy humans and cognitive disorders. In: Wu J, editor. *Early Detection and Rehabilitation Technologies for Dementia: Neuroscience and Biomedical Applications*. Hershey, PA: IGI Global (2011). p. 156–61.
61. Yamasaki T, Inamizu S, Goto Y, Tobimatsu S. Visual system: clinical applications. In: Tobimatsu S, Kakigi R, editors. *Clinical Applications of Magnetoencephalography*. Tokyo: Springer Japan KK (2016). p. 145–59.
62. Huk AC, Dougherty RF, Heeger DJ. Retinotopy and functional subdivision of human area MT and MST. *J Neurosci.* (2002) 22:7195–205. doi: 10.1523/JNEUROSCI.22-16-07195.2002
63. McKhann G, Drachman D, Folstein M, Katzman R, Price D, Stadlan EM. Clinical diagnosis of alzheimer's disease: report of the NINCDS-ADRDA work group under the auspices of department of health and human services task force on Alzheimer's disease. *Neurology* (1984) 34:939–44.
64. Yamasaki T, Goto Y, Ohyagi Y, Monji A, Munetsuna S, Minohara M, et al. A deficit of dorsal stream function in patients with mild cognitive impairment and Alzheimer's disease. In: *2012 IEEE/ICME International Conference on Complex Medical Engineering* (Kobe) (2012). p. 28–31.
65. Ikari Y, Nishio T, Makishi Y, Miya Y, Ito K, Koeppe RA, et al. Head motion evaluation and correlation for PET scans with 18F-FDG in the Japanese Alzheimer's disease neuroimaging initiative (J-ADNI) multi-center study. *Ann Nucl Med.* (2012) 26:535–44. doi: 10.1007/s12149-012-0605-4
66. Vilhelmsen K, van der Weel FR, van der Meer ALH. A high-density EEG study of differences between three high speeds of simulated forward motion from optic flow in adult participants. *Front Syst Neurosci.* (2015) 9:146. doi: 10.3389/fnsys.2015.00146

Conflict of Interest Statement: The authors declare that the research was conducted in the absence of any commercial or financial relationships that could be construed as a potential conflict of interest.

The reviewer DS and handling editor declared their shared affiliation.

Advantages of publishing in Frontiers

OPEN ACCESS
Articles are free to read for greatest visibility and readership

FAST PUBLICATION
Around 90 days from submission to decision

HIGH QUALITY PEER-REVIEW
Rigorous, collaborative, and constructive peer-review

TRANSPARENT PEER-REVIEW
Editors and reviewers acknowledged by name on published articles

Frontiers
Avenue du Tribunal-Fédéral 34
1005 Lausanne | Switzerland

Visit us: www.frontiersin.org
Contact us: info@frontiersin.org | +41 21 510 17 00

REPRODUCIBILITY OF RESEARCH
Support open data and methods to enhance research reproducibility

DIGITAL PUBLISHING
Articles designed for optimal readership across devices

FOLLOW US
@frontiersin

IMPACT METRICS
Advanced article metrics track visibility across digital media

EXTENSIVE PROMOTION
Marketing and promotion of impactful research

LOOP RESEARCH NETWORK
Our network increases your article's readership